RING-FAULTING AND ASSOCIATED INTRUSIONS, GLENCOE, SCOTLAND

by

Jennifer Ann Garnham

A thesis submitted for the degree of Doctor of Philosophy, University of London

Department of Geology
Royal School of Mines
Imperial College
London SW7 2BP

April 1988

RING-FAULTING AND ASSOCIATED INTRUSIONS, GLENCOE, SCOTLAND.

ABSTRACT

Ring-faulting and intrusive activity occurred in Glencoe during the lower Devonian, after subduction beneath the area had ceased, and extensional tectonics prevailed. The region is an example of cauldron subsidence, and is interpreted as the root of an ash-flow caldera. A down-faulted block is surrounded by a sub-cylindrical ring-fault, and ring-intrusion which displays calc-alkaline geochemical affinities. The volcanic rocks which are preserved within the down-faulted block are not considered in this study to be related to the ring-faulting event.

A fine-grained fault rock ('flinty crush-rock') is present, and has been extensively sampled. A range of ring-intrusion samples have also been collected and analysed. The intrusion is heterogeneous, varying in shape, mineralogy and chemistry. The underlying magma-chamber is believed to have been zoned as a result of fractional crystallisation.

Some areas have been mapped in detail, in order to elucidate the complexities associated with the interaction of ring-faulting and intrusion. Detailed qualitative and quantitative studies using Scanning Electron Microscopy have shown that the 'flinty crush-rock' is of mixed origin. Intimate mixing of rhyolitic magma with unconsolidated cataclasite has occurred contemporaneously with cauldron-subsidence.

Two examples of early igneous activity have been studied in detail, and give important clues regarding the evolution of the magma-chamber and cauldron.

Firstly, in the west of the area is An-t-sron pluton. This represents the roots of early volcanoes. High heat flow, due to the continual throughput of magma, led to thermal metamorphism and partial-melting of the country-rock in this area. Secondly, in the eastern part of Glencoe, a series of rhyolite and breccia dykes, sub-parallel to the ring-fault are present. These fed surface eruptions of pyroclastic breccias, tuffs and lavas at the base of the volcanic sequence.

Comparisons with Tertiary and Recent calderas in the Western U.S.A. have helped to build up a 3-dimensional picture of cauldrons and calderas, leading to a better understanding of their formation and relationship to one-another.

This project and additional fieldwork was funded by N.E.R.C., which is gratefully acknowledged. I am indebted to Drs Bob Thompson and Kate Brodie for their patient and helpful supervision in my time at Imperial College.

The acquisition of analytical data and the presentation of this work would have been impossible without the help of Peter Watkins, Dick Giddens, Alan Hill, Alan Jones, Ken O'Hara, Barry Coles, Dr Susan Parry, Nick Royall and the Photography and Cartography sections of Imperial College. I am very thankful for the advice and support of numerous colleagues and friends, particularly, Mick Rutter, Ian Kille, Mike Fowler, Paul Suddaby, Paul Grant, Greig Cowan, Dr Chris Halls, Dr Paul Garrard, Fraser Wigley, John Wolff, Phil Leat, Caroline Spark, Steve Rouse, Bob Anderson and everyone from 31, Mapesbury Road. Also, I wish to thank my friends in Glencoe for their kindness and hospitality which made up for the inclement weather.

Special thanks go Dr Jack Nolan for his unerring patience and help in the face of adversity, Dr Ernie Rutter, whose advice has been invaluable, Drs Roy Bailey and Peter Lipman for their kindness and time in the field, and Robert Maddock for his help and support.

Finally, I wish to thank my parents, without whom none of this would have been possible. This work is dedicated to them.

LIST OF CONTENTS

	PAGE
ABSTRACT	1
ACKNOWLEDGEMENTS	3
LIST OF CONTENTS	4
LIST OF FIGURES	9
LIST OF PLATES	12
LIST OF TABLES	13
CHAPTER 1 INTRODUCTION AND LITERATURE REVIEW	14
1.1 INTRODUCTION	14
1.2 EARLY PIONEERING WORK	18
1.3 THE 'FLINTY CRUSH-ROCK' CONTROVERSY	23
1.4 THE RELATIONSHIP BETWEEN CAULDRON AND CALDERA-COLLAPSE	23
1.5 SUMMARY	25
1.6 AIMS	26
CHAPTER 2 FIELD OUTCROP OF THE RING-FAULT AND ASSOCIATED INTRUSIONS	27
2.1 INTRODUCTION	27
2.2 THE FAULT ROCKS	30
2.2.1 General features	30
2.2.2 Stob Mhic Mhartuin	33
2.2.3 F.C.R. away from the fault	37
2.2.4 Association with the red felsite	41
2.2.5 Variability of the fault rock along the ring-fault	43
2.3 THE RING-INTRUSION	45
2.3.1 Introduction	45
2.3.2 Distribution of different types of intrusion and their relative age	45
2.3.3 Width of the intrusions and marginal relationships	48
2.4 SENSE OF MOVEMENT INDICATORS AND	

SUBSIDIARY STRUCTURES 50
2.5 THE BRECCIA AND RHYOLITE DYKES 52
2.6 SUMMARY 54
2.6.1 Fault rocks 54
2.6.2 Ring-intrusion 54
2.6.3 Sense of movement 55

CHAPTER 3 PETROGRAPHY AND MINERAL CHEMISTRY OF THE RING-INTRUSION 56

3.1 INTRODUCTION 56
3.2 THE GABBROS AND DIORITIC GABBROS 57
3.3 THE DIORITES 68
3.4 THE MONZONITES AND GRANITES 69
3.4.1 The fine-grained porphyries 69
3.4.2 The coarse-grained granophyric granite 69
3.4.3 A note on the "early fault-intrusion" 70
3.5 AMPHIBOLES 70
3.6 SUMMARY 73

CHAPTER 4 GEOCHEMISTRY OF THE RING-INTRUSION ROCKS 78

4.1 INTRODUCTION 78
4.2 MAJOR AND TRACE ELEMENT VARIATIONS 80
4.2.1 Major elements 80
4.2.2 Trace elements 84
4.3 RARE EARTH ELEMENTS 91
4.4 RHYOLITES 96
4.5 MAJOR ELEMENT MODELLING 97
4.5.1 Crystal fractionation 97
4.5.2 Partial-melt addition 101
4.5.3 Addition-subtraction diagrams 103
4.5.4 Partial-melt addition followed by crystal fractionation 103
4.6 TRACE ELEMENT MODELLING 107
4.6.1 Based on major element models 107
4.6.2 Based on actual data 112
4.7 SOURCE OF THE RING-INTRUSION MAGMAS 112
4.8 SUMMARY AND CONCLUSIONS 115

CHAPTER 5 EARLY IGNEOUS ACTIVITY ASSOCIATED WITH THE RING-FAULT: PART 1, AN-T-SRON 122

5.1 INTRODUCTION 122
5.2 THE INTRUSIVE ROCKS OF AN-T-SRON 124
5.2.1 Introduction 124
5.2.2 Field relationships 124
5.2.3 Xenoliths 128
5.2.4 The felsites 130
5.2.5 Relationship between intrusion and the marginal breccias 130
5.3 CONTACT METAMORPHISM OF THE ADJACENT COUNTRY-ROCK 131
5.3.1 Dalradian metamorphism 131
5.3.2 The calc-schists 131
5.3.3 The quartzites and pelites 132
5.3.4 Rocks of uncertain origin (nebulite) 133
5.3.5 Breccias 133
5.3.6 Summary 135
5.4 GEOCHEMISTRY OF THE INTRUSIVE ROCKS 137
5.4.1 Range of composition 137
5.4.2 Evidence for fractional crystallisation 137
5.4.3 Evidence for partial-melting 142
5.5 INTERPRETATION OF FIELD AND GEOCHEMICAL OBSERVATIONS 147
5.6 MATHEMATICAL MODELLING OF THE THERMAL HISTORY OF AN-T-SRON 149
5.6.1 Possible causes of the occurrences observed in the field 149
5.6.2 Assumptions 149
5.6.3 Computer programs used to model the heating of the country-rock adjacent to the intrusion 153
5.6.4 Discussion 163

CHAPTER 6 EARLY IGNEOUS ACTIVITY ASSOCIATED WITH THE RING-FAULT: PART 2, BRECCIAS AND ASSOCIATED RHYOLITE DYKES 166

6.1 INTRODUCTION 166

6.2 FIELD RELATIONSHIPS AND PETROGRAPHY 167
6.2.1 Distribution and outcrop of the breccias 167
6.2.2 Breccia types 170
6.2.3 Intrusive rhyolites 174
6.3 FORMATION OF THE BRECCIAS 176
6.3.1 Intrusive and explosion breccias 176
6.3.2 Pyroclastic breccias 177
6.4 SUMMARY AND INTERPRETATION 180
6.4.1 Conclusions 180
6.4.2 A 3-dimensional model 181

CHAPTER 7 THE ORIGIN AND NATURE OF THE FLINTY CRUSH-ROCK 186

7.1 INTRODUCTION AND TERMINOLOGY 186
7.2 FIELD EVIDENCE AND THEORIES OF FORMATION 189
7.3 F.C.R. TEXTURES AND MINERALOGY 190
7.3.1 Marginal breccias 190
7.3.2 Cataclasite 191
7.3.3 The flinty crush-rock 193
7.3.4 Red felsite 195
7.3.5 Mixing relationships 186
7.4 THE GEOCHEMISTRY OF THE FAULT ROCKS 199
7.4.1 Analytical methods 199
7.4.2 Results 199
7.4.3 Origin of the rhyolite (red felsite) 201
7.5 DISCUSSION AND INTERPRETATION 202
7.5.1 Summary 202
7.5.2 Discussion of previous models for the origin of the F.C.R. 203
7.5.3 Alternative hypotheses 207

CHAPTER 8 THE RELATIONSHIPS BETWEEN THE GLENCOE CAULDRON AND YOUNGER CALDERAS 212

8.1 INTRODUCTION 212
8.2 A 3-DIMENSIONAL VIEW 214
8.3 EARLY VOLCANISM 216
8.4 ASH-FLOW TUFF ERUPTIONS 217
8.5 THE INYO-MONO VOLCANIC CHAIN 218

CHAPTER 9 CONCLUSIONS 223

LIST OF REFERENCES 227

APPENDICES 238
APPENDIX A ANALYTICAL TECHNIQUES 238
APPENDIX B SAMPLE LOCALITIES 255
APPENDIX C MAJOR AND TRACE ELEMENT DATA 259
APPENDIX D MINERAL ANALYSES 280
APPENDIX E S.E.M. BULK ANALYSES 300
APPENDIX F NORMALISATION FACTORS 304

BACK POCKET ENCLOSURE
FIGURE 5.01 A simplified map of An-t-sron

LIST OF FIGURES

	PAGE
FIGURE 1.01 Dalradian stratigraphy	15
FIGURE 1.02 Dalradian of the western highlands	16
FIGURE 1.03 Dalradian structures around Loch Leven	17
FIGURE 1.04 Dalradian metamorphic zones	17
FIGURE 1.05 Scottish Devonian igneous rocks	19
FIGURE 1.06 Southwest highlands location map	20
FIGURE 1.07 Sketch map of Glencoe	21
FIGURE 1.08 Sketch section through a cauldron/caldera complex	22
FIGURE 2.01 Sketch map of Glencoe	28
FIGURE 2.02 Section through the cauldron margin	29
FIGURE 2.03 Inner ring-fault, Stob Mhic Mhartuin	31
FIGURE 2.04 Exposure map, Stob Mhic Mhartuin	35
FIGURE 2.05 Cross-section, Stob Mhic Mhartuin	36
FIGURE 2.06 Fractured ring-intrusion	39
FIGURE 2.07 Branching of the F.C.R.	39
FIGURE 2.08 F.C.R. pods and stringers	40
FIGURE 2.09 F.C.R. and felsite mixing	42
FIGURE 2.10 Sketch section, An-t-sron	44
FIGURE 2.11 Multiple intrusion, Cam Ghleann	47
FIGURE 2.12 Ring-fault at Atriochtan	51
FIGURE 2.13 Ring-fault at An-t-sron	53
FIGURE 3.01 Feldspar analyses expressed in terms of An-Ab-Or	65
FIGURE 3.02 Pyroxene analyses expressed in terms of Wo-En-Fs	67
FIGURE 3.03 Amphibole analyses	71

FIGURE 3.04 Phenocryst content vs. SiO2 74
FIGURE 3.05 Crystallisation interval of phenocrystal phases 76
FIGURE 4.01 Geochemical plot of K2O/SiO2 79
FIGURE 4.02 Major element analyses 81
FIGURE 4.03 Trace element analyses 85
FIGURE 4.04 Rare-earth element analyses 92
FIGURE 4.05 Chondrite-normalised REE plots 94
FIGURE 4.06 Flow diagram for element modelling 98
FIGURE 4.07 Addition-subtraction diagram 104
FIGURE 4.08 Trace element variations with respect to residual melt 113
FIGURE 4.09 Chondrite-normalised multi -element plots 120
FIGURE 5.01 Sketch map of An-t-sron Back Pocket
FIGURE 5.02 Field relationships at An-t-sron 125
FIGURE 5.03 Petrogenetic grid showing An-t-sron metamorphism 136
FIGURE 5.04 Ternary phase diagram for granite minimum melting 138
FIGURE 5.05 Major element plots for An-t-sron 139
FIGURE 5.06 Trace element plots for An-t-sron 140
FIGURE 5.07 Trace element plots for An-t-sron 141
FIGURE 5.08 Plagioclase core and rim plots 143
FIGURE 5.09 Chondrite-normalised multi -element plots 144
FIGURE 5.10 Sketch of a foundered cauldron 150
FIGURE 5.11 Estimated radius of An-t-sron pluton 152
FIGURE 5.12 Thermal profiles of cooling intrusions 155
FIGURE 5.13 Equation for determining the motion of a solidification boundary 159
FIGURE 5.14 Temperature vs. time plot for contact metamorphism 160
FIGURE 5.15 Temperature vs. time plote for contact metamorphism 162
FIGURE 5.16 Temperature vs. time plot for contact metamorphism 164
FIGURE 6.01 Sketch map of eastern Glencoe 169

FIGURE 6.02 Sketch section through a pyroclastic breccia 173
FIGURE 6.03 Relationships between breccias and rhyolites 175
FIGURE 6.04 Evolution of the breccia and rhyolite dykes 183
FIGURE 6.05 3-Dimensional view of eastern Glencoe 184
FIGURE 7.01 Fault rock classification 187
FIGURE 7.02 Major element plots 200
FIGURE 7.03 Model for F.C.R. formation 209
FIGURE 8.01 Geological map of Long Valley 213
FIGURE 8.02 Map of the Inyo Volcanic Chain 219
FIGURE 8.03 Cross-section through a rhyolite dome conduit 219
FIGURE 8.04 Cross-section through Long Valley magma-chambers 221
FIGURE 9.01 Cross-section through Glencoe 223
FIGURE 9.02 Sequence of magmatic events 225
FIGURE A1 Errors in chondrite-normalised multi-element plots 249

LIST OF PLATES

		PAGE
2.01	Fault rocks at Atriochtan	32
2.02	Inner ring fault at Stob Mhic Mhartuin	38
2.03	Ring-intrusion in Cam Ghleann	38
2.04	Ring-fault at An-t-sron	38
2.05	Sheared F.C.R. vein	38
3.01	Photomicrograph of a gabbro, 2JG1	63
3.02	Photomicrograph of a diorite, 2JG35	63
3.03	Photomicrograph of a monzonite, 2JG9	63
3.04	Photomicrograph of a granophyric granite, 1JG61	63
5.01	Ring-fault at An-t-sron	123
5.02	Pelitic xenolith, An-t-sron	126
5.03	Felsite, pelite and tonalite, River Coe	126
5.04	Pelite band, River Coe	127
5.05	Foliated 'nebulite', River Coe	127
5.06	Pelitic xenoliths, River Coe	129
5.07	Photomicrograph of a calc-schist, 3JG56	129
5.08	Photomicrograph of a pelite, 3JG10	129
5.09	Photomicrograph of a felsite, 4JG2	129
5.10	Photomicrograph of a felsite segregation, 3JG10	129
6.01	Intrusive breccia vein	168
6.02	Intrusive breccia	171
6.03	Photomicrograph of an intrusive breccia	171
6.04	Pyroclastic breccia	171
6.05	Photomicrograph of a pyroclastic breccia	171
6.06	Photomicrograph of an intrusive tuff	171
7.01	Photomicrograph of a breccia, 1JG21	192
7.02	Photomicrograph of fault rock, 1JG35	192
7.03	Photomicrograph of F.C.R.	194
7.04	BEI image of a megacryst	194
7.05	BEI image of a megacryst	194
7.06	BEI image of F.C.R.	194
7.07	BEI image of F.C.R. matrix	194
7.08	Photomicrograph of spherulitic rhyolite, 3JG64	194
7.09	BEI image of acidic rhyolite	197
7.10	BEI image of rhyolite	197
7.11	Photomicrograph of immiscible mixing	197
7.12	Photomicrograph of F.C.R. eddies	197
7.13	Photomicrograph of F.C.R. mixing	197

LIST OF TABLES

		PAGE
TABLE 3.01	Selected modal compositions	58
TABLE 3.02	Typical mineral compositions	59
TABLE 4.01	Crystal fractionation mixing model	99
TABLE 4.02	Partial-melt mixing model	102
TABLE 4.03	Crystal fractionation with partial-melt mixing model	105
TABLE 4.04	Trace element modelling	108
TABLE 4.05	Maximum and minimum bulk distribution coefficients	110
TABLE 4.06	Actual bulk distribution coefficients	111
TABLE 4.07	Magma source mixing model	116
TABLE 4.08	Magma source mixing model	117
TABLE 4.09	Trace element modelling of the magma source	118
TABLE 5.01	Mixing model for granite genesis	146
TABLE 5.02	Heat flux across the pluton wall	155
TABLE A1	Major element precision data	240
TABLE A2	Comparison between X.R.F. and I.C.P.	241
TABLE A3	U.S.G.S. standard trace element values	243
TABLE A4	Precision data for trace elements	244
TABLE A5	Trace element detection limits	246
TABLE A6	Precision data for REE	248
TABLE A7	REE standard concentrations from I.C.P.	250
TABLE A8	REE standard concentrations from I.N.A.A.	251
TABLE A9	Comparative REE data for I.C.P. and I.N.A.A.	252
TABLE A10	Precision data for a jadeite standard mineral	254

CHAPTER 1

INTRODUCTION AND LITERATURE REVIEW

1.1 INTRODUCTION

Ring-faulting and intrusion occurred in Glencoe during Lower Devonian times (approx. 400my, see footnote at end of chapter). This was at the end of the Caledonian Orogeny, when subduction under Scotland had ceased, and the Iapetus Ocean had closed (Lambert and McKerrow 1976).

The fault and intrusion have cut through a crystalline basement of Dalradian metasediments (Fig. 1.01). These were deposited in Late Precambrian - Cambrian times (700-550my; Anderton et al. 1979), and subsequently folded and metamorphosed during the Ordovician (500-490my; Fettes 1979) under a compressional tectonic regime (Fig. 1.02; Fig. 1.03; Fig. 1.04).

By the Lower Devonian, an extensional tectonic regime was prevalent, which facilitated the upwelling of subduction-related magmas. This led to the eruption of lavas near Oban, Glencoe and in the Midland Valley, as well as the intrusion of the 'Newer Granites' (Fig. 1.05), (Anderton et al. 1979; Bluck 1985)

Glencoe is located in the northwestern corner of the Etive granite complex, (and is partially intruded by it). The ring-fault and ring-intrusion (previously named "fault-intrusion" by other workers) surround a downfaulted block of Dalradian basement overlain by Lower Devonian sediments and volcanics (Fig. 1.06; Fig. 1.07). This was recognised by Clough et al. (1909) to be an example of cauldron subsidence, now interpreted as the erosional remnant of an ash-flow caldera (Fig. 1.08)(Roberts 1963; 1966a)

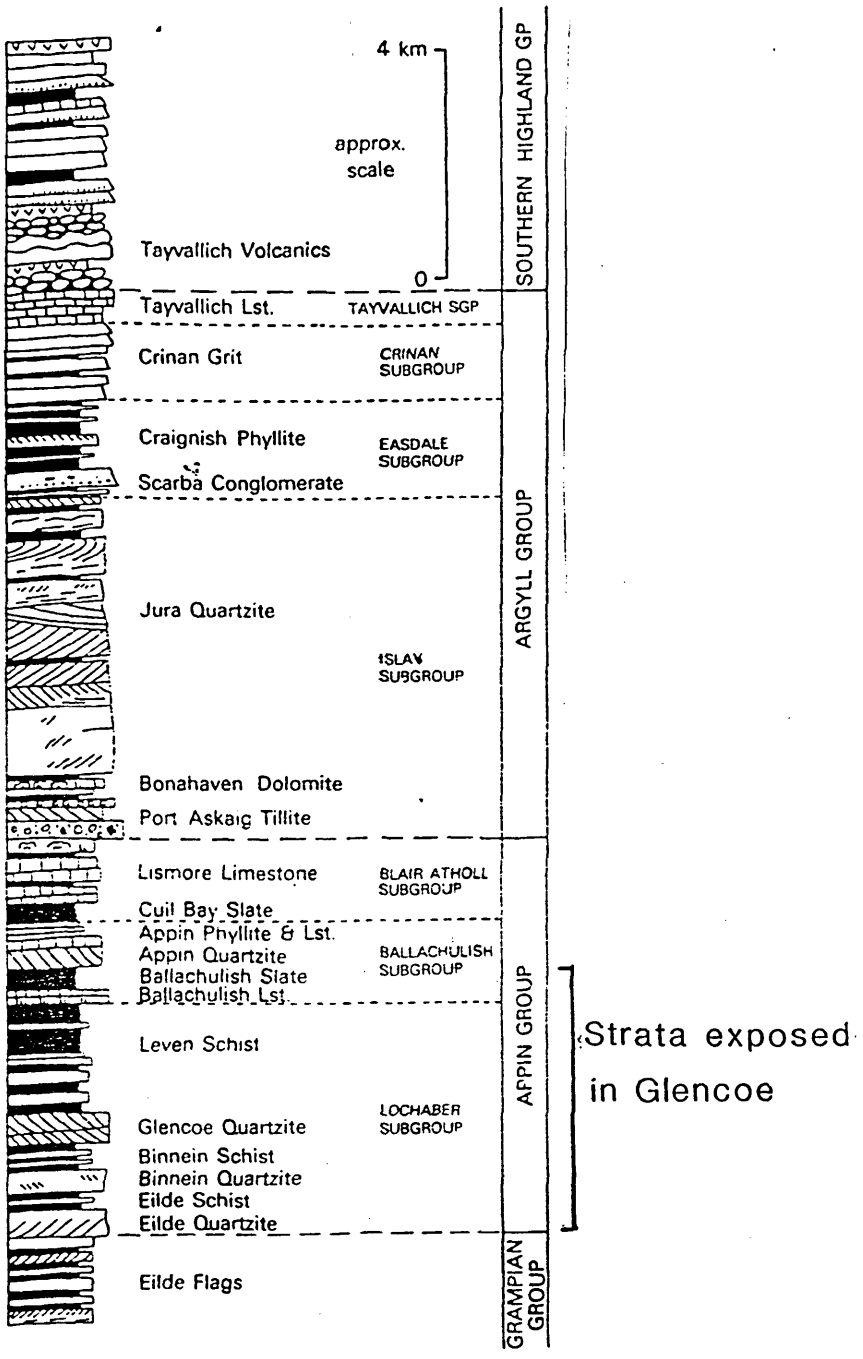

FIGURE 1.01 Stratigraphy of the Dalradian showing the rocks exposed in the Glencoe area. After Anderton et al. (1979).

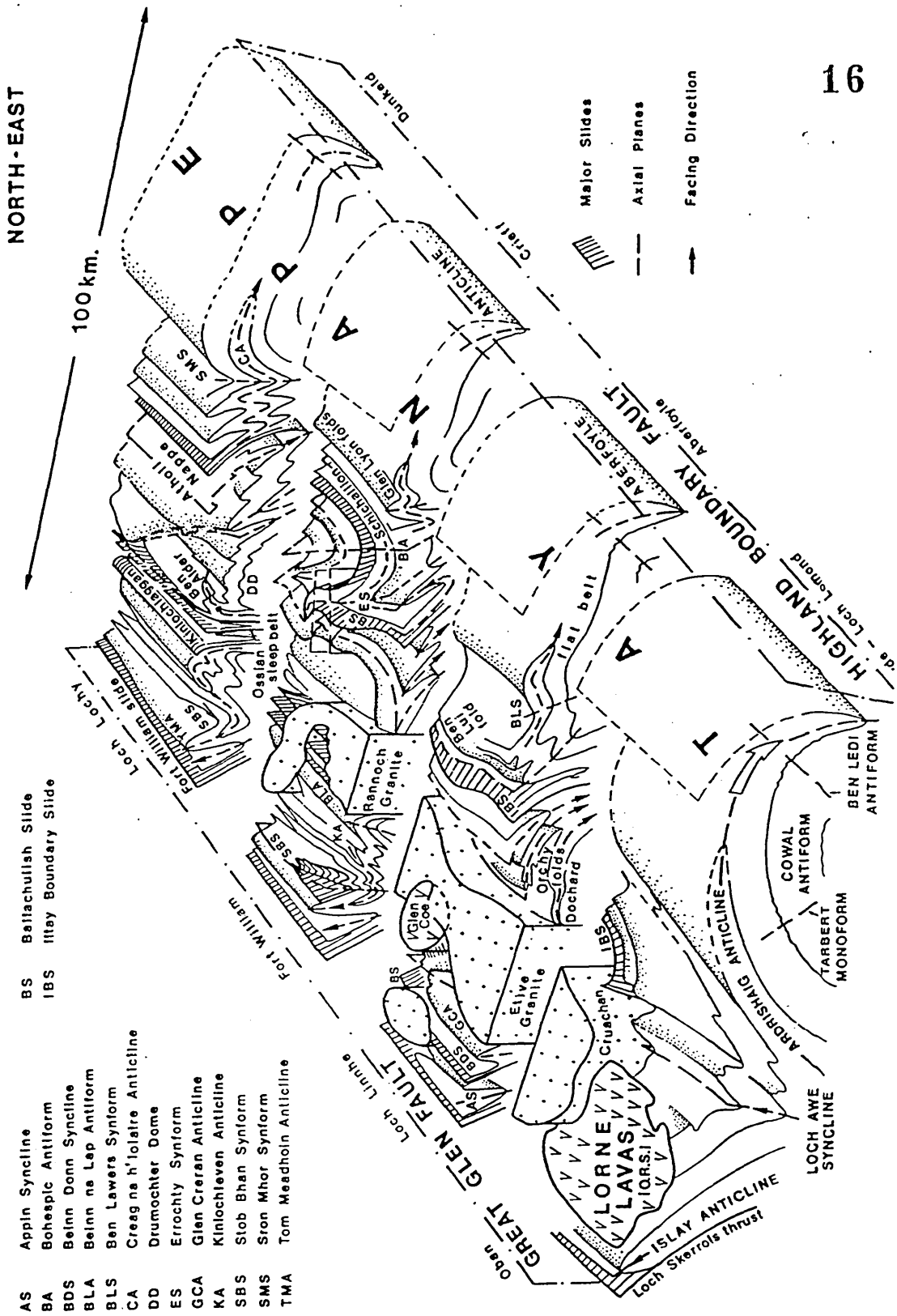

FIGURE 1.02 A 3D block diagram showing the structure of the Dalradian in the Western Highlands, and its cross-cutting relationship to Devonian igneous activity. After Roberts and Treagus (1979)

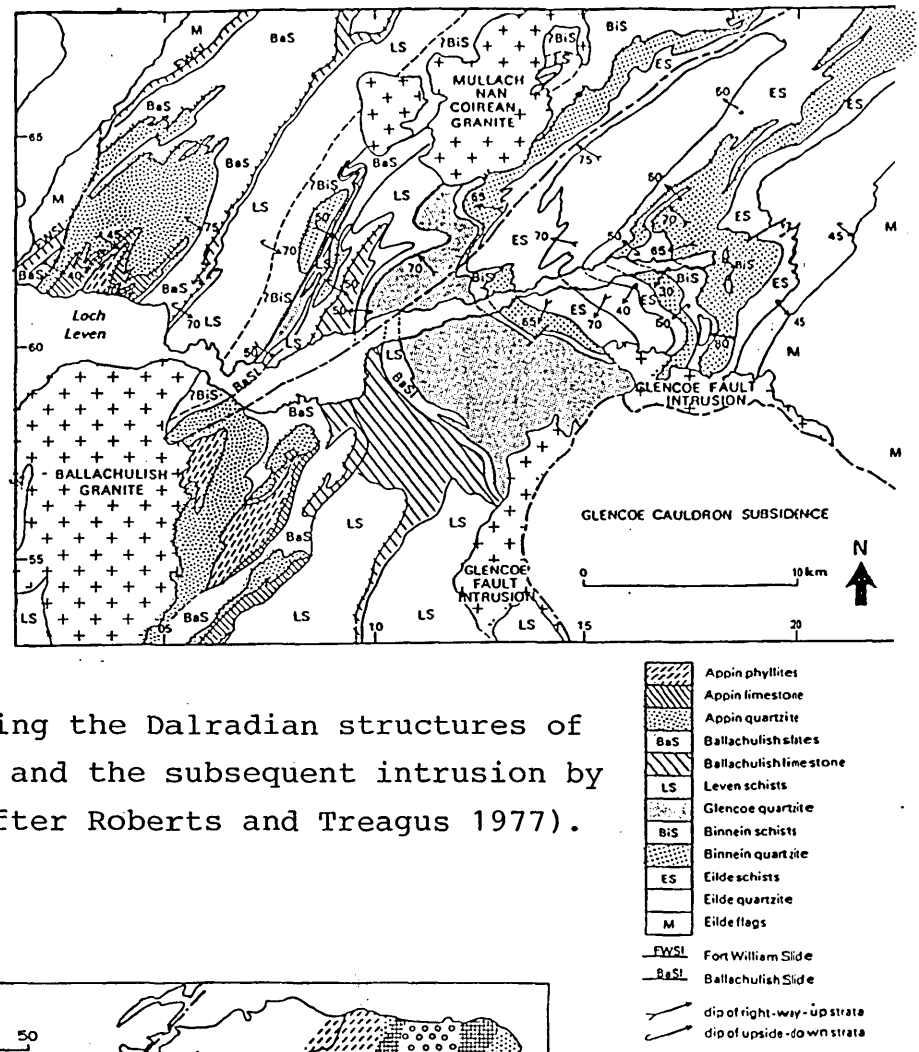

FIGURE 1.03 Map showing the Dalradian structures of the Loch Leven area, and the subsequent intrusion by Devonian granites (after Roberts and Treagus 1977).

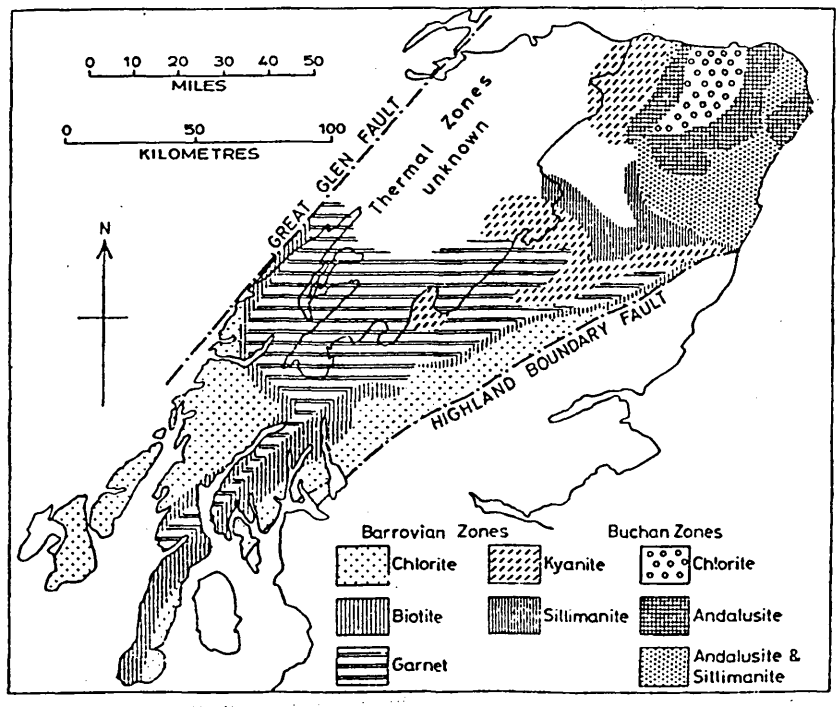

FIGURE 1.04 Metamorphic zones of the Dalradian rocks (after Johnson 1963).

The extrusives and intrusives are calc-alkaline in composition, ranging from basalt/andesite (gabbro/diorite) to rhyolite (granite). These rocks are thought to have been erupted and crystallised from a compositionally layered magma chamber.

The author would like to stress that for reasons which are considered later, she believes that the extrusive rocks exposed in Glencoe, which are preserved within the down-faulted block, are not directly related to the cauldron-subsidence event.

1.2 EARLY PIONEERING WORK

The earliest detailed study of Glencoe was undertaken at the beginning of the century by the British Geological Survey, (Bailey and Maufe 1916, 2nd Ed. Bailey 1960; Clough et al. 1909). In the course of regional mapping, Bailey and co-workers recognised an incomplete outward-dipping ring fault with an associated intrusion, enclosing a down-faulted block. This was interpreted as cauldron subsidence.

The ring-fault, which occasionally splits into two is marked by a black, very fine-grained rock, called the 'flinty crush-rock' (Clough et al. 1909). Due to its sub-vitreous texture, and the presence of small, rounded quartzite grains, it was thought to be a pseudotachylite, derived by the frictional melting of the country rock. It was noted that the ring-intrusion occurred almost exclusively outside the ring fault. Clough et al. (1909) describe four main types of intrusion : grey tonalite, pink granitite, grey porphyrite and pink porphyrite (the relevence of these terms is discussed in chapters 3 and 4). In addition, Bailey (1916) observed a separate grey hornblendic porphyrite known as the 'early fault-intrusion'. (Due to practical difficulties and poor exposure, the mapping of the

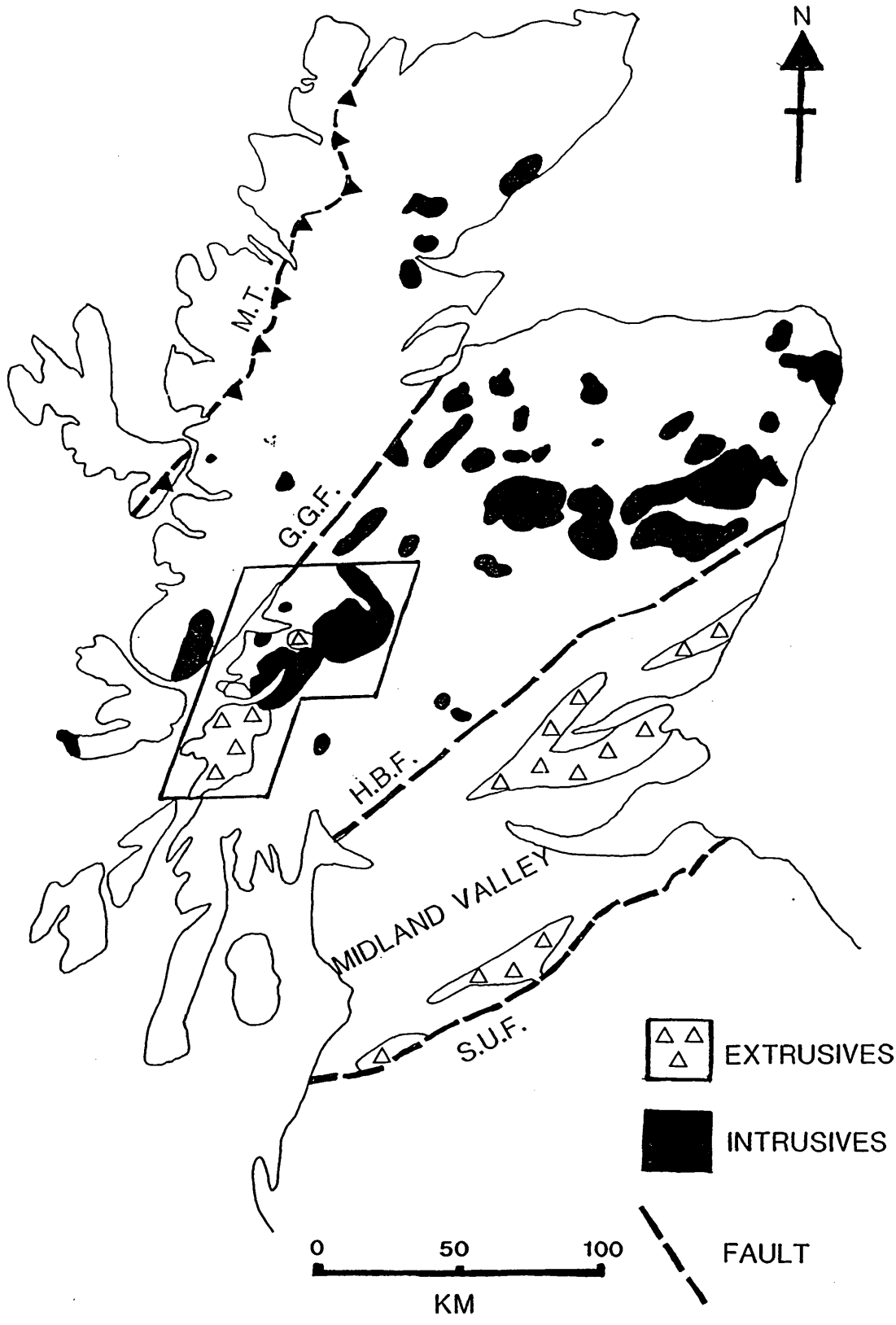

FIGURE 1.05 Map showing the distribution of Devonian igneous rocks of Scotland. M.T. is the Moine Trust, G.G.F. is the Great Glen Fault, H.B.F. is the Highland Boundary Fault and S.U.F. is the Southern Uplands Fault. Detail of the area marked is shown in Fig. 1.06

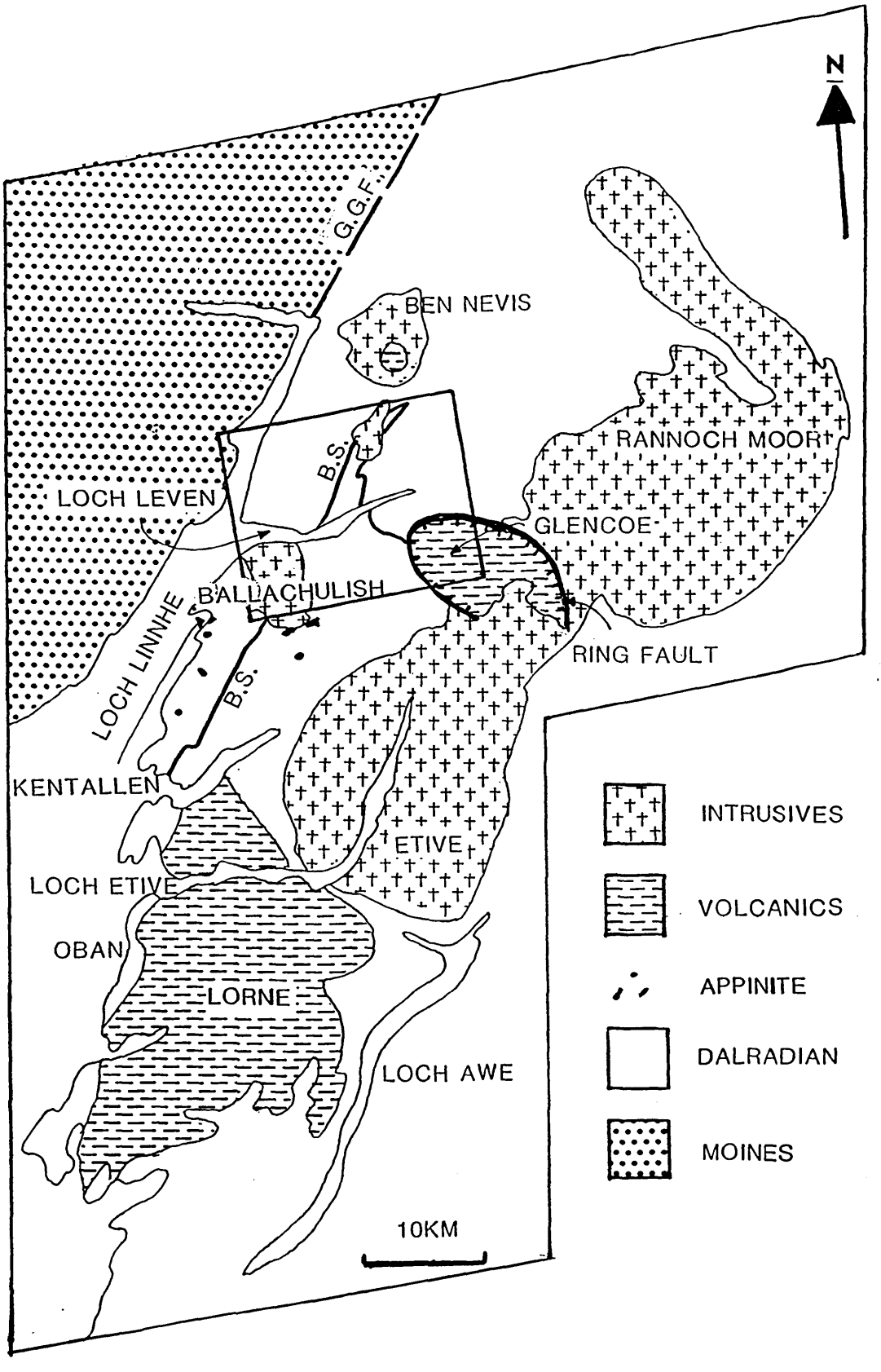

FIGURE 1.06 A location map of the Southwest Highland region showing the Devonian igneous activity including the small appinite (dioritic) plugs in the Appin region. Detail of the area marked is shown in Fig. 1.03

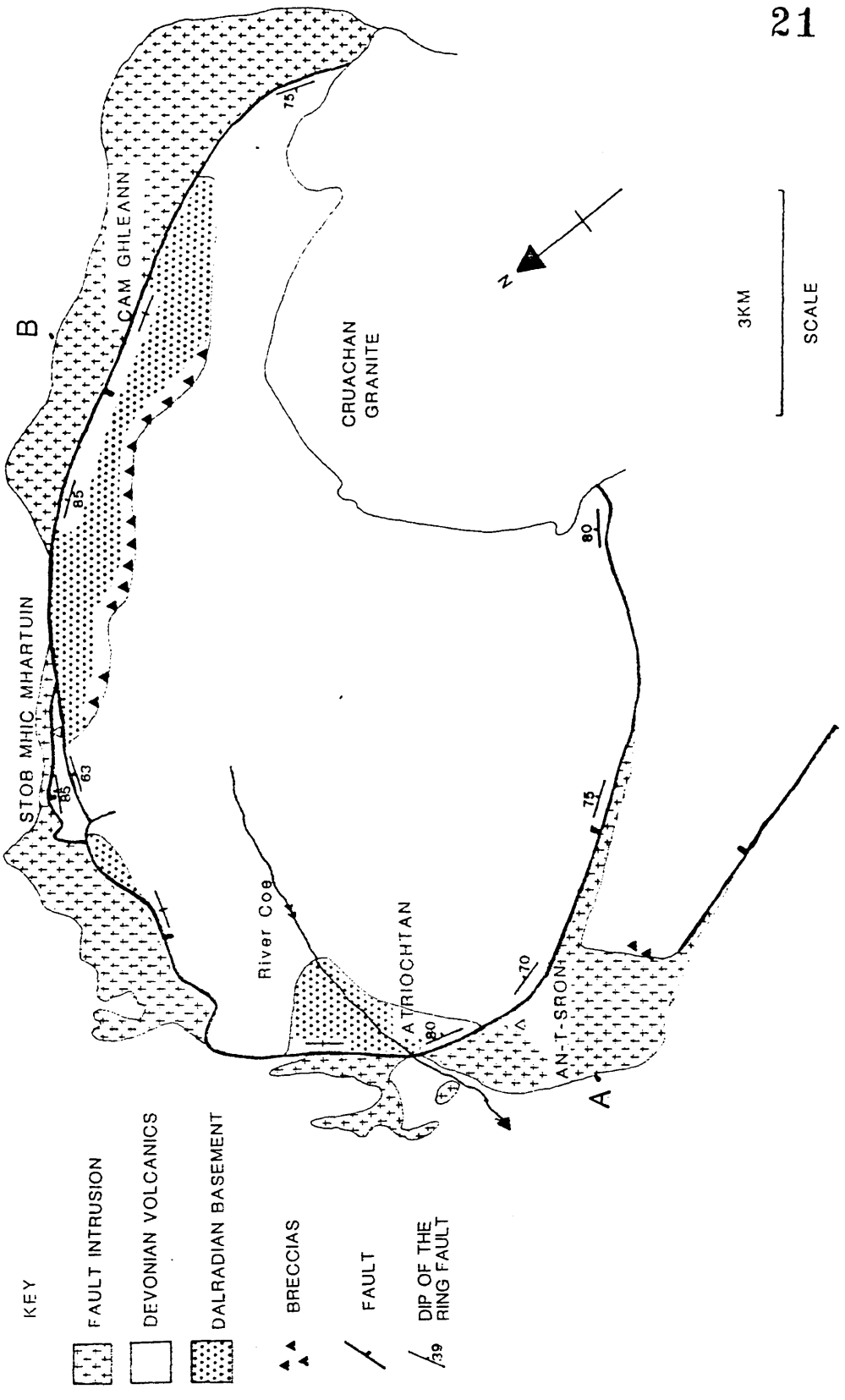

FIGURE 1.07 Simplified sketch map of the Glencoe cauldron subsidence. Dalradian rocks outside the fault intrusion are not marked.

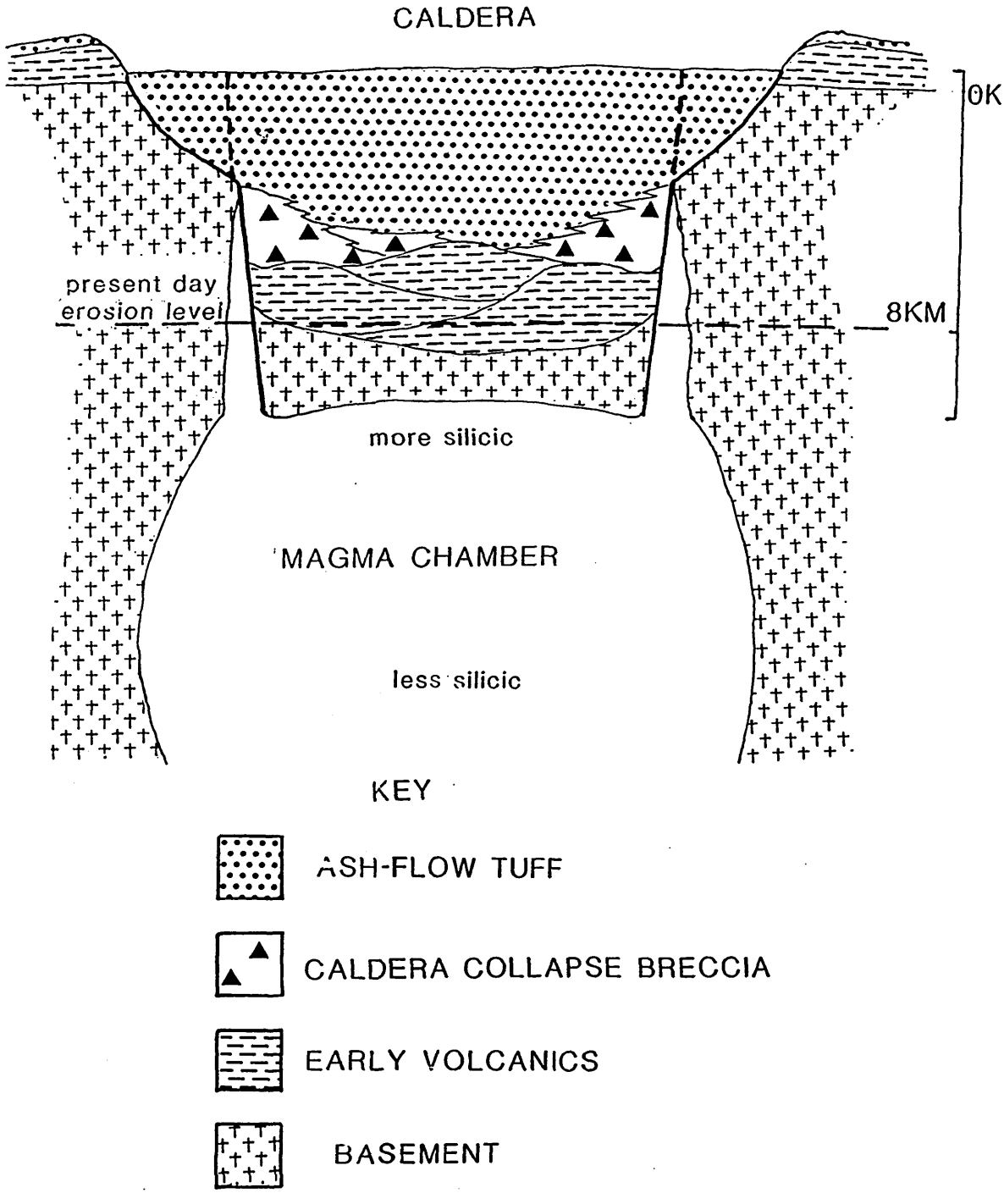

FIGURE 1.08 A sketch section through a typical ash-flow cauldron/caldera complex with associated magma chamber. After Lipman (1984). The dashed line represents the present day erosion level of Glencoe.

intrusive rocks was not considered to be a worthwhile exercise in this study.) It was inferred that simultaneous faulting and intrusion had occurred due to a) a lack of deformation of the ring-intrusion, and b) a lack of thermal metamorphism of the country-rock within the ring-fault.

The volcanic rocks were found to be of Lower Devonian age from the evidence of plant fossils discovered in the basal sediments, and were considered to have been derived from more than one centre. This is due to their bimodal nature (andesite and rhyolite), and variations of the thickness of different units in different areas.

1.3 THE 'FLINTY CRUSH-ROCK' CONTROVERSY

The flinty crush-rock, which is located along the ring-fault, is best exposed at Stob Mhic Mhartuin, Cam Ghleann and Atriochtan (Fig. 1.06) (flinty crush-rock is used in this work as a field term for the ultra fine-grained fault rocks, but for a full definition of the fault rock terminology used, see chapter 7). It was originally thought to be a melt generated by frictional heating (Clough et al. 1909), but Reynolds (1956) disputed this theory, and likened the formation of flinty crush-rock to the industrial process of gas-fluidisation. Other workers also agreed with this view (Hardie 1963; Taubeneck 1967; Roberts 1974). They proposed that the flinty crush-rock was a fine-grained intrusive breccia carried by magmatic gases which cored and brecciated the country-rock, rounding and 'polishing' fragments by attrition. Roberts (1966b) concluded that the flinty crush-rock was the 'advanced guard' for the ring-intrusion, whereby crystals and liquid droplets of magma were entrained into their present position by gases during cauldron subsidence. A similar rock type to the flinty crush-rock is also found at Slieve

Gullion (Reynolds 1956), in the Irish Tertiary Province, and was thought to have been generated by a gas-fluidised system. The origin of this rock-type is considered further in chapters 2 and 7.

1.4 THE RELATIONSHIP BETWEEN CAULDRON AND CALDERA-COLLAPSE

The discovery of two ignimbrite (ash-flow tuff) horizons preserved within the lava sequence inside the ring-fault (Roberts 1963, 1966a) led to a more integrated discussion about the evolution of Glencoe in relation to ash-flow caldera-collapse (Roberts 1966a, 1966b, 1974; Taubeneck 1967). Cycles of volcanism involving the andesites and rhyolites and culminating in the eruption of the ignimbrites were postulated (Roberts 1966b, 1974; Taubeneck 1967). The occurrence in places of two distinct, sub-parallel faults and associated ring-intrusions led to the suggestion that they were related to the two ignimbrite horizons. That is, the earliest ring fault was formed during the eruption of the lower ignimbrite, resulting in the emplacement of the 'early ring-intrusion', and the later ring-fault was formed during the eruption of the upper ignimbrite resulting in the emplacement of the later ring-intrusion (Roberts 1966a, 1974; Taubeneck 1967). (These points are considered further in chapters 8 and 9.) Roberts (1966a) suggested that a layered magma-chamber was the source for the compositional range of the associated volcanics and intrusives.

There has been much discussion concerning the evolution of a group of rhyolite-associated breccias on the eastern side of the cauldron (Clough et al. 1909; Bailey 1960; Hardie 1963; 1968; Taubeneck 1967; Roberts 1974) (see chapter 6). Clough et al. (1909) and Taubeneck (1967) believe these to be sedimentary breccias, however Hardie (1963), using the

nomenclature of Wright and Bowes (1963), interpreted them as a group of intrusive, explosion breccias, caused by the release of magmatic gases. Many of the breccia bodies are elongate, and sub-parallel to the ring-fault (Fig. 1.06). Hardie (1963, 1968) noted the similarity between the fine-grained breccia matrix, and the flinty crush-rock at Stob Mhic Mhartuin, using this similarity between the two as evidence for the gas-fluidisation theory for flinty crush-rock formation (section 1.3). Roberts (1974) noted that the boundary between the Dalradian basement and the Devonian volcanics was marked by a band of these breccias, and considered this boundary to be sub-vertical. From this he postulated that the breccia band represented an early, crescentic caldera wall fault.

1.5 SUMMARY

There has been little work published on Glencoe in recent times. The regional geochemistry of the Devonian lavas and intrusions of Scotland has been assessed (Thirlwall 1981, 1982), as well as the geochemistry and isotope systematics of the Etive pluton (Clayburn 1981; Clayburn et al. 1984; Frost and O'Nions 1985), incorporating the Glencoe ring-intrusion.

A small region on the slopes of An-t-sron has been mapped in detail (Bussell 1979). A full assessment of this work is given in chapter 5.

As a result of the work discussed so far, this present study began given the following scenario:

1) That Glencoe was a cauldron-subsidence feature, linked to the Etive granite complex, which in turn was a member of the 'Newer Granites' (Halliday and Stephens 1984).

2) Some of the volcanics in the down-faulted plug may have been erupted during cauldron-subsidence

and associated emplacement of the ring-intrusion, and may have formed an extension of the Lorne Lava Plateau prior to erosion.

3) There were conflicting ideas about the formation of the 'flinty crush-rock', and its relationship to the ring-intrusion.

4) The fault intrusion was known to be of variable composition, and there was no clear consensus on its relation to the volcanics, its mode of emplacement, nor its temporal relation to the ring-fault.

5) In the light of more recent work on calderas and ash-flow tuffs (e.g. Smith et al. 1961; Lipman 1984; Walker 1984), previous evolutionary interpretations of Glencoe were in need of updating (Bailey 1960; Roberts 1974).

1.6 AIMS

The main aim of this work is to determine the nature and origin of the flinty crush-rock, particularly in terms of the relationship between faulting, intrusion and cauldron-subsidence/caldera collapse. This is intergrated with an assessment of the magma-chamber evolution, via the study of the petrography, mineral chemistry and geochemistry of the ring-intrusion rocks. Additional aims are to examine the temporal relationship between ring-faulting and intrusion, and to assess evidence of early, fault-associated intrusion in terms of the evolution of the Glencoe igneous complex. Since the extrusive rocks which are spatially associated with the ring-fault are not considered to be related to the cauldron-subsidence event (chapters 8, 9), they are not discussed in detail in this work.

Footnote: The term Lower Devonian is used in this text for simplicity. However, the author is aware of the fact that rocks such as these, which are associated with the deposition of the Old Red Sandstone, may have Wenlockian ages.

CHAPTER 2

FIELD OUTCROP OF THE RING-FAULT AND ASSOCIATED INTRUSIONS

2.1 INTRODUCTION

The ring-fault in Glencoe is an incomplete ellipse, 14Km by 8Km. It is believed to have originally been sub-circular, and was extended by the later intrusion of the Etive dyke swarm (Bailey 1960).

In places the fault is well-exposed, though less than 10% of the total circumference of the ring-fault is seen (Fig. 2.01). The classic exposure is at Stob Mhic Mhartuin, but the fault and associated intrusions are also well-exposed at Cam Ghleann, Atriochtan and An-t-sron. The intrusive igneous rocks form a ring-intrusion ranging in width from 1m to 2Km.

The fault is steeply dipping, ranging from 85° outwards to 60° inwards (Taubeneck 1967; present work Fig. 1.06). These measurements suggest a tapering, subsided block (as in Fig. 1.08), but the lack of more complete exposure, combined with the inhomogeneity of dip, leads to speculation about this assumption. For the purpose of this study, the original ring-fault is taken to be vertical.

The fault zone varies in width from 10cm up to 1m. Aswell as the typical range of brecciated rocks seen in fault zones, this particular fault is characterised by an ultra fine-grained, black rock, known as the 'flinty crush-rock' (F.C.R.). The F.C.R. is not only found along the fault plane, but it is also seen intruding the country-rock and ring-intrusion. The presence of two sub-parallel ring-faults has been described in a number of places (Clough et al. 1909; Bailey 1960), with one case of

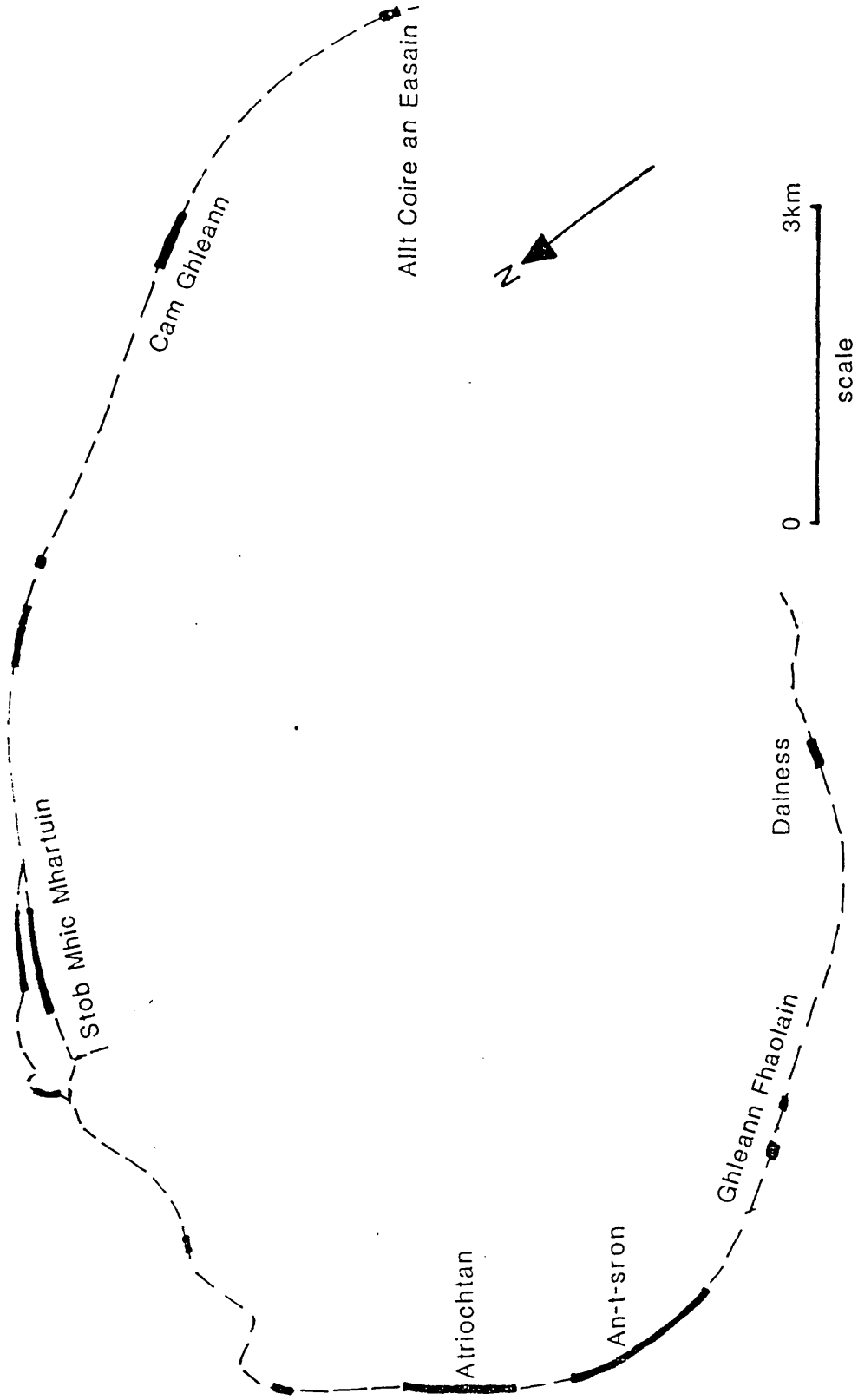

FIGURE 2.01 A sketch map of the Glencoe ring fault indicating the extent of exposure (solid lines, not to scale), and the localities mentioned in the text.

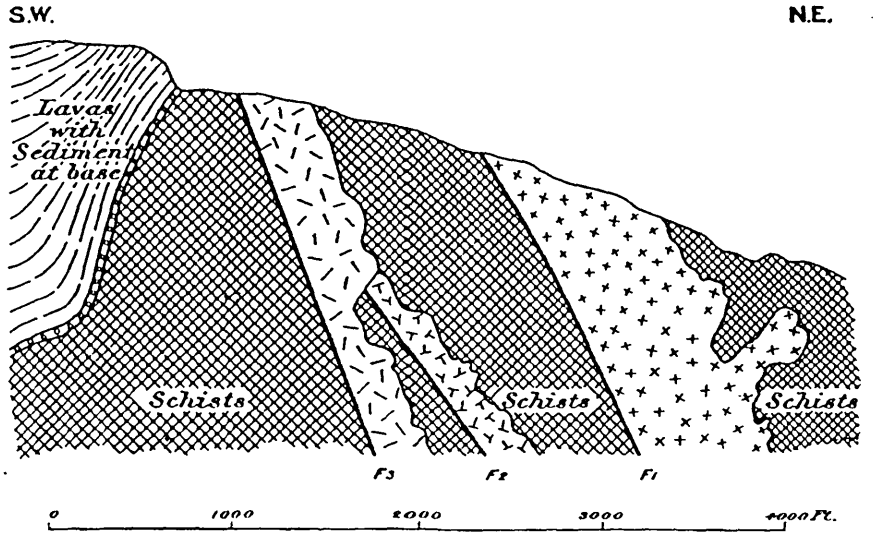

. Section through ridge W. of Coire Odhar-mhòr

F1 and F2 Early Boundary-Faults accompanied by Early Fault-Intrusions. F3 Main Boundary-Fault with Main Fault-Intrusion

FIGURE 2.02 A cross-section through the cauldron margin west of Coire Odhair Mhor showing the presence of three ring-faults and associated intrusions. (After Bailey 1960). F1 and F2 are faults accompanied by deformed ring-intrusions, F3 is the main boundary fault, with accompanying tonalitic ring-intrusion.

three faults (Bailey 1960) (Fig.2.02). The outermost fault is considered to be the earliest (Bailey 1960).

Much of the fieldwork concentrated on Stob Mhic Mhartuin and An-t-sron. More general observations were made from other areas, combined with comprehensive sampling of the fault-rocks and intrusions for petrographical and geochemical analyses. A map of the northern part of the area is soon to be published (W.G. Hardie pers. comm.).

2.2 THE FAULT-ROCKS

2.2.1 General features

The fault rocks separate the ring-intrusion from the country-rocks within the subsided block. These are Dalradian quartzites and pelites, with Devonian volcanics and sediments. The fault zone is up to 1m wide ranging from a country-rock breccia which grades into a white, fine-grained crush-rock, through a grey crush-rock to black 'flinty crush-rock' (F.C.R.) (Fig. 2.03). This gradation correlates with an apparent decrease in grainsize. A fine-grained, red felsite is commonly found at, or near, the outer margin of the fault zone, or intimately associated with the F.C.R. (section 2.2.4).

The F.C.R. is extremely fine-grained, diplays a conchoidal fracture and is banded. This banding is presumed to be flow-banding. Small, rounded quartz grains are found within the F.C.R., and are particularly common near the inner, country-rock margin, even if the in situ country-rock is not a quartzite (Plate 2.01). Tabular feldspar megacrysts are also found in the F.C.R. and are commonest near the outer, ring-intrusion margin.

Shear zones running parallel to the main fault can be seen in the country-rocks within the downfaulted block (Fig. 2.04). These are

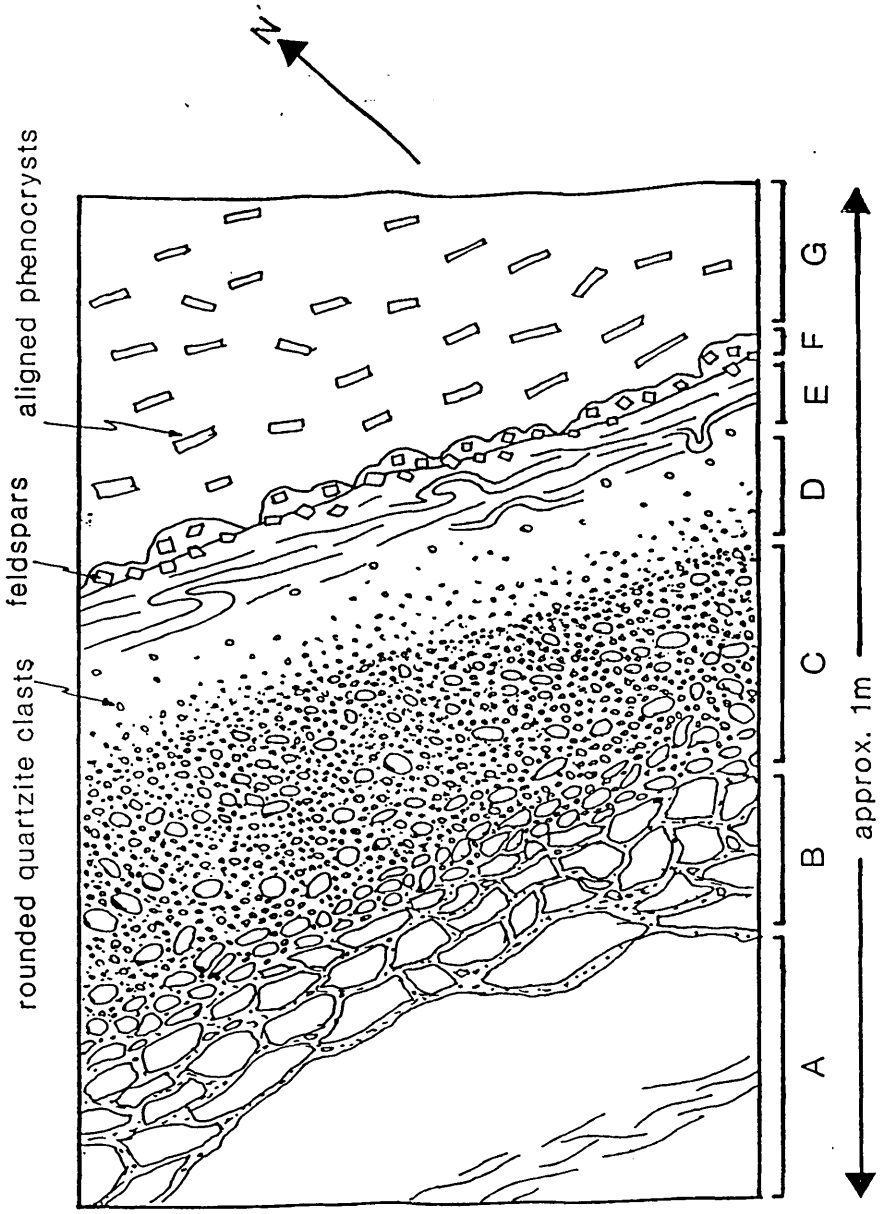

FIGURE 2.03 A schematic map showing the gradation from quartzitic country-rock to flinty crush-rock as seen on the inner ring fault at Stob Mhic Mhartuin (partly after Roberts 1966b). A is flaggy quartzite, B is brecciated and shattered quartzite, C is 'white' crush-rock, D is grey crush-rock, E is black, flinty crush-rock with flow-banding, F is red felsite with phenocrysts and G is inner ring-intrusion.



PLATE 2.01 Outcrop of the fault rocks showing relationship B (Fig. 2.09) between the black F.C.R. and the red felsite. Note the small rounded white quartzite clasts, and the pink feldspar megacrysts within the F.C.R.

approximately 5cm wide, and are composed of fractured and sheared fragments of country-rock up to 10cm in length. These structures are considered to be subsidiary to the main ring-faulting event.

A full assessment of the fault rocks is covered in chapter 7.

2.2.2 Stob Mhic Mhartuin

The best exposure of the ring-fault and F.C.R. is at Stob Mhic Mhartuin (Figs. 2.04, 2.05), which is a prominent crag in the northeastern part of the area. Here a number of aspects of the cauldron subsidence can be observed at the one locality. Other ring-fault and F.C.R. localities (e.g Cam Ghleann, Atriochtan) display many of the features described here.

Two faults are present, with a slice of flaggy quartzite preserved between them. Quartzite is present adjacent to the inner ring-fault within the subsided block. A tonalite, which intrudes quartzite, is present outside the outer ring-fault. The area has subsequently been intruded by a number of Etive dykes, which are omitted from both the map and the present discussion.

The outer ring-fault dips outwards at 85°, and is marked by a wide zone of F.C.R. up to 15cm wide. The crush-rock is black to a purplish-red in colour, and is characterised by abundant tabular feldspar crystals. At locality D (Fig. 2.04), the fault cuts through a patch of breccia (similar to those discussed in chapter 6), and fragments of the breccia become incorporated by the F.C.R.. A similar relationship between breccia and F.C.R. is seen on an outcrop of the inner ring-fault 300m to the West (G.R. NN208578). Exposures of the breccia do not appear outside the ring-fault, hence it is inferred that the brecciation event was pre-faulting (chapter 6).

The inner ring-fault has an outward dip ranging

FIGURE 2.04 An exposure map of Stob Mhic Martuin showing the two ring faults and associated intrusions. The cross-section from X to Y is shown in Fig. 2.05. Details of localities A to H are described in the text.

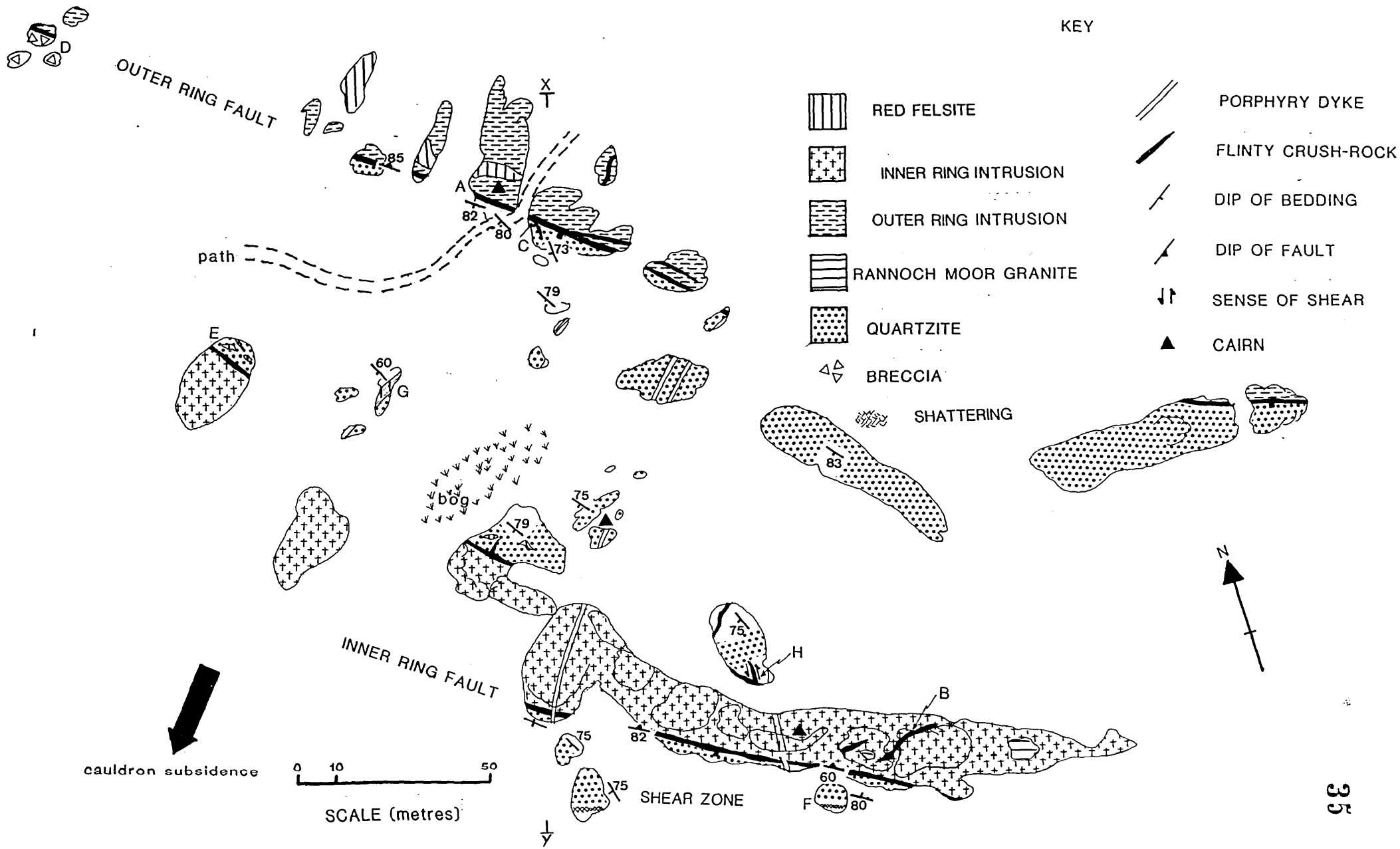
KEY
RED FELSITE
INNER RING INTRUSION
OUTER RING INTRUSION
RANNOCH MOOR GRANITE
QUARTZITE
BRECCIA
SHATTERING
PORPHYRY DYKE
FLINTY CRUSH-ROCK
DIP OF BEDDING
DIP OF FAULT
SENSE OF SHEAR
CAIRN
OUTER RING FAULT
INNER RING FAULT
path
bog
SHEAR ZONE
cauldron subsidence
SCALE (metres)
0
10
50
N
A
B
C
D
E
F
G
H
X
Y
85
82
80
73
79
60
75
83

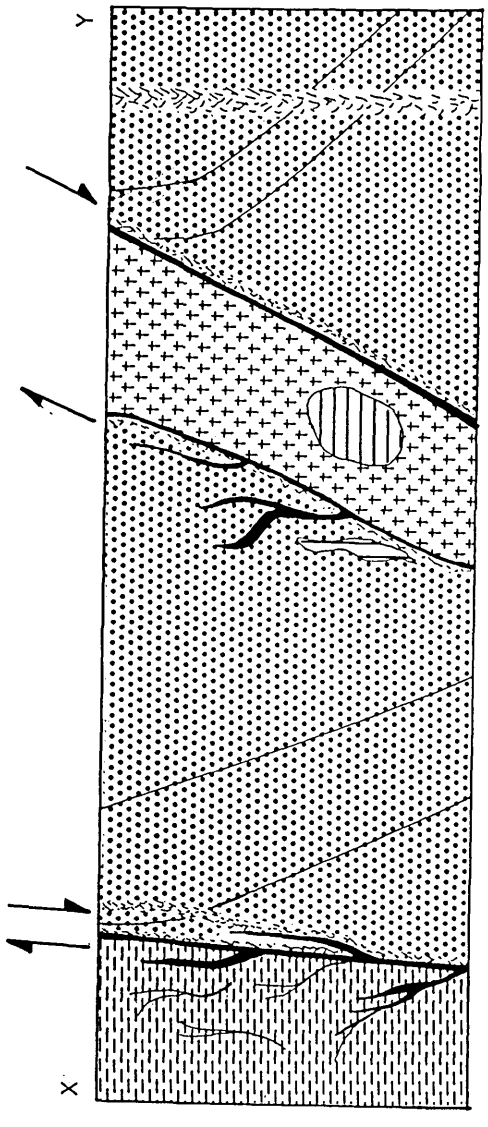

FIGURE 2.05 An idealised cross-section through Stob Mhic Mhartuin along the line X to Y. For the legend see Fig. 2.04.

from 60° to 85° (Plate 2.02). The typical gradation from brecciated quartzite to F.C.R. is very well developed here (Fig. 2.03).

Between the F.C.R. and the ring-intrusion, there is commonly a thin band of red felsite (section 2.2.3). Where this felsite displays a porphyritic nature, phenocrysts are seen at the margin, partly, and in places totally enclosed by the F.C.R. (Fig 2.03).

2.2.3 F.C.R. away from the fault

There are a number of localities where F.C.R. is found away from the ring-fault:

1) The outer ring-intrusion at Stob Mhic Mhartuin is 'intruded' by thin veins of F.C.R. (Fig. 2.06; see section 2.3.2).

2) The outer margin of the inner ring-intrusion at Stob Mhic Mhartuin is marked by a band of F.C.R. (section 2.3.3.2).

3) Splays of the F.C.R. linked to the fault zones at Stob Mhic Mhartuin 'intrude' both the country-rock and the ring-intrusion. These are up to 5cm wide and can be seen at localities B,C and H (Fig. 2.07). Where they 'intrude' the country-rock and outer ring-intrusion the margins around the splay are shattered. At locality B, a splay 'intrudes' the inner ring-intrusion. It does not appear to have fractured the phenocrysts, but has forcibly pushed them aside, suggesting that the rock was not brittle at the time of F.C.R. 'intrusion'.

4) Pods and stringers of F.C.R. are seen within the country-rock at locality E on Stob Mhic Mhartuin (Fig. 2.08).

5) At Atriochtan (G.R.NN142571), there are two sigmoidal intrusions of F.C.R. (section 2.4).

6) At Cam Ghleann, a band of F.C.R. 'intrudes' the country-rock within the cauldron, and is associated with multiple igneous intrusions (section 2.3.2).

PLATE 2.02 The inner ring-fault at Stob Mhic Mhartuin looking northwest, with subsidence to the left. Accompanying line drawing depicts the F.C.R., felsite, ring-intrusion, and one of the sub-parallel shear bands within the subsided block.

PLATE 2.03 Outcrop showing multiple intrusion as depicted in Fig. 2.11. G = gabbro, T = tonalite, PR = porphyritic rhyolite, AR = aphyric rhyolite, Q = quartzite.

PLATE 2.04 View of the ring-fault at An-t-sron and subsidiary faults within the subsided block. The photograph was taken looking south, with subsidence to the left.

PLATE 2.05 A thin vein of F.C.R. within quartzite at Stob Mhic Mhartuin which shows shearing. Q = quartzite.



2.02

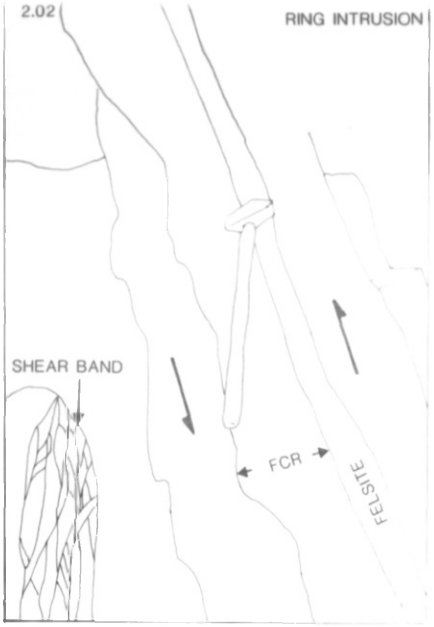
2.02
RING INTRUSION
SHEAR BAND
FCR
FELSITE


2.03
G
T
PR
AR
FCR
Q

2.04




2.05
Q
SHEARED FCR
Q

2.04

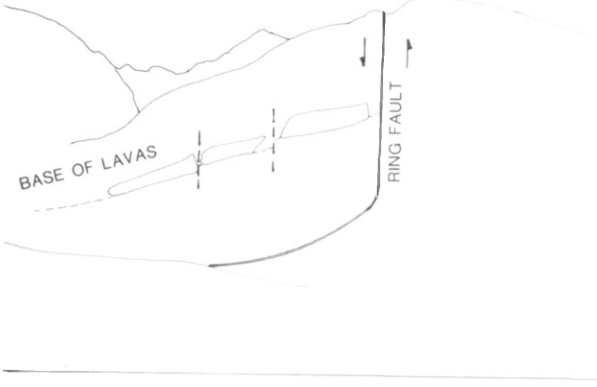
BASE OF LAVAS
RING FAULT

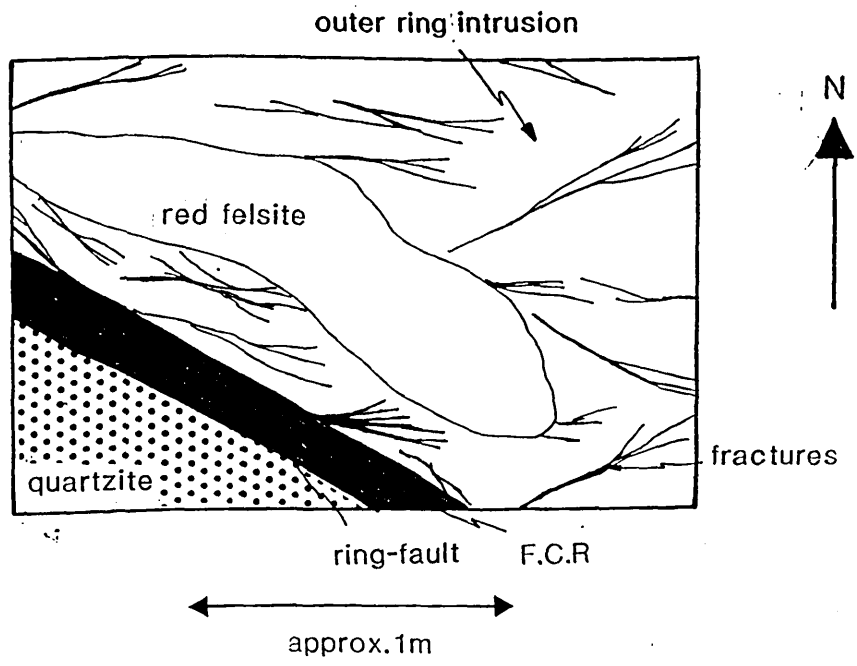

FIGURE 2.06 Detail of locality A (Fig. 2.04), showing the fracturing in the outer ring-intrusion.

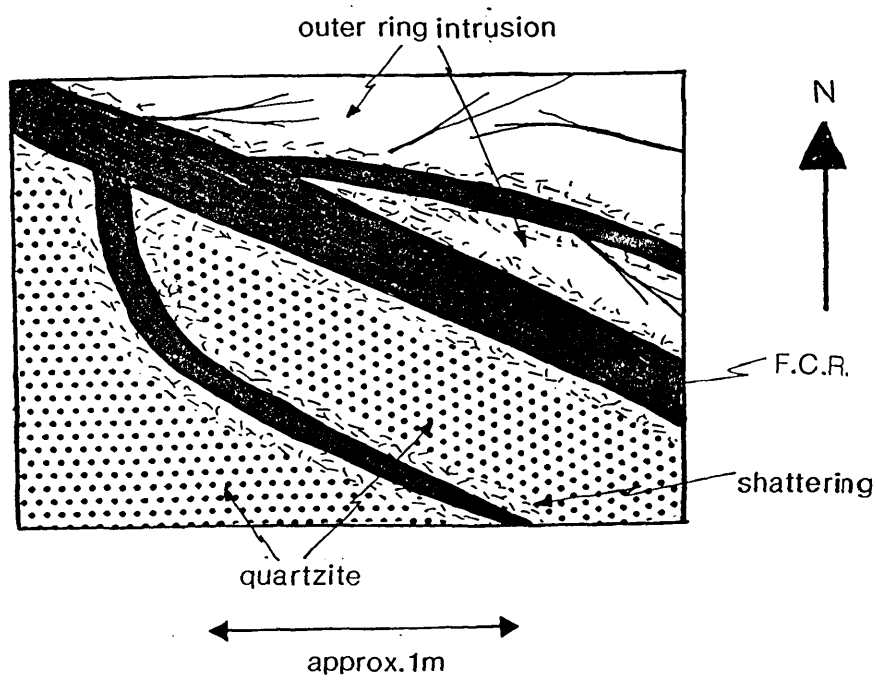

FIGURE 2.07 Detail of locality C (Fig. 2.04), showing the branching of the F.C.R. into both the quartzites and the outer ring-intrusion.

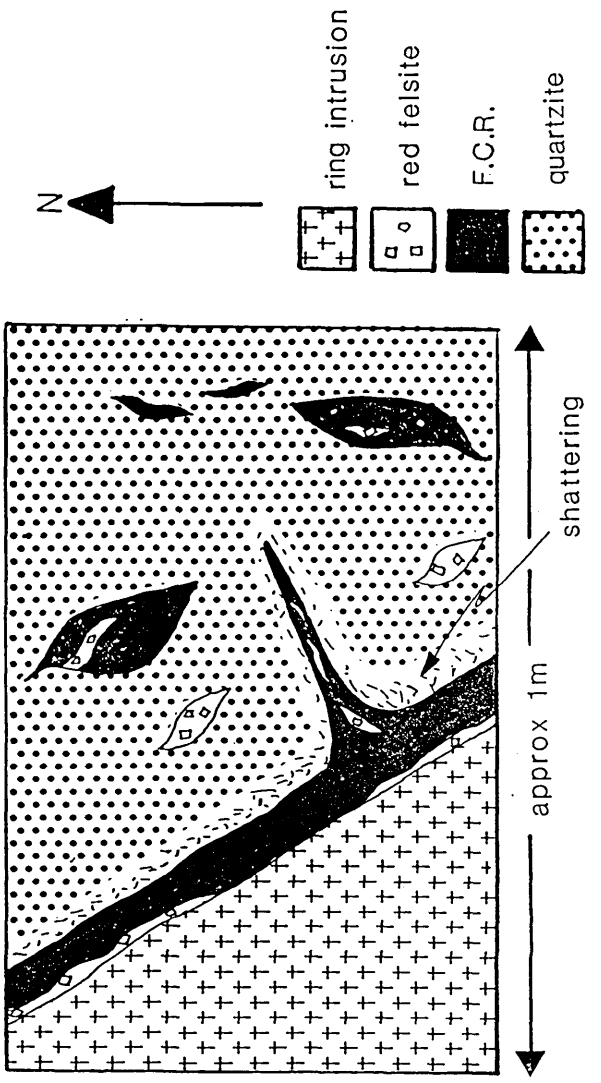

FIGURE 2.08 Detail of locality E (Fig. 2.04), showing the presence of pods and stringers of both red felsite and F.C.R. in quartzites near the outer margin of the inner ring-intrusion.

2.2.4 Association with the red felsite

The flinty crush-rock is commonly associated with a fine-grained, red felsite. In general, the felsite appears as a thin band between the flinty crush-rock and the ring-intrusion (Plate 2.01). It has been previously described as the chilled margin of the ring-intrusion (Bailey 1960), but close examination reveals it to be separate from the adjacent ring-intrusion. The felsite is fine-grained, and aphyric where it exists as small patches and stringers. Larger pods and sheets containing feldspar phenocrysts, and chloritic patches, which may be replacing a mafic phenocryst phase, are seen. (For a detailed petrographic assessment of the red felsite, see chapter 7).

In certain places, thin stringers of felsite are seen interfingering with the F.C.R.. On close examination, there are six different mixing relationships between the red felsite and the F.C.R. which are summarised in Figure 2.09. Type A is a simple planar relationship with no apparent cooling of the felsite against the F.C.R. (e.g. Atriochtan G.R.NN142571). In type B, feldspar megacrysts are present in the F.C.R., which were originally phenocrysts in the felsite. These are sometimes seen to span the boundary between the two rock-types (e.g. the inner ring-fault at Stob Mhic Mhartuin). Types C1 and C2 involve the presence of stringers of one rock-type in the other. Individual stringers can be very small (just visible to the naked eye), and do not gradually 'blend' with their host rock (e.g. locality H at Stob Mhic Mhartuin). Types D1 and D2 involve the formation of a hybrid rock which appears to be a 'blended' mixture of felsite and F.C.R. (e.g. the outer ring-fault at Stob Mhic Mhartiun).

The red felsite is also found at Stob Mhic Mhartuin in places where it is not obviously related to the F.C.R. Sizeable bodies (up to 15m long)

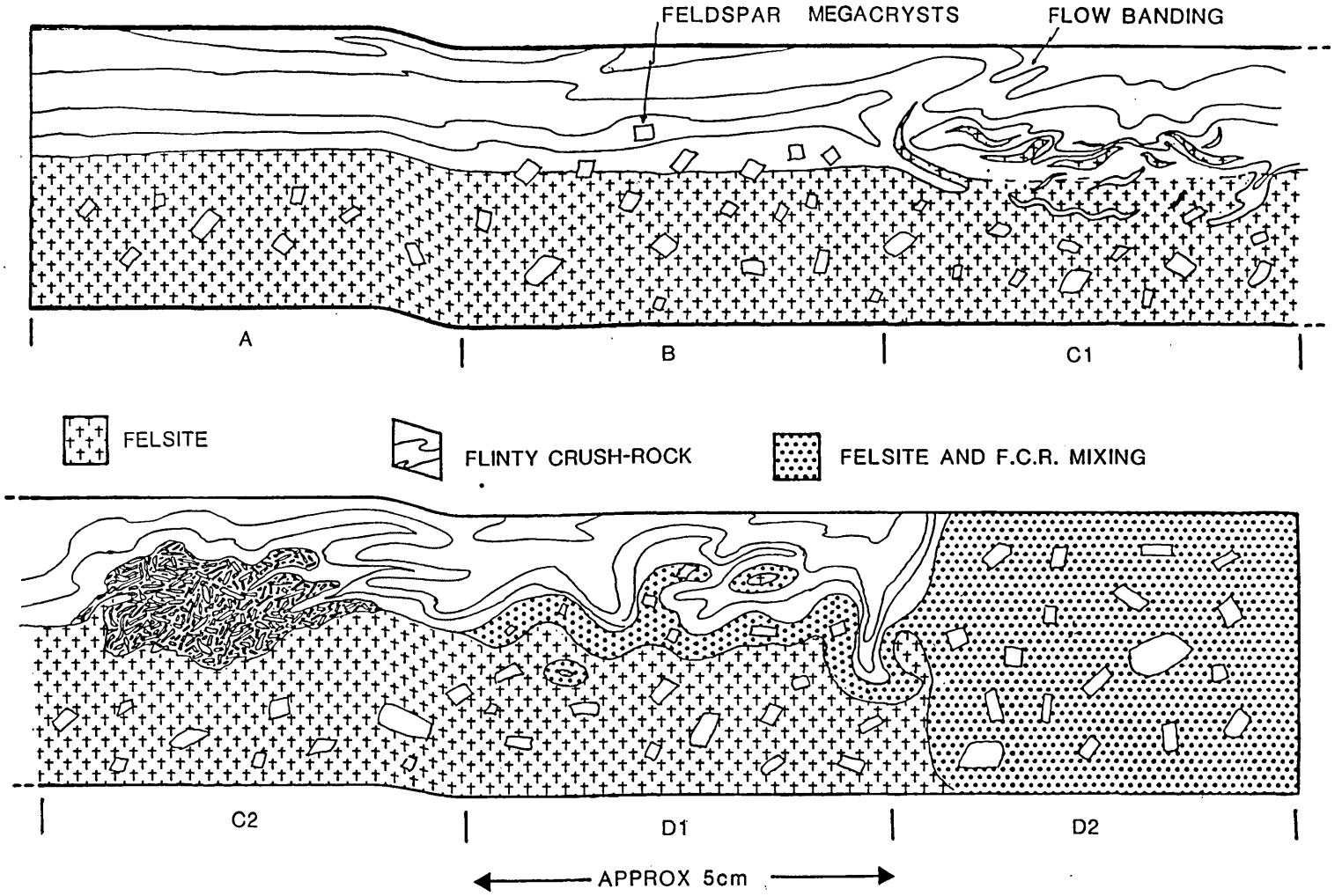

FIGURE 2.09 A schematic diagram showing the different types of mixing between the F.C.R. and the felsite. A is a planar contact with no mixing, B is the total and partial enclosure of feldspar megacrysts in F.C.R., C1 is the interfingering of the felsite and the F.C.R., C2 is a smaller scale version of C1, D1 is the mixing of felsite and F.C.R. to produce a hybrid margin and D2 is the total mixing of the felsite and F.C.R. to produce a purplish-black rock with feldspar megacrysts.

intrude the outer ring-intrusion, but have no associated crush-rock. This is probably a slightly later intrusion of material from the same source as the felsite previously described. At locality E (Fig. 2.04), small pods of felsite are present, seen both with and without the F.C.R. (Fig. 2.08). Nearby, at locality G, felsite is found forming a dyke within the quartzites.

2.2.5 Variability of the fault-rock along the ring fault

The majority of the fault-rock exposed is similar to that described above (section 2.2.1). There are, however, two localities where it is different:

1) The southern slopes of Bidean nam Bian in Ghleann Fhaolain (e.g. G.R. NN147529). The ring-fault here is exposed in a number of stream sections. The fault is displacing Devonian volcanics against Dalradian metasediments (with the ring-intrusion intervening between the two). The dark, fine-grained volcanics have been faulted and brecciated during the ring-faulting event. The fault-rock here has a more rubbly, unconsolidated texture, and may be rich in clays. It has also been brecciated, and veined by quartz and epidote. F.C.R. is not observed.

2) An-t-sron ridge (G.R. NN135547). The ring-fault is well-exposed crossing the ridge, and splits into a number of subsidiary faults. Each subsidiary fault has an associated granitic intrusion similar to the ring-intrusion adjacent to the main ring-fault at this locality (Fig. 2.10). Neither F.C.R. nor red felsite are observed, just the rubbly fault-rock described above. As is the case with the southern slopes of Bidean nam Bian, the fault cuts through Devonian volcanics.

It seems that wherever the fault displaces metasediment against metasediment, F.C.R. is present. However, wherever the ring fault cuts through

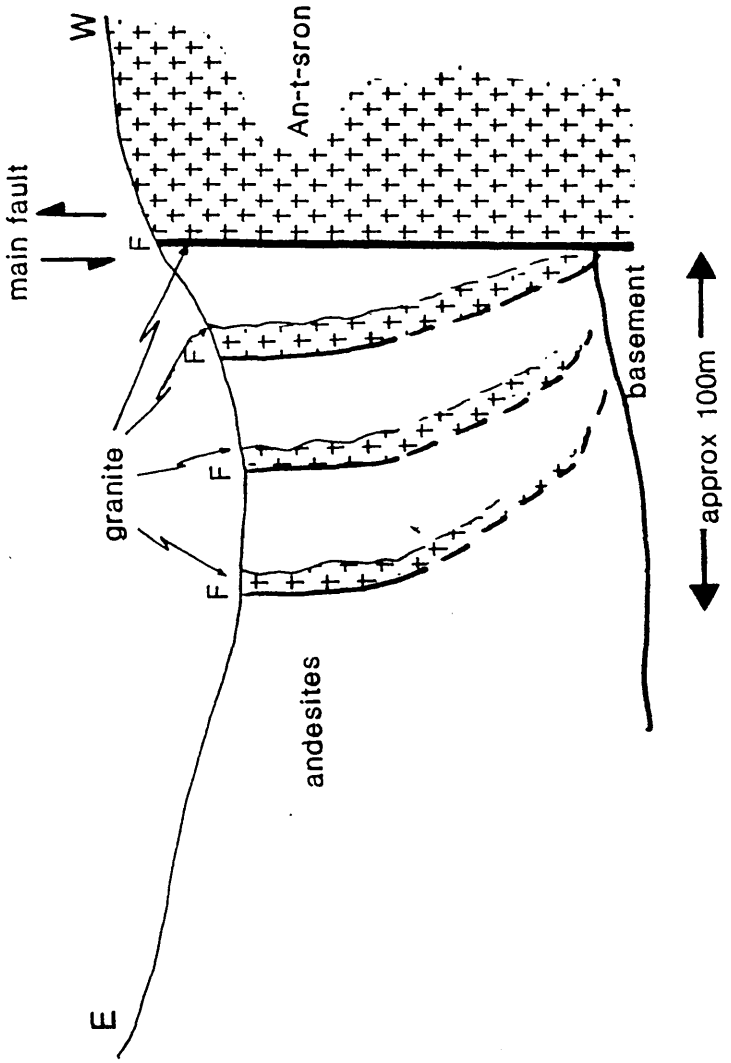

FIGURE 2.10 A schematic cross-section of upper An-t-sron showing the multiple faulting and intrusion in the Devonian volcanic sequence.

Devonian volcanics, a less-well consolidated fault-rock is found, and the fault anastomoses.

2.3 THE RING-INTRUSION

2.3.1 Introduction

The ring-intrusion is a porphyry of variable composition, which varies in width and style along the circumference of the fault. The main rock-types seen in the field fit into a 4-fold classification (Clough et al. 1909; Bailey 1960). This does not, however, cover the full range of rocks exposed, which vary from gabbro to granite. A detailed petrographic and geochemical assessment and classification of the intrusion is covered in chapters 3 and 4.

2.3.2 Distribution of different types of intrusion and their relative age

The distribution of the different types of intrusion follows no apparent pattern. A lack of exposure, combined with obscure boundaries between units made mapping unfeasible within the scope of this study.

The most basic rocks are found in fairly small bodies (approximately 10m maximum diameter). They are usually located near to the ring-fault (e.g G.R. NN138566), and are free of xenoliths.

The 'typical', and most voluminous rock-type, is a tonalite. This forms most of the intrusion in Cam Ghleann and at An-t-sron. It also forms the inner ring-intrusion at Stob Mhic Mhartuin.

The granitic rocks occur more commonly in the outer part of the ring-intrusion. To the west, north of the River Coe (e.g. G.R. NN129569), granite occurs as sheeted intrusions, with sheets (up to 10m wide) exploring bedding and joint planes (section 5.2).

The relative ages of the different types of intrusion are difficult to discern. The basic rocks, however, seem to be much fresher than the other rock-types, and do not contain country-rock xenoliths, which suggests that they are the youngest. The porphyritic granites appear altered and in places shattered (section 2.5.2). Red, hydrothermal veins lined with epidote commonly criss-cross the granites, and can be very pervasive. This suggests that the granites are probably older then the less altered tonalites. Much of the tonalite is believed to have been emplaced simultaneously with faulting (Clough et al. 1909; Bailey 1960; section 2.3.3.3). The question of how much of the intrusion was emplaced at this time is as yet unresolved, but will be dealt with more fully in chapters 7 and 9.

There are two clear examples of the ring-intrusion where an age relationship between different compositions can be easily inferred:

1) The intrusion associated with the outer fault at Stob Mhic Mhartuin. This is a fine-grained, tonalitic porphyry, which has been pervasively fractured and hydrothermally altered. These brittle fractures are infilled with thin veins of F.C.R., which was probably generated simultaneously with the F.C.R. along the main ring-fault. This suggests that the intrusion here was emplaced and consolidated prior to ring-faulting.

2) Cam Ghleann.

Much of the ring-intrusion present in Cam Ghleann consists entirely of tonalite. However, at one locality (G.R. NN250523) several pulses of intrusion of different composition are seen (Fig 2.11; Plate 2.03). These occur within the main ring-fault, but are separated from the country-rock within the cauldron by a band of F.C.R.. This is one of the many exposures of F.C.R. which is not adjacent to the fault. Although this is a small outcrop, four different types of intrusion are present. These are a) gabbro, b) tonalite, c) porphyritic felsite

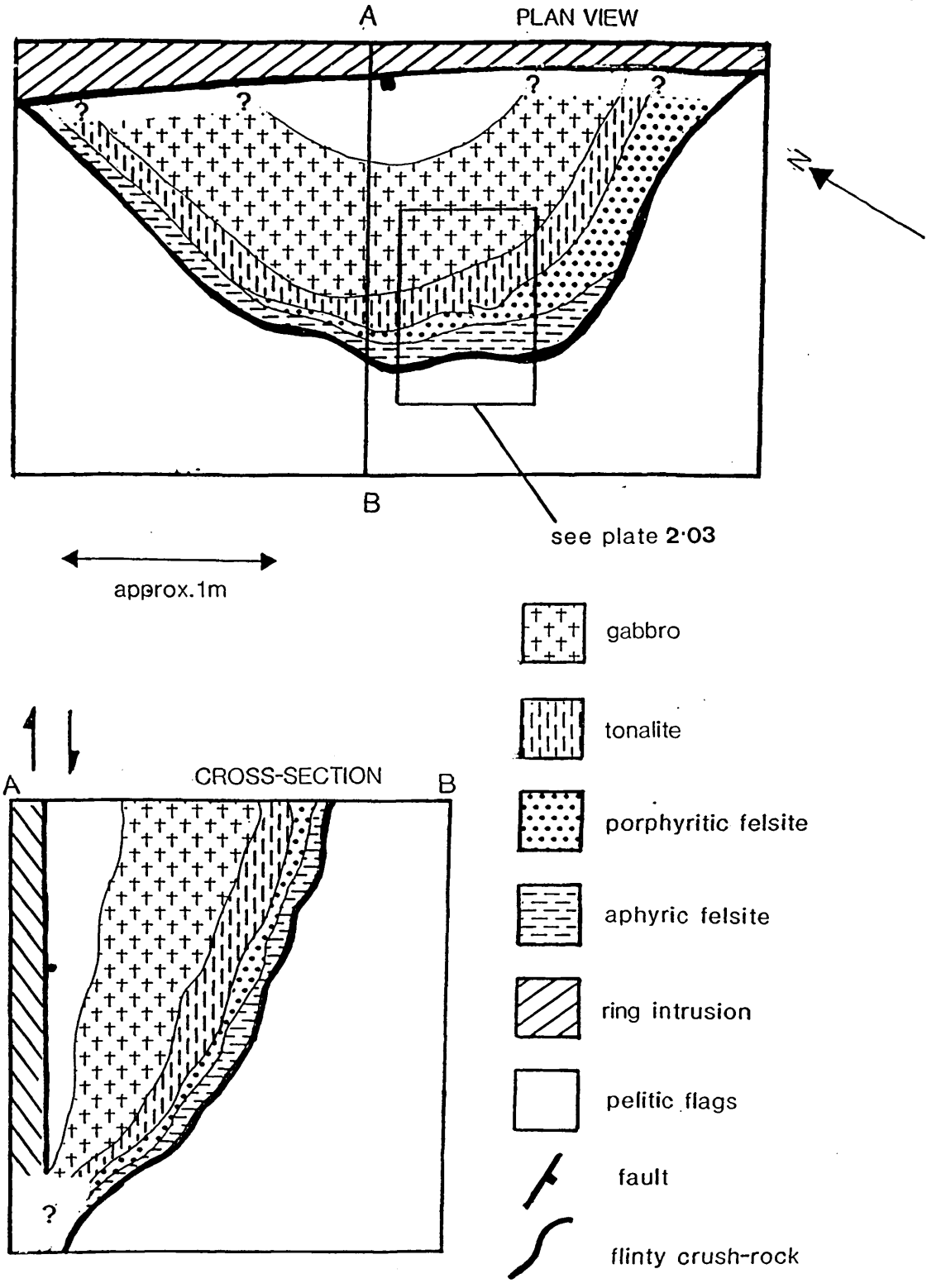

FIGURE 2.11 Sketch map and cross-section of the ring-fault seen in Cam Ghleann (G.R. NN250523), showing the multiple intrusion of gabbro, tonalite and felsites (rhyolites) within the cauldron, as shown in Plate 2.03.

(rhyolite), d) aphyric felsite (rhyolite). Chilled relationships show that the gabbro is the youngest, and the aphyric felsite the oldest. The felsite is very similar to the red felsite previously described (section 2.2.3), and is at all times in contact with the F.C.R..

2.3.3 Width of the intrusions and marginal relationships

2.3.3.1 General

The composition of the intrusion varies along the circumference of the ring-fault, as does the width, which ranges from 1m to 2Km. This, combined with the age relationships described above, leads to the conclusion that the ring-intrusion is composed of a number of smaller bodies of variable dimensions which intruded over a period of time.

The outer, irregular margin of the ring-intrusion is considered in relation to the country-rocks. The inner,planar margin is obviously different in style, and is considered in relation to the fault-rock.

2.3.3.2 Outer margin

The outer margin of the ring-intrusion has a chilling relationship to the Dalradian country-rocks. There is not a 'typical' margin, but a number of varieties which are described below. The outer margin at An-t-sron is considered in detail later (chapter 5). In other areas there are variable relationships with the adjacent rocks:

1) The margin with the Cruachan granite. The Cruachan granite intrudes the "Glencoe cauldron subsidence" in the southeast (Fig. 1.06). In Allt Coire an Easain, the contact is planar. At Dalness, in Glen Etive (G.R. NN199513), the Cruachan margin is variable, consisting of a number of irregular shaped

bodies, of different composition intruding the lavas and ring-intrusion.

2) At Cam Ghleann the ring-intrusion is adjacent to the Rannoch Moor granite. This was emplaced prior to the ring-intrusion, and in the River Etive (G.R.NN198513) the ring-intrusion is seen enclosing xenoliths of Rannoch Moor granite. The contact between the ring-intrusion and the Rannoch Moor granite is fairly planar, and sometimes has an intervening thin screen of Dalradian metasediments. Hence, it is thought that the ring-intrusion came up alongside the Rannoch Moor pluton, in a non-forceful manner, and did not intrude it, except to the extent of deta ching parts of the margin as xenoliths.

3) In Ghleann Fhaolain the ring-intrusion is narrow (only 10m wide), and typical of the tonalites seen at Dalness and Cam Ghleann. Again the country-rock margin is very planar, and more representative of a ring-dyke.

4) In the area north of the Aonach Eagach ridge the intrusion is very variable. In one place (G.R. NN192583) Bailey (1960) recognised three faults, each with an associated ring-intrusion. The outer margins of these intrusions are very irregular, with veins extending into the country- rock over a wide area (W.G. Hardie, pers. comm.).

5) The outer margin of the inner ring-intrusion at Stob Mhic Mhartuin is planar, and separated from the country-rock by a band of F.C.R. (Fig. 2.04). This is discussed further in section 2.6.

2.3.3.3 Inner margin

The inner margin of the ring-intrusion is adjacent to the ring-fault. In certain areas the intrusion has been fractured and intruded by F.C.R. (e.g. the outer ring-intrusion at Stob Mhic Mhartuin, and at Atriochtan, G.R. NN143571). In other areas where tonalitic intrusion is adjacent to the ring-fault, there is no faulting or fracturing of the

intrusion, but there is no chilling of the intrusion against the ring-fault, and no thermal metamorphism of the country-rock within the cauldron. Also the inner ring-intrusion at Stob Mhic Mhartuin shows sub-parallel alignment of phenocrysts close to the ring-fault. It has therefore been suggested that this intrusion was emplaced simultaneously with faulting (see chapter 7).

2.4 SENSE OF MOVEMENT INDICATORS AND SUBSIDIARY STRUCTURES

1) At Stob Mhic Mhartuin shear zones are present within the quartzites, running sub-parallel to the ring-faults (e.g. locality F, Fig. 2.04). Although fragmentation is complex, minor shear structures suggest downdrop to the southwest, i.e. they indicate cauldron subsidence.

2) On a larger scale, at An-t-sron, a group of normal faults appear to segment the basal lavas within the cauldron (Plate 2.04). These are sub-parallel to the ring-fault, and indicate a step-wise downfaulting within the cauldron. These faults are wider-spaced than the faults described in section 2.2.5 (Fig 2.10), and the two groups are considered unrelated.

3) Near the ring-fault exposed at Atriochtan (G.R.NN142571), F.C.R. has 'intruded' the metasediments within the subsided block (Fig. 2.12). The F.C.R. takes the form of tension-gash fillings, with their shape indicating downdrop to the east, i.e cauldron subsidence. Close by, there are also shear zones sub-parallel to the ring-fault, which are similar to those described at Stob Mhic Mhartuin.

4) In the proximity of both ring-faults at Stob Mhic Mhartuin and the ring-fault at An-t-sron the strike of the within-cauldron country-rock bedding

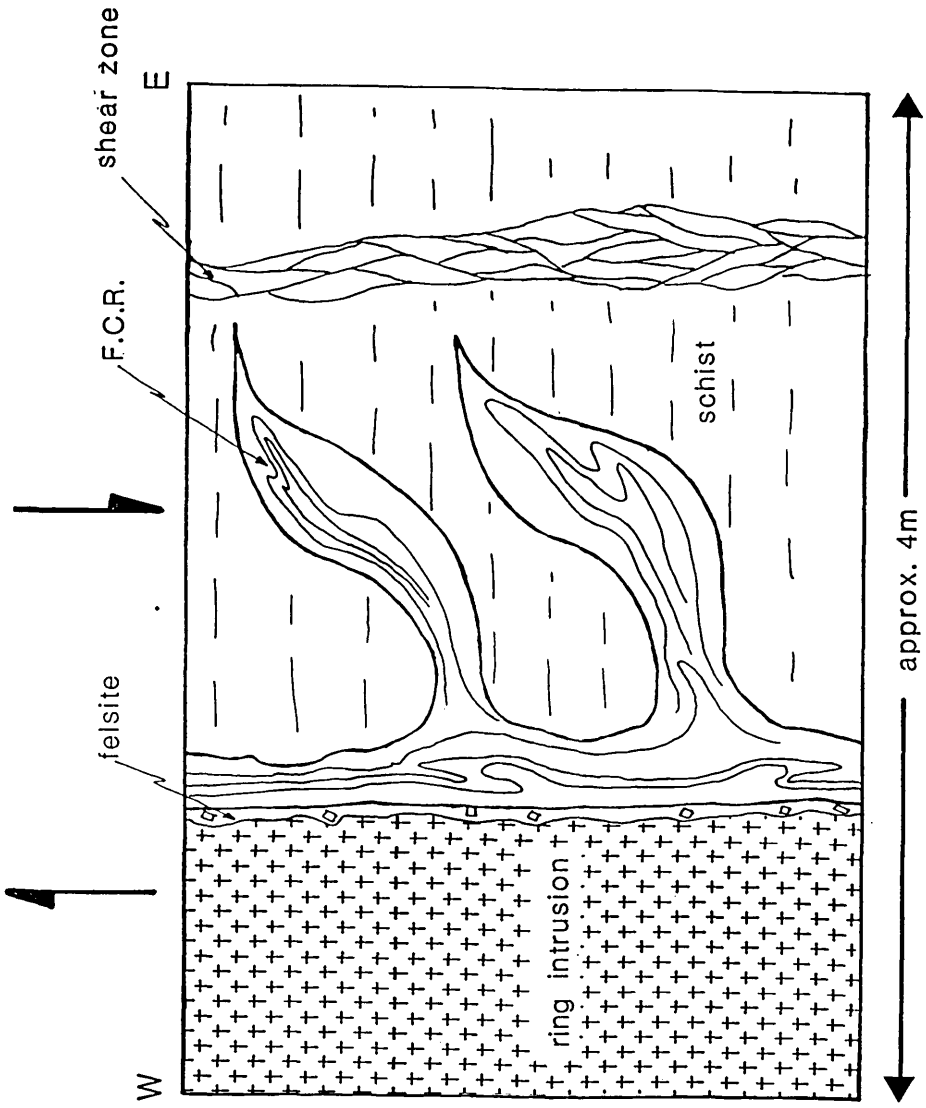

FIGURE 2.12 A schematic cross-section through the ring-fault north of Atriochtan (G.R.143571), where the flow-banded flinty crush-rock (F.C.R.) has intruded the country-rock schists within the cauldron (flow-banding is purely schematic). These intrusions have a shape similar to tension-gashes, and give a sense of movement consistent with cauldron subsidence (i.e. east side down). There is also a shear zone sub-parallel to the ring-fault.

changes, such that it becomes sub-parallel. Also the dip of the bedding steepens to near-vertical, indicating cauldron subsidence.

5) At Stob Mhic Mhartuin many of the splays of F.C.R. which intrude the country-rock are near-normal to the ring-faults, as is the dyke of red felsite (locality G). The splay at locality H (Fig. 2.04) displays a shear structure on its horizontal surface (Plate 2.05). This indicates a sinistral sense of movement, and leads to the speculation that, in addition to the downfaulting of the cauldron, strike-slip processes may have been operating.

6) The ring-fault exposed on the lower slopes of An-t-sron has undergone later brecciation, this has disrupted parts of the ring-intrusion, red felsite and much of the F.C.R. (Fig.2.13). The brecciated rocks have been recemented by quartz and epidote (which also occurs in adjacent areas, as described in section 2.2.4). The brecciated ring-intrusion rocks are intruded by an undeformed Etive dyke, dating the brecciation to post ring-faulting, pre dyke intrusion. A sheared quartzite clast is caught up in the brecciated shear zone, the shearing indicates a reverse sense of movement to cauldron subsidence.

2.5 THE BRECCIA AND RHYOLITE DYKES

Breccia-associated rhyolite dykes intrude the Eilde flags and quartzites located within the ring-fault on the eastern side of the cauldron (Fig. 1.07).

The breccias were originally considered to be sedimentary (Bailey 1960; Clough et al. 1909), but have been re-interpreted as intrusive and pyroclastic breccias (Hardie 1963, 1968; Roberts 1974), a view supported by this present study. A full field and petrographic description of these rocks is included in chapter 6.

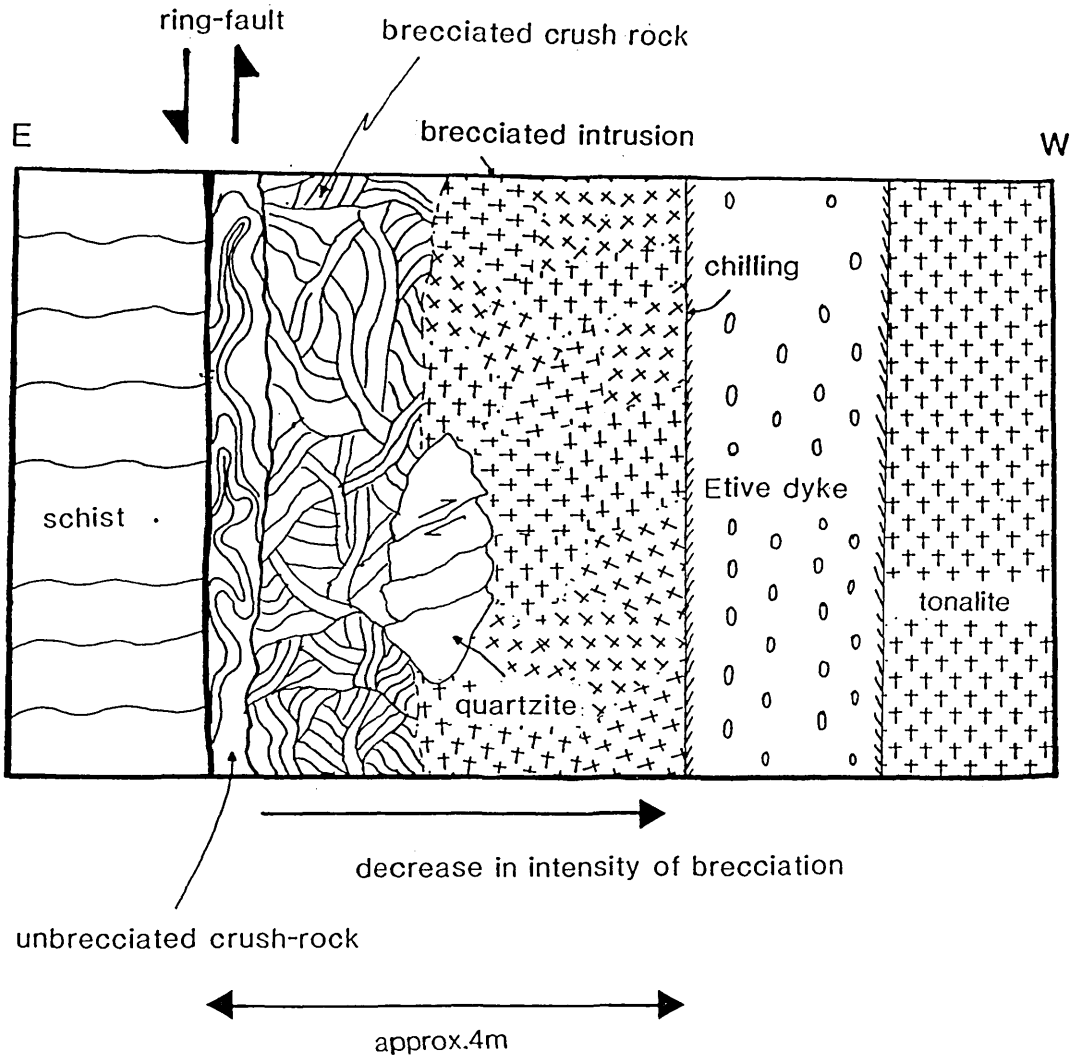

FIGURE 2.13 A schematic field sketch section of the ring-fault at An-t-sron showing later brecciation of the F.C.R. and ring-intrusion.

2.6 SUMMARY

2.6.1 Fault rocks

The ring-faults are marked by breccias and ultra fine-grained F.C.R.. F.C.R. can also be seen 'intruding' both metasedimentary country-rock, and parts of the ring-intrusion.

The occurrence of the F.C.R. is nearly always associated with the intrusion of a red felsite. There is a variety of mixing relationships between these two which suggests that they might have coexisted as fluids, prior to consolidation.

Where F.C.R. is not present along the ring-fault, the fault rock is more rubbly and has the appearance of a fault gouge. This is seen to occur only where Devonian volcanics and sediments have been displaced against Dalradian metasediments.

2.6.2 Ring-intrusion

The ring-intrusion is of variable width and composition. Some of the rocks were intruded prior to ring-faulting, and some are believed to have been emplaced contemporaneously with ring-faulting. There is little evidence for post-faulting intrusion.

The inner ring-intrusion at Stob Mhic Mhartuin is bounded by F.C.R. on both margins. This has been interpreted as an example of syn-faulting intrusion, whereby the F.C.R. was plastered on the walls of a fracture as the vanguard to tonalitic ring-intrusion (Roberts 1966b).

Where there is evidence of an age-relationship between rocks of different composition, the more acidic rocks were emplaced before the basic rocks. This is typical of the systematic tapping of a layered magma source.

2.6.3 Sense of movement

Most minor structures associated with the ring-faulting indicate downdrop of the cauldron. The one exception is at An-t-sron, where the fault rocks have been re-brecciated, and minor structures indicate a reverse sense of movement. This activity seems to be associated with a later quartz-epidote veining event.

At Stob Mhic Mhartuin there is evidence for a component of strike-slip faulting in the country-rock slice preserved between the two ring-faults. This is thought to be the result of accommodation necessary between the two main faults.

CHAPTER 3

PETROGRAPHY AND MINERAL CHEMISTRY OF THE RING INTRUSION

3.1 INTRODUCTION

The intrusive rocks of the ring-intrusion show distinct variations in both texture and mineralogy. Their large phenocrystal contents and general paucity of groundmass prompted Taubeneck (1967) to refer to them as porphyries. In this study the author has adopted a combination of both petrography and geochemistry for the rock classification. The rocks range in composition from gabbros through dioritic gabbros, diorites and monzonites to granites. In general, the range of porphyries previously described by Clough et al. (1909) are covered by the diorite - monzonite suites in this study.

The lack of exposure in many areas of the ring-intrusion, plus the marked heterogeneity in the available outcrop pattern makes a quantitative determination of the relative volumes of the different rock-types within the intrusive suite extremely difficult. However, it would appear that the relative abundances are: diorite$>$ monzonite$\gg$ dioritic gabbro$>$ granite$\gg$ gabbro.

Many of the intrusive rocks show distinct signs of alteration by later hydrothermal events. These manifest themselves as quartz-epidote veins, pervasive Fe-oxidation (reddening) and minor local abundances of such secondary minerals as epidote, white mica and iron pyrites. No detailed investigation of these hydrothermal products has been undertaken. In addition to these localised late hydrothermal events, many of the mineral phases display a more pervasive alteration typically resulting in cloudy feldspars with chloritised

biotites and amphiboles.

Table 3.1 shows a representative set of modal mineral proportions of the main rock types within the ring-intrusion. Mineral compositions, determined by electron microprobe analysis, are given in appendix D. A selection of probe analyses of the major rock-forming minerals are listed in Table 3.2.

In classifying the amphiboles, the ratio of Fe2+/Fe3+ used, is such that on the basis of 23 oxygens, the tetrahedral, M1, M2 and M3 sites contain exactly 13 cations (Leake 1978; Hawthorn 1983).

3.2 THE GABBROS AND DIORITIC GABBROS

These rocks are very porphyritic (up to 85% phenocrysts), comprised largely of plagioclase, augite and Fe-Ti oxides within the gabbros, and plagioclase, biotite and Fe-Ti oxides within the dioritic gabbros. Amphibole first appears as a phenocrystal phase within the dioritic gabbros, but remains subordinate to plagioclase and biotite within the suite.

The groundmass consists of large green amphibole and granular plagioclase, biotite, and Fe-Ti oxides. Alkali feldspar may occasionally be found in some samples. The grain-size of the groundmass varies from 0.04 to 0.5mm. A typical gabbro is shown in plate 3.01.

The plagioclase phenocrysts vary in size from 1mm to 1cm in length, and all exhibit normal zoning. In the gabbros, the plagioclases range from An59 (cores) to An31 (rims), whilst the dioritic gabbros show a zonal range from An54 to An27 (Fig. 3.01).

Some of the plagioclases show distinct oligoclase overgrowths, which have grown over broken phenocrysts and are clearly in optical discontinuity with their host (Plate 3.02). The groundmass plagioclases are not zoned, but do exhibit a

TABLE 3.1
MODAL COMPOSITIONS OF A SELECTION OF RING-INTRUSION ROCKS
(based on 2000 points per sample)

GABBRO 2JG1 75% phenocryst

PL PHEN	AUG PHEN	OP PHEN	PL	AMPH	BIOT
. 54	18	3	10	7	7

OTHERS (zircon and groundmass opaques)
. 1

DIORITIC GABBRO 1JG10 76% phenocryst

PL PHEN	BIOT PHEN	AMPH PHEN	OP PHEN	PL
. 52	12	9	1	25

OTHERS (zircon, phenocrystal apatite, groundmass opaques)
. 1

DIORITE 2JG35 69% phenocryst

PL PHEN	BIOT PHEN	AMPH PHEN	OP PHEN	PL	KSPAR	QTZ
. 42	14	11	2	18	2	10

OTHERS (zircon, phenocrystal apatite, sphene, groundmass opaques)
. 1

MONZONITE 1JG80 44.5% phenocryst

PL PHEN	BIOT PHEN	AMPH PHEN	OP PHEN	PL	KSPAR	QTZ
. 34	7	2	0.5	23	2	31

OTHERS (zircon, phenocrystal apatite, sphene, groundmass opaques)
. 0.5

MONZONITE 1JG9 29% phenocryst

PL PHEN	BIOT PHEN	PL	KSPAR	QTZ
. 23	5.5	23	3	45

OTHERS (zircon, groundmass opaques)
. 0.5

GRANITE 1JG61 30% phenocryst

PL PHEN	QTZ	KSPAR	MUSC	BIOT
. 30	22	44	1	3

OTHERS (zircon)
. 0.01

PHEN - phenocryst
PL - plagioclase
AUG - augite
OP - opaques
BIOT - biotite
AMPH - amphibole
QTZ - quartz
KSPAR - alkali feldspar
MUSC - muscovite

All values are percentages, all phenocryst forming minerals are labelled PHEN.

TABLE 3.2 'TYPICAL MINERAL COMPOSITIONS OF THE RING-INTRUSION ROCKS
(phenocryst unless stated otherwise)

Feldspars: Number of ions on the basis of 8 oxygens
Clinopyroxene: Number of ions on the basis of 6 oxygens
Biotite: Number of ions on the basis of 22 oxygens. H2O determined by stoichiometry.
Amphibole: Number of ions on the basis of 24 oxygens. H2O determined by stoichiometry.

OXIDE	1		2		3		4	
Na2O	5.05		5.92		5.66		8.57	
Al2O3	27.73		26.11		27.94		23.82	
SiO2	54.26		55.70		56.14		61.85	
K2O	.34		.52		.33		.29	
CaO	11.39		9.74		10.15		5.42	
FeO	.57		.53		.16		.43	
SUM	99.34		98.52		100.38		100.38	
Si	2.476	*	2.553	*	2.518	*	2.742	*
Al	1.491	*	1.410	*	1.476	*	1.244	*
Fe	.022	3.988	.020	3.984	.006	4.000	.016	4.002
Ca	.557	*	.478	*	.488	*	.257	*
Na	.447	*	.526	*	.492	*	.737	*
K	.020	1.023	.030	1.035	.019	.999	.016	1.010
O	8.000	*	8.000	*	8.000	*	8.000	*
AN	54.41		46.22		48.83		25.48	
AB	43.66		50.84		49.28		72.90	
OR	1.93		2.94		1.89		1.62	

1 - feldspar core in gabbro 2 - feldspar rim in gabbro
3 - feldspar core in tonalite 4 - feldspar rim in tonalite

TABLE 3.2 (continued)

OXIDE	5	6	7	8	9
Na2O	7.52	9.59	9.77	1.12	10.00
Al2O3	23.81	22.21	21.36	18.76	20.55
SiO2	61.06	64.56	65.07	64.18	65.26
K2O	.80	.22	.56	14.99	.76
CaO	6.06	3.11	2.59	.22	2.23
FeO	.40	.09	.21	.08	.21
SUM	99.65	99.78	99.56	99.35	99.01

Si	2.731	*	2.850	*	2.881	*	2.977	*	2.907	*
Al	1.255	*	1.155	*	1.114	*	1.025	*	1.079	*
Fe	.015	4.001	.003	4.008	.008	4.003	.003	4.005	.008	3.993
Ca	.290	*	.147	*	.123	*	.011	*	.106	*
Na	.652	*	.821	*	.839	*	.101	*	.864	*
K	.046	.988	.012	.980	.032	.993	.887	.988	.043	1.013
O	8.000	*	8.000	*	8.000	*	8.000	*	8.000	*
AN	29.39		15.01		12.37		1.09		10.50	
AB	65.99		83.73		84.44		10.09		85.23	
OR	4.62		1.26		3.18		88.82		4.26	

5 - feldspar core in granite 6 - feldspar rim in granite
7 - feldspar overgrowth rim 8 - feldspar overgrowth rim
9 - groundmass feldspar

TABLE 3.2 (continued)

OXIDE	10		11		12		13	
Na2O	.58		Na2O	.75	.60		.38	
MgO	15.23		MgO	14.78	13.75		13.77	
Al2O3	2.62		Al2O3	14.65	13.45		13.55	
SiO2	51.49		SiO2	36.87	37.78		37.82	
CaO	21.58		K2O	8.77	9.43		9.67	
TiO2	.49		CaO	.03	.35		.20	
Cr2O3	.26		TiO2	5.76	3.52		2.92	
MnO	.26		MnO	.09	.17		.17	
FeO	7.53		FeO	13.97	16.29		15.96	
SUM	100.04		H2O	4.04	3.97		3.94	
.			SUM	99.71	99.31		98.38	
Si	1.912	*	Si	5.464	*	5.698	*	5.748	*
Al	.088	2.000	Al	2.536	8.000	2.302	8.000	2.252	8.000
Al	.027	*	Al	.022	*	.088	*	.174	*
Ti	.014	*	Ti	.642	*	.399	*	.334	*
Cr	.008	*	Mg	3.265	*	3.091	*	3.119	*
Fe	.234	*	Fe	1.731	*	2.055	*	2.028	*
Mg	.843	*	Mn	.011	5.672	.022	5.655	.022	5.678
Ca	.859	*	K	1.658	*	1.814	*	1.874	*
Mn	.008	*	Ca	.005	*	.057	*	.033	*
Na	.042	2.034	Na	.215	1.878	.175	2.046	.112	2.019
O	6.000	*	H	4.000	4.000	4.000	4.000	4.000	4.000
WO	44.18		O	24.000	*	24.000	*	24.000	*
EN	43.37		ANN	34.80		40.18		39.66	
FS	12.45		PHLOG	65.20		59.82		60.34	
F/M	.287		F/M	.534		.672		.657	
F/FM	.223		F/FM	.348		.402		.397	

10 - clinopyroxene 11 - biotite core 12 - biotite rim
13 - groundmass biotite

TABLE 3.2 (continued)

OXIDE	14		15		16	
SiO2	42.10		50.32		45.01	
Al2O3	11.65		4.84		9.65	
FeO	10.39		9.81		10.97	
Fe2O3	1.34		3.24		2.02	
MgO	13.65		15.13		13.07	
MnO	0.00		.43		.21	
TiO2	4.33		1.26		2.56	
CaO	11.65		11.99		11.59	
Na2O	2.94		1.26		1.96	
K2O	.78		.36		.78	
H2O	2.05		2.09		2.04	
SUM	100.88		100.73		99.86	
Si	6.141	*	7.226	*	6.600	*
Al	1.859	8.000	.774	8.000	1.400	8.000
Al	.143	*	.045	*	.267	*
Ti	.475	*	.136	*	.282	*
Fe3+	.147	*	.350	*	.223	*
Mg	2.968	*	3.238	*	2.856	*
Fe2+	1.267	*	1.178	*	1.345	*
Mn	0.000	*	.052	*	.026	*
Ca	1.821	*	1.845	*	1.821	*
Na	.180	7.000	.155	7.000	.179	7.000
Na	.652	*	.195	*	.378	*
K	.145	.797	.066	.261	.146	.524
H	2.000	2.000	2.000	2.000	2.000	2.000
O	24.000	*	24.000	*	24.000	*
Mg	70.07		72.47		67.57	
FeMn	29.93		27.53		32.43	
F/M	.427		.380		.480	
F/FM	.299		.275		.324	

14 - brown magnesio-hastingsite 15 - green actinolitic hornblende 16 - brown/green edenite

PLATE 3.01 Photomicrograph under crossed polars of a gabbro (2JG1). P = plagioclase, C = clinopyroxene, A = groundmass amphibole.

PLATE 3.02 Photomicrograph under crossed polars of a diorite (2JG37). P = plagioclase, B = biotite, A = amphibole, Q = quartz. Note the optically discontinuous overgrowths on plagioclase, biotite and amphibole.

PLATE 3.03 Photomicrograph under plane polarised light of a monzonite (2JG9). P = plagioclase, B = biotite (partly replaced by chlorite).

PLATE 3.04 Photomicrograph under crossed polars of a granophyric granite (1JG61). P = plagioclase, K = alkali feldspar, Q = quartz.

3·01



3·02

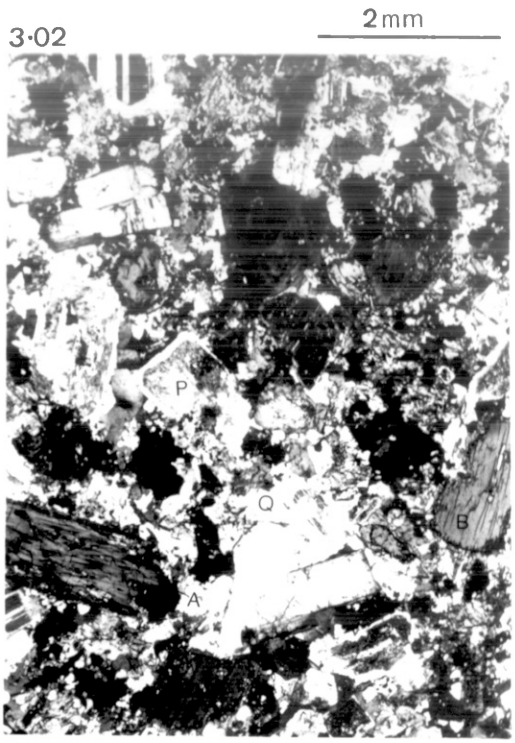

3.03

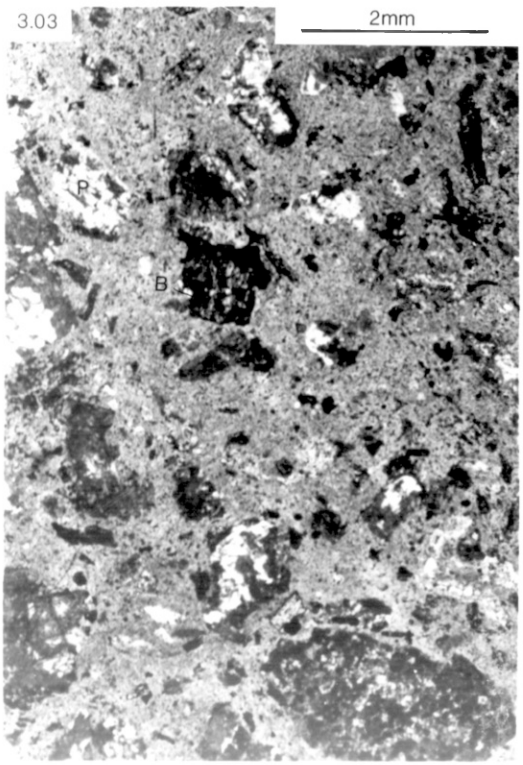

3.04



variation in composition from grain to grain. In the gabbros for instance, their compositions generally span the compositional range An28 to An15. In the dioritic gabbros the groundmass plagioclases cover the range from An25 to An11.

Modally the clinopyroxenes constitute the next most abundant phenocrystal phase in the gabbros, forming up to 25% of the total phenocrystal content (Table 3.1). Their grain-size varies from 0.2 to 1mm, and chemically they are calcic augites (Wo44 En44 Fs12). Although such clinopyroxenes have also been found in the dioritic gabbros, they are very sparse, occurring either as isolated grains which have been pseudomorphed, or as small nuclei within amphibole phenocrysts. Electron microprobe analysis of the more suitable grains shows a slight enrichment in the orthoferrosilite molecule (Wo42 En43 Fs15) in comparison to the clinopyroxenes within the more gabbroic members of the suite.

Individual analyses of the calcic augites have been plotted in Fig. 3.02. In general they show a very restricted range in composition.

Both brown and green amphibole phenocrysts may be found in the dioritic gabbros, the significance of which will be discussed in section 3.5.

Phenocrystal biotites occur in the dioritic gabbros. They are well-formed and have pleochroic haloes, occasionally individuals display kink-bands. The phenocrysts are brown Ti-rich crystals of composition Ann 35. In contrast, the groundmass biotites are very small, thin plates, and are poorer in Ti, and richer in Fe (Ann 40) (Table 3.2). In those dioritic gabbros containing both two amphiboles and exhibiting feldspar overgrowths, the biotite phenocrysts show a distinctive zone of small opaque crystals (partial microprobe analysis indicates an ilmenite composition) which in turn is overgrown by biotite similar in composition to those found in the groundmass. Taubeneck (1967) observed similar textures but did not report the further overgrowth of

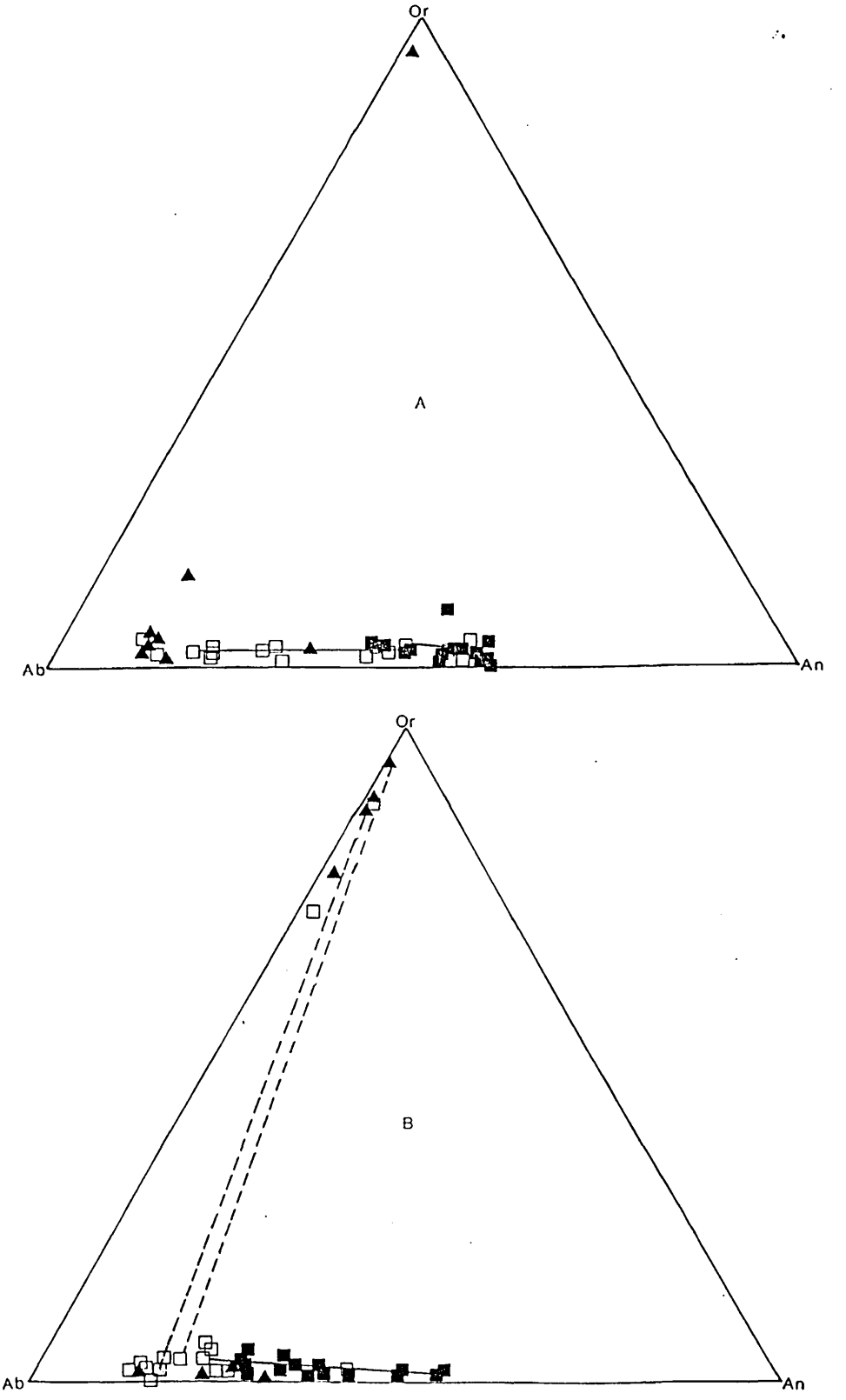

FIGURE 3.01 Microprobe analyses of feldspars expressed in terms of the end-members An-Ab-Or: A: gabbros and dioritic gabbros; B: diorites and monzonites. Solid tie-lines indicate typical core/rim pairs, dashed tie-lines indicate typical rim/groundmass pairs. (Filled squares = phenocryst cores, open squares = phenocryst rims, triangles = groundmass.)

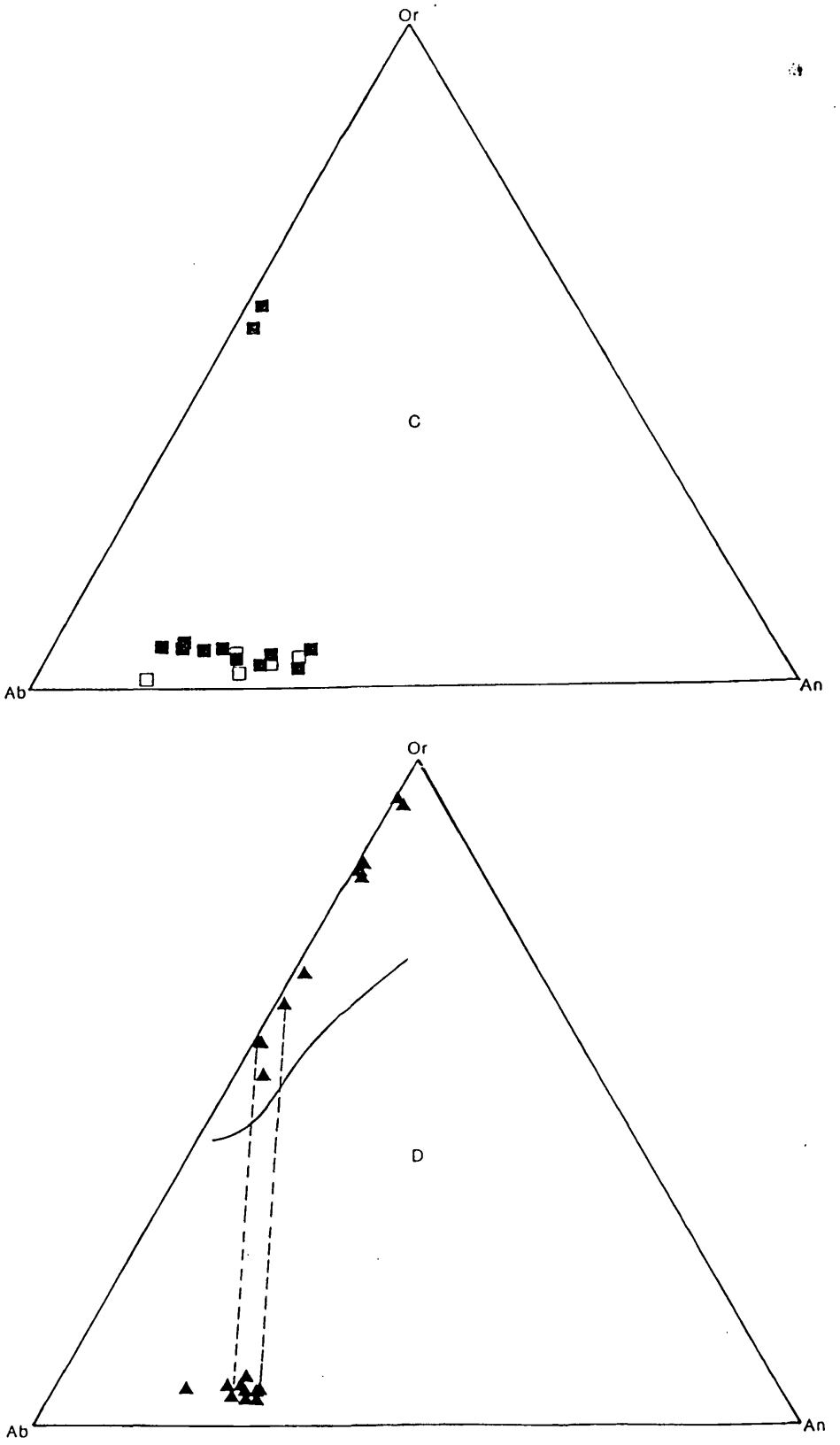

FIGURE 3.01 (continued) C: porphyritic granites; D: granophyric granites. Dashed tie-lines indicate typical rim/groundmass pairs. Curved line is the cotectic in a quartz-saturated ternary feldspar system at PH2O = 1Kb (after James and Hamilton 1969).

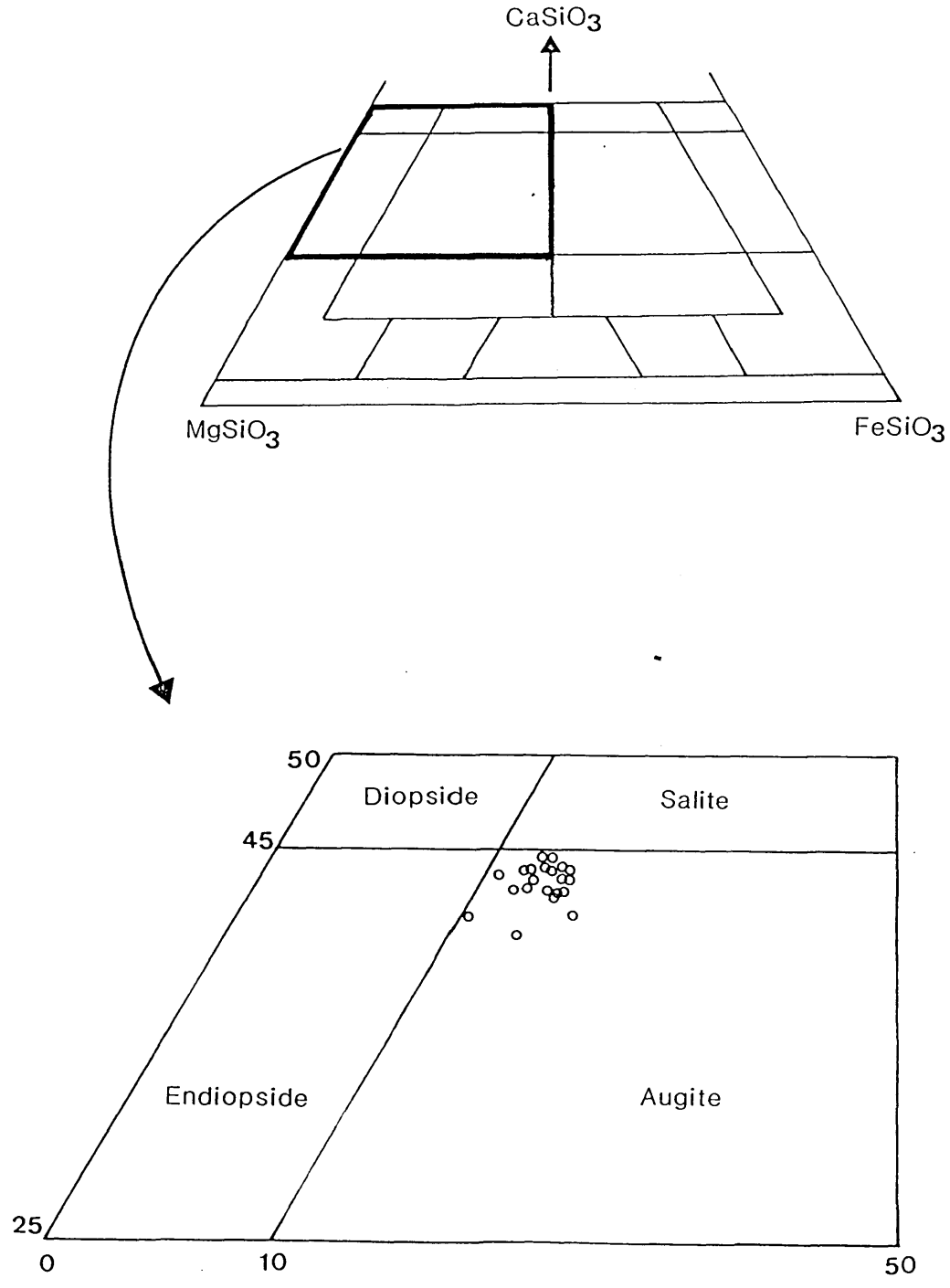

FIGURE 3.02 Microprobe analyses of pyroxene phenocrysts from the gabbros and dioritic gabbros expressed in terms of the end-members Wo-En-Fs.

biotites outside the opaque zone. He commented on their similarity to the resorption rims found in many biotites and hornblendes in intermediate and acid extrusive rocks and suggested some volatile loss prior to the crystallisation of the groundmass.

Accessory apatite, sphene and zircon are present, although only zircon is observed in the more basic rocks.

3.3 THE DIORITES

The diorites are the most abundant rock type found, and together with the monzonites form the bulk of the ring-intrusion rocks in Glencoe. They are again very porphyritic with phenocrystal phases making up 69% of the rock. The phenocrysts are plagioclase (42% modal content), biotite (14%), amphibole (11%) and opaques (2%).

The plagioclase phenocrysts range in size from 0.5mm to 1cm and display normal zoning from An54 (cores) to An13 (rims) (Fig. 3.01). Again in certain samples they are mantled with an optically discontinuous overgrowth of oligoclase or alkali feldspar (Plate 3.02).

The biotite phenocrysts range in size from 0.1 to 1.5mm and are of the same composition as those in the gabbros and dioritic gabbros (section 3.2). As with the dioritic gabbros, some samples containing two amphibole phases display overgrowths on the feldspars, and zones of opaque granules within the overgrowths on the biotites. Very rare augitic pyroxenes are sometimes found forming minute nuclei in the amphibole phenocrysts.

The groundmass of the dioritic rocks has a variable grain-size (0.04 to 0.5mm) and consists of plagioclase feldspar (An30 to An12), essential quartz, opaques, minor biotite, alkali feldspar, together with the accessory phases apatite, sphene

and zircon.

3.4 THE MONZONITES AND GRANITES

These can be divided into two groups:

a) Fine-grained porphyritic monzonites and granites.

b) Coarse-grained granophyric granite.

3.4.1 The fine-grained porphyries

These rocks are far less porphyritic than those previously described in sections 3.2 and 3.3 (with phenocrystal contents ranging between 30 and 40%). The dominant phenocrystal phase is plagioclase feldspar ranging in size from 0.25 to 2mm. The plagioclases are again zoned from An33 to An14, and often show a mantle of alkali feldspar. Amphibole phenocrysts are quite rare, but when present are dominantly the brown variety with a green overgrowth (see section 3.5). Biotite is present both as a phenocrystal phase, and in the groundmass, their respective compositions are very similar to those previously described. Quartz may also appear in the granites as a phenocrystal phase.

The groundmass is composed of fine-grained quartz, with plagioclase, alkali feldspar and minor biotite. Apatite and sphene may be seen in some of the monzonites as accessory phases, accessory zircon is found in rocks of all compositions. A typical monzonite is shown in Plate 3.03.

3.4.2 The coarse-grained granophyric granite

These rocks are mainly found in the northwest margin of the An-t-sron pluton (see chapter 5). They are relatively coarse-grained (0.2-4mm), and are composed mainly of alkali feldspar (Or58 Ab41

An0.65), quartz and plagioclase (Plate 3.04). The plagioclase is generally unzoned (one notable exception being 1JG61, An24 cores to An17 rims). Amphibole and pyroxene are absent from these rocks, and biotite has only been recorded in 1JG61. Primary muscovite is however a ubiquitous phase in all samples of this rock-type. Graphic intergrowths between quartz and either alkali feldspar or plagioclase are common. Zircon is the only accessory phase.

3.4.3 A note on the "early fault-intrusion"

This is a lithology referred to in the early literature (Clough et al. 1909; Bailey 1960), and is generally found in the northern part of the area (e.g. G.R. NN208577). It is a field term used to describe an intrusion that has been altered and sheared, and as a result of which, is considered to have been emplaced prior to ring-faulting and the main intrusive events. In composition it ranges from monzonite to granite, and displays the same petrographic features as those described in sections 3.3 and 3.4.1.

3.5 AMPHIBOLES

Amphibole is present in nearly all the rock-types observed. They are calcic amphiboles, mainly euhedral, brown, edenitic-hornblendes, magnesio-hastingsitic hornblendes and magnesio-hastingsites (Fig. 3.03) (Leake 1978). Some rocks also contain green actinolites, actinolitic hornblendes and magnesio-hornblendes (Leake 1978). The latter occur as anhedral clots or sub-euhedral phenocrysts. They are commonly seen overgrowing brown amphiboles, and occasionally biotites. One sample (1JG51) has brown/green amphiboles of an intermediate

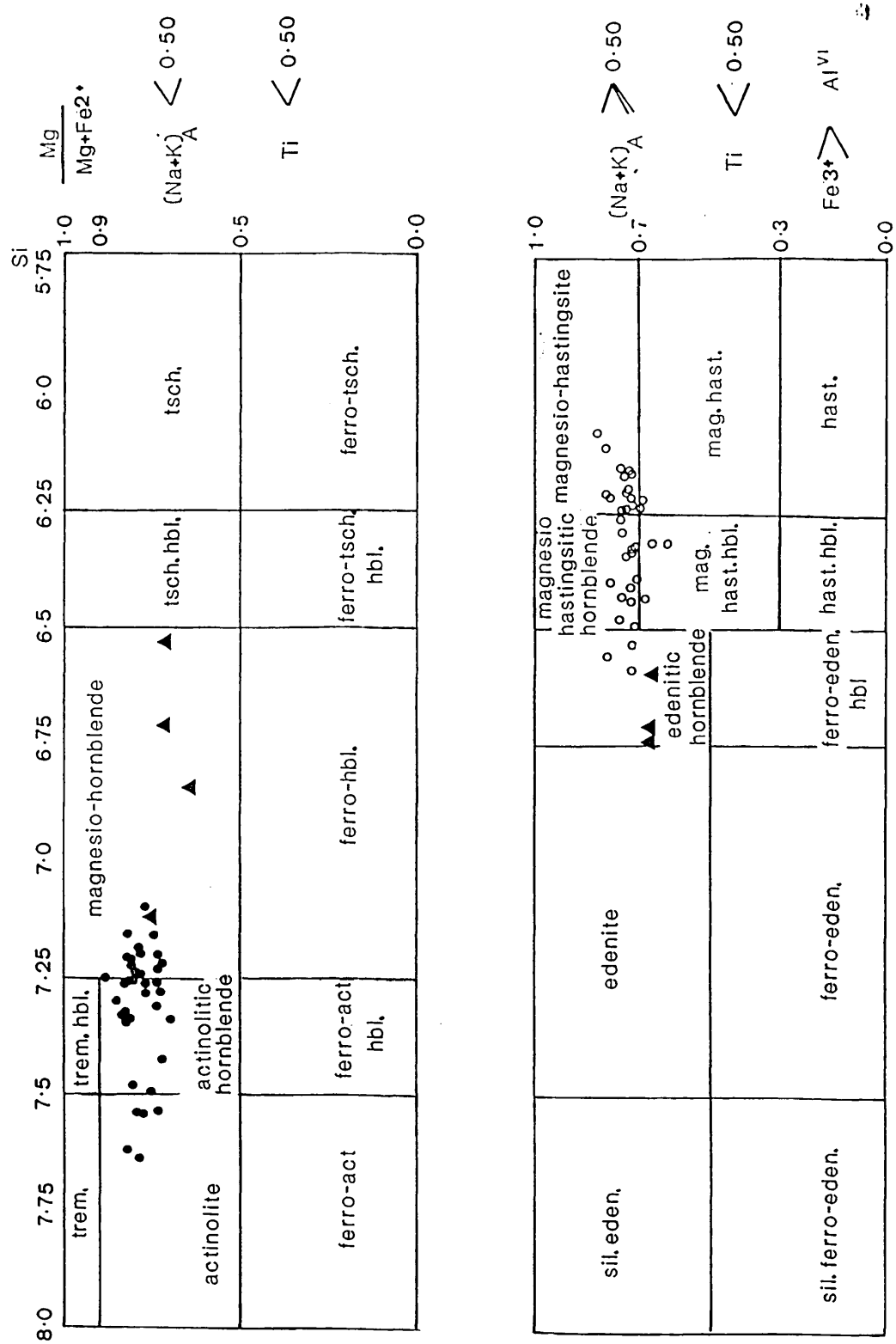

FIGURE 3.03 Microprobe analyses of amphiboles (classification after Leake 1978). Closed circles represent green amphiboles, open circles represent brown amphiboles, and triangles represent brown/green amphiboles from sample 1JG51.

edenitic hornblende and magnesio-hornblende compositions.

The rocks which contain brown amphiboles with green fringes also have feldspars with overgrowths and biotites with opaque horizons and overgrowths (Plate 3.4). This suggests a major change in the chemical environment. The decrease in Ti and Na in amphiboles in general, indicates a drop in pressure (Cawthorn 1976; Stephenson and Upton 1982). These amphibole compositions are found in both igneous and metamorphic rocks (Richardson 1968; Wones and Gilbert 1981). The literature concerning igneous and metamorphic amphiboles provides no concensus view for determining the difference between the two on textural grounds in deformed rocks (Richardson 1968; Otten 1984; Fowler 1985). However, in this particular case, the potential metamorphism would be contact metamorphism rather than regional metamorphism. There are three clear, possible reasons for the presence of different amphibole compositions:

1) Brown amphibole crystallised as a phenocrystal phase at high pressure, from a melt, probably in a magma-chamber. After emplacement at higher crustal levels, sub-solidus actinolitic hornblende grew in response to the heat produced by the emplacement of other igneous bodies in the surrounding area.

2) Brown amphibole crystallised from a liquid, which was then emplaced rapidly at higher crustal levels. However amphibole crystallisation continued, but as the pressure was lower, actinolitic hornblendes were formed instead.

3) Magma-mixing led to a change in the melt composition, which either led to the growth of a different type of amphibole, or the two mixed magmas contained different amphiboles prior to mixing.

There are three pieces of evidence that point to the second interpretation being the most probable.

a) The presence of intermediate, edenitic hornblende and magnesio-hornblende in sample 1JG51,

which provides a link between the brown and green amphiboles. This suggests that this particular magma batch intruded slowly, allowing amphibole crystallisation to take place at intermediate levels.

b) Opaque horizons within the amphiboles and biotites. Both amphibole and biotite contain less TiO2 at lower pressures (Cawthorn 1976). Hence, if a crystallising liquid were to be rapidly emplaced at higher crustal levels, TiO2 would not be accommodated in amphibole and biotite and is most likely to crystallise out as an oxide, hence ilmenite. Experimental evidence suggests that in a crystal-liquid environment, ilmenite would be likely to nucleate around amphibole and biotite (Piwinskii and Wyllie 1968). If sub-solidus crystallisation had taken place, one would expect to see opaque minerals forming intergrowths with amphiboles and biotites, and not euhedral crystals. Also there would probably be geochemical differences between groundmass and phenocryst biotite (Rock 1982).

c) Magma-mixing is not thought to have caused the different amphibole populations as one would expect to see two feldspar core populations. Also there would not be any amphiboles of intermediate composition present, such as those present in 1JG51.

3.6 SUMMARY

The intrusive rocks of the Glencoe cauldron are essentially porphyries with compositions ranging from gabbroic types through dioritic gabbros, diorites and monzonites to granites. The diorite and monzonite porphyries make up the bulk of the intrusive rocks, with the end members, gabbro and granite being greatly subordinate. The phenocrystal contents of the rocks show a progressive percentage decrease with increasing acidity of the rock-type, greater than 70% in the gabbros and averaging about 30% in the granites (see Fig 3.04). In addition to the change in phenocrystal content, the sizes of the phenocrysts

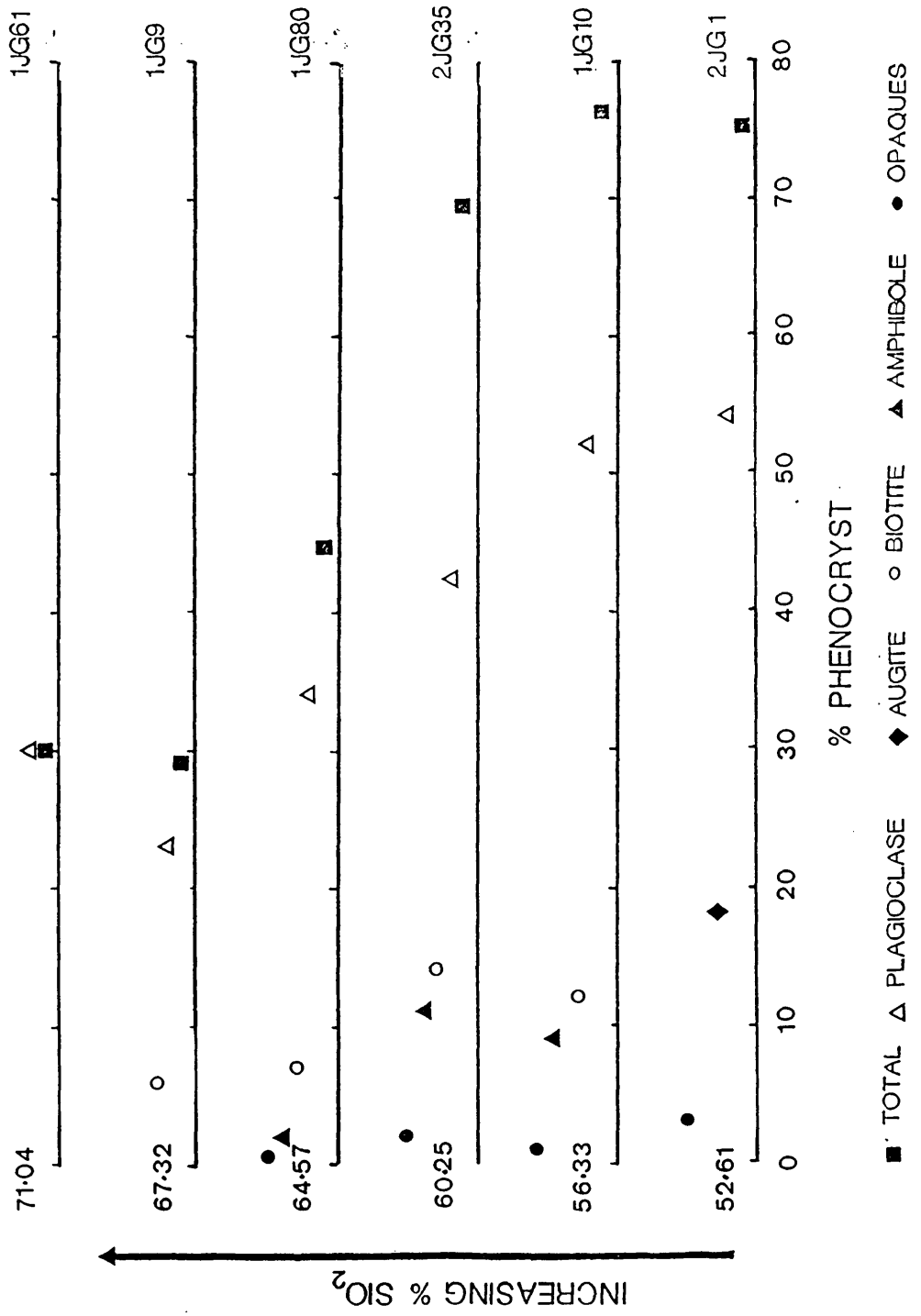

FIGURE 3.04 A diagram showing the change in phenocryst content of the magma with increasing SiO2 over the range of ring-intrusion rocks.

also show a progressive decrease with decreasing basicity of the rock. The increase of both the modal content and size of the phenocrysts with increasing basicity has been reported by Nakada (1983) for a series of lavas and pyroclastics erupted from a compositionally zoned magma chamber, which became progressively poorer in SiO2 with depth.

The major phenocrystal phases display a change in composition in keeping with a series of liquids undergoing fractional crystallisation. This is clearly seen in the normally zoned plagioclase feldspars whose core compositions change from An59 in the gabbroic porphyries to An33 in the granites, with a similar trend in rim compositions from An31 to An17 (Fig. 3.01).

The amphiboles also show a change in composition with change in rock type, although this is less obvious than that previously described for the plagioclase feldspars. In the dioritic gabbros the brown amphibole approaches an edenitic hornblende composition, but with increasing acidity, magnesio hastingsite becomes the dominant amphibole phase within the monzonites (Fig. 3.03).

The clinopyroxenes have a much shorter crystallisation interval (Fig. 3.05), and show very little change in crystal chemistry (Fig. 3.02). The biotite phenocrysts do show some substitution of the phlogopitic end member by annite, albeit small, with increasing fractionation.

Alkali feldspar begins to nucleate either as small groundmass crystals or as rims on some plagioclase phenocrysts in certain dioritic porphyries, but it is not until the granitic compositions that it takes on any major modal significance along with quartz. The presence of alkali feldspar as an overgrowth on plagioclase phenocrysts may lead one to the conclusion that alkali feldspar was an important fractionating phase. However, it is believed that these overgrowths, together with the associated rims (and opaque

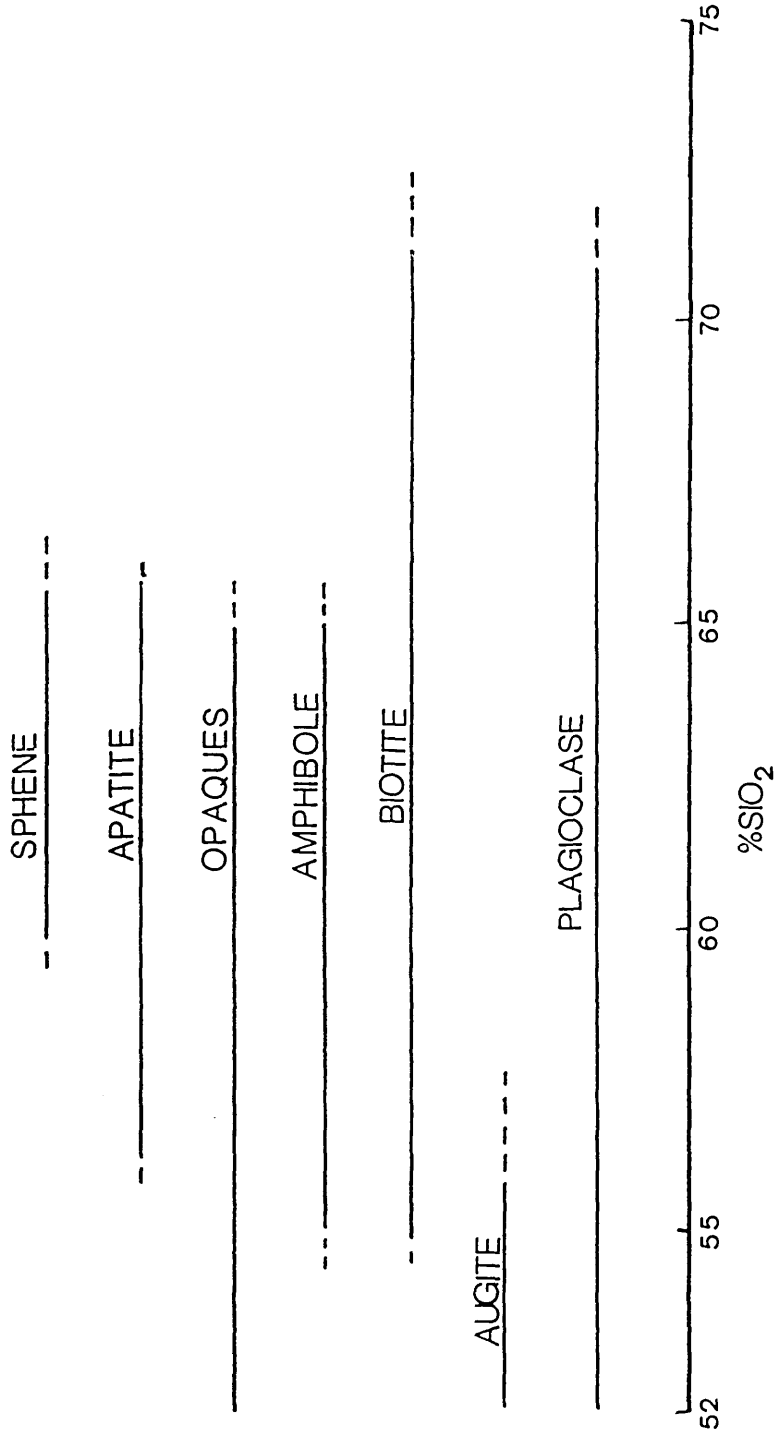

FIGURE 3.05 The crystallisation interval of phenocrystal phases within the magma chamber with increasing silica.

horizons) around amphibole and biotite phenocrysts probably represent post-emplacement crystallisation of individual batches of magma at lower pressure in a crystal-liquid environment. Significant crystal fractionation is not considered to have occurred under these conditions.

Apatite, sphene and zircon are not modally important, although, the fractionation of small amounts of these phases will have a significant effect upon the whole-rock geochemistry. Apatite and sphene are found as phenocrysts in rocks of composition ranging from dioritic gabbro to monzonite. Zircon is present throughout the range of rock compositions, however, some of these crystals may be inherited from crustal melts.

CHAPTER 4

THE GEOCHEMISTRY OF THE RING-INTRUSION ROCKS

4.1 INTRODUCTION

A range of major and trace elements have been analysed for 56 samples from the Glencoe ring-intrusion. These cover the compositional range from gabbro (52.61 wt.% SiO2) through diorites and monzonites to granites (71.93 wt.% SiO2). A smaller number of samples (14) have been analysed for rare earth elements (REEs), tantalum, hafnium and uranium. Also analysed were four samples of granophyric granite (associated with the ring-intrusion as is discussed in chapter 5), four samples of intrusive and extrusive rhyolites, two samples of red felsite associated with the ring-fault (chapter 7), and an intrusive suite from the neighbouring Etive and Ballachulish plutons (Fig. 1.02).

The rocks have high-K calc-alkaline affinities (Fig. 4.01). All the rocks except one (1JG18) are quartz-normative. Some rocks are corundum-normative, and others diopside-normative. This reflects a variable Ca/Al ratio. Normative values are shown in Appendix C.

The rocks are rich in phenocrysts, mainly plagioclase, but also augite, biotite, amphibole, and opaque minerals (chapter 3). The chemical variations in the rocks are discussed below mainly in terms of crystal fractionation.

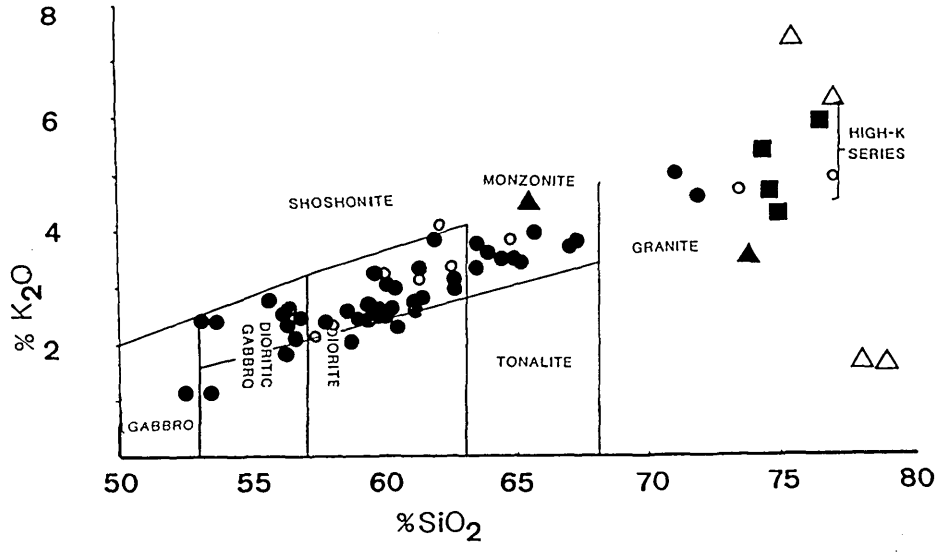

● RING INTRUSION
■ RHYOLITE
○ ETIVE GRANITOID
△ GRANOPHYRIC GRANITE
▲ FAULT FELSITE

FIGURE 4.01 K2O against SiO2 for the Glencoe igneous rocks, showing the geochemical classification (after Taylor et al. 1981).

4.2.1 Major Elements

All the major and trace element concentrations have been plotted against SiO2 in a series of Harker variation diagrams (Figs. 4.02, 4.03). Although the rocks have a consistently high phenocrystal content which could possibly mask the trend of magma evolution, it is believed that fractional crystallisation was important in the generation of the chemical variations displayed in Fig. 4.02. Inflection points in some of the major element trends for samples of the ring-intrusion mark either the end or the beginning of fractionation of a particular phase. Some of the major and trace element plots show a scatter of points, i.e. Na2O, K2O, FeO/Fe2O3, MnO, Sr, Rb, Ba, Nb, Th, Cr and Y. Much of this randomness is thought to be due to the effect of sub-solidus hydrothermal alteration (see chapter 3). However, some plots (MnO, Cr, Th, Nb) may show scatter due to either heterogeneous phenocrystal accumulation, or analytical uncertainty at low concentrations.

Throughout the evolution of the more basic and intermediate magma compositions plagioclase feldspar is a dominating fractionating phase. This is reflected by the general decrease in both Al2O3 and CaO with increasing SiO2. From approximately 52 wt.% SiO2 to 60% the Al2O3 values are fairly constant, which suggests that plagioclase was not the only phase being fractionated. Petrographic evidence from both the gabbroic and dioritic porphyries indicate that the additional phase is calcic augite. This interpretation is in keeping with the variation diagrams for both CaO and MgO+FeO, the latter clearly indicating the removal of ferro-magnesian phases throughout the evolution of the liquid. Augite is removed early in the fractionation process, and is superceded by biotite and amphibole as the liquid

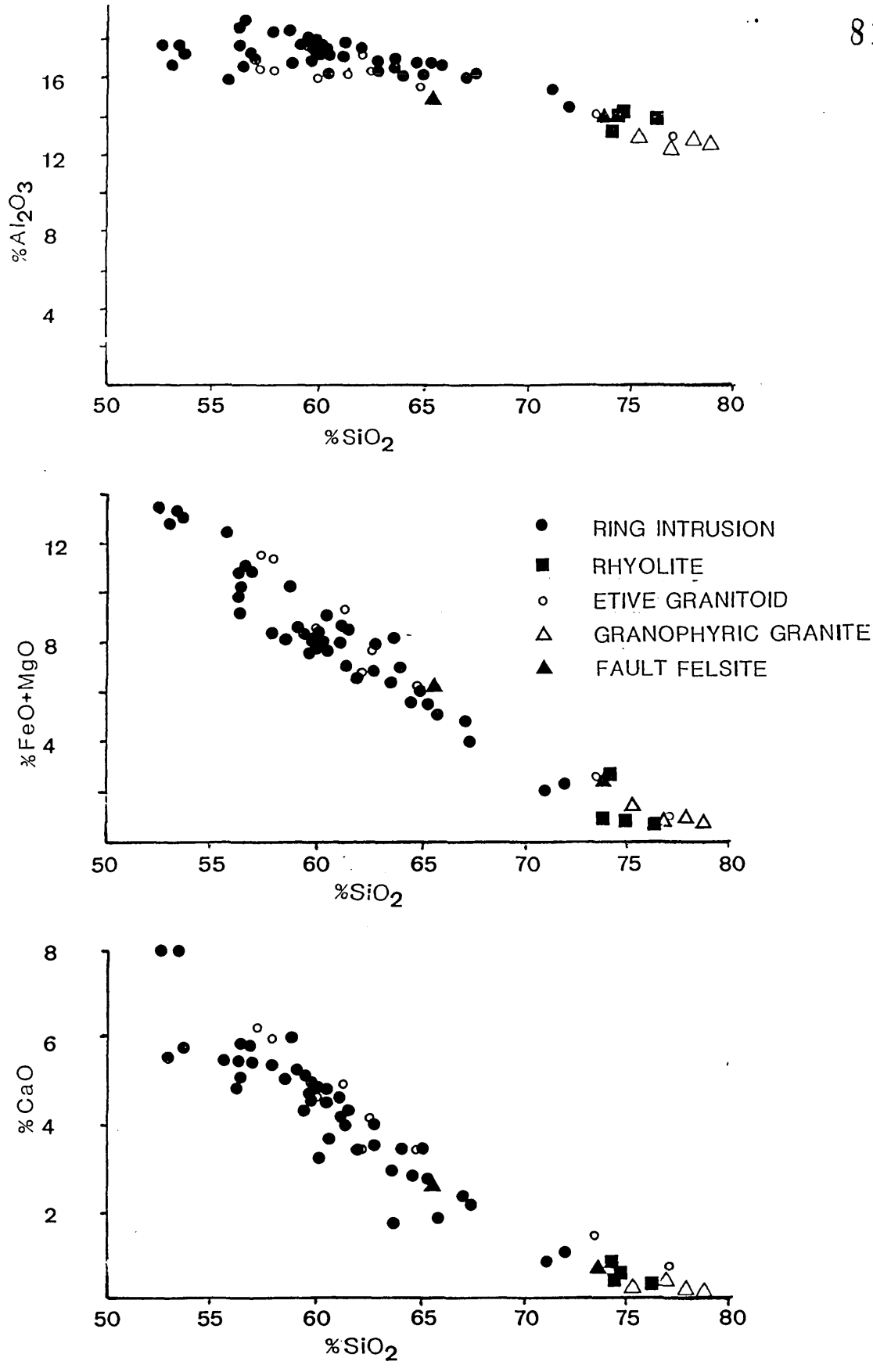

FIGURE 4.02 Major element chemical variations for the Glencoe igneous rocks.

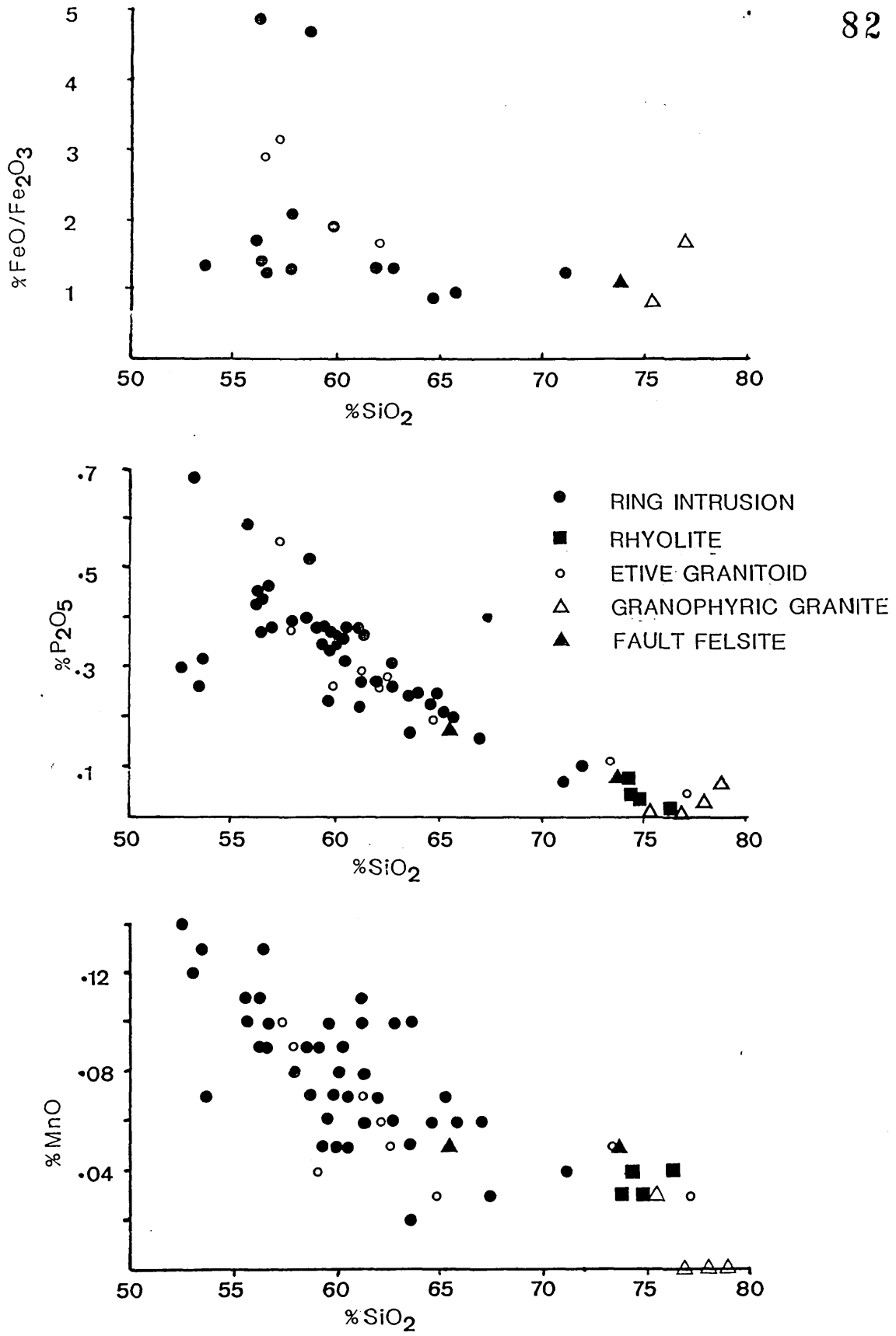

FIGURE 4.02 (continued)

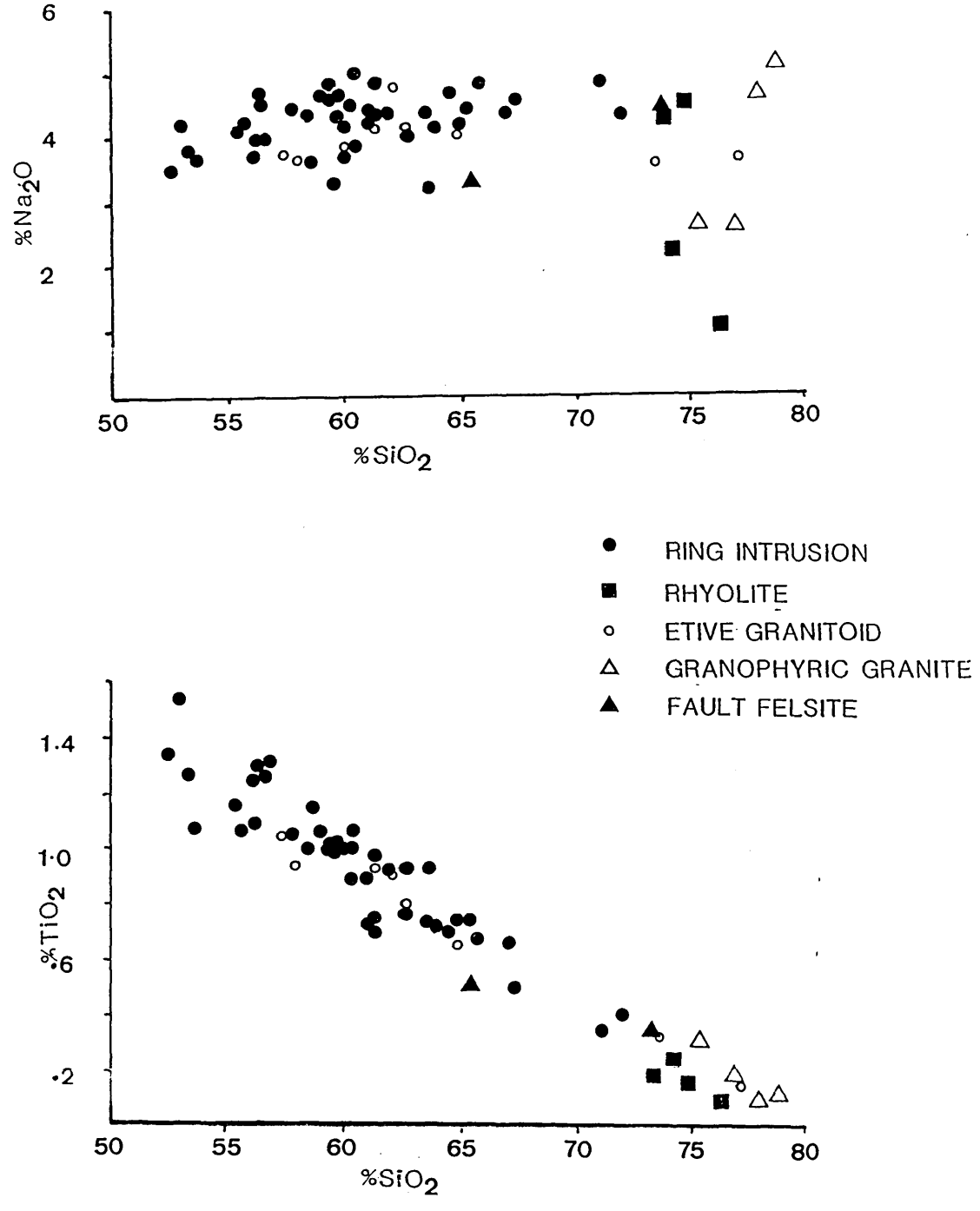

FIGURE 4.02 (continued)

becomes more SiO2 rich. Opaque phases (Fe-Ti oxides) accompany the removal of augite, as well as amphibole and biotite (Fig. 3.05).

The variation of TiO2 with SiO2 shows a very marked negative correlation, adding further evidence for the removal of such phases as biotite, amphibole, Fe-Ti oxides (particularly ilmenite) and sphene. Apart from two anomolous values above 0.55 wt.% P2O5, the P2O5 trend shows an inflection at around 57 wt.% SiO2. The oxide was obviously behaving incompatibly up to this point, which is substantiated by the lack of apatite in the more basic members of the series. Apatite is seen in more acidic compositions (above 57% SiO2), which accounts for the compatible geochemical behaviour in these latter compositions.

K2O shows a marked positive correlation with SiO2, even though in the intermediate stages of liquid evolution the fractionating phases biotite and amphibole both contain small amounts of K2O. Na2O shows a very flat trend with a much wider scatter than that displayed by K2O.

In the majority of the variation diagrams both the granophyric granites (except 1JG61) and the rhyolites do not conform to the general trends discussed above. The reasons for this will be discussed in sections 4.4 and 4.5.2.

4.2.2 Trace elements

Rb increases with increasing SiO2 content of the ring-intrusion rocks. There is a tendency for the trend to show more scatter at higher values of SiO2. Sr, as expected, behaves in a similar fashion to CaO and shows a steady decrease with fractionation.

The incompatible elements Th, Nb, Ta and Hf all show a general increase in concentration with fractionation, although the individual trends do show a marked scatter throughout the rock series. The variation diagrams for Ba, Y and Zr show far more scatter than the rest of the incompatible elements.

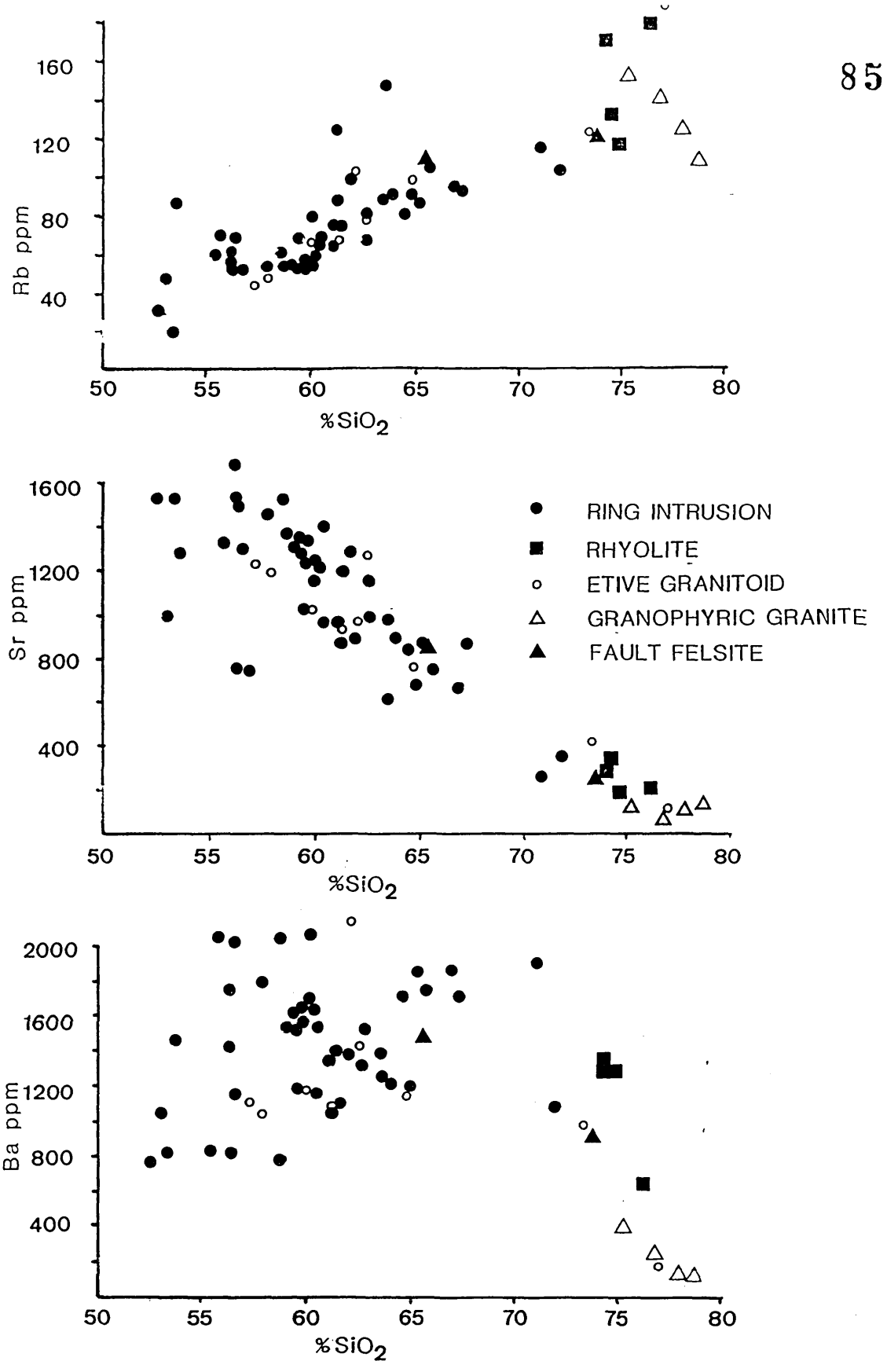

FIGURE 4.03 Trace element chemical variations for the Glencoe igneous rocks.

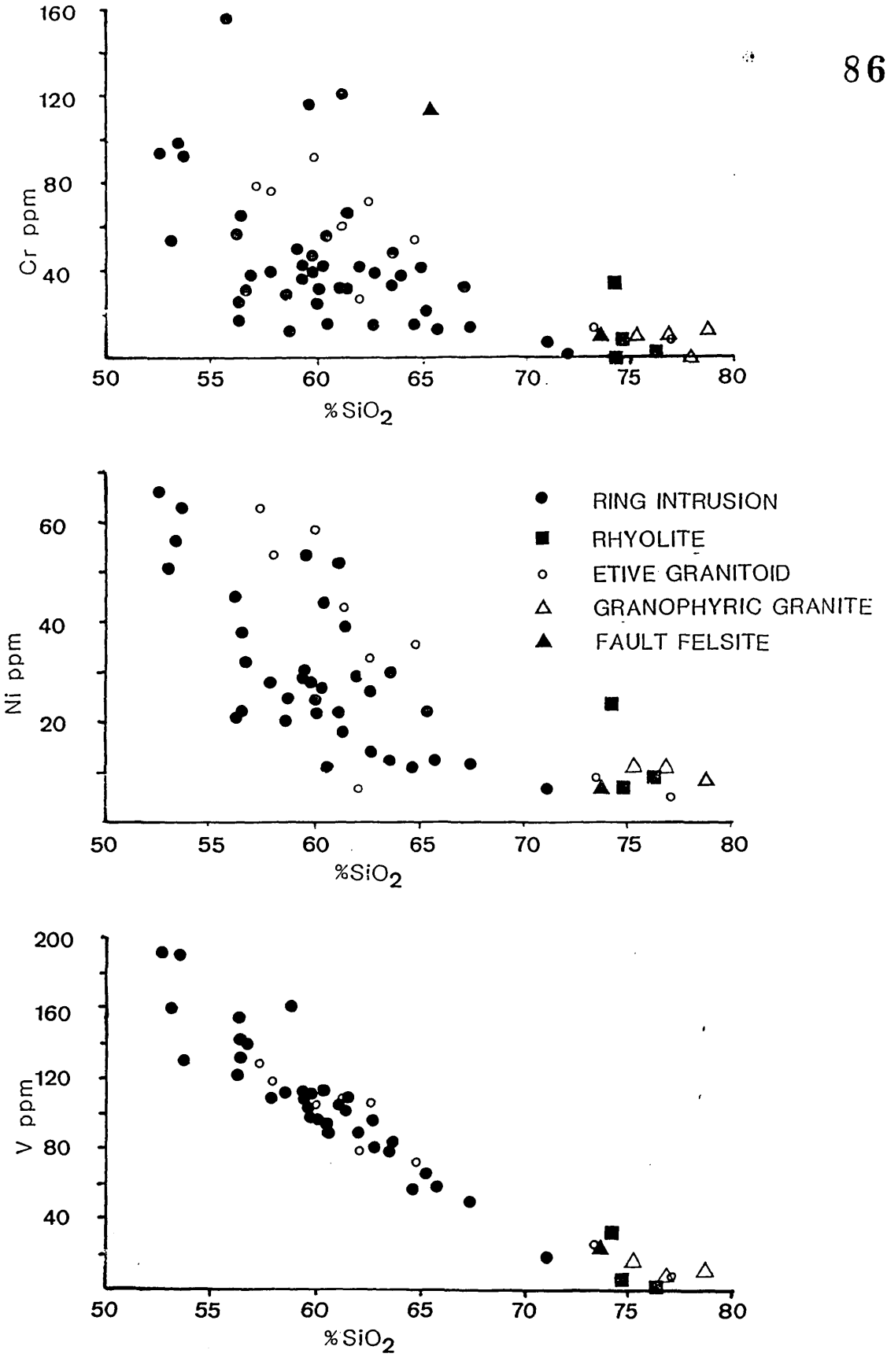

FIGURE 4.03 (continued)

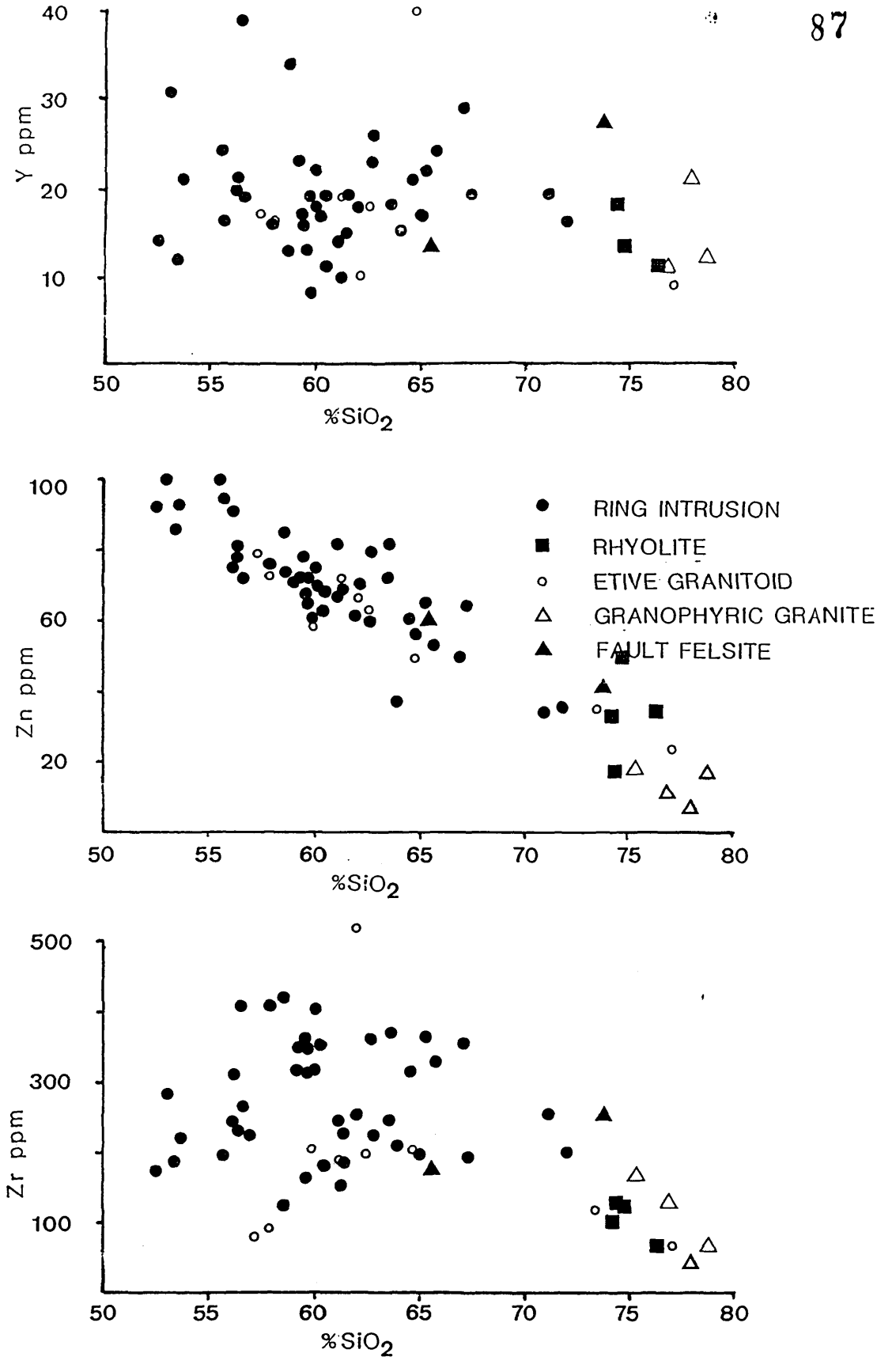

FIGURE 4.03 (continued)

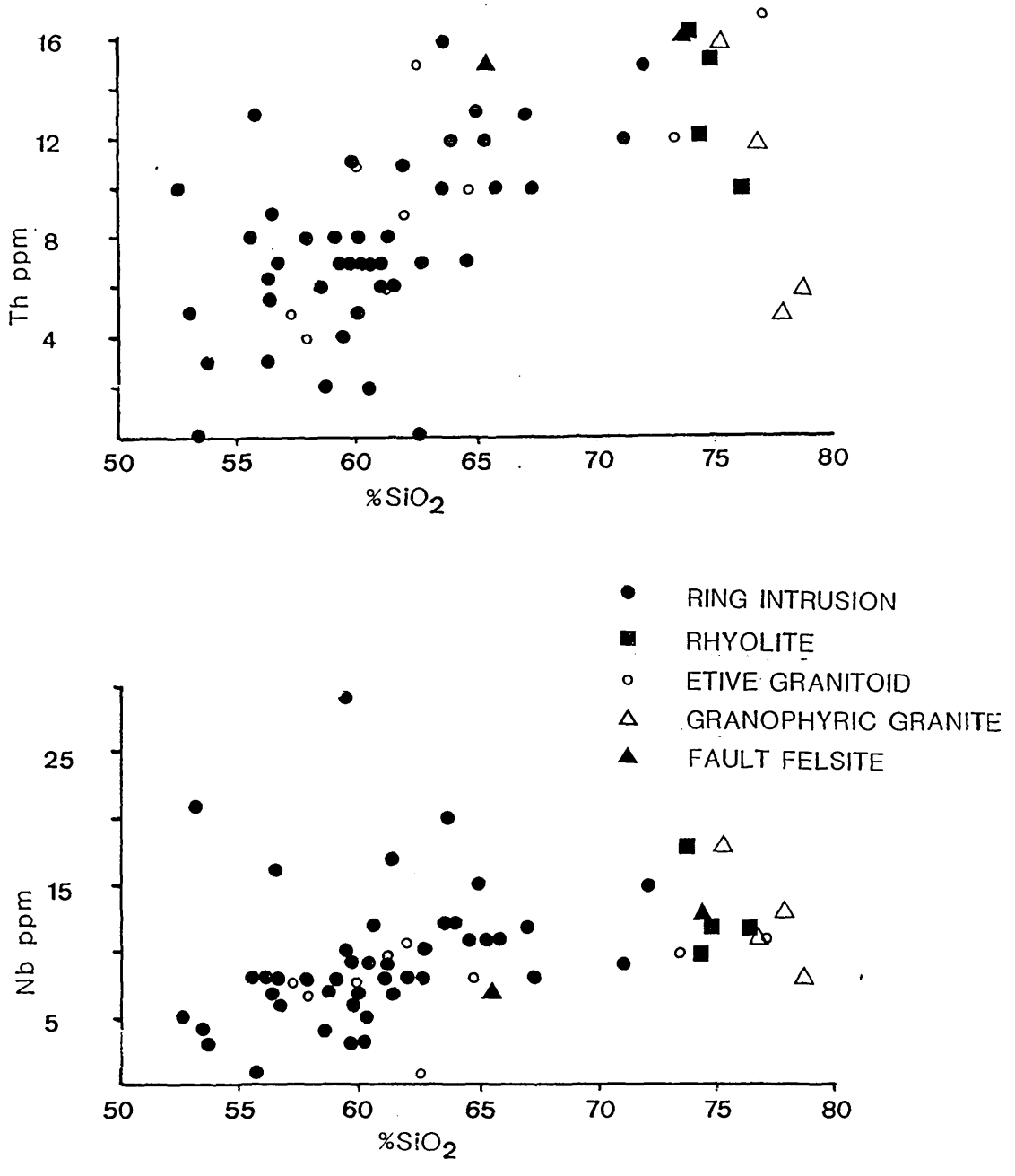

FIGURE 4.03 (continued)

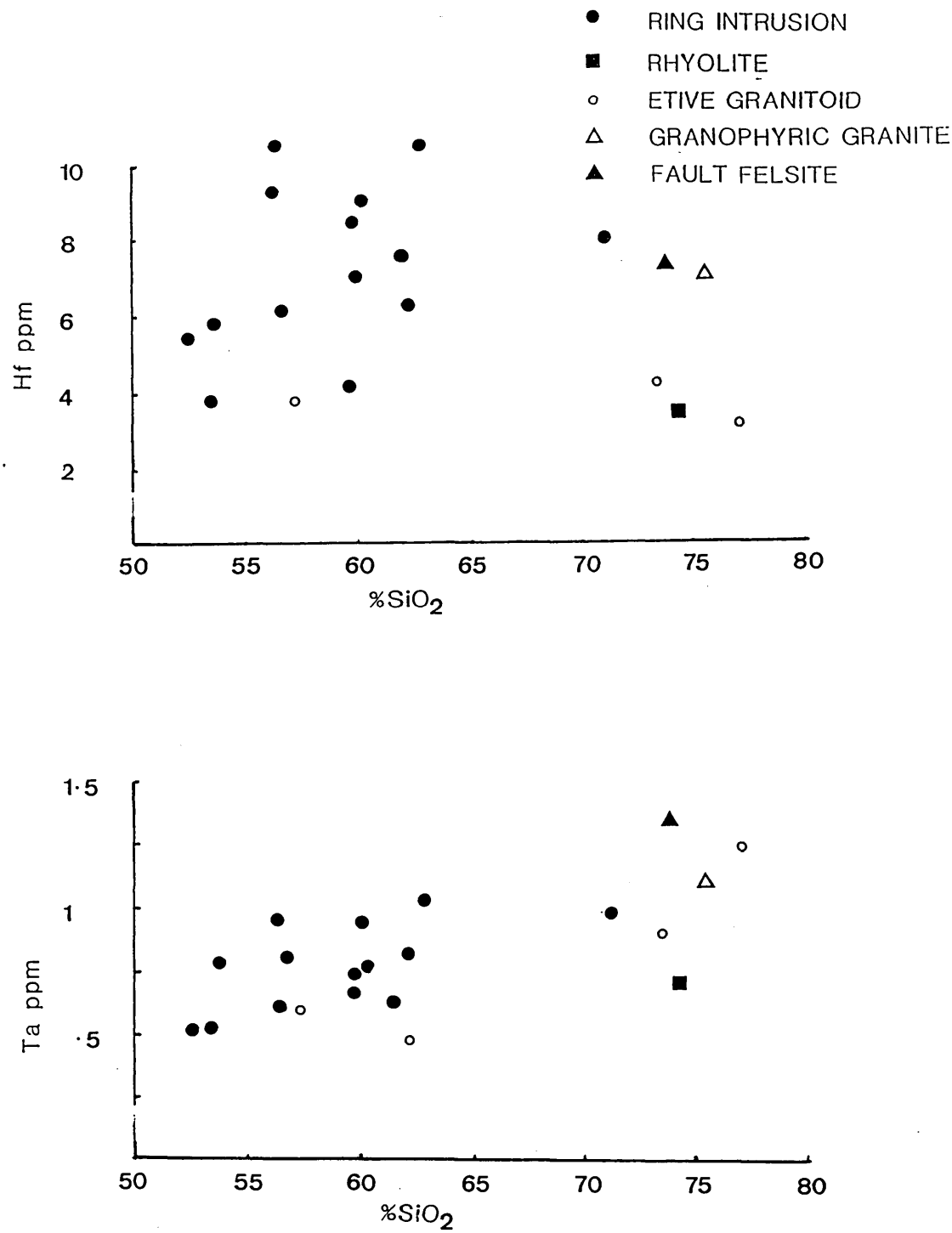

FIGURE 4.03 (continued)

The scatter previously mentioned for Zr may reflect the variable assimilation of inherited zircons. Although the Ba variation diagram does show a lot of scatter, it does appear that for the ring-intrusion samples an inflection point is present at approximately 70 wt.% SiO2. This inflection correlates with the appearance of alkali feldspar in the more acid members of the suite, in addition to the biotite which appears somewhat earlier. However, there does not appear to be a correlation between the variation in the Ba content of the rocks and the presence of alkali feldspar overgrowths on plagioclase phenocrysts which occur in samples throughout the range of ring-intrusion rocks.

Of the remaining trace elements Ni, Cr, V and Zn, all behave in a compatible manner. Cr reaches low concentrations at around 60 wt.% SiO2, possibly indicating the last stages of augite removal from the liquid. V shows a much smoother trend decreasing with increasing SiO2 content. The compatible nature of this element can be ascribed to the removal of augite in the early period of fractionation, with Fe-Ti oxides (magnetite KD = 30), and later biotite (KD = 50) and hornblende (KD = 32). The preceeding KD values are approximations from Gill (1978) for liquids of andesitic composition. Zn also shows a marked negative correlation with increasing SiO2, and again the compatible nature of this element can be explained by the removal of the phases biotite (KD = 20), hornblende (KD = 7) and Fe-Ti oxides (magnetite KD = 12). All these phases have been identified as modally important phases within the suite of ring-intrusion rocks (partition coefficients from Henderson 1982).

The low Nb abundances are typical of calc-alkaline rocks, and are believed to be due to the retention of such minor phases as ilmenite and sphene in the residue (Saunders et al. 1980), although the retention of such high-Ti phases is not universally accepted (Thompson et al. 1984).

4.3 RARE EARTH ELEMENTS

Rare Earth Element (R.E.E) values for a selection of the igneous rocks have been plotted against silica (Fig. 4.04). All the R.E.E.'s except Eu behave incompatibly for the ring-intrusion rocks. Most samples of rhyolite and granophyric granite do not fall into this pattern (see section 4.8).

The R.E.E.'s of individual samples are also displayed in chondrite-normalised incompatible element plots (Fig. 4.05). The salient features of these plots are listed below:

1) All the rocks are light R.E.E. enriched.

2) Light R.E.E. enrichment increases with fractionation.

3) All, except the most basic rocks, have a flat or concave upwards heavy R.E.E. pattern. This reflects the fractionation of amphibole (Rutter 1985).

4) Most of the ring-intrusion rocks have a positive Eu anomaly, or a flat profile. This occurs despite the obvious fractionation of large amounts of plagioclase (section 4.4). The absence of a negative Eu anomaly probably indicates that Eu had a trivalent oxidation state in the magma (Eu^{3+}), and hence behaved in a similar fashion to the other R.E.E.'s. The positive anomalies probably reflect the large amounts of plagioclase phenocrysts present in each sample. The granophyric granites have a negative Eu anomaly, the significance of which is discussed in chapter 5.

5) Most rocks display a small negative Ce anomaly. This could be due to the fractionation of sphene. The available KDs for Ce in sphene are rather sparse, but are generally large showing a range of values between 30 and 80 depending on the liquid composition (Tindle and Pearce 1981).

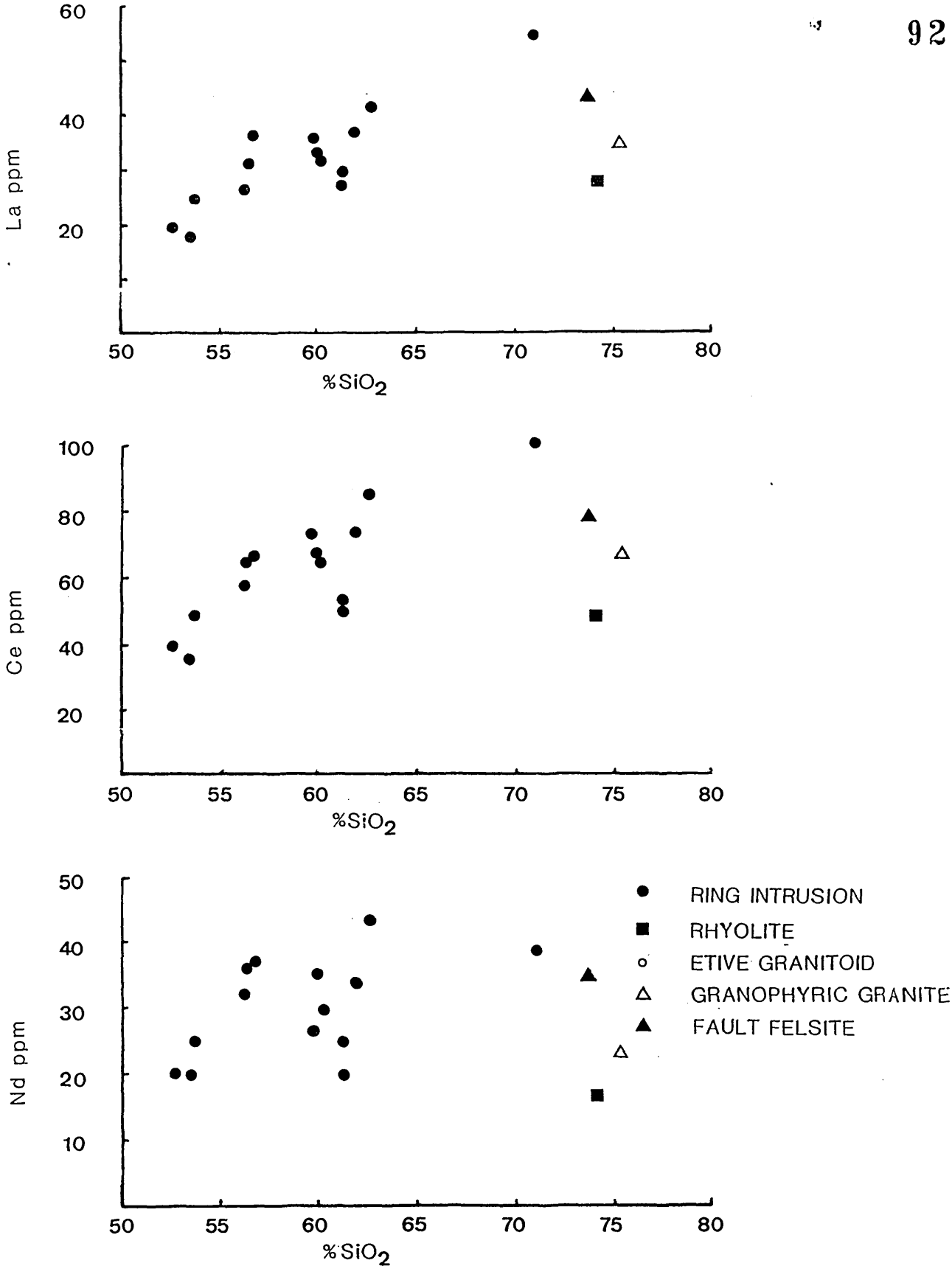

FIGURE 4.04 Rare Earth Element (R.E.E.) chemical variations for a selection of Glencoe igneous rocks.

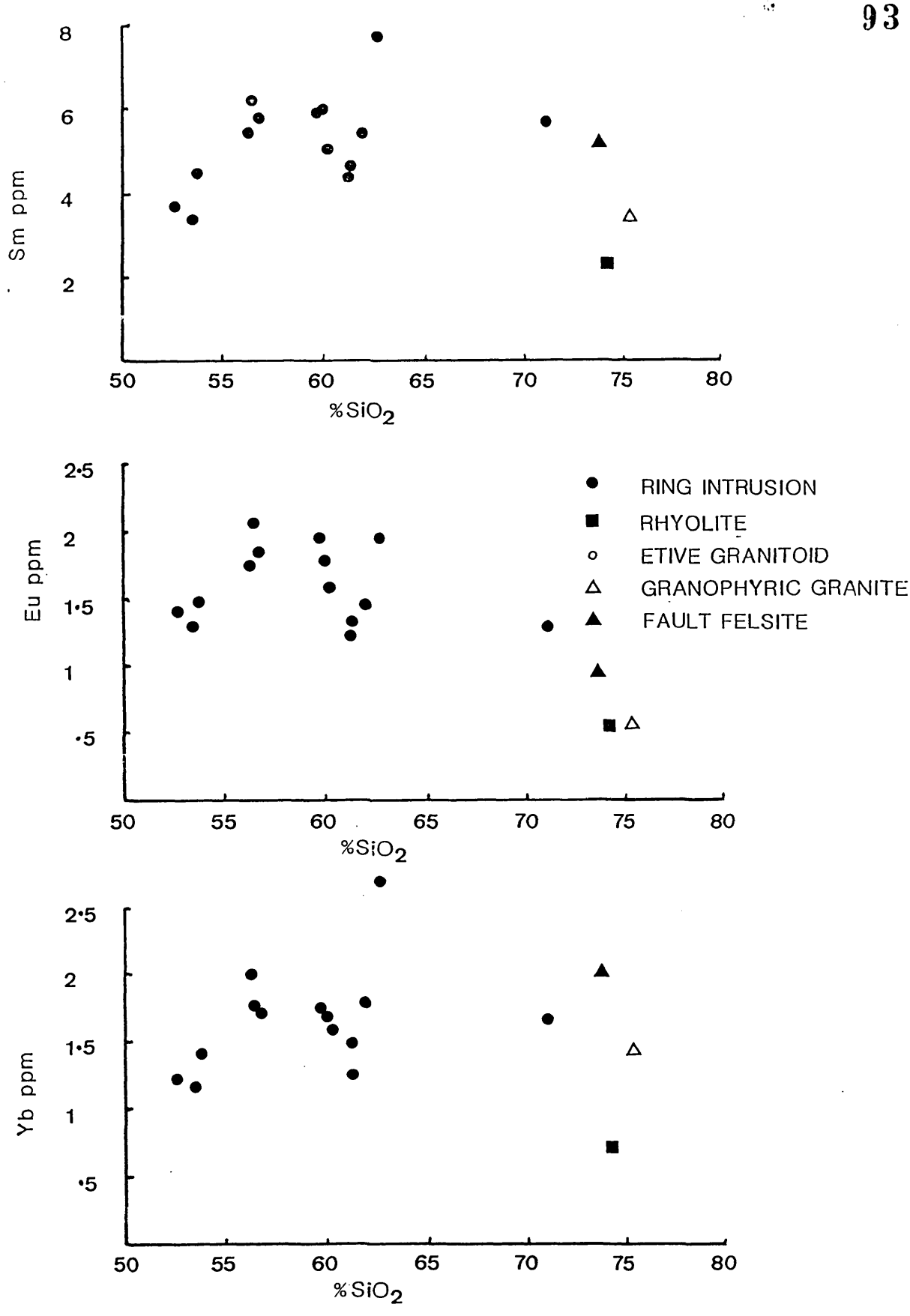

FIGURE 4.04 (continued)

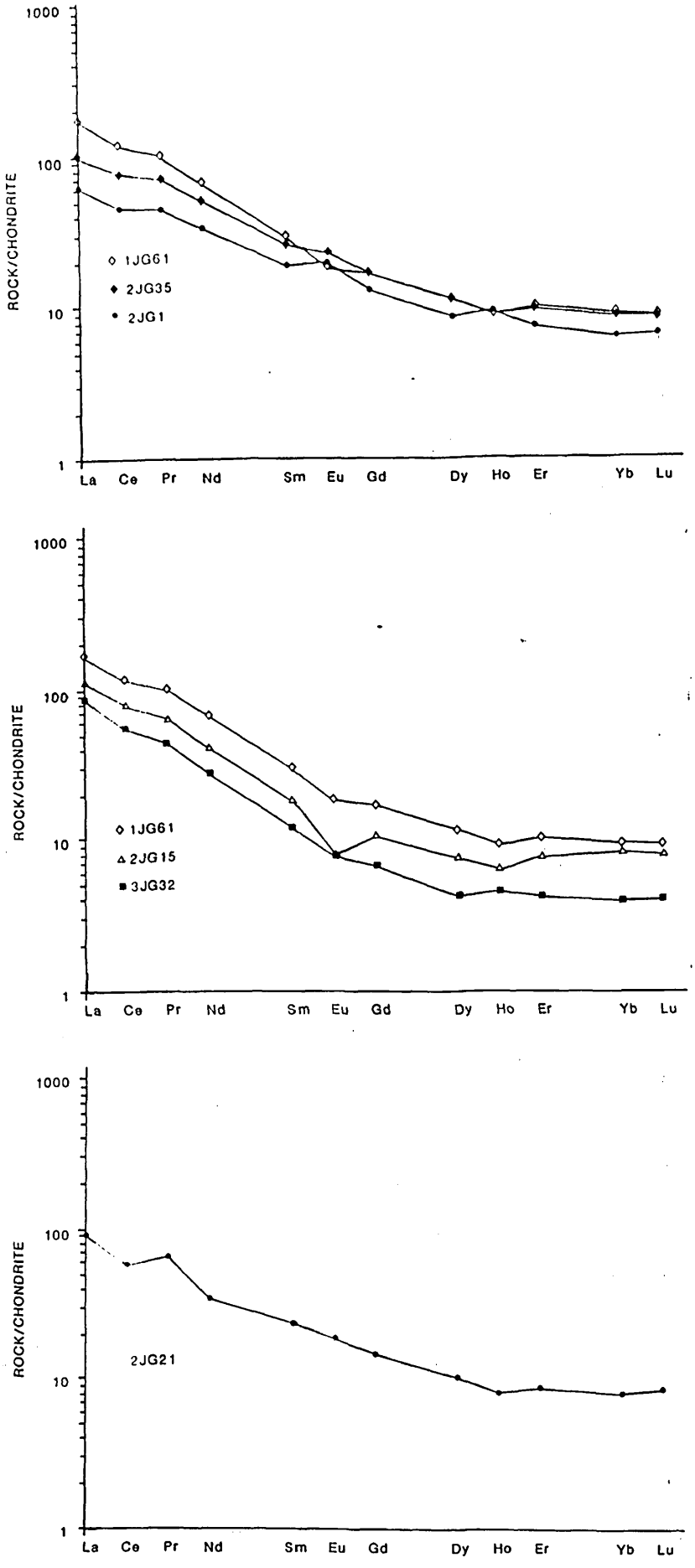

FIGURE 4.05 Chondrite-normalised R.E.E. data for selected Glencoe igneous rocks. Gabbro (2JG1), dioritic gabbro (1JG18, 3JG47), diorite (2JG35, 2JG21, 3JG29), granophyric granite (1JG61, 2JG15), rhyolite (3JG32), fault felsite (1JG24).

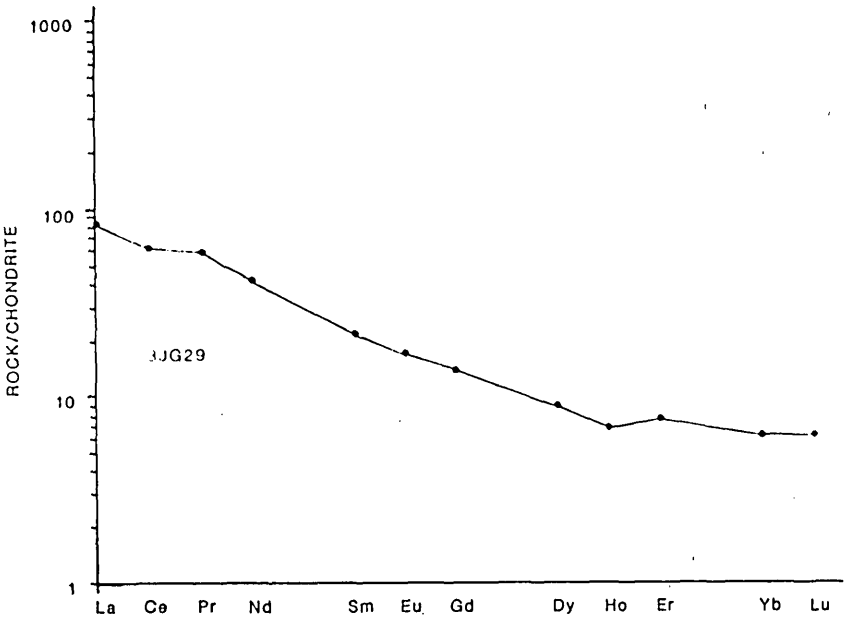

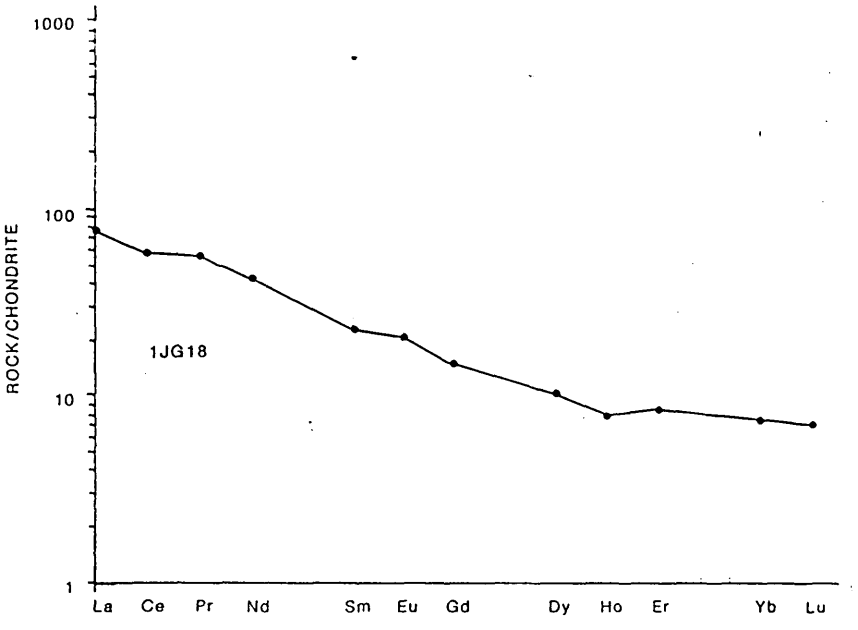

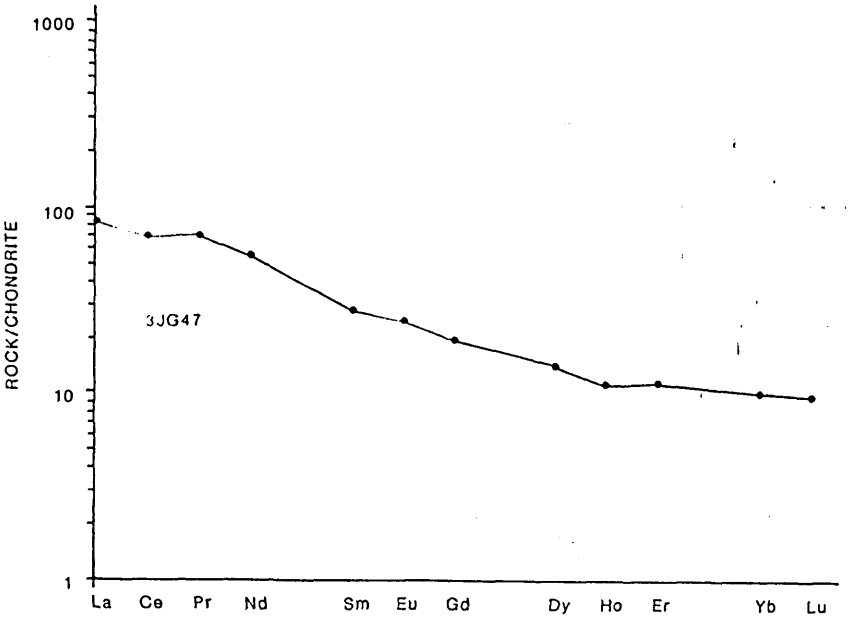

FIGURE 4.05 (continued)

6) The granophyric granites (1JG61) and rhyolites (3JG32) have different patterns from the ring-intrusion rocks, and are much poorer in REEs. The origin of these two groups of rocks are considered separately (granophyric granites in chapter 5 and rhyolites in section 4.4). However, it is possible that their origins may be similar, or related to one another.

7) Sample 1JG24 (fault felsite or rhyolite) has very similar R.E.E values to 1JG61 (granophyric granite) (chapter 7).

4.4 RHYOLITES

The samples of rhyolite studied are different both petrographically and chemically from the ring-intrusion rocks. They are poorly porphyritic, containing a few small, altered mafic crystals, and small unzoned feldspars (whereas the ring-intrusion rocks contain large, zoned feldspars).

Analyses of the rhyolites do not lie on any of the incompatible trends produced by the ring-intrusion rocks and displayed in the variation diagrams (Figs. 4.02, 4.03). The four analyses are spread out, and range between the main ring-intrusion trends, and the analyses for the granophyric granites. This could be caused by the fractionation of phases such as K-feldspar, sphene and allanite, but neither sphene nor allanite are observed in thin-section, plus it is also difficult to wholly remove crystals from a viscous rhyolitic magma.

It is probable that these rocks have been derived by a process other than crystal fractionation of the ring-intrusion magmas. The data set seems to show a mixing relationship between the main batch of data and the granophyric granites, which are believed to represent upper crustal partial-melt compositions (see chapter 5). Alternatively, the rhyolitic magmas

could originate from a completely different source. However, the spread of data points does suggest that variable amounts of partial-melt material have been incorporated in these rocks.

4.5 MAJOR ELEMENT MODELLING

Element modelling has been carried out using different approaches which are summarised in a flow-diagram (Fig. 4.06). A mass balance approach has been used to model the major element chemical variations within the ring-intrusion suite. A simple least squares fractionation model (LeMaitre 1979) was used to calculate the proportion of each mineral which must be removed from a parent magma in order to produce a supposed derivative magma.

This type of modelling does, however, have certain limitations:

1) The modelling is purely mathematical, and some results, such as negative values for components, cannot be correlated to geological processes.

2) Only fractional crystallisation is considered in the modelling, rather than the more complex situation generally considered to occur in natural crystal/liquid assemblages.

From this initial modelling, a number of other options for element modelling are studied.

4.5.1 Crystal fractionation models

The ring-intrusion rocks were modelled in five stages from gabbro to granite (Table 4.01). This approach enables the changes in both phenocrystal type and composition to be taken into account in the fractionating series. The phenocryst analyses were obtained using the electron microprobe, and are listed in Appendix D. Results of the different stages of the modelling are given in Table 4.01. An

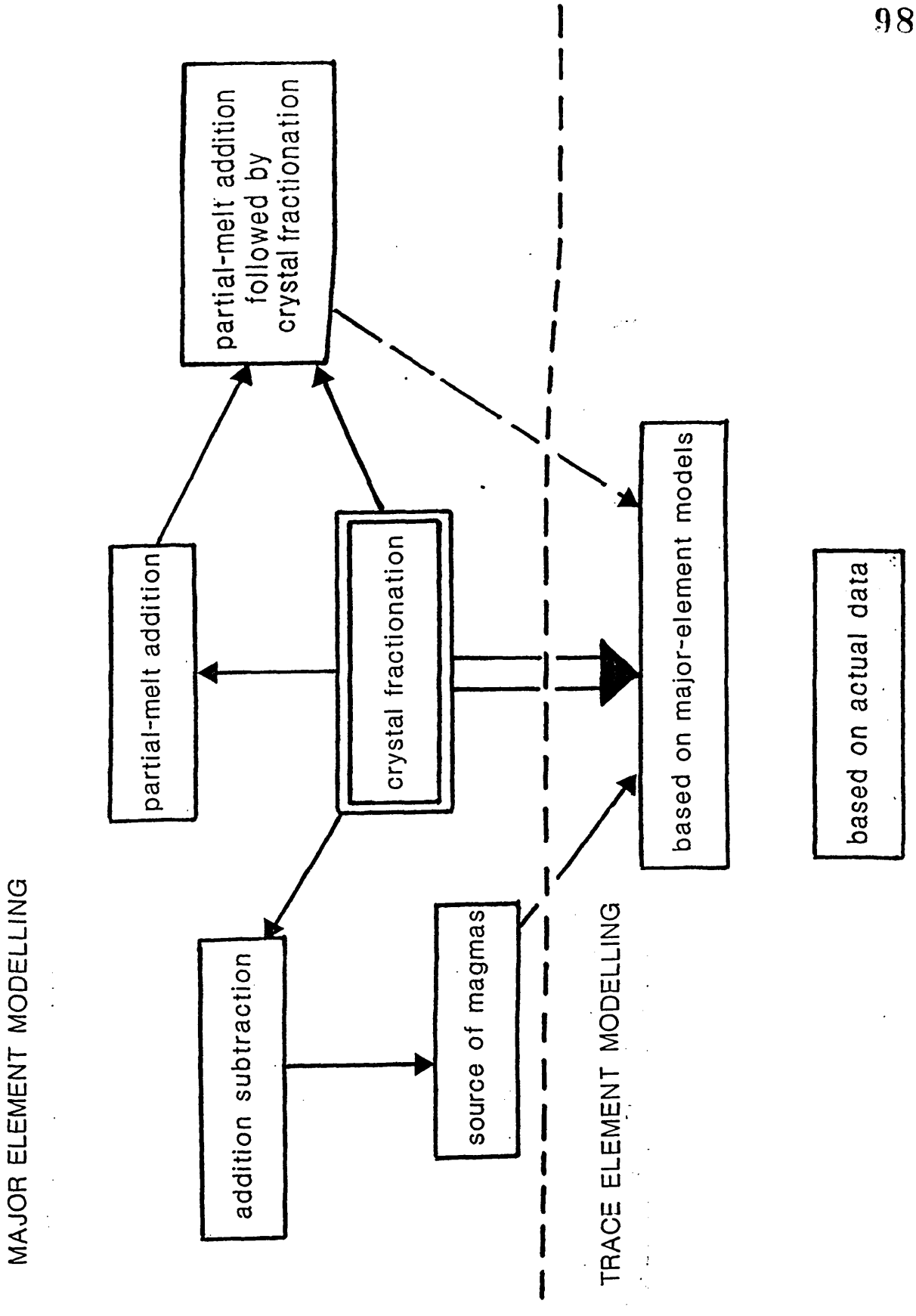

FIGURE 4.06 Flow-diagram illustrating the element modelling which was used in this study

TABLE 4.01 Results of major element fractional crystallisation modelling of samples 2JG1, 1JG10, 2JG35, 1JG80, 1JG9, 1JG61.

-****** LEAST-SQUARES SOLUTION TO GENERALISED MIXING MODEL NO. 1 ******

0	AMOUNTS	SI	TI	AL	FE	MN	MG	CA	NA	K	P	TOTAL
REACTANTS USED												
1 GABBRO(2JG1)	100.00	52.61	1.35	17.75	8.61	.14	4.82	8.01	3.51	1.24	.30	98.34
OPRODUCTS USED												
2 1JG10	44.98	56.33	1.10	18.66	6.78	.09	3.12	5.44	3.94	2.68	.45	98.59
3 AUGITE	17.88	54.51	.30	1.89	10.53	.19	18.74	11.02	1.73	.60	.05	99.04
5 PLAGIOCLASE	32.35	54.26	0.00	27.72	.57	0.00	0.00	11.39	5.00	.13	.00	99.09
6 MAGNATITE	2.87	.43	.24	.08	98.56	0.00	.15	.36	0.00	0.00	.00	99.82
7 ILMENITE	1.92	3.88	46.25	.52	39.10	3.06	.43	2.55	0.00	0.00	0.00	95.79
OESTIMATED COMPOSITIONS												
REACTANTS		52.61	1.35	17.75	8.61	.14	4.82	8.01	3.51	1.24	.30	98.34
PRODUCTS		52.73	1.44	17.72	8.69	.13	4.77	8.16	3.72	1.33	.20	98.87
DIFFERENCES		-.12	-.09	.03	-.08	.01	.05	-.15	-.21	-.08	.10	
ORESIDUAL SUM OF SQUARES = .1134												
DISTANCE BETWEEN TWO ESTIMATED COMPOSITIONS = .3367												
0****** ****** ****** ****** ****** ******												

-****** LEAST-SQUARES SOLUTION TO GENERALISED MIXING MODEL NO. 1 ******

0	AMOUNTS	SI	TI	AL	FEFE	MN	MG	CA	NA	K	P	TOTAL
REACTANTS USED												
1 1JG10	100.00	56.33	1.10	18.66	6.78	.09	3.12	5.44	3.94	2.68	.45	98.59
OPRODUCTS USED												
2 2JG35	64.24	60.25	1.01	17.43	5.74	.09	2.27	4.81	4.51	2.75	.36	99.22
3 PLAGIOCLASE	23.05	59.13	0.00	25.54	.31	0.00	0.00	7.74	.23	.00	.00	99.74
4 MAGNETITE	1.48	.43	.24	.08	98.56	0.00	.15	.36	0.00	0.00	.00	99.82
5 AMPHIBOLE	.92	43.71	3.17	10.00	12.35	.03	13.53	11.70	2.00	.60	.05	97.06
6 APATITE	.61	0.00	0.00	0.00	0.00	.07	.10	55.84	0.00	0.00	.00	99.64
11 BIOTITE	9.71	36.42	5.38	13.54	14.53	.15	15.61	.20	1.07	8.84	.00	95.74
OESTIMATED COMPOSITIONS												
REACTANTS		56.33	1.10	18.66	6.78	.09	3.12	5.44	3.94	2.68	.45	98.59
PRODUCTS		56.28	1.20	18.49	6.74	.07	3.10	5.34	3.59	2.66	.40	98.99
DIFFERENCES		.05	-.10	.17	.04	.02	.02	.10	-.65	-.00	-.04	
ORESIDUAL SUM OF SQUARES = .4719												
DISTANCE BETWEEN TWO ESTIMATED COMPOSITIONS = .6869												
0****** ****** ****** ****** ****** ******												

-****** LEAST-SQUARES SOLUTION TO GENERALISED MIXING MODEL NO. 1 ******

0	AMOUNTS	SI	TI	AL	FEFE	MN	MG	CA	NA	K	P	TOTAL
REACTANTS USED												
1 2JG35	100.00	60.25	1.01	17.43	5.74	.09	2.27	4.81	4.51	2.75	.36	99.22
OPRODUCTS USED												
2 1JG80	67.89	64.57	.71	16.74	4.01	.06	1.63	2.84	4.70	3.57	.23	99.06
3 PLAGIOCLASE	20.92	60.48	0.00	24.30	.30	0.00	0.00	6.84	6.75	1.02	.00	99.71
4 AMPHIBOLE	8.07	42.77	3.20	10.41	12.21	.22	13.78	11.51	2.59	.79	.05	97.53
5 APATITE	.46	0.00	0.00	0.00	0.00	.07	.10	55.84	0.00	0.00	.00	99.64
6 BIOTITE	.11	36.42	5.38	13.54	14.53	.15	15.61	.20	1.07	8.84	.00	95.74
9 MAGNETITE	1.92	.43	.24	.08	98.56	0.00	.15	.36	0.00	0.00	.00	99.82
10 SPHENE	.63	30.75	37.97	.69	1.77	0.00	0.00	27.77	0.00	0.00	.00	98.95
OESTIMATED COMPOSITIONS												
REACTANTS		60.25	1.01	17.43	5.74	.09	2.27	4.81	4.51	2.75	.36	99.22
PRODUCTS		60.19	.99	17.31	5.69	.06	2.24	4.72	4.31	2.71	.35	99.07
DIFFERENCES		.06	.02	.12	.05	.03	.03	.09	-.30	.04	.01	
ORESIDUAL SUM OF SQUARES = .1244												
DISTANCE BETWEEN TWO ESTIMATED COMPOSITIONS = .3527												
0****** ****** ****** ****** ****** ******												

TABLE 4.01 (continued)

```
-****** LEAST-SQUARES SOLUTION TO GENERALISED MIXING MODEL NO.  1 ******
O                    AMOUNTS      SI      TI      AL      FEFE      MN      MG      CA      NA      K       P      TOTAL
 REACTANTS USED
   1   1JG80          100.00     64.57     .71   16.74    4.01     .06    1.63    2.84    4.70    3.57     .23    99.06
OPRODUCTS USED
   2   1JG9            81.73     67.32     .50   16.12    2.97     .03    1.06    2.18    4.60    3.91     .40    99.09
   3   PLAGIOCLASE     12.09     61.06    0.00   23.81     .40    0.00    0.00    6.06    7.52     .80    0.000   99.65
   4   AMPHIBOLE        2.40     42.77    3.20   10.41   12.21     .22   13.78   11.51    2.59     .79    0.000   97.48
   6   BIOTITE          2.92     36.89    5.38   13.51   16.03     .16   13.90     .19     .69    9.11    0.000   95.48
   7   MAGNETITE         .76      .43     .24     .08   98.56    0.00     .15     .36    0.00    0.00    0.000   99.82
   8   SPHENE            .10     30.75   37.97     .69    1.77    0.00    0.00   27.77    0.00    0.00    0.00    98.95
OESTIMATED COMPOSITIONS
       REACTANTS                  64.57     .71   16.74    4.01     .06    1.63    2.84    4.70    3.57     .23    99.06
       PRODUCTS                   64.54     .68   16.70    3.99     .03    1.60    2.83    4.75    3.58     .33    99.03
          DIFFERENCES               .03     .03     .04     .02     .03     .03     .01    -.05    -.01    -.10
ORESIDUAL SUM OF SQUARES =        .0174
 DISTANCE BETWEEN TWO ESTIMATED COMPOSITIONS =          .1317
O******       ******      ******      ******       ******       ******


-****** LEAST-SQUARES SOLUTION TO GENERALISED MIXING MODEL NO.  1 ******
O                    AMOUNTS      SI      TI      AL      FEFE      MN      MG      CA      NA      K       P      TOTAL
 REACTANTS USED
   1   1JG9           100.00     67.32     .50   16.12    2.97     .03    1.06    2.18    4.60    3.91     .40    99.09
CPRODUCTS USED
   2   1JG61           54.70     71.04     .34   15.29    1.77     .04     .32     .89    4.85    5.12     .07    99.72
   3   PLAGIOCLASE     27.49     62.41    0.00   23.43     .31    0.00    0.00    5.10    8.27     .77    0.000  100.29
   6   BIOTITE         10.13     36.89    5.38   13.51   16.03     .16   13.90     .19     .69    9.11    0.000   95.86
   7   QUARTZ           7.64    100.00    0.00    0.00    0.00    0.00    0.00    0.00    0.00    0.00    0.000  100.00
OESTIMATED COMPOSITIONS
       REACTANTS                  67.32     .50   16.12    2.97     .03    1.06    2.18    4.60    3.91     .40    99.09
       PRODUCTS                   67.40     .73   16.18    2.68     .04    1.59    1.90    5.00    3.94     .04    99.51
          DIFFERENCES              -.08    -.23    -.06     .29    -.01    -.53     .28    -.40    -.03     .36
ORESIDUAL SUM OF SQUARES =        .7927
 DISTANCE BETWEEN TWO ESTIMATED COMPOSITIONS =          .8903
O******       ******      ******      ******       ******       ******
```

acceptable upper limit for the sum of residual squares of 1.0 was arbitrarily taken for the calculations. The modelling was successful with all the residual sums of squares being less than 1.0. Some values are rather high, but this is probably a result of cation exchange caused by the sub-solidus circulation of hydrothermal fluids.

The most basic magma (2JG1) is believed to have fractionated plagioclase, augite and Fe-Ti oxides. These are the only phenocrysts observed, and modelling of fractional crystallisation from 2JG1 to 1JG10 produces a low residual sum of squares.

In the dioritic rocks, augite is rarely seen as a phenocryst phase, but biotite and amphibole are observed as phenocrysts. Also, accessory phenocrysts of apatite and sphene are present. These phenocryst phases, along with plagioclase and magnetite, produce good mixing models for the intermediate steps (Table 4.01). Ilmenite is not seen in these rocks, and does not fit into the model. This reflects the ability of sphene to incorporate the excess TiO2.

In the granites, only plagioclase, biotite and quartz are present as phenocrysts. When modelling the fractionation of these phases, the residual sum of squares is a little high. It is possible that processes other than fractional crystallisation have been operating, especially as it is more difficult to remove crystals from a viscous, granitic magma.

4.5.2 Partial-melt addition

The author believes that the granophyric granites are derived by the partial-melting of the Dalradian country-rock (see Ch.5 for detailed discussion). Hence it is possible that the range of intrusives could have been derived by the addition of partial-melt material to a more basic magma to produce an intermediate magma. This theory has been tested using least-squares modelling, and produces variable results (Table 4.02). Some steps have high

TABLE 4.02 Results of major element modelling of the mixing of basic rocks with partial-melt to produce intermediate rocks.

-****** LEAST-SQUARES SOLUTION TO GENERALISED MIXING MODEL NO. 2 ******

O	AMOUNTS	SI	TI	AL	FE	MN	MG	CA	NA	K	P	TOTAL
REACTANTS USED												
2 1JG10	100.00	56.33	1.10	18.66	6.78	.09	3.12	5.44	3.94	2.63	.45	98.59
OPRODUCTS USED												
1 GABBRO(2JG1)	83.58	52.61	1.35	17.75	8.61	.14	4.82	8.01	3.51	1.24	.30	98.34
9 PART MELT	16.42	78.01	.08	12.89	1.11	.06	0.00	.25	4.73	1.64	.03	98.80
OESTIMATED COMPOSITIONS												
REACTANTS		56.33	1.10	18.66	6.78	.09	3.12	5.44	3.94	2.68	.45	98.59
PRODUCTS		56.78	1.14	16.95	7.38	.13	4.03	6.74	3.71	1.31	.26	98.42
DIFFERENCES		-.45	-.04	1.71	-.60	-.04	-.91	-1.30	.23	1.37	.19	

ORESIDUAL SUM OF SQUARES = 7.9656

DISTANCE BETWEEN TWO ESTIMATED COMPOSITIONS = 2.8223

O****** ****** ****** ****** ****** ******

-****** LEAST-SQUARES SOLUTION TO GENERALISED MIXING MODEL NO. 2 ******

O	AMOUNTS	SI	TI	AL	FEFE	MN	MG	CA	NA	K	P	TOTAL
REACTANTS USED												
2 2JG35	100.00	60.25	1.01	17.43	5.74	.09	2.27	4.81	4.51	2.75	.36	99.22
OPRODUCTS USED												
1 1JG10	81.84	56.33	1.10	18.66	6.78	.09	3.12	5.44	3.94	2.68	.45	98.59
10 PART MELT	18.16	78.01	.08	12.89	1.11	.06	0.00	.25	4.73	1.64	.03	98.80
OESTIMATED COMPOSITIONS												
REACTANTS		60.25	1.01	17.43	5.74	.09	2.27	4.81	4.51	2.75	.36	99.22
PRODUCTS		60.27	.91	17.61	5.75	.08	2.55	4.50	4.08	2.49	.37	98.83
DIFFERENCES		-.02	.10	-.18	-.01	.01	-.28	.31	.43	.26	-.01	

ORESIDUAL SUM OF SQUARES = .4698

DISTANCE BETWEEN TWO ESTIMATED COMPOSITIONS = .6854

O****** ****** ****** ****** ****** ******

-****** LEAST-SQUARES SOLUTION TO GENERALISED MIXING MODEL NO. 2 ******

O	AMOUNTS	SI	TI	AL	FEFE	MN	MG	CA	NA	K	P	TOTAL
REACTANTS USED												
2 1JG9	100.00	67.32	.50	16.12	2.97	.03	1.06	2.18	4.60	3.91	.40	99.09
OPRODUCTS USED												
1 1JG80	79.56	64.57	.71	16.74	4.01	.06	1.63	2.84	4.70	3.57	.23	99.06
9 PART MELT	20.44	78.01	.08	12.89	1.11	.06	0.00	.25	4.73	1.64	.03	98.80
OESTIMATED COMPOSITIONS												
REACTANTS		67.32	.50	16.12	2.97	.03	1.06	2.18	4.60	3.91	.40	99.09
PRODUCTS		67.32	.58	15.95	3.42	.06	1.30	2.31	4.71	3.18	.19	99.01
DIFFERENCES		.00	-.08	.17	-.45	-.03	-.24	-.13	-.11	.73	.21	

ORESIDUAL SUM OF SQUARES = .9038

DISTANCE BETWEEN TWO ESTIMATED COMPOSITIONS = .9507

O****** ****** ****** ****** ****** ******

-****** LEAST-SQUARES SOLUTION TO GENERALISED MIXING MODEL NO. 2 ******

O	AMOUNTS	SI	TI	AL	FEFE	MN	MG	CA	NA	K	P	TOTAL
REACTANTS USED												
2 1JG80	100.00	64.57	.71	16.74	4.01	.06	1.63	2.84	4.70	3.57	.23	99.06
OPRODUCTS USED												
1 2JG35	74.65	60.25	1.01	17.43	5.74	.09	2.27	4.81	4.51	2.75	.36	99.22
11 PART MELT	25.35	78.01	.08	12.89	1.11	.06	0.00	.25	4.73	1.64	.03	98.80
OESTIMATED COMPOSITIONS												
REACTANTS		64.57	.71	16.74	4.01	.06	1.63	2.84	4.70	3.57	.23	99.06
PRODUCTS		64.75	.77	16.28	4.57	.08	1.69	3.65	4.57	2.47	.28	99.11
DIFFERENCES		-.18	-.06	.46	-.56	-.02	-.06	-.81	.13	1.10	-.05	

ORESIDUAL SUM OF SQUARES = 2.4597

DISTANCE BETWEEN TWO ESTIMATED COMPOSITIONS = 1.5684

O****** ****** ****** ****** ****** ******

-****** LEAST-SQUARES SOLUTION TO GENERALISED MIXING MODEL NO. 2 ******

O	AMOUNTS	SI	TI	AL	FEFE	MN	MG	CA	NA	K	P	TOTAL
REACTANTS USED												
2 1JG61	100.00	71.04	.34	15.29	1.77	.04	.32	.88	4.35	5.12	.07	99.72
OPRODUCTS USED												
1 1JG9	67.19	67.32	.50	16.12	2.97	.03	1.06	2.18	4.60	3.91	.40	99.09
9 PART MELT	32.81	78.01	.08	12.89	1.11	.06	0.00	.25	4.73	1.64	.03	98.80
OESTIMATED COMPOSITIONS												
REACTANTS		71.04	.34	15.29	1.77	.04	.32	.88	4.35	5.12	.07	99.72
PRODUCTS		70.83	.36	15.06	2.36	.04	.71	1.55	4.64	3.17	.26	98.99
DIFFERENCES		.21	-.02	.23	-.59	.00	-.39	-.67	.21	1.95	-.21	

ORESIDUAL SUM OF SQUARES = 4.9524

DISTANCE BETWEEN TWO ESTIMATED COMPOSITIONS = 2.2254

O****** ****** ****** ****** ****** ******

residual sums of squares, and others are low. However, those models with a low residual sum of squares use samples which have a high phenocryst content, which would suggest that crystal fractionation was a more likely process to have caused their evolution.

4.5.3 Addition-subtraction diagrams

Addition-subtraction diagrams (Bowen 1928) have also been used to test for the addition of partial-melts. An example is shown for the first stage of modelling (Fig. 4.07). This produces two hypothetical rock-types which may have been 'added' or 'subtracted' from the more basic magma to produce the less basic magma.

The composition of the 'added' material is most unusual, and bears no relation to any rock composition found in Glencoe, particularly sedimentary and partial-melt rocks.

The 'subtracted' material is also dissimilar to any rocks in Glencoe. However, it is very similar to a basalt (L23) from the nearby Lorne Lava Plateau (Thirlwall 1982). It seems more likely that 2JG1 and 1JG10 are genetically related to a basic rock of similar composition to L23.

4.5.4 Partial-melt addition followed by crystal fractionation

In modelling the evolution of sample 1JG61 (granite) from sample 1JG9 (monzonite) using partial-melt addition, a relatively high residual sum of squares results. These rocks also contain some phenocrysts. Hence, least-squares mixing models have been used to model the addition of partial-melt material, followed by fractional crystallisation (Table 4.03). The modelling is successful for the stage 1JG9 to 1JG61, and this sort of process is considered more likely to have occurred in such

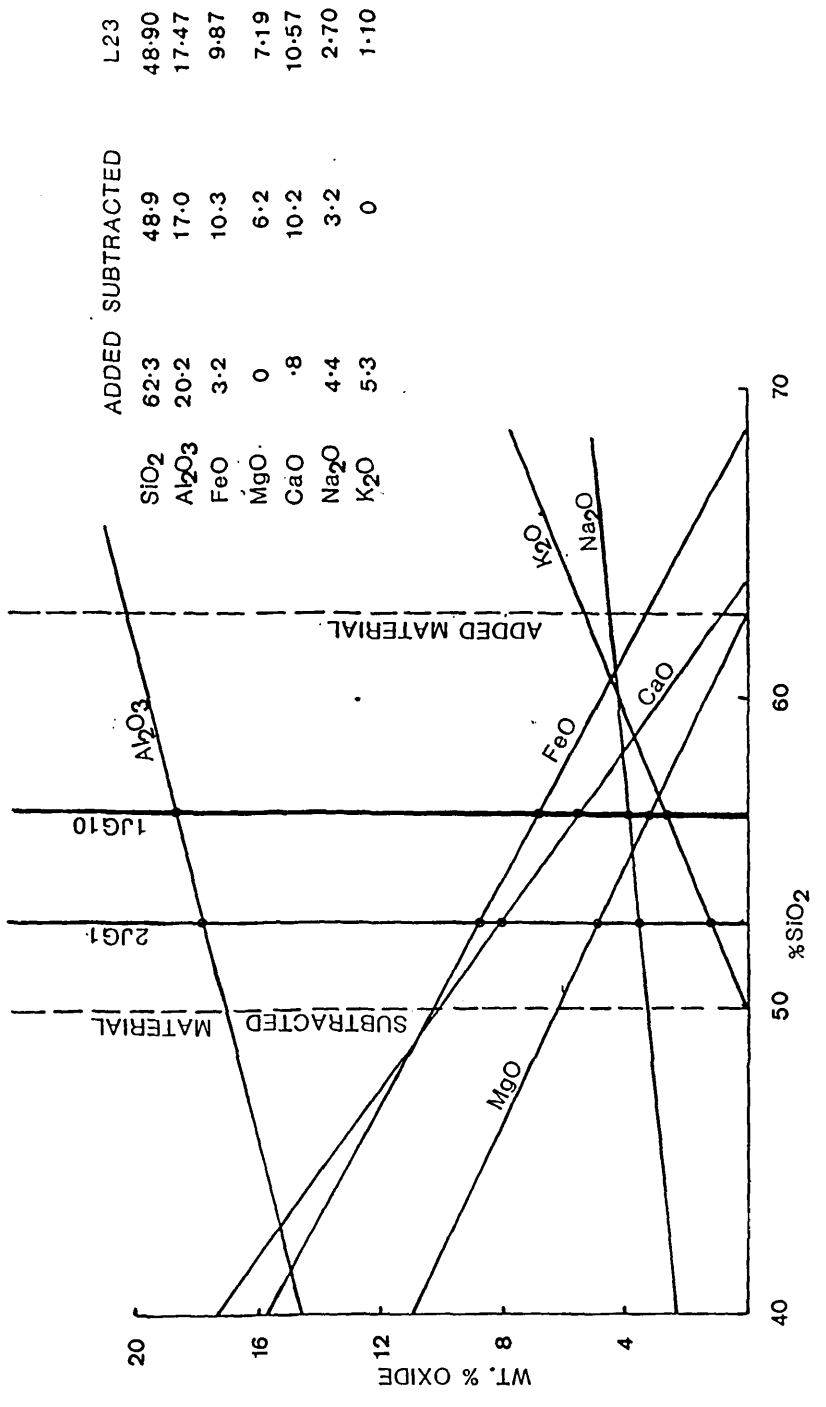

FIGURE 4.07 An addition-subtraction diagram modelling the chemical variations between samples 2JG1 (gabbro) and 1JG10 (dioritic gabbro).

-****** LEAST-SQUARES SOLUTION TO GENERALISED MIXING MODEL NO. 3 ******

O	AMOUNTS	SI	TI	AL	FE	MN	MG	CA	NA	K	P	TOTAL
REACTANTS USED												
1 GABBRO(2JG1)	98.32	52.61	1.35	17.75	8.61	.14	4.82	9.01	3.51	1.24	.30	99.34
9 PART MELT	1.68	78.01	.08	12.89	1.11	.06	0.00	.25	4.73	1.64	.03	98.80
OPRODUCTS USED												
2 1JG10	49.03	56.33	1.10	18.66	6.78	.09	3.12	5.44	3.94	2.68	.45	98.59
3 ALGITE	17.17	54.51	.30	1.89	10.53	.19	18.74	11.02	1.73	0.00	0.00	99.91
5 PLAGIOCLASE	29.52	54.26	0.00	27.73	.57	0.00	0.00	11.39	5.05	.30	0.00	99.34
6 MAGNATITE	2.61	.43	.24	.08	98.56	0.00	.15	.36	0.00	0.00	0.00	99.82
7 ILMENITE	1.68	3.88	46.25	.52	39.10	3.06	.43	2.55	0.00	0.00	0.00	95.79
OESTIMATED COMPOSITIONS												
REACTANTS		53.04	1.33	17.67	8.48	.14	4.74	7.88	3.53	1.25	.30	98.35
PRODUCTS		53.07	1.37	17.67	8.52	.13	4.76	7.97	3.72	1.41	.22	98.85
DIFFERENCES		-.03	-.05	-.00	-.04	.01	-.02	-.09	-.19	-.17	.07	

ORESIDUAL SUM OF SQUARES = .0834
DISTANCE BETWEEN TWO ESTIMATED COMPOSITIONS = .2888
O****** ****** ****** ****** ****** ******

-****** LEAST-SQUARES SOLUTION TO GENERALISED MIXING MODEL NO. 3 ******

O	AMOUNTS	SI	TI	AL	FEFE	MN	MG	CA	NA	K	P	TOTAL
REACTANTS USED												
1 1JG10	87.10	56.33	1.10	18.66	6.78	.09	3.12	5.44	3.94	2.68	.45	98.59
10 PART MELT	12.90	78.01	.08	12.89	1.11	.06	0.00	.25	4.73	1.64	.03	98.80
OPRODUCTS USED												
2 2JG35	88.33	60.25	1.01	17.43	5.74	.09	2.27	4.81	4.51	2.75	.36	99.22
3 PLAGIOCLASE	7.28	59.13	0.00	25.54	.31	0.00	0.00	7.74	6.77	.23	0.00	99.72
4 MAGNETITE	.36	.43	.24	.08	98.56	0.00	.15	.36	0.00	0.00	0.00	99.82
5 AMPHIBOLE	.76	43.71	3.17	10.00	12.35	.03	13.53	11.70	2.65	.60	0.00	97.74
6 APATITE	-.12	0.00	0.00	0.00	0.00	.07	.10	55.84	0.00	0.00	42.00	97.93
11 BIOTITE	3.40	36.42	5.38	13.54	14.53	.15	15.61	.20	1.07	8.84	0.00	95.74
OESTIMATED COMPOSITIONS												
REACTANTS		59.13	.97	17.92	6.05	.09	2.72	4.77	4.04	2.55	.40	98.62
PRODUCTS		59.09	1.10	17.79	6.03	.08	2.64	4.84	4.53	2.75	.27	99.13
DIFFERENCES		.04	-.13	.13	.01	.00	.08	-.07	-.49	-.20	.13	

ORESIDUAL SUM OF SQUARES = .3451
DISTANCE BETWEEN TWO ESTIMATED COMPOSITIONS = .5874
O****** ****** ****** ****** ****** ******

-****** LEAST-SQUARES SOLUTION TO GENERALISED MIXING MODEL NO. 3 ******

O	AMOUNTS	SI	TI	AL	FEFE	MN	MG	CA	NA	K	P	TOTAL
REACTANTS USED												
1 2JG35	93.37	60.25	1.01	17.43	5.74	.09	2.27	4.81	4.51	2.75	.36	99.22
11 PART MELT	6.63	78.01	.08	12.89	1.11	.06	0.00	.25	4.73	1.64	.03	98.80
OPRODUCTS USED												
2 1JG80	76.15	64.57	.71	16.74	4.01	.06	1.63	2.84	4.70	3.57	.23	99.06
3 PLAGIOCLASE	15.14	60.48	0.00	24.30	.30	0.00	0.00	6.84	6.75	1.02	0.00	99.69
4 AMPHIBOLE	8.78	42.77	3.20	10.41	12.21	.02	13.78	11.51	2.59	.79	0.00	97.40
5 APATITE	.22	0.00	0.00	0.00	0.00	.07	.10	55.84	0.00	0.00	42.00	98.04
6 BIOTITE	-2.41	36.42	5.38	13.54	14.53	.15	15.61	.20	1.07	8.84	0.00	95.74
9 MAGNETITE	1.58	.43	.24	.08	98.56	0.00	.15	.36	0.00	0.00	0.00	99.82
10 SPHENE	.54	30.75	37.97	.69	1.77	0.00	0.00	27.77	0.00	0.00	0.00	98.95
OESTIMATED COMPOSITIONS												
REACTANTS		61.43	.95	17.13	5.43	.09	2.12	4.51	4.52	2.69	.34	99.19
PRODUCTS		61.37	.90	17.02	5.39	.06	2.08	4.48	4.25	2.73	.27	99.11
DIFFERENCES		.05	.05	.11	.04	.03	.04	.02	-.23	-.05	.07	

ORESIDUAL SUM OF SQUARES = .1070
DISTANCE BETWEEN TWO ESTIMATED COMPOSITIONS = .3272
O****** ****** ****** ****** ****** ******

TABLE 4.03 Results of major element modelling of the mixing of basic magmas with partial-melt, followed by fractional crystallisation.

TABLE 4.03 (continued)

-****** LEAST-SQUARES SOLUTION TO GENERALISED MIXING MODEL NO. 3 ******

O		AMOUNTS	SI	TI	AL	FEFE	MN	MG	CA	NA	K	P	TOTAL
REACTANTS USED													
1	1JG80	101.08	64.57	.71	16.74	4.01	.06	1.63	2.84	4.70	3.57	.23	99.06
9	PART MELT	-1.08	78.01	.08	12.89	1.11	.06	0.00	.25	4.73	1.64	.03	98.80
OPRODUCTS USED													
2	1JG9	80.78	67.32	.50	16.12	2.97	.03	1.06	2.18	4.60	3.91	.40	99.09
3	PLAGIOCLASE	12.75	61.06	0.00	23.81	.40	0.00	0.00	6.06	7.52	.80	0.00	99.65
4	AMPHIBOLE	2.30	42.77	3.20	10.41	12.21	.22	13.78	11.51	2.59	.79	0.00	97.47
6	BIOTITE	3.28	36.89	5.38	13.51	16.03	.16	13.90	.19	.69	9.11	0.00	95.86
7	MAGNETITE	.77	.43	.24	.08	98.56	0.00	.15	.36	0.00	0.00	0.00	99.82
8	SPHENE	.12	30.75	37.97	.69	1.77	0.00	0.00	27.77	0.00	0.00	0.00	98.95
OESTIMATED COMPOSITIONS													
	REACTANTS		64.42	.72	16.78	4.04	.06	1.65	2.37	4.70	3.59	.23	99.06
	PRODUCTS		64.40	.70	16.74	4.02	.03	1.63	2.84	4.76	3.53	.29	99.02
	DIFFERENCES		.03	.02	.04	.02	.03	.02	.03	-.06	.01	-.06	
ORESIDUAL SUM OF SQUARES =		.0164											
DISTANCE BETWEEN TWO ESTIMATED COMPOSITIONS =						.1281							
O******		******	******		******		******						

-****** LEAST-SQUARES SOLUTION TO GENERALISED MIXING MODEL NO. 1 ******

O		AMOUNTS	SI	TI	AL	FEFE	MN	MG	CA	NA	K	P	TOTAL
REACTANTS USED													
1	1JG9	73.90	67.32	.50	16.12	2.97	.03	1.06	2.18	4.60	3.91	.40	99.09
9	PART MELT	26.10	78.01	.08	12.89	1.11	.06	0.00	.25	4.73	1.64	.03	98.80
OPRODUCTS USED													
2	1JG61	52.36	71.04	.34	15.29	1.77	.04	.32	.88	4.85	5.12	.07	99.72
3	PLAGIOCLASE	26.81	62.41	0.00	23.43	.31	0.00	0.00	5.10	8.27	.77	0.00	100.29
6	BIOTITE	7.27	36.89	5.38	13.51	16.03	.16	13.90	.19	.69	9.11	0.00	95.86
7	QUARTZ	13.56	100.00	0.00	0.00	0.00	0.00	0.00	0.00	0.00	0.00	0.00	100.00
OESTIMATED COMPOSITIONS													
	REACTANTS		70.11	.39	15.28	2.48	.04	.78	1.68	4.63	3.32	.30	99.01
	PRODUCTS		70.17	.57	15.27	2.18	.03	1.18	1.84	4.81	3.55	.04	99.63
	DIFFERENCES		-.06	-.18	.01	.31	.01	-.40	-.17	-.17	-.23	.27	
ORESIDUAL SUM OF SQUARES =		.4695											
DISTANCE BETWEEN TWO ESTIMATED COMPOSITIONS =						.6852							
O******		******	******		******		******						

viscous magmas than pure fractional crystallisation. However, other processes, such as liquid fractionation (McBirney et al. 1985) cannot be ruled out.

The other stages of fractionation were also modelled in this manner, and some produced residual sums of squares (Table 4.03). However, the results are discounted as either:

1) There is a negative component present.

2) The amount of partial-melt used is negligable.

4.6 TRACE ELEMENT MODELLING

Trace element modelling has been approached in two ways. The initial approach is to use major element models as a basis for trace element modelling, in which the anticipated trace element concentrations (from major element models) are compared with the actual concentrations. The second approach is partly based on the major element models, but utilises the actual trace element concentrations of the rocks concerned to determine their distribution coefficients (KD) throughout the range of rocks.

4.6.1 Based on major element models

Table 4.04 compares the calculated concentrations with the actual concentrations of trace elements for the first stage of modelling, from 2JG1 to 1JG10. This was done by taking the percentage of residual liquids calculated in the least squares modelling. Rayleigh fractionation was assumed, and the concentrations of elements in the residual liquid

TABLE 4.04 Trace element modelling, assuming 55% fractional crystallisation of a starting composition 2JG1.
The fractionating assemblage consists of 32% augite, 59% plagioclase and 9% Fe-Ti oxides (as calculated using least squares major element modelling). Distribution coefficients were taken from weighted averages in Gill (1977) and Henderson (1982). All values are in ppm.

Element	2JG1 (parent)	1JG10	model
Ba	761	1750	1560
Cr	94	18	24
Ni	66	21	14
Rb	31	56	64
Sr	1547	1539	1440
V	191	122	37
Zn	93	75	66

were calculated using the equation:

$$\frac{Cl}{Co} = F^{(D-1)}$$

where

Cl is the concentration of the element in the residual liquid

Co is the concentration of the element in the original magma

F is the weight percent fraction of the liquid

D is the bulk distribution coefficient

The individual distribution coefficient values (KD) were taken from weighted averages (Gill 1977; Henderson 1982).

There are, however, large variations in experimentally determined KD values for trace element partitioning into minerals. Table 4.05 shows the maximum and minimum possible values of calculated trace element bulk distribution coefficients for all stages of modelling. These can be compared with the actual values calculated and shown in Table 4.06. All the observed trace element bulk distribution coefficients (Table 4.06) except V and Ce fall within the range, however, some are close to the limits.

The apparent relative 'compatibility' of Ce (i.e. it is behaving less incompatibly than is expected from Table 4.05) can be explained by the fractionation of sphene (which is not considered in the trace element modelling). However, the apparent relative 'incompatibility' of V (i.e. it is behaving more compatibly than is expected from Table 4.05), and the general variation in the data cannot be explained by such simple processes as the fractionation of accessory phases. This problem is not uncommon in other subduction-related suites (Luhr and Carmichael 1981; Mann 1983; Rutter 1985). The differences between calculated and actual concentrations for Rb, Sr, Cr, Ni and Ba, as well as their scatter in the variation diagrams, may well be due to the mobility of these elements in the presence

TABLE 4.05 The maximum and minimum bulk distribution coefficients that can be calculated using the available range range of experimental data for 45%, 29%, 20%, 16% and 9% residual melt fractions. Distribution coefficients were obtained from Gill (1977) and Henderson (1982).

% residual	D(Ba)		D(Cr)		D(Ni)	
melt (F)	max.	min.	max.	min.	max.	min.
45	.48	.03	27.62	1.60	4.27	.36
29	.91	.09	23.28	1.68	4.86	.32
20	.96	.09	21.04	1.46	4.17	.32
16	1.06	.10	19.96	1.49	4.11	.28
9	1.16	.11	19.44	1.51	4.94	.28

% residual	D(Rb)		D(Sr)		D(V)	
melt (F)	max.	min.	max.	min.	max.	min.
45	.38	.01	5.33	.79	11.43	2.42
29	.58	.01	5.32	.79	12.54	2.12
20	.55	.01	5.51	.84	12.94	2.82
16	.59	.01	5.52	.82	13.11	2.57
9	.62	.01	5.51	.82	12.95	2.38

% residual	D(Zn)		D(Ce)		D(Sm)	
melt (F)	max.	min.	max.	min.	max.	min.
45	1.75	1.05				
29	2.78	.96	.47	.05	1.13	.04
20	2.79	.96				
16	2.91	.88				
9	3.04	.87	.47	.06	1.17	.04

TABLE 4.06 Actual bulk distribution coefficients of the Glencoe series using weighted means (Gill 1977; Henderson 1982). Fractionating assemblages calculated by least squares modelling are used.

% residual melt (F)	D(Ba)	D(Cr)	D(Ni)	D(Rb)	D(Sr)	D(V)
45	0	3.06	2.43	.24	.99	1.56
29	.39	1.63	1.72	.48	1.19	1.41
20	.50	2.14	2.11	.40	1.38	1.74
16	.56	2.04	1.93	.46	1.32	1.73
9	.62	2.07	1.93	.46	1.75	1.95

% residual melt (F)	D(Zn)	D(Ce)	D(Sm)	D(Eu)	D(Yb)
45	1.27				
29	1.23	.99	.77	.91	.80
20	1.27				
16	1.20				
9	1.42	.61	.83	1.04	.87

of hydrothermal fluids (chapter 3). The variations in other elements may be due to either open-system magmatism, or source heterogeneity.

4.6.2 Based on actual data

The trace element data can also be modelled by calculating the KD for individual elements through the fractionating range. Again this was done by taking the residual liquids calculated in the least squares mixing models, and assuming Rayleigh fractionation. The results are shown in Table 4.06 and are graphically displayed in Figure 4.08. The KD for some elements, e.g. Rb, Sr and the R.E.E.'s consistently increase with fractionation and form a smooth curve as shown in Fig.4.08. Eu changes from being incompatible to becoming compatible, probably due to an increase in its uptake in plagioclase (maybe as a result of different oxygen fugacities).

Other elements show an ill-defined curve on Fig. 4.08, and their apparent KDs vary randomly with fractionation. This may be due to changes of the fractionating phases, but is more likely to be due to either hydrothermal alteration, open-system magmatism, or source heterogeneity.

4.7 SOURCE OF THE RING-INTRUSION MAGMAS

A detailed investigation into the ultimate source of the Glencoe magmas is beyond the scope of this study. However, previous workers have speculated upon the source of both the Lorne lavas (Thirlwall 1981, 1982), and the Etive igneous complex (Clayburn 1981; Clayburn et al. 1984; Frost and O'Nions 1985). The above studies have incorporated data from both the intrusive and extrusive suites from Glencoe, as it is generally believed that there is a close petrogenetic association between the Lorne and

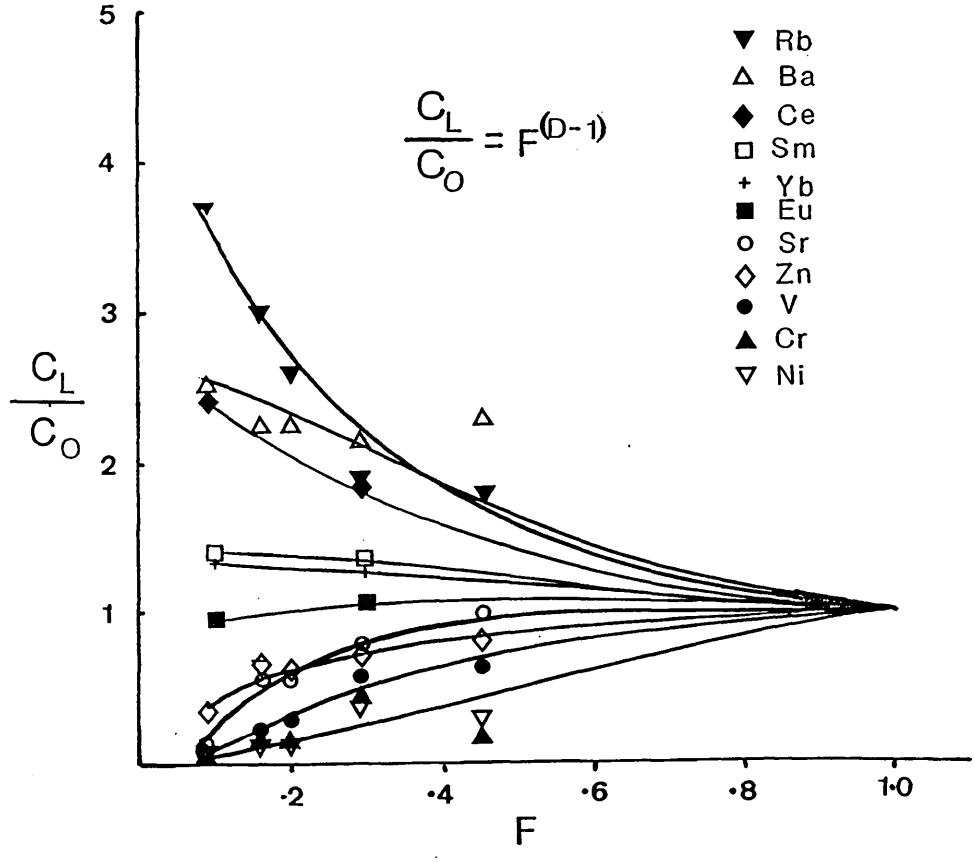

FIGURE 4.08 The actual variation of trace element concentrations (Cl/Co) relative to the residual melt fraction (F) assuming Rayleigh fractionation in a range of Glencoe igneous rocks. The melt fraction was calculated using least squares element modelling (Table 4.01). Individual bulk distribution coefficients are listed in Table 4.06.

Glencoe volcanics, and the Etive and Glencoe extrusives (Bailey 1960). It is also possible that the whole intrusive and extrusive suite of the Western Highlands is petrogenetically linked.

Thirlwall (1982) believes that primitive basalts (similar to L23) and andesites rich in Mg, Ni and Cr are primitive melts from the mantle, and that there has been selective contamination from the lower crust to produce the range of compositions of volcanic rocks present in Lorne. He proposed a layered mantle source, with the upper layer feeding eruptions in the Midland Valley, and the lower layer feeding the Lorne volcanics at this time. He also believed that subduction was still occurring beneath Scotland at the time of these eruptions. However, many of these theories concerning the spatial relationship between the Midland valley volcanics and Lorne must be considered in the light of more recent discussions concerning strike-slip faulting and suspect terranes (Bluck 1985; J. Leggett pers. comm.).

Clayburn (1981) and Clayburn et al. (1984) believe that the Etive source magma was a melt from an enriched mantle overlying a subducted slab, which mixed in a lower crustal reservoir with a lower crustal melt. For Etive (although perhaps not Glencoe) they suggested that the magmas were rapidly intruded, and that there was minor upper crustal contamination. However, Frost and O'Nions (1985) stressed the importance of Dalradian xenolith digestion in these rocks, particularly in the latter stages of intrusion, and proposed that there was a continental lithospheric source for the Etive rocks.

In section 4.5.3 it was noted that a potential source magma for the Glencoe rocks (as calculated in the addition-subtraction diagram) was very similar in composition to rock L23 (Thirlwall 1982), which is a primitive basalt from the Lorne region. It is commonly believed that the Glencoe and Lorne volcanics have a similar source (Bailey 1960; Thilwall 1982), and it is also likely that all of the

igneous rocks in this area are genetically related. Hence, an attempt has been made to link the primitive basalt from the Lorne volcanics with the most basic of the Glencoe intrusive rocks.

In trying to establish a link between the Lorne basalts and the Glencoe intrusives, the least squares mixing model was used (LeMaitre 1979). Various fractionation combinations of augite, plagioclase, olivine and opaque minerals were tried, but none was successful (Table 4.07).

The influence of partial-melt additions upon a fractionating magma chamber beneath Glencoe has already been considered, and it is possible that partial-melt material was a significant factor in the generation of some of the rock compositions. The introduction of substantial amounts of basaltic magma into the upper crust is likely to induce such partial-melting. Hence least squares mixing models were used to determine the effect of partial-melt being mixed with a Lorne basalt (Table 4.08). The direct mixing of partial-melt with a Lorne basalt to produce 2JG1 was not successful. However, the mixing of a partial-melt with a Lorne basalt, followed by the fractionation of augite, plagioclase and opaque minerals, produced a low residual sum of squares.

Trace element modelling of this process was unsuccessful (Table 4.09). This may be due to different chemical conditions affecting the partitioning of certain elements in minerals. Alternatively, any one of the reasons discussed in section 4.6 may be responsible for the lack of correlation between major and trace-element modelling.

4.8 SUMMARY AND CONCLUSIONS

A summary of the geochemistry of the intrusive rocks in Glencoe is listed below. Many of the

TABLE 4.07 Results of major element fractional crystallisation modelling of the Glencoe magma source.

```
-****** LEAST-SQUARES SOLUTION TO GENERALISED MIXING MODEL NO.  1 ******
O                      AMOUNTS        SI      TI      AL      FE      MN      MG      CA      NA      K       P     TOTAL
 REACTANTS USED
    8   LCRNE BAS       100.00      48.90    1.54   17.47    9.87     .14    7.19   10.57    2.70    1.10     .40   99.38
OPRODUCTS USED
    1   GABBRO(2JG1)    -16.50      52.61    1.35   17.75    8.61     .14    4.82    8.01    3.51    1.24     .11   98.34
    3   AUGITE           38.04      54.51     .30    1.89   10.53     .19   18.74   11.02    1.73     .40     .00   99.31
    5   PLAGIOCLASE      68.73      54.26    0.00   27.73     .57    0.00    0.00   11.39     .05     .04     .00   99.34
    6   MAGNATITE         5.61       .43     .24     .08   88.56    0.00     .15     .36     .00     .00     .00   89.82
    7   ILMENITE          4.12      3.88   46.25     .52   39.10     .06     .43    2.55     .00     .00     .00   95.79
OESTIMATED COMPOSITIONS
        REACTANTS                  48.90    1.54   17.47    9.87     .14    7.19   10.57    2.70    1.10     .40   99.82
        PRODUCTS                   49.53    1.81   16.87   10.12     .18    6.36   10.82    3.55     .03     .00   99.27
            DIFFERENCES             -.63    -.27     .60    -.25    -.04     .83    -.25    -.85    1.07     .41
ORESIDUAL SUM OF SQUARES =      3.7138
 DISTANCE BETWEEN TWO ESTIMATED COMPOSITIONS =      1.9271
O******      ******      ******      ******      ******      ******
-****** LEAST-SQUARES SOLUTION TO GENERALISED MIXING MODEL NO.  2 ******
O                      AMOUNTS        SI      TI      AL      FE      MN      MG      CA      NA      K       P     TOTAL
 REACTANTS USED
    8   LCRNE BAS       100.00      48.90    1.54   17.47    9.87     .14    7.19   10.57    2.70    1.10     .40   99.38
OPRODUCTS USED
    1   GABBRO(2JG1)    -25.60      52.61    1.35   17.75    8.61     .14    4.82    8.01    3.51    1.24     .11   98.34
    3   AUGITE           30.76      54.51     .30    1.89   10.53     .19   18.74   11.02    1.73     .40     .00   99.31
    5   PLAGIOCLASE      76.47      54.26    0.00   27.73     .57    0.00    0.00   11.39     .05     .04     .00   99.34
    6   MAGNATITE         1.72       .43     .24     .08   88.56    0.00     .15     .36     .00     .00     .00   89.82
    7   ILMENITE          4.14      3.88   46.25     .52   39.10     .06     .43    2.55     .00     .00     .00   96.92
   12   OLIVINE          12.50     34.04     .43     .91   41.83     .68   20.32     .81    0.00    0.00     .00   99.02
OESTIMATED COMPOSITIONS
        REACTANTS                  48.90    1.54   17.47    9.87     .14    7.19   10.57    2.70    1.10     .40   99.82
        PRODUCTS                   49.22    1.72   17.38   10.02     .23    7.09   10.26    3.50    -.06     .00   99.36
            DIFFERENCES             -.32    -.18     .09    -.15    -.09     .10     .31    -.80    1.16     .40
ORESIDUAL SUM OF SQUARES =      2.4760
 DISTANCE BETWEEN TWO ESTIMATED COMPOSITIONS =      1.5735
O******      ******      ******      ******      ******      ******
-****** LEAST-SQUARES SOLUTION TO GENERALISED MIXING MODEL NO.  3 ******
O                      AMOUNTS        SI      TI      AL      FE      MN      MG      CA      NA      K       P     TOTAL
 REACTANTS USED
    8   LCRNE BAS       100.00      48.90    1.54   17.47    9.87     .14    7.19   10.57    2.70    1.10     .40   99.38
OPRODUCTS USED
    1   GABBRO(2JG1)     22.74      52.61    1.35   17.75    8.61     .14    4.82    8.01    3.51    1.24     .11   98.34
    5   PLAGIOCLASE      50.48      54.26    0.00   27.73     .57    0.00    0.00   11.39     .05     .04     .00   99.34
    6   MAGNATITE        -5.72       .43     .24     .08   88.56    0.00     .15     .36     .00     .00     .00   89.82
    7   ILMENITE          3.26      3.88   46.25     .52   39.10     .06     .43    2.55     .00     .00     .00   96.92
   12   OLIVINE          29.24     34.04     .43     .91   41.83     .68   20.32     .81    0.00    0.00     .00   99.02
OESTIMATED COMPOSITIONS
        REACTANTS                  48.90    1.54   17.47    9.87     .14    7.19   10.57    2.70    1.10     .40   99.82
        PRODUCTS                   49.41    1.93   16.31   10.11     .33    7.04    7.87    3.35     .45     .03   96.83
            DIFFERENCES             -.51    -.39    -.84    -.24    -.19     .15    2.70    -.65     .65     .37
ORESIDUAL SUM OF SQUARES =      9.4708
 DISTANCE BETWEEN TWO ESTIMATED COMPOSITIONS =      3.0775
O******      ******      ******      ******      ******      ******
```

		AMOUNTS	SI	TI	AL	FE	MN	MG	CA	NA	K	P	TOTAL
****** LEAST-SQUARES SOLUTION TO GENERALISED MIXING MODEL NO. 6 ******													
REACTANTS USED													
1	GABBRO(2JG1)	100.00	52.61	1.35	17.75	8.61	.14	4.82	8.01	3.51	1.24	.30	98.34
PRODUCTS USED													
8	LORNE BAS	85.29	48.90	1.54	17.47	9.87	.14	7.19	10.57	2.70	1.10	.40	99.88
9	PART MELT	14.71	78.01	.08	12.89	1.11	.06	0.00	.25	4.73	1.64	.03	98.80
ESTIMATED COMPOSITIONS													
	REACTANTS		52.61	1.35	17.75	8.61	.14	4.82	8.01	3.51	1.24	.30	98.34
	PRODUCTS		53.18	1.33	16.80	8.58	.13	6.13	9.05	3.00	1.19	.35	99.72
	DIFFERENCES		-.57	.02	.95	.03	.01	-1.31	-1.04	.51	.06	-.05	
RESIDUAL SUM OF SQUARES = 4.3136													
DISTANCE BETWEEN TWO ESTIMATED COMPOSITIONS = 2.0769													
******		******	******		******		******						
****** LEAST-SQUARES SOLUTION TO GENERALISED MIXING MODEL NO. 7 ******													
		AMOUNTS	SI	TI	AL	FE	MN	MG	CA	NA	K	P	TOTAL
REACTANTS USED													
8	LORNE BAS	86.47	48.90	1.54	17.47	9.87	.14	7.19	10.57	2.70	1.10	.40	99.88
9	PART MELT	13.53	78.01	.08	12.89	1.11	.06	0.00	.25	4.73	1.64	.03	98.80
PRODUCTS USED													
1	GABBRO(2JG1)	69.09	52.61	1.35	17.75	8.61	.14	4.82	8.01	3.51	1.24	.30	98.34
3	ALGITE	15.00	54.51	.30	1.89	10.53	.19	18.74	11.02	1.73	0.00	.10	98.99
5	PLAGIOCLASE	14.84	54.26	0.00	27.73	.57	0.00	0.00	11.39	5.05	.70	.10	99.80
6	MAGNATITE	.77	.43	.24	.08	98.56	0.00	.15	.36	0.00	0.00	0.00	99.82
7	ILMENITE	.31	3.88	46.25	.52	39.10	3.06	.43	2.55	0.00	0.00	0.00	95.79
ESTIMATED COMPOSITIONS													
	REACTANTS		52.84	1.34	16.85	8.68	.13	6.22	9.17	2.97	1.17	.35	99.71
	PRODUCTS		52.59	1.12	16.66	8.49	.13	6.14	8.89	3.43	.91	.21	99.56
	DIFFERENCES		.25	.22	.19	.20	-.01	.07	.29	-.46	.27	.14	
RESIDUAL SUM OF SQUARES = .5733													
DISTANCE BETWEEN TWO ESTIMATED COMPOSITIONS = .7571													
******		******	******		******		******						

TABLE 4.08 Results of major element modelling of partial melt mixing with a basalt Glencoe magma source, followed by fractional crystallisation.

TABLE 4.09 Trace element modelling assuming 40% fractional crystallisation from a parent magma composed of 86.5% L23 (Lorne basalt), 13.5% partial-melt. The fractionating assemblage consists of 49% augite, 48% plagioclase and 3% Fe-Ti oxides as calculated using least squares major element modelling. Distribution coefficients were taken from Gill (1977) and Henderson (1982). All values are in ppm.

Element	parent	2JG1	model
Ba	619	761	987
Cr	129	94	22
Ni	80	66	25
Rb	29	31	47
Sr	976	1547	1025
V	178	191	142
Zn	61	93	76

important points can be best summed up using chondrite-normalised incompatible element plots (Fig. 4.09).

1) The rocks are calc-alkaline, and have evolved from subduction-related magmas, as exemplfied by troughs at Nb and Ta, and peaks at Rb, K and Sr (Fig. 4.09A) (Thompson et al. 1984).

2) Fractional crystallisation is the dominant process which operated in the generation of the range of compositions for the ring-intrusion rocks.

3) Major element modelling has shown that the fractionating assemblage was dominated by plagioclase. Augite was removed early in the sequence, but was subsequently superceded by biotite and amphibole as fractionating phases. Magnetite and ilmenite were removed in the earlier stages of fractionation, with Ti continuing to become depleted by the removal of sphene. This has led to a steepening in the La/Ce ratio (Fig. 4.09A). Apatite was removed in the intermediate stages, as is shown by the initial incompatibility, followed by depletion of P2O5.

4) Trace element modelling does not concur with the results produced by the major element modelling. This is due to, a) only Rayleigh fractionation being considered. This does not allow for the mixture of large phenocrysts with trapped interstitial melt, as occurs in all the Glencoe rocks. b) The effects of cation exchange caused by hydrothermal fluid circulation.

5) The parental magma to the ring-intrusives is considered to be basaltic, and of a similar composition to basalts from the Lorne Lava Plateau. This source has been contaminated by upper crustal partial-melt material prior to fractionation.

6) The rhyolites are not derived by fractional crystallisation of the main magma batch represented by the ring-intrusives. However, the elemental pattern is still typical of a calc-alkaline magma (Fig. 4.09B).

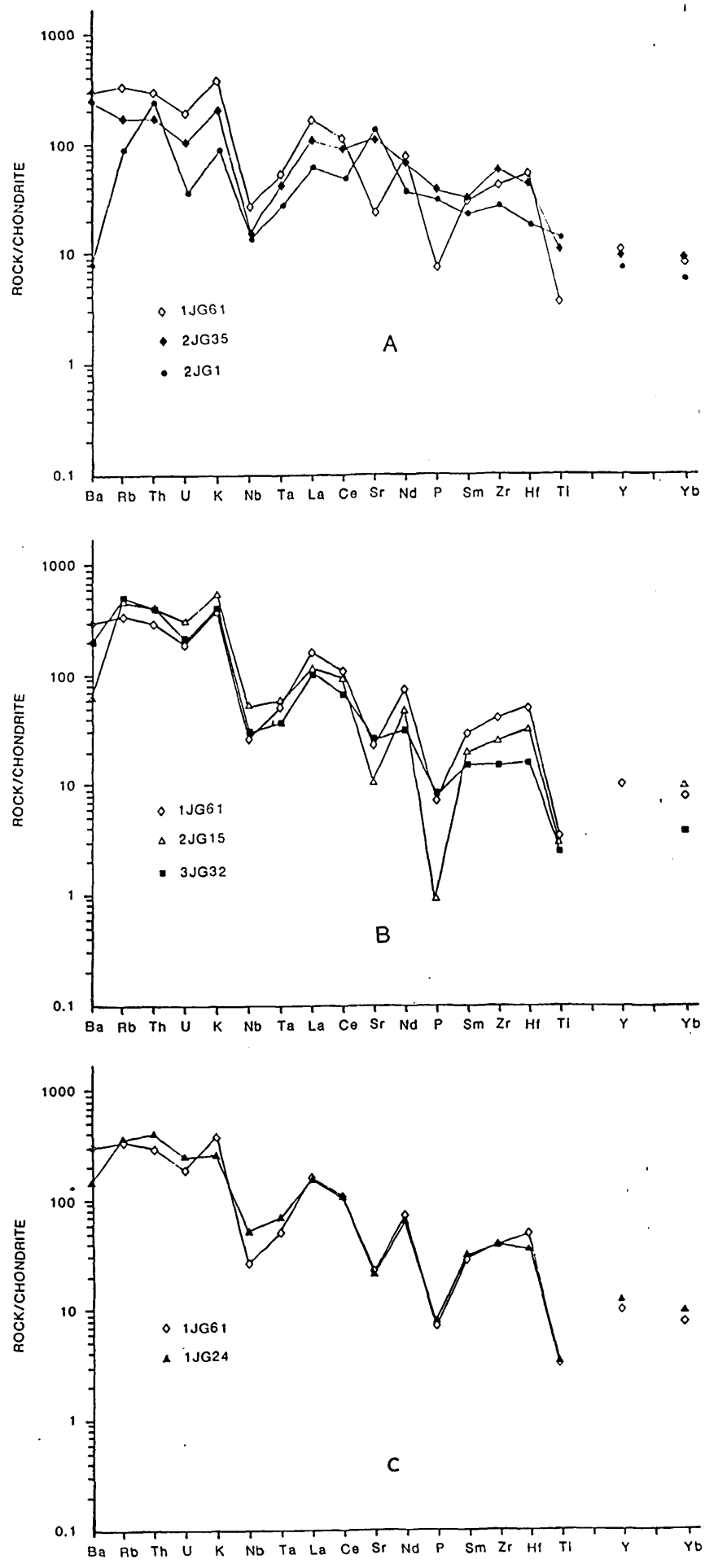

FIGURE 4.09 Chondrite-normalised multi-element plots of a selection of Glencoe igneous rocks. Gabbro (2JG1), diorite (2JG35), granophyric granite (1JG61, 2JG15), rhyolite (3JG32), fault felsite (1JG24).

7) The more basic members of the Etive granitoid suite show similar chemical characteristics to the ring-intrusion magmas. However, the more acidic rocks do not.

In conclusion, it seems that a parental basalt magma was injected into the upper crust to form a high level magma-chamber. As a result of the input of hot magma, partial-melting of the country-rock occurred. The partial-melt mixed with the basalt magma , which then evolved into a range of compositions by a process of fractional crystallisation. An open system was operating, with the magma being periodically tapped from above, and probably refilled from below. Following consolidation of the magma, circulating hydrothermal fluids altered many minerals, and changed the concentrations of mobile elements in the rocks.

The rhyolites were not derived by a process of fractional crystallisation from the main magma batch sampled, and may have come from a separate source.

Different processes may have also been operating in parts of the magma chamber, such as liquid fractionation (McBirney et al. 1985). This is common in calc-alkaline magma chambers, and is caused by the rapid removal of buoyant rhyolitic magma up the walls of the chamber. It is likely that mixing between this rhyolitic fraction and partial-melt material would have occurred, and this may have been variable, which would produce a range of trace element concentrations.

Alternatively, other complex processes may have been operating, such as the existence of different fractionation cells, which would produce a spread of data (Fridrich and Mahood 1987).

CHAPTER 5

EARLY IGNEOUS ACTIVITY ASSOCIATED WITH THE RING FAULT: PART I, AN-T-SRON

5.1 INTRODUCTION

In the western part of the Glencoe cauldron the fault intrusion expands into a crescent-shaped body, approximately 2km wide. The major part of this body forms the western side of An-t-sron (Fig. 5.01). The eastern, concave margin is adjacent to the ring fault (Plate 5.01), and has undergone later shearing. This boundary is sharp, and faulting is thought to have occurred after the intrusion because there is no evidence of contact metamorphism east of the fault within the downfaulted block. This is in contrast to the western margin of An-t-sron pluton (see section 5.3)

The adjacent country rock west of the intrusion is a series of folded Dalradian metasediments of variable composition (Roberts and Treagus 1977; Soper and Anderton 1984). The pluton intrudes mainly pelites of the Leven Schist series, but also calc-schists and quartzites (Fig. 1.03). Regional metamorphism is middle to upper greenschist facies (Fettes 1979), with some garnet-bearing pelites. The structure is complex, with displacement occurring early in the history between the Dalradian units along the Ballachulish slide (Roberts and Treagus 1977). The slide has been folded, serving to intensify the complexity, and obscuring relationships between individual units (Fig. 5.01).

PLATE 5.01 A view of An-t-sron showing the ring-fault and its relationship to the ring-intrusion, Dalradian basement and Devonian volcanics.



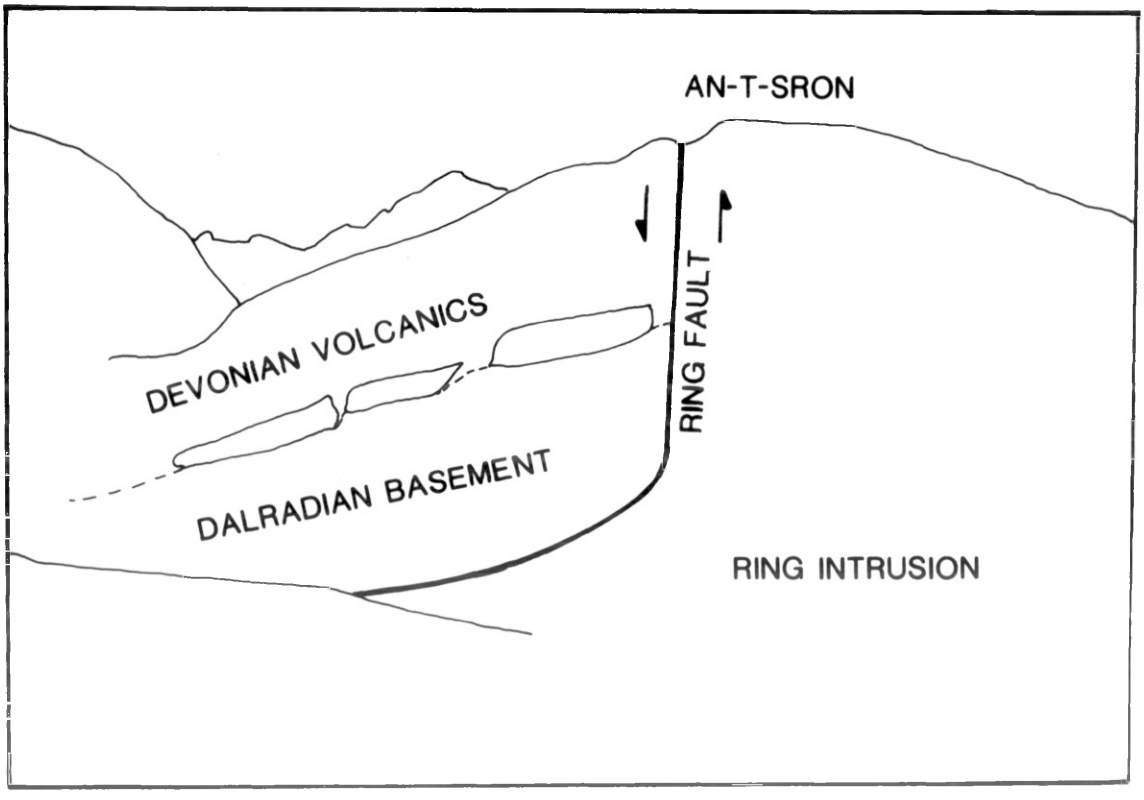
AN-T-SRON
RING FAULT
DEVONIAN VOLCANICS
DALRADIAN BASEMENT
RING INTRUSION

5.2.1 Introduction

The petrography, mineral chemistry and geochemistry of all the ring-intrusion rocks have been discussed in chapters 3 and 4, including the intrusive rocks of An-t-sron. It is believed that the main An-t-sron intrusives were derived from the same fractionating magma chamber as the other ring-intrusion rocks. However, at An-t-sron the intrusion is wider, and has very different marginal relationships from the rest of the ring-intrusion. Small, pink, felsitic intrusions are also unique to the region. It is with these points in mind that the An-t-sron region has been examined in more detail than other parts of the Glencoe intrusion.

5.2.2 Field relationships

The relationships in time and space between intrusions of different composition are difficult to discern. Boundaries between the diorites and tonalites appear to be gradational. However, the diorites are the least altered of all of the intrusive rocks at An-t-sron, hence it is inferred that they are the youngest.

There is evidence in the River Coe to suggest that the more granitic intrusions are older than the tonalite (G.R. NN137567) (Fig. 5.02). A small finger of this rock-type has intruded quartzite, which was then taken up as a xenolith within the main An-t-sron tonalite. It is interesting to note that this granitic rock-type is similar to the "early fault-intrusion" described by Bailey and Maufe (1916) and Bailey (1960) (chapters 1,2).

The distribution of the different rock-types within An-t-sron intrusion appears to be fairly random. The gradational boundaries between rocks of

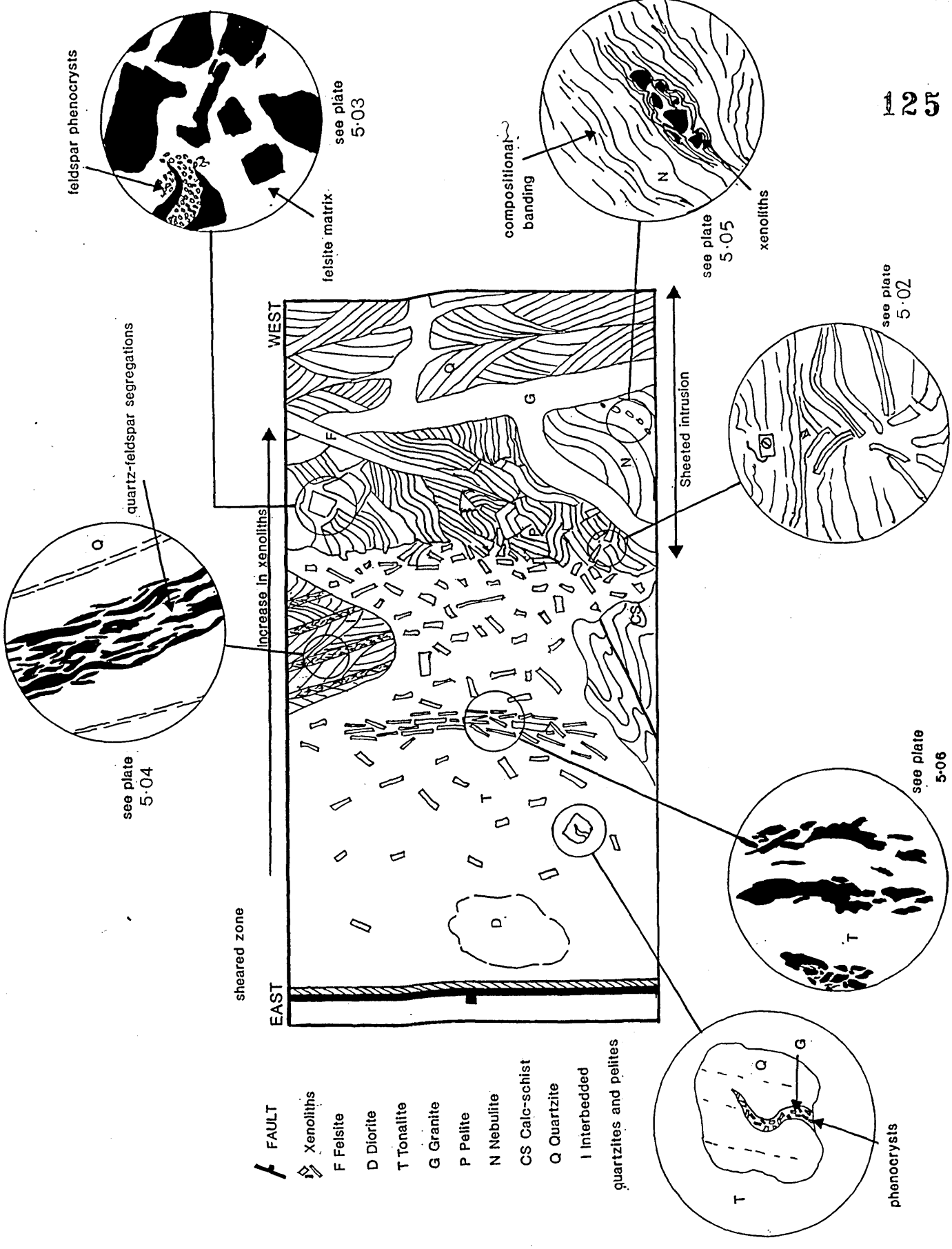

FIGURE 5.02 A schematic diagram of the An-t-sron area, showing the different field relationships between the intrusion and the country-rock. Five of the smaller individual sketches are illustrated in plates 5.02 to 5.06, the black material in these sketches represents pelite. Although the diagram is not to scale, these features are seen over a stretch approximately 2Km long.



PLATE 5.02 The fragmentation of a pelitic xenolith within tonalite as shown in Fig. 5.02. Note the fractured fold hinge.



PLATE 5.03 The relationship between felsite, pelite and tonalite in the River Coe, as shown in Fig. 5.02.



PLATE 5.04 A pelitic band within flaggy quartzites as shown in Fig. 5.02. Note the segregation of quartz and feldspar from the pelite.

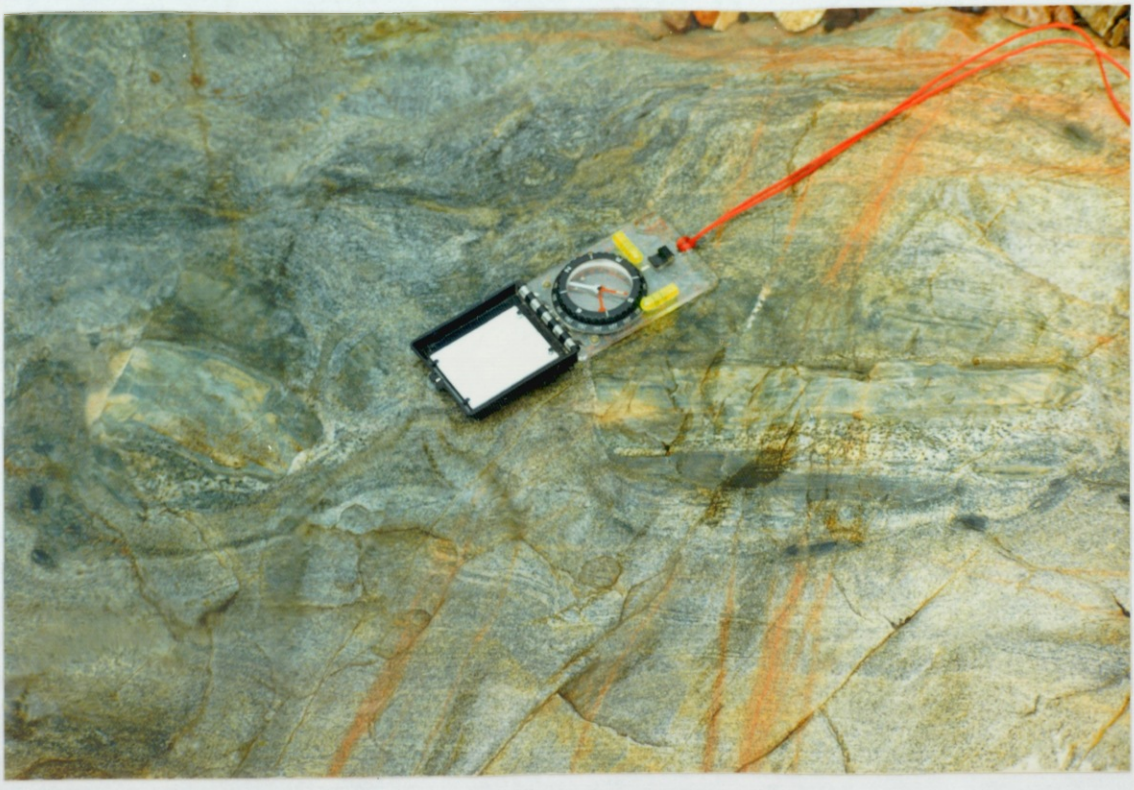

PLATE 5.05 Foliated 'nebulite' enclosing two xenoliths. These xenoliths are part of a chain of xenoliths which run parallel to the foliation, as shown in Fig. 5.02.

different composition make mapping unfeasible. In general, however, tonalite is found in the centre of the intrusion. Diorite is found in small pockets near the eastern, faulted margin. The granites are found around the western margin, and form sheeted intrusions along joints and bedding planes within the country-rock (e.g. 1JG61). Many of the field relationships described in this section and in section 5.3 are summarised in a schematic sketch diagram of the area (Fig. 5.02, Plates 5.02 - 5.06).

5.2.3 Xenoliths

In the greater part of the intrusion pelitic xenoliths are present, becoming more abundant towards the western margin. No volcanic or mafic cognate xenoliths have been observed. Quartzite xenoliths can be common, usually in close proximity to quartzite country rock. The increase in xenoliths and the appearance of a sheeted margin appear to be complementary. There is a gradational area between the sheets and the main body of the intrusion where neither the intrusion nor the metasediments can be considered to be the 'host rock'. An example of this in the River Coe (G.R. NN136567) shows concentrated bands of aligned xenoliths parallel to the strike of the country rock (Plate 5.06). Some xenoliths seem to be 'peeling off', and becoming incorporated in the main part of the intrusion. This may represent the 'in situ' disintegration of a sheet of wall-rock that passively became deta ched and incorporated in the intrusion. Further away from the intrusion, interconnecting sheets enclose large blocks of country rock (e.g. G.R. NN130567). Some large quartzite blocks outcrop nearer the centre of the intrusion, just south of the A82 road (G.R. NN135563). Again these blocks seem to be in structural continuity with the country-rock, indicating little or no rotation or convective movement of the blocks. However structural

PLATE 5.06 The alignment of pelitic xenoliths as shown in Fig. 5.02. X = xenolith, T = tonalite.

PLATE 5.07 Photomicrograph in plane polarised light of a contact metamorphosed calc-schist (3JG56). Q = quartz, P = phlogopite, W = wollastonite, D = diopside.

PLATE 5.08 Photomicrograph in plane polarised light of a contact metamorphosed pelite (3JG10). S = sillimanite, C = corundum.

PLATE 5.09 Photomicrograph in crossed polars of a granitic pod (4JG2). Q = quartz, M = muscovite, P = plagioclase, K = alkali feldspar.

PLATE 5.10 Photomicrograph in crossed polars of a thin felsite band in sample 3JG10. Q = quartz, K = alkali feldspar. Note the euhedral feldspar crystals enclosed in quartz.


5.06
X


5.07
1mm
W
Q
P
D

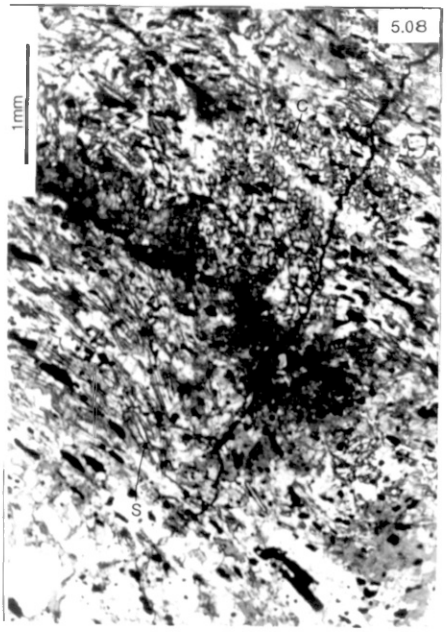
5.08
1mm
C
S

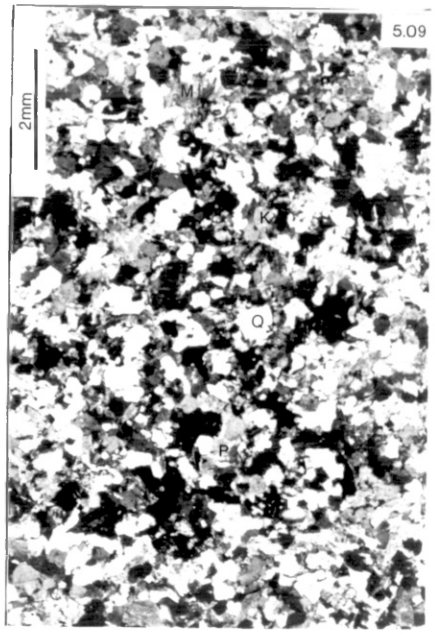
5.09
2mm
M
K
Q
P

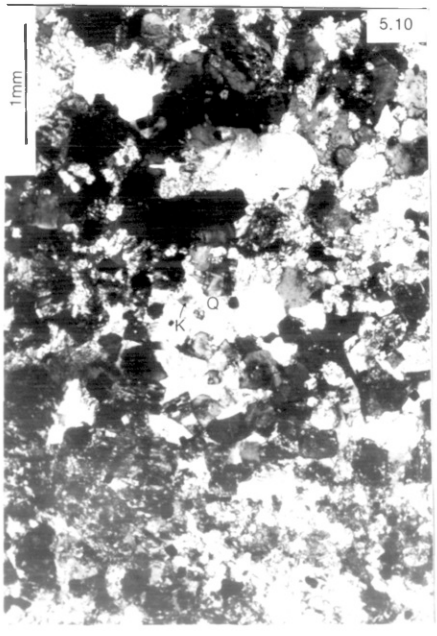
5.10
1mm
K
Q

complexities associated with the Ballachulish slide have obscured many of these features.

5.2.4 The felsites

Felsite intrusions form significant, although volumetrically unimportant, intrusive bodies. These range in width from 1cm to 40cms. When intruding quartzites and calc-schists they occur as dykes. However, in the pelites they occur as small, irregular bodies, often associated with brecciation of the country-rock. The significance of this will be discussed in section 5.5. The felsites are composed mainly of quartz and feldspar, and primary muscovite is common, although it is only found as a secondary mineral in the main part of the intrusion (chapter 2,3). There are cavities lined with drusy quartz and feldspar present in the felsites, but again these are not found in the main part of the intrusion.

5.2.5 Relationship between intrusion and the marginal breccias

As mentioned previously, brecciation of the pelitic country-rock occurs in some marginal areas. Complex intrusive relationships between the brecciated pelite, the tonalitic ring-intrusion and felsitic bodies have been mapped in detail on the southwestern side of An-t-sron (Bussell, 1979). An explosive origin for the breccia has been invoked, and the whole series interpreted as the interaction of felsic intrusion, brecciation, followed by tonalitic intrusion. Thermal metamorphism was thought not to be important. Bussell has also recognised the lack of transport of the breccia blocks, and refers to them being 'jumbled up essentially in situ'.Many of the brecciated margins seem to grade into xenolith-rich intrusion, similar to the marginal sequences seen in the River Coe (section 5.3.5).

5.3 CONTACT METAMORPHISM OF THE ADJACENT COUNTRY ROCK.

5.3.1 Dalradian metamorphism

Regional metamorphism of the Dalradian rocks in this part of the Highlands was of middle to upper greenschist facies (Fettes 1979). As a result chlorite and biotite had grown in the pelites, with occasional small garnets. The steeply-dipping garnet isograd is situated just to the west of An-t-sron (Fig. 1.04).

In the calc-schists, phlogopite is present, and there has been recrystallisation of calcite and dolomite. Recrystallisation has also occurred in the quartzites.

5.3.2 The calc-schists

The calc-schist (Ballachulish Limestone) is a siliceous marble of variable composition. Exposures in the small crossroads quarry (G.R. NN138567) show that the rock had behaved in a very plastic manner, but was later cut by brittle, extensional fractures. Different compositional bands display intimate interfingering, and mixing with fingers of acidic, igneous material. These features totally overprint Dalradian structures and textures. In thin section the growth of diopside, phlogopite and wollastonite is seen, again overprinting the regional metamorphic textures (Plate 5.07). Rare forsterite may also be observed in certain rock compositions. On a larger scale,the development of phlogopite-rich and phlogopite-poor bands is evident. These represent a regionally developed Dalradian texture, but the segregation is accentuated, and more phlogopite is developed. Despite compositional segregation, the

rock has not undergone partial melting.

5.3.3 The quartzites and pelites

In the quartzites, the only evidence of heating is the growth of large alkali feldspars in arkosic bands (though even these may be detrital). The rock is massive, showing no evidence of pervasive deformation, but like the calc-schists has undergone brittle, extensional fracture. This may be a response to ballooning of the pluton, but is more likely to be related to the regional extensional regime.

As the proportion of pelitic material begins to increase, the response of the rock-type to heat changes. Plate 5.02 shows a pelitic band within the quartzite. The quartzite shows no effect of being heated, but the pelite is disrupted, and quartz and feldspar have started to segregate. These segregations often occur in boudinaged veins in close association with the quartzite. As the country rock becomes increasingly pelitic, the amount of quartz and feldspar segregation increases. These segregational and ductile features are displayed by large pelitic xenoliths, and become well developed in the Leven Schist group of pelites. The restite bands contain plagioclase, biotite, sillimanite (fibrolitic and prismatic), corundum and cordierite (Plate 5.08). No andalusite is observed. The segregated material, typical of granite minimum melt, is composed of euhedral quartz and alkali-feldspar, commonly displaying polygonal grain boundaries (Plate 5.09). Drusy cavities are often present, aswell as muscovite. In places, quite large segregations are present. These are similar in mineralogy, colour and texture to the felsites previously described (section 5.2.4). This implies that the felsites may be a product of partial-melting.

5.3.4 Rocks of uncertain origin (nebulite)

In some areas (G.R. NN132565), the partially-melted rocks described above grade into a foliated, crystalline rock called nebulite . The crystalline texture suggests that it is a plutonic igneous rock, but the foliation, picked out mainly by biotites, suggests that the rock has a metasedimentary origin, especially as the foliation i in structural continuity with the local Dalradian rocks. On one part of the outcrop there is a trail of xenolith-like features (Plate 5.05) within the foliated, crystalline rock. The mineralogy of this crystalline rock is essentially the same as the partially melted pelites. In thin-section, there are small patches where one can see the initiation of partial-melting (Plate 5.10). A quartz-feldspar segregation can be observed, where the minerals are fresh and recrystallised, with polygonal grain boundaries. This type of segregation is on a very small scale, and only visible in thin-section. It seems that in this particular area the rock composition is similar to the granite minimum melt. The rock has therefore become totally recrystallised without undergoing obvious partial-melting. This accounts for the 'ghost' foliation, and the gradation from migmatite. On a smaller scale, compositional differences between bands is shown by localised partial-melting and 'xenolith' formation. It is likely that the train of xenoliths (Plate 5.05), represents an original sedimentary band of a more refractory composition - hence the crystalline rock is enclosing xenoliths of itself.

5.3.5 Breccias

Evidence for partial-melting ceases at approximately 200m away from the main intrusion. Temperatures were not high enough for sillimanite-corundum assemblages to form, with

andalusite being the aluminium silicate phase present. In these lower temperature areas west of the intrusion (G.R. NN126558) brecciation of the pelites is common. The brecciated bodies are quite large and totally structureless. Within 200m of the intrusion they are intimately associated with igneous material (Bussell 1979). Two types of breccia are seen:

(1) The first occurs in more distal areas to the south of the region (Fig. 5.01). Individual breccia clasts are sub-rounded and 2-4cm in size. The clast-to- matrix ratio is high, with an interstitial matrix composed of fine-grained quartz and phyllosilicates, presumably derived from the country rock. These are referred to as explosion breccias.

(2) The second occurs nearer the intrusion and at its margins. Clasts vary in size, with some up to 20cm in length. They are elongate, and can be seen breaking-off from the country-rock at fold hinges. These clasts are breaking up along lines of partial melt segregation (Plate 5.11). These are referred to as melt breccias. Much of the matrix is igneous material, with little or no fine-grained quartz.

At some outcrops on An-t-sron the clasts are smaller, and the rock seems to be a mixture of (1) and (2). The distal breccias in the lower grade rocks have many similarities with the explosion breccias described in Chapter 6 (Hardie 1963).

A small area of the brecciated margin on An-t-sron has been mapped by Bussell (1979) in which both breccia types are exposed. Bussell divides the breccias into four groups based on clast size and the type of matrix (i.e. crushed quartzite, tonalite or felsite). Ductile deformation and contact metamorphism of the country-rock by the An-t-sron intrusion are not considered by Bussell, despite recording sillimanite-andalusite-cordierite assemblages. Bussell notes that the felsites are "true granite in composition", but believes their origin to be from a gravity-stratified magma-chamber. As a result, Bussell has postulated a rather

disjointed series of brecciation events, interspersed with tonalitic and felsitic permeation and intrusion. However, if the brecciation and felsite 'intrusion' are considered interactively (i.e. the formation of a melt-breccia due to quartz and feldspar segregation), the picture becomes easier to comprehend.

5.3.5 Summary

Figure 5.03 shows the estimated pressure and temperature field for the country rock in the vicinity of An-t-sron intrusion. The wollastonite and diopside stability curves assume 0.4 XCO2 in the calc-schists. Although andalusite is recorded at distances greater than 200m away from the intrusion margin, sillimanite is the aluminium silicate phase present close to the intrusion. Hence pressures in excess of 2Kb prevailed, although the complete lack of kyanite gives a maximum of 4Kb pressure. The presence of cordierite further constrains the maximum pressure, to about 3.5 Kbars. Temperatures grade away from the intrusion, but wollastonite, sillimanite and corundum are found up to 200m from the margin, in conjunction with partial melting. This gives a minimum of 650°C (Tuttle and Bowen 1958), although the extent of sillimanite development and partial melting suggests much higher temperatures.

Clearly the regional greenschist facies metamorphism (Fettes 1979) has been overprinted by the low P, high T assemblages, suggesting erosion and uplift, plus a strong thermal input. This requires time, and a large heat source, namely magma. The only major igneous event in the area since the end of regional metamorphism, is the Lower Devonian igneous activity, leaving little doubt that the textures and assemblages seen were caused by the intrusion at An-t-sron.

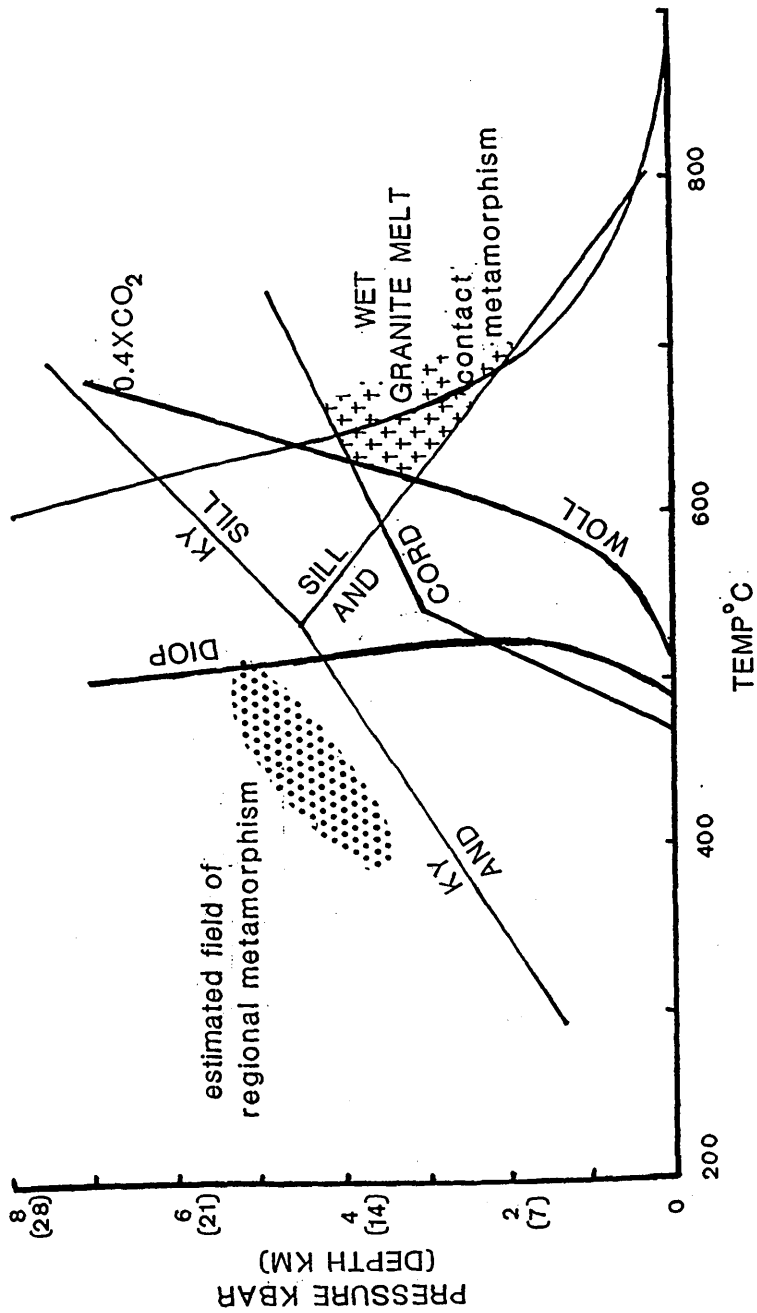

FIGURE 5.03 Petrogenetic grid demonstrating the stability limits of cordierite, sillimanite, andalusite, diopside, wollastonite and the wet granite solidus. The shaded areas represent the estimated pressure and temperature conditions at An-t-sron during regional and contact metamorphism associated with An-t-sron intrusion. Stability limits are taken from Hyndman (1972).

5.4.1 Range of composition

The geochemistry of the ring-intrusion as a whole has been discussed in chapter 4. However, in addition to the main ring-intrusion at An-t-sron, pink felsite bodies occur, with a composition close to the granite minimum melt (Fig. 5.04).

There are three possible reasons for the variation in the composition of the intrusion.

(1) Magma fractionation in a convective-cooling pluton, such as the magma chamber beneath the Glencoe cauldron. The rocks exposed range from dioritic gabbro, to high-Si rhyolite (representative of the felsites).

(2) Excessive heating of the country rock by magmatic intrusion producing partial-melts (i.e. the felsites).

(3) There may be a multiple source for the magmas. For example, the felsites could be associated with the later Etive dyke swarm, and having no relation to the ring-intrusion.

The third explanation is unlikely, as (a) the Etive dykes occur as discrete sheets, and do not occur as amorphous, coalescing bodies, as seen at G.R. NN134566. (b) The mineralogy and textures of the Etive dykes are totally different from those of the An-t-sron felsites.

5.4.2 Evidence for fractional crystallisation

The chemical evidence discussed in chapter 4 supports a fractional crystallisation process to have been responsible for the variation in the composition of the ring-intrusion. In addition, many of the chemical plots indicate that this is the case for the felsites aswell (Figs. 5.05, 5.06, 5.07). The most obvious feature is the negative correlation between

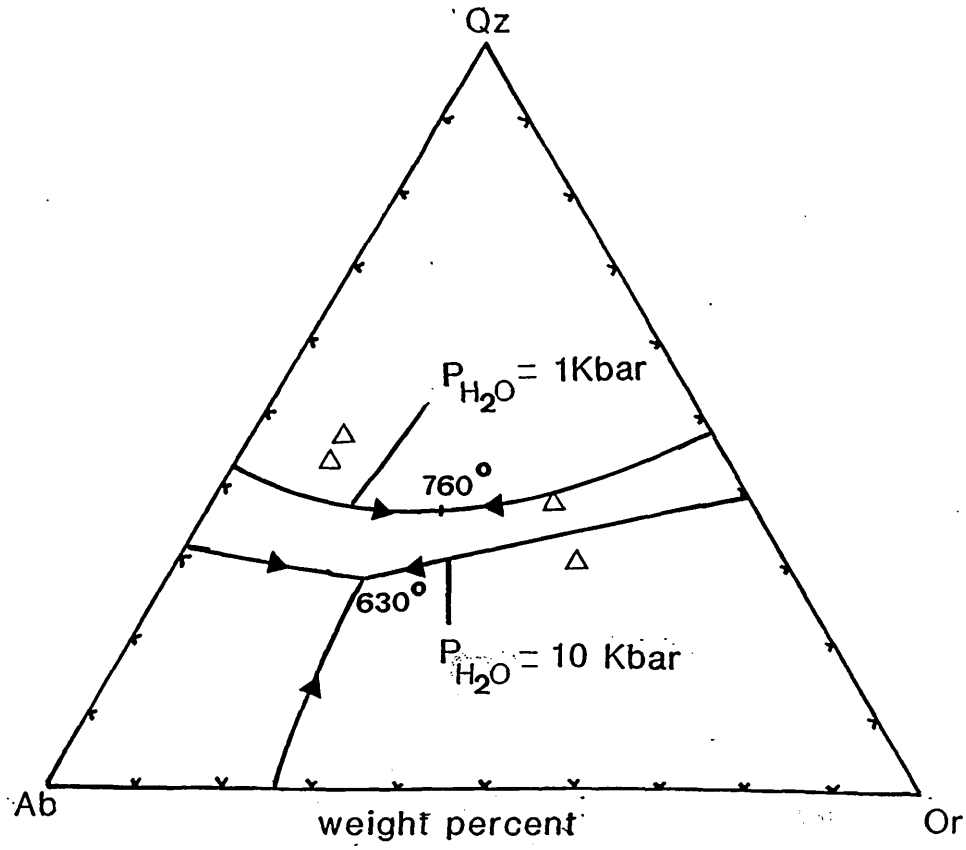

FIGURE 5.04 The system albite-orthoclase-silica-H2O at water pressures of 10 Kbars and 1Kbar. Open triangles are felsite compositions. (Data taken from Tuttle and Bowen 1958; Luth et al. 1964).

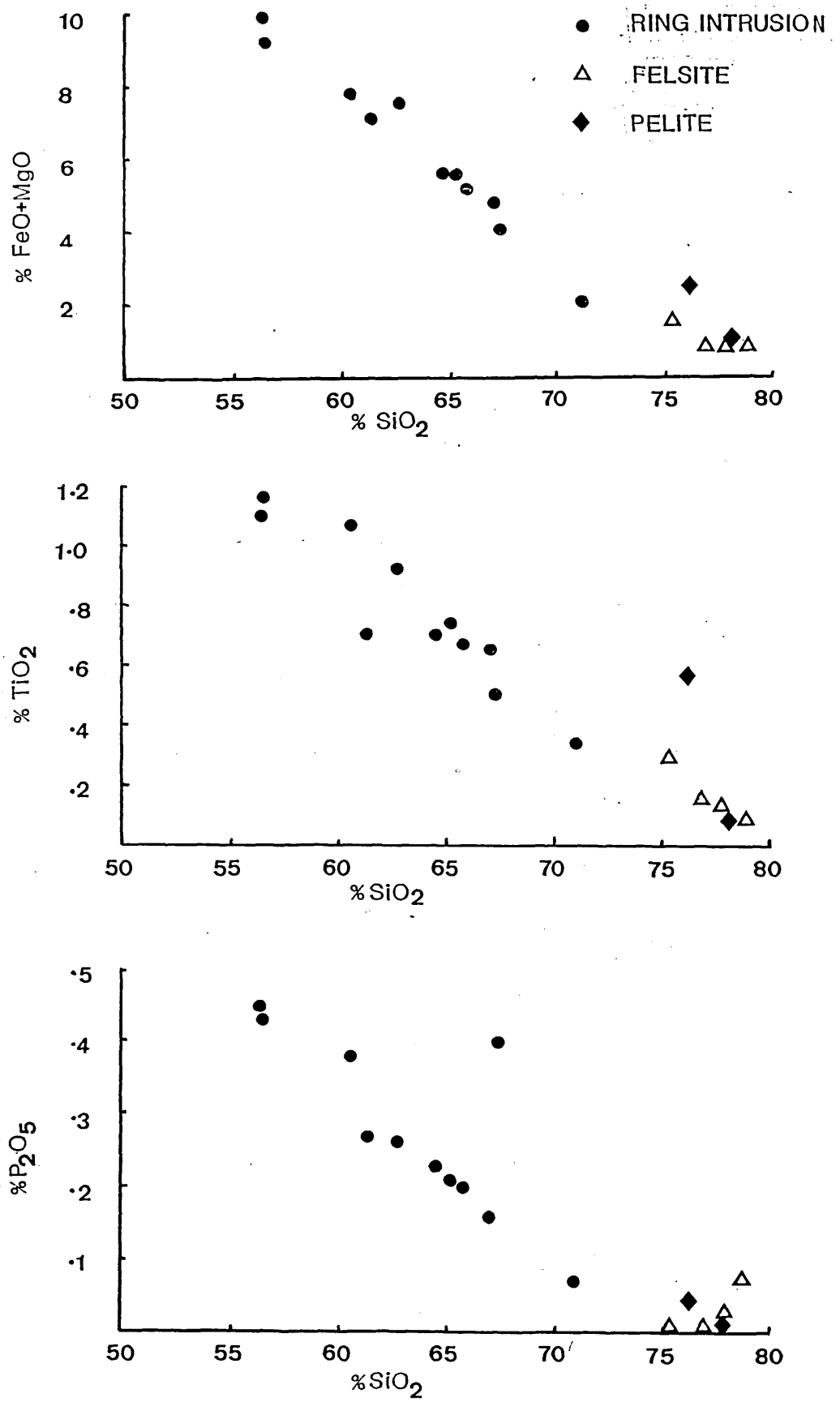

FIGURE 5.05 . Oxide plots of MgO+FeO, TiO2 and P2O5 against SiO2.

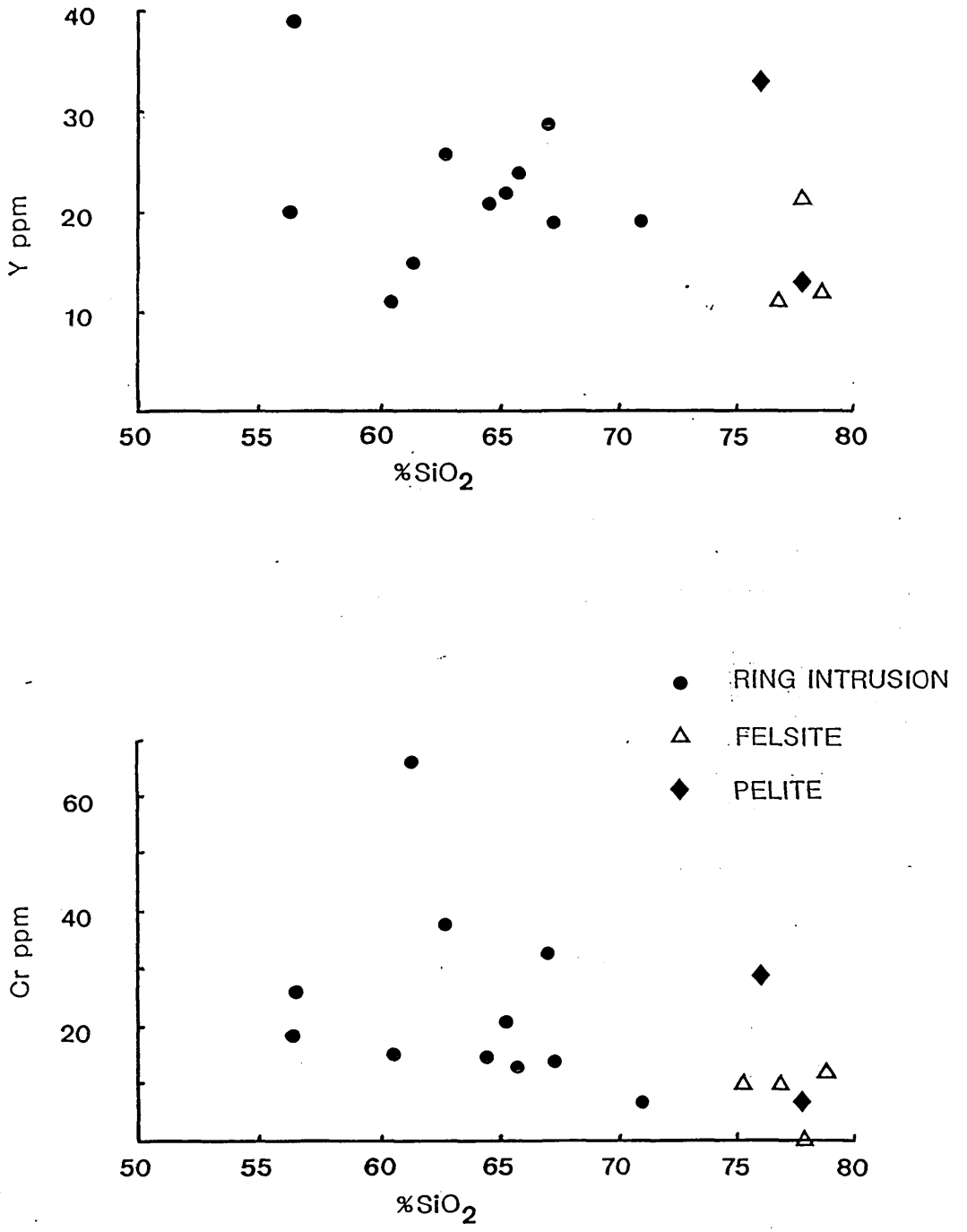

FIGURE 5.06 Elemental plots of Y and Cr against SiO2.

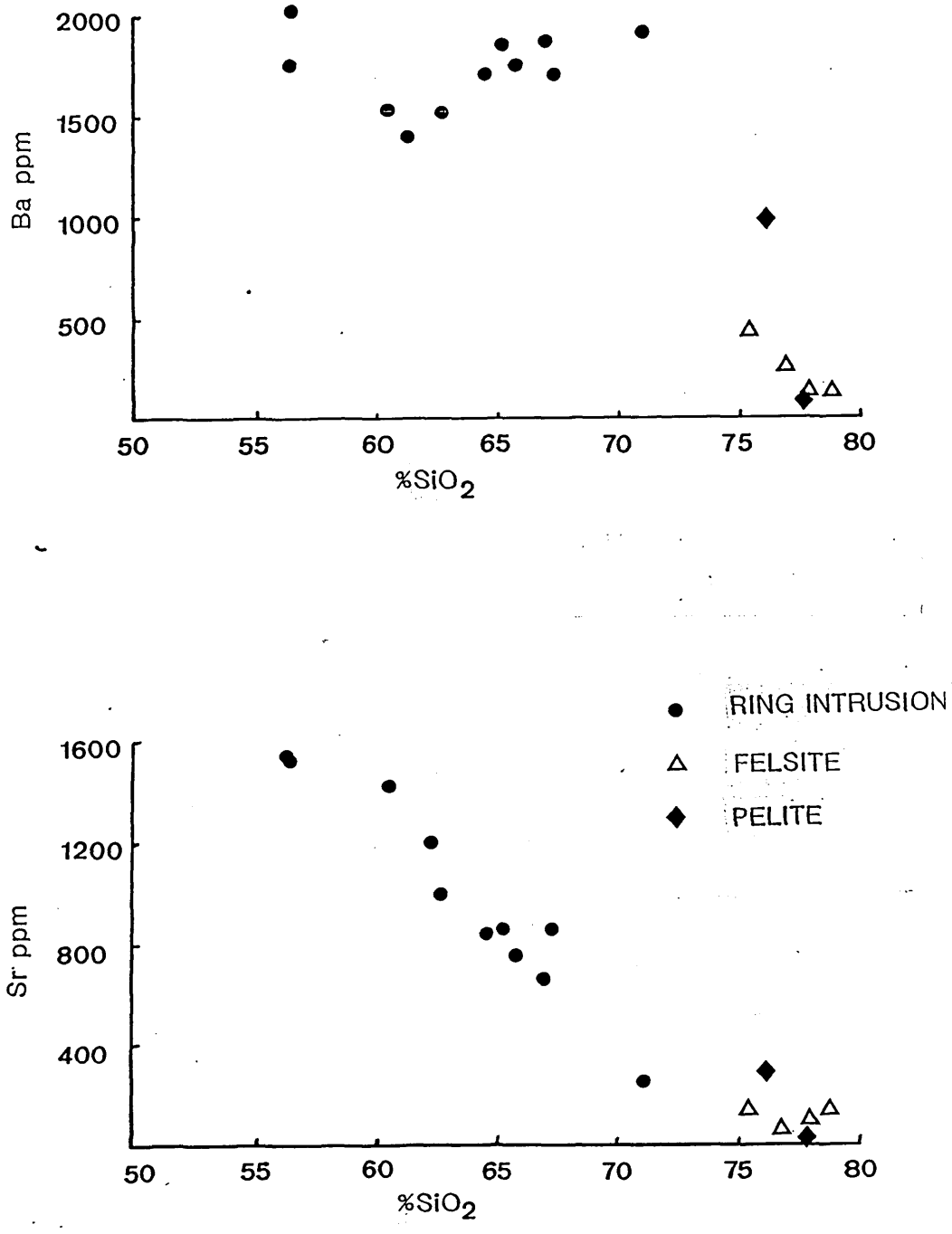

FIGURE 5.07 Elemental plots of Ba and Sr against SiO2.

iron and magnesium oxides against silica. This demonstrates the fractionation of ferro-magnesian minerals such as augite and amphibole. This is supported by the strong, early depletion of chromium (in augite), and the compatibility of yttrium (in amphibole) throughout the silica range shown by the analysed rocks. Titanium oxide shows a good negative correlation with silica, reflecting the fractionation of Fe-Ti oxides and sphene. Also phosphorus depletion demonstrates apatite fractionation. Plagioclase fractionation can be shown clearly by the loss of strontium with increasing silica, and is confirmed by the normal zoning observed in plagioclase phenocrysts (Fig. 5.08). However the plagioclase crystals in the felsites are not zoned.

The general form of multi-element plots and rare earth element (REE) plots in Fig. 5.09 showsa typical calc-alkaline pattern for all the rocks, which is steep and enriched in light REE's, showing a peak at potassium, and depletion of niobium and tantalum. The development of a negative europium anomaly may indicate plagioclase fractionation. The plots are of samples ranging from dioritic gabbro (3JG20) through granite (1JG61), to felsite (2JG15). Here the evidence again points to a simple fractionation history.

5.4.3 Evidence for partial-melting

To argue for partial-melting within the thermal aureole, one must first look at the possible sources and their chemical characteristics. The most likely source rock is the Leven Schist series. These are the pelitic rocks which appear to exhibit partial-melting textures in the field, and near the fault intrusion are commonly host to the felsite (section 5.3.3). Similar partial-melting characteristics have been noted by Platten (1983) in Dalradian pelites and quartzo-feldspathic rocks around dioritic plugs in Appin. Here, the micas have been converted into

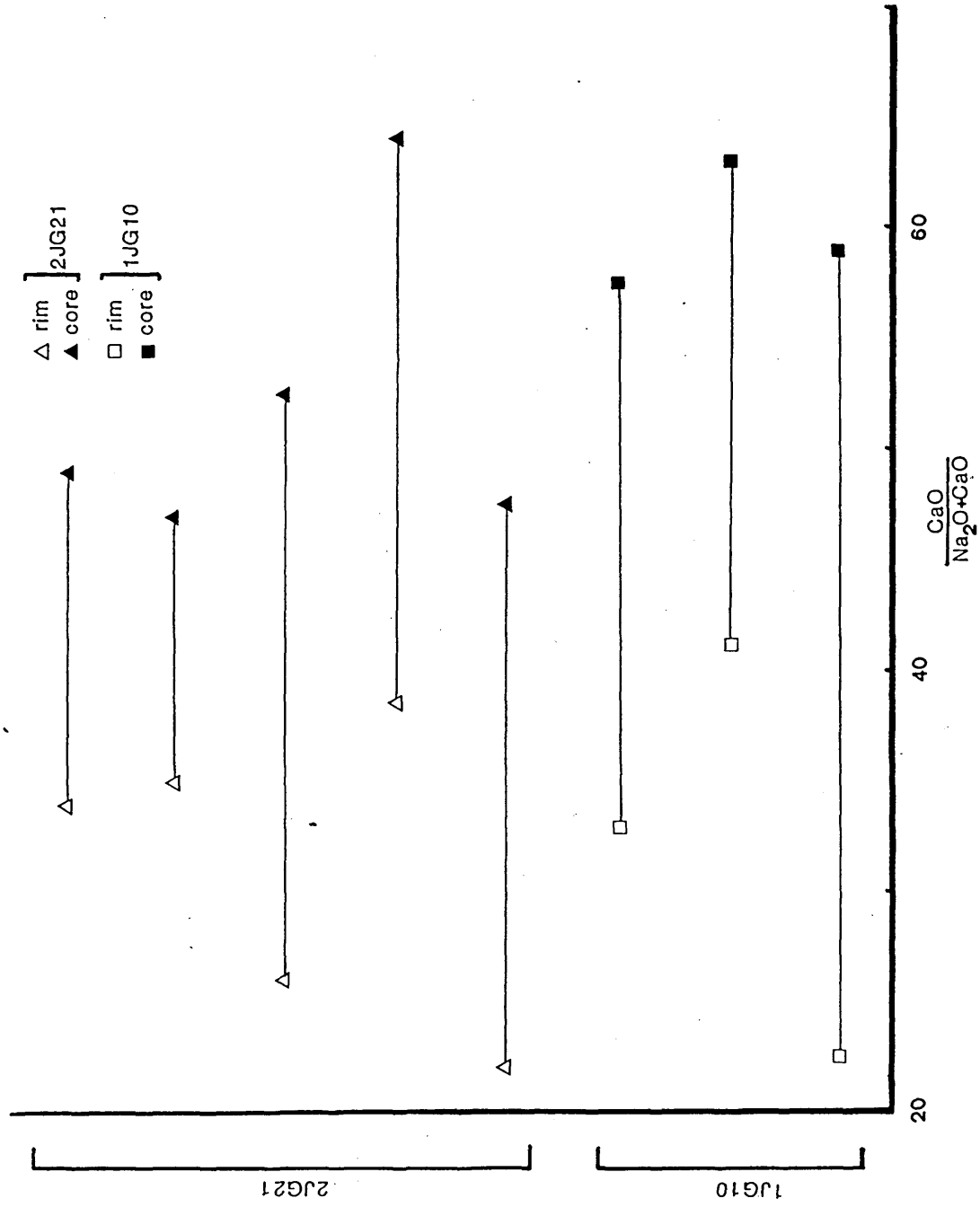

FIGURE 5.08 Plagioclase core and rim plots for samples 1JG10 and 2JG21.

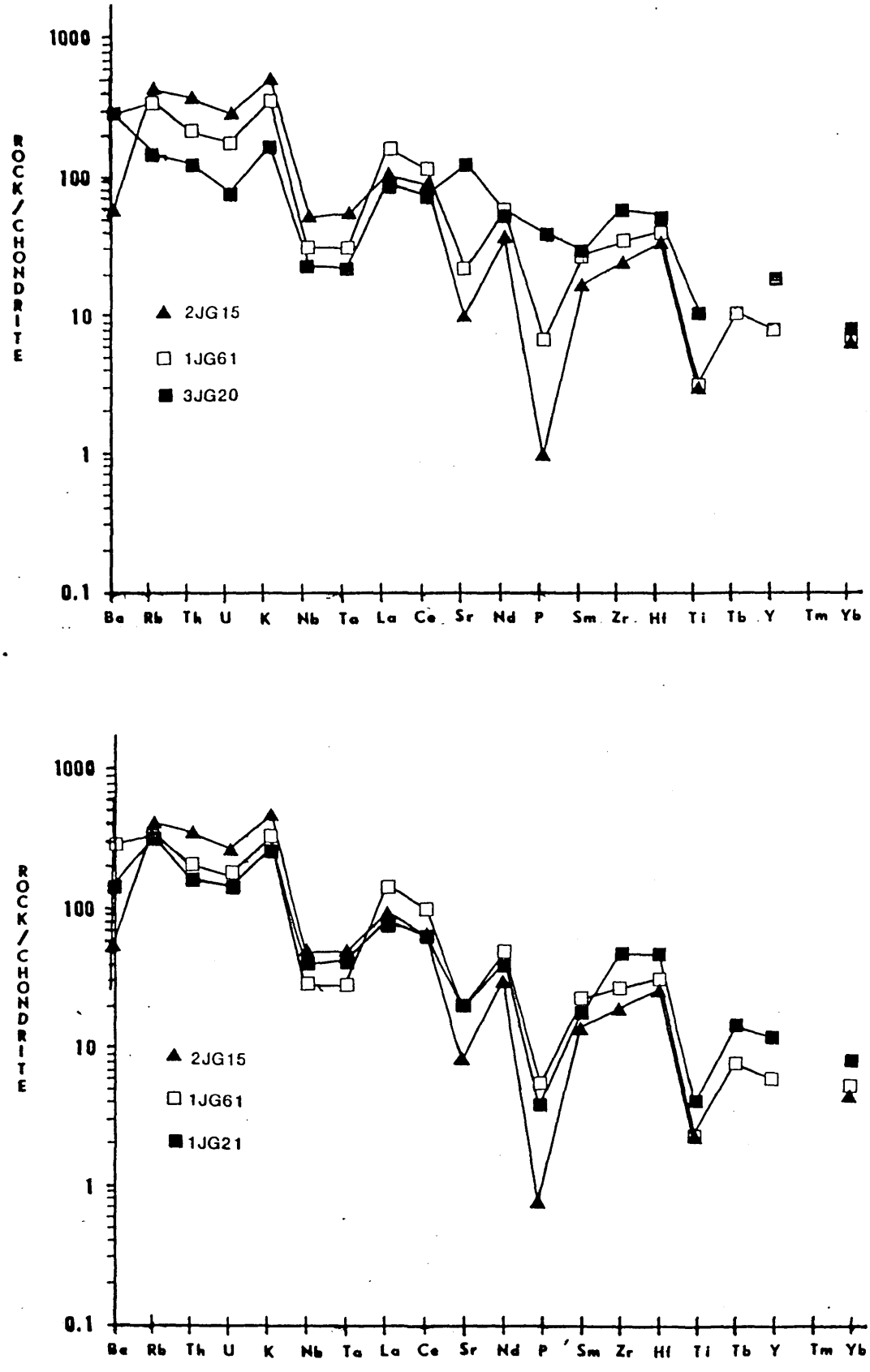

FIGURE 5.09 Multi-element plots for samples 2JG15, 1JG61, 1JG21 and 3JG20.

aluminium silicates to form restite bands, and enabling water to be released. It was calculated that the water residing in the pelites, if completely released, would oversaturate the amount of granitic melt produced in the heating. This would lead to the formation of drusy cavities, similar to those described in section 5.24, being formed by the excess vapour phase.

Samples 2JG25 and 1JG21 have been taken as representative pelites of the Glencoe area, and analysed for a wide range of elements. However their composition for all the elements discussed so far is in line with the fractionation trend of the ring-intrusion! The same applies for many incompatible elements (Fig. 5.09), where the pelite seems to be the end member of a logical fractionation trend! All this implies is that the original depositional source of the country-rock is calc-alkaline. It also suggests that the origin of the felsites may be from either fractionation of magma, or partial-melting of the country-rock. As the composition of the pelites is similar to that of the evolved intrusion, they are difficult to characterise chemically.

By examining a number of elemental plots, similarities between the felsites and the country-rock can be seen, which cannot be explained by simple fractionation.

(1) The variation in barium with silica compared with strontium versus silica (Fig. 5.07). The Sr variation demonstrates constant plagioclase fractionation. Barium behaves incompatibly in the ring-intrusion rocks, but the felsites have very low concentrations. It is possible that fractionation of alkali feldspar and biotite may have caused this variation. Major element least squares mixing models show that plagioclase was a necessary fractionating phase aswell as biotite and alkali feldspar (Table 5.01). However plagioclase crystals in 1JG61 show minimal zoning, and they are not zoned in 4JG2. Also,

****** LEAST-SQUARES SOLUTION TO GENERALISED MIXING MODEL ******

	AMOUNTS	SI	TI	AL	FEFE	MN	MG	CA	NA	K	P	TOTAL
REACTANTS USED												
2 1JG61	100.00	71.04	.34	15.29	1.77	.04	.32	.88	4.85	5.12	.07	99.72
PRODUCTS USED												
5 KSPAR	37.85	64.20	0.00	18.41	.17	0.00	0.00	.54	4.66	9.45	0.00	97.43
6 BICTITE	3.65	36.89	5.38	13.51	16.03	.16	13.90	.19	.69	9.11	0.00	95.86
7 QUARTZ	-1.70	100.00	0.00	0.00	0.00	0.00	0.00	0.00	0.00	0.00	0.00	100.00
9 4JG2	60.20	78.01	.08	12.89	1.11	.06	0.00	.25	4.73	1.64	.03	98.80
ESTIMATED COMPOSITIONS												
REACTANTS		71.04	.34	15.29	1.77	.04	.32	.88	4.85	5.12	.07	99.72
PRODUCTS		70.91	.24	15.22	1.32	.04	.51	.36	4.64	4.90	.02	98.15
DIFFERENCES		.13	.10	.07	.45	-.00	-.19	.52	.21	.22	.05	

RESIDUAL SUM OF SQUARES = .6377

DISTANCE BETWEEN TWO ESTIMATED COMPOSITIONS = .7985

****** ****** ****** ****** ****** ******

****** LEAST-SQUARES SOLUTION TO GENERALISED MIXING MODEL ******

	AMOUNTS	SI	TI	AL	FEFE	MN	MG	CA	NA	K	P	TOTAL
REACTANTS USED												
2 1JG61	100.00	71.04	.34	15.29	1.77	.04	.32	.88	4.85	5.12	.07	99.72
PRODUCTS USED												
3 PLAGIOCLASE	5.46	62.41	0.00	23.43	.31	0.00	0.00	5.10	8.27	.77	0.00	100.29
5 KSPAR	38.68	64.20	0.00	18.41	.17	0.00	0.00	.54	4.66	9.45	0.00	97.43
6 BICTITE	3.92	36.89	5.38	13.51	16.03	.16	13.90	.19	.69	9.11	0.00	95.86
7 QUARTZ	3.14	100.00	0.00	0.00	0.00	0.00	0.00	0.00	0.00	0.00	0.00	100.00
9 4JG2	48.80	78.01	.08	12.89	1.11	.06	0.00	.25	4.73	1.64	.03	98.80
ESTIMATED COMPOSITIONS												
REACTANTS		71.04	.34	15.29	1.77	.04	.32	.88	4.85	5.12	.07	99.72
PRODUCTS		70.89	.25	15.22	1.25	.04	.55	.62	4.59	4.85	.01	98.27
DIFFERENCES		.15	.09	.07	.52	.00	-.23	.26	.26	.27	.06	

RESIDUAL SUM OF SQUARES = .5628

DISTANCE BETWEEN TWO ESTIMATED COMPOSITIONS = .7502

****** ****** ****** ****** ****** ******

TABLE 5.01 Least squares mixing modelling of major elements in the An-t-sron intrusive rocks.

neither 1JG61 nor 4JG2 contain feldspar phenocrysts. This suggests an alternative to crystal fractionation for the origin of the felsites.

(2) On the multi-element plot (Fig. 5.09), Ce and La are lower in the felsites than in the ring-intrusion rocks. This apparent compatibility of LREE's may be due to allanite and sphene fractionation, but allanite is not seen petrographically, and sphene fractionated at an earlier stage (chapters 3 and 4).

These points clearly suggest that the felsites cannot have been derived purely by fractionation of the ring-intrusion magma. Thesechemical data confirm the field and petrographic evidence and point to extreme heating and partial-melting of the country-rock having taken place during intrusion.

5.5 INTERPRETATION OF FIELD AND GEOCHEMICAL OBSERVATIONS

The Western quarter of the Glencoe cauldron subsidence consists of a small pluton, cut by a ring fault. The body has a wide-ranging chemical composition, but is mainly tonalite. There are associated small, felsitic bodies, not seen in other areas of the ring-intrusion. The pluton intrudes the crystalline country-rock. Competent country-rock quartzites have been fragmented in a block-like manner, occasionally forming large xenoliths. The calc-schists have behaved in a ductile manner, but have not been greatly disrupted by the intrusion. The pelitic schists were the major source for the country-rock xenoliths, and in marginal areas have undergone partial-melting and disruption.

Some interesting features of the area are the distal explosion breccias found in Fionn Ghlean (G.R. NN126558; NN129532). These rocks were incorporated in Bussell's (1979) discussion of the area (section

5.3.4). He went on to interpret other features, such as the intimate association between fault intrusion, felsite and melt breccia, in relation to the explosion breccias. By studying a wider area around the margin of the pluton, it has become clear to the author that the explosion breccias are not intimately related to the melt breccias. The latter were formed at a much higher temperature, and were able to generate liquid in situ. The explosion breccias were probably caused by the release of gases from a high-level magma body prior to volcanic eruption.

The felsites (section 5.2.4) are partial-melts, and are close to the granite minimum melt composition (Fig 5.04). Initial melts would have been vapour-saturated and were likely to be more sodic. As the temperature increased, the vapour became dissolved in the melt, and the melt composition became increasingly more potassic (Steiner et al. 1975). This is supported by petrography, as the two sodic melts (2JG19,4JG2) contain drusy cavities, and the other melts do not. In the area that Bussell studied in detail, the felsites do appear to have crystallised from an independent magma, and intrude the breccias. However, by looking at the whole of the An-t-sron area, one can see the progressive formation of thin stringers and melt segregations bands, which coalesced to form the larger magma bodies that Bussell mapped.

In summary, the An-t-sron area today displays a small, zoned plutonic body intruding a variety of crystalline metasediments. These have undergone thermal metamorphism, with pelitic compositions being partially-melted up to 200m away from the pluton. Early explosion breccias suggest that volcanic activity occurred prior to the intrusion.

5.6 MATHEMATICAL MODELLING OF THE THERMAL HISTORY OF AN-T-SRON.

5.6.1 Possible causes of the occurrences observed in the field

One major problem with the interpretation of the field and geochemical observations is the question of how the intrusion of such a small body of tonalite can lead to partial-melting up to 200m away from the margin. There are a number of hypotheses which may be advanced to explain the evidence that has been discussed so far.

A) The intrusion is a small mainly tonalitic body that cools in a simple fashion.

B) An-t-sron is the 'corner' of the much larger Glencoe magma chamber, of which the central block has foundered (Fig. 5.10) (Bailey 1969). This would have been a convective, cooling magma chamber.

C) An-t-sron forms part of the feeder system for early volcanic activity. This is an open system with a continual throughput of hot magma, and in situ cooling only occurring at the end of intrusive activity.

Platten (1983) concluded that the partial-melting generated around the dioritic plugs in Appin was due to "either vigorous convection, or an open system in the magmas filling the plugs."

In order to test these hypotheses, mathematical modelling of the heat-flow from intruding bodies has been attempted.

5.6.2 Assumptions

A number of assumptions must be made concerning the physical properties of the rocks involved in the calculations.

1) Depth from the surface. The stability curves (Fig. 5.03) suggest that the distance from the

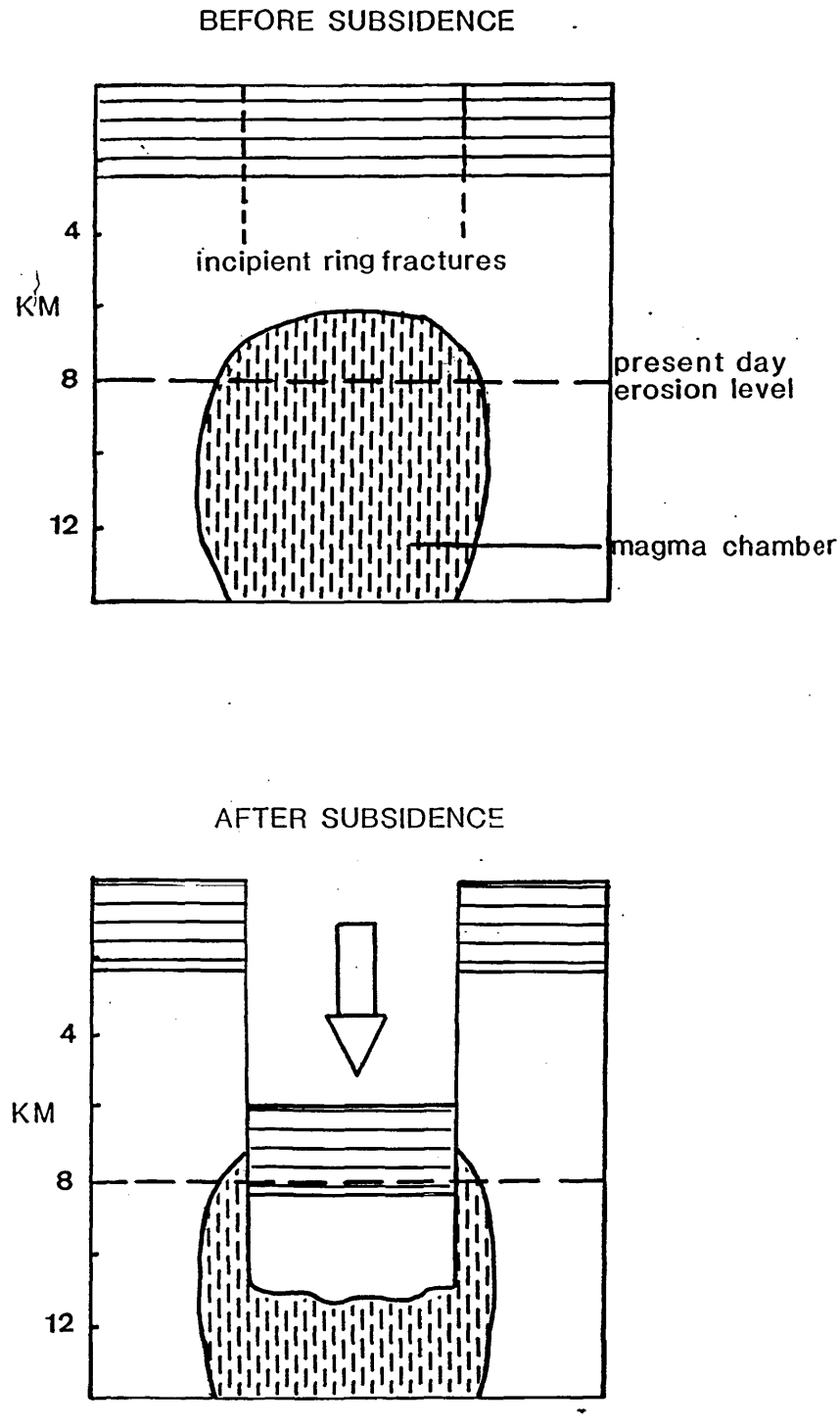

FIGURE 5.10 Sketch diagram of a foundered cauldron, where a magma chamber has intruded a crystalline basement, overlying which is a cover sequence contemporaneous with cauldron subsidence. This diagram also shows the estimated present day erosion level in Glencoe which has been used in section 5.6.

surface is between 5 and 12 Km. However sillimanite coexists with partially-melted material, which could indicate shallower depths of intrusion. Bailey (1960) believed the Dalradian cover to be 2 Km. Although the mineralogy suggests approximately 8 Km, I believe a more realistic value to be 5 Km. For the modelling, however, to maximise the heating effect, a depth of 8 Km has been used, giving an initial country-rock temperature of 200°C prior to intrusion. Wet granite melting in the country-rock is assumed, as this lowers the solidus.

2) The An-t-sron intrusion is assumed to be an open-ended cylinder, with a radius of 2.4 Km (Fig. 5.11). If a more elongate shape were assumed for An-t-sron, such as a dyke, the surface area of the body would increase, hence lowering the temperature to which the country-rock would rise during intrusion. Therefore, by considering radial heat-flow from a cylinder, the potential heat output is maximised. Also, an open-ended cylinder assumes no heat loss from above.

3) The main rock-type is a tonalite, hence an arbitrary initial magma temperature has been taken as 1000 C. The model also assumes that the intrusion was emplaced instantaneously into colder surroundings. Considering the rock-types exposed, the magma could not conceivably be hotter, hence the upper limit to the thermal effects is calculated.

4) As the rock is very porphyritic, 50% crystallisation at the time of intrusion has been assumed. If this were different, it would affect the total heat produced by the latent heat of crystallisation. In order to deduce this, albite is assumed to be the groundmass constituent, which has a latent heat of crystallisation of 61.3 cal/g (Robie and Waldbaum 1968).

5) The density, thermal conductivity, thermal diffusivity and specific heat used are those given for an average crystalline rock by Carslaw and Jaeger (1980). These values vary very little over the range

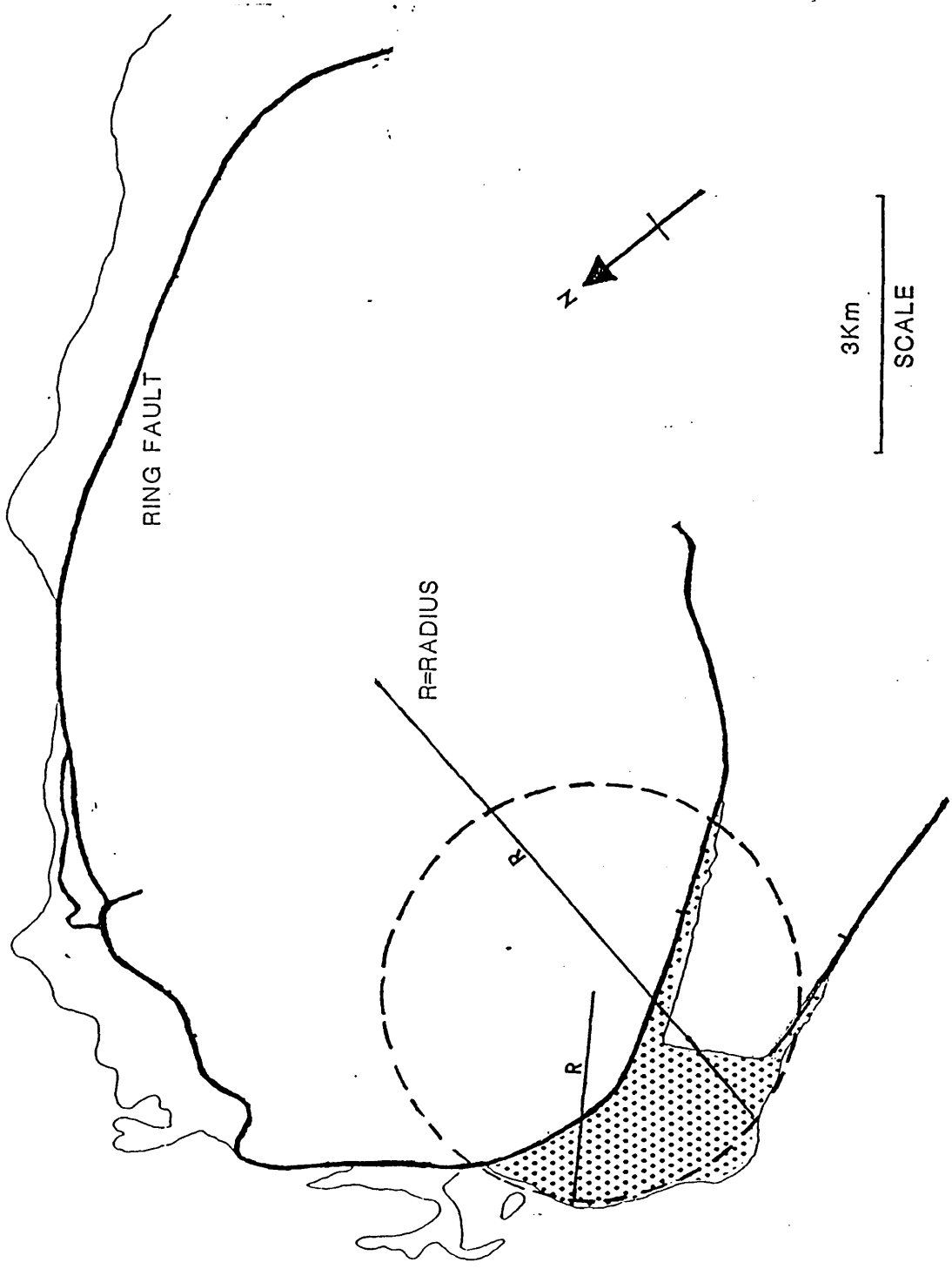

FIGURE 5.11 Sketch of Glencoe showing the estimated radius of An-t-sron pluton, in relation to the rest of Glencoe. See text for assumptions used in determining this distance.

of crystalline rocks, so any inaccuracies in these assumptions will have little effect on the model.

6) No convective heat transfer has occurred. There is very little evidence of hydrothermal fluids circulating in the country-rock during intrusion. The minerals in An-t-sron intrusion have undergone some hydrothermal alteration, but as this affects the whole rock, it is considered to be late stage. This is in accordance with Lipman (1984), who suggests that hydrothermal circulation occurs at the end of a caldera sequence. If there was convective heat transfer, the effects could be extremely variable, as they are dependent upon the permeability, width of conduit, and the topology of the conduit network.

5.6.3 Computer programs used to model the heating of the country-rock adjacent to the intrusion

Two computer programs were developed by Dr E.H. Rutter (Imperial College) to evaluate heat flow from an open-ended cylinder using appropriate solutions to the heat flow equations given by Carslaw and Jaeger (1980). The first examines the thermal consequences of a simple cooling pluton (hypothesis A). The second looks at continuous magmatic throughput as might be expected if the An-t-sron intrusion acted as a magma conduit. As a result, the temperature of the intrusion is held constant for a given period of time (hypothesis C). The latent heat of crystallisation is considered when examining hypothesis A, but is not considered in hypothesis C, as the magma is kept at a constant temperature.

5.6.3.1 Simulation of hypothesis A

This program simulates the cooling of an open-ended cylindrical body, when it is instantaneously emplaced in colder surroundings. This is given by the equation (Carslaw and Jaeger 1980,

2nd Ed., page 56, Eqn. 9):

Eqn. 1

$$V(rt) = \frac{1}{2}V\left[\operatorname{erf}\left(\frac{a-r}{2\sqrt{kt}}\right) + \operatorname{erf}\left(\frac{a+r}{2\sqrt{kt}}\right)\right]$$

where

a = radius of cylinder

r = distance from the centre of the intrusion

t = time

V = initial difference in temperature between the intrusion and its surroundings

k = thermal diffusivity

$$\operatorname{erf}(x) = \frac{2}{\sqrt{\pi}} \int_{x}^{\infty} e^{u^2}\, du$$

This gives the temperature profile (with radial distance) of the area at certain periods of time after the intrusion (Fig. 5.12). By measuring the gradient of these temperature profiles, the heat flux can be found, hence the change in the heat output with time can be calculated (Table 5.02).

As a cooling and crystallising body is being studied, the latent heat of crystallisation must be taken into account. For each 1km length of the cylinder the volume is 18.1 x 10 cm. The density is taken to be 2.5 g/cm. As most of the groundmass is feldspar, the latent heat of crystallisation of albite was used, which is 61.3 cal/g.

Firstly, the total heat content of the intrusion associated with the temperature rise above ambient for a 1km section was calculated. Where :

total heat = Vdct

where

V = volume

d = density

c = specific heat

t = temperature rise

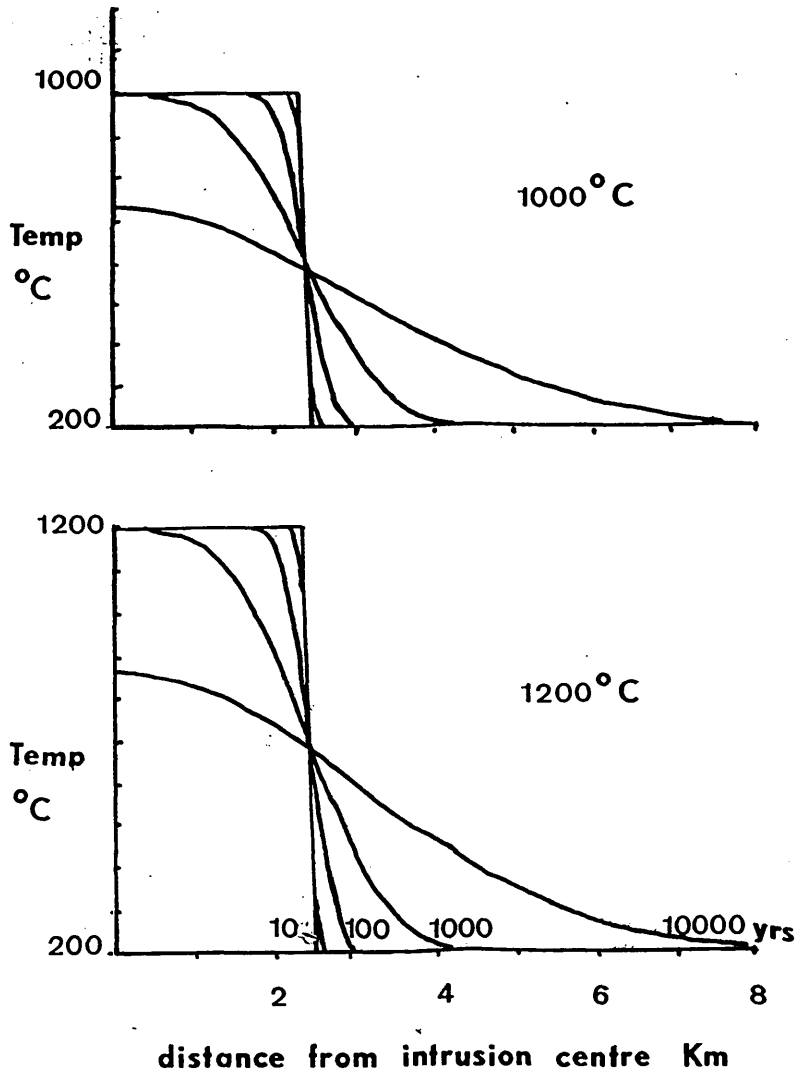

FIGURE 5.12 Thermal profiles of cooling intrusions of temperatures 1000 C and 1200 C, and their thermal effect upon the country-rock at time intervals of 10, 100, 1000 and 10000 years after intrusion.

TABLE 5.02 The heat flux as a result of conduction across a liquid solid interface

TIME ELAPSED (Yrs) .	TOTAL FLUX PER YEAR	%HEAT LOST FOR 1000 Yr PERIOD	%HEAT LOST FOR 10000 Yr PERIOD	%HEAT LOST FOR 100000 Yr PERIOD
10	2.34 x 10	0.31%	3.1%	31%
10	7 x 10	0.09%	0.9%	9%
10	2 x 10	0.03%	0.3%	3%
10	2 x 10	0.003%	0.03%	0.3%

Hence for a cooling body with an original temperature of 1000°C, the total heat content is 7.6 x 10 calories.

The heat produced by the latent heat of crystallisation is given by :

total latent heat = LVd

total heat = 1.38×10^{18} cal

where

L = latent heat/unit mass

Therefore the total heat conducted to the country-rock is

$(7.6 + 1.38) \times 10^{18} = 8.98 \times 10^{18}$ cal.

hence, the latent heat is approximately 15% of the total.

This is a significant amount of heat, but its affect upon the country-rock is dependent on two factors :

a) The temperature of crystallisation. During the period of production of latent heat the temperature of the interface between liquid and solid will remain constant. Heat can only be transported away by conduction at a certain rate (as determined in Table 5.02). If crystallisation occurs at 1000°C, the latent heat produced will be carried away quickly, and will probably have a significant effect on the country-rock. If however, the crystallisation temperature is 800°C, this will be less effective as the heat flux will be lower.

b) The time taken for the heat to dissipate. This is given by the equation (Turcotte and Schubert 1982, page 173, Eqn. 4-143):

Eqn. 2

$$t_s = \frac{b^2}{4k\lambda^2}$$

where

t_s = solidification time

b = radius of the pluton

k = thermal diffusivity

λ can be obtained from the equation (Turcotte and Schubert 1982, page 173, Eqn. 4-142):

Eqn. 3

$$\frac{L\sqrt{\pi}}{cT} = \frac{e^{-\lambda^2}}{\lambda(1+\mathrm{erf}\lambda)}$$

where

L = latent heat

c = specific heat

T = Tm - To = temperature difference between the crystallising intrusion and the country-rock

The solution to λ is read from the graph (Fig. 5.13) (after Turcotte and Schubert 1982, page 174). The temperature of the crystallising intrusion is taken as 800°C (which constitutes a 600°C rise, as the country-rock is at 200°C), Thus, λ = 0.55, and t is 150000 yrs. This gives an average flux of 6 x 10^{13} cal/yr over the entire surface of the pluton.

The heat produced by the latent heat of crystallisation is dissipated over a long period of time. One semi-quantitative method of taking this into consideration, and maximising any effect that it might have, is to use the cooling curves produced by a magma at 1200°C (Fig. 5.12).

By extrapolating the data for the cooling curves at 200m away from the intrusion margin, a set of country-rock heating curves can be produced (Fig. 5.14). Even with an intrusion temperature of 1200°C, the country-rock only reaches a maximum of 650°C. This is not sufficient to produce the partial-melting features seen in the field.

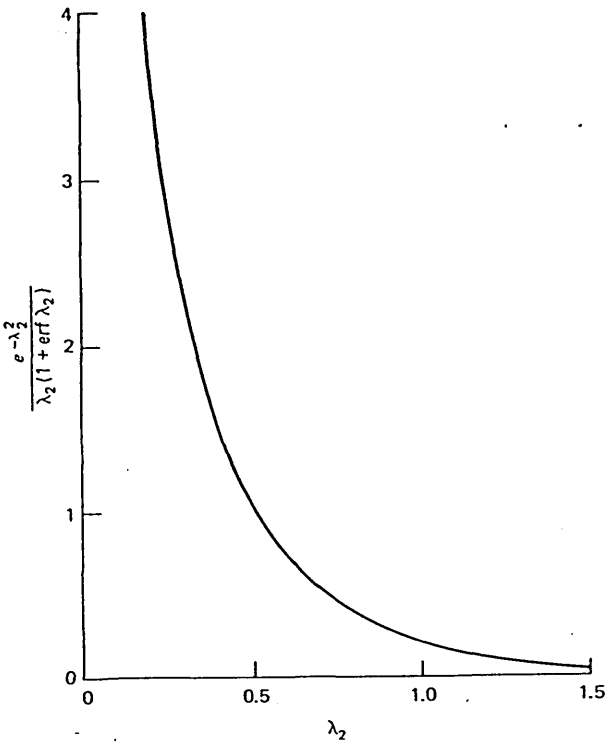

FIGURE 5.13 The right side of the transcendental equation (3) for determining the motion of the solidification boundary, . (After Turcotte and Schubert 1982).

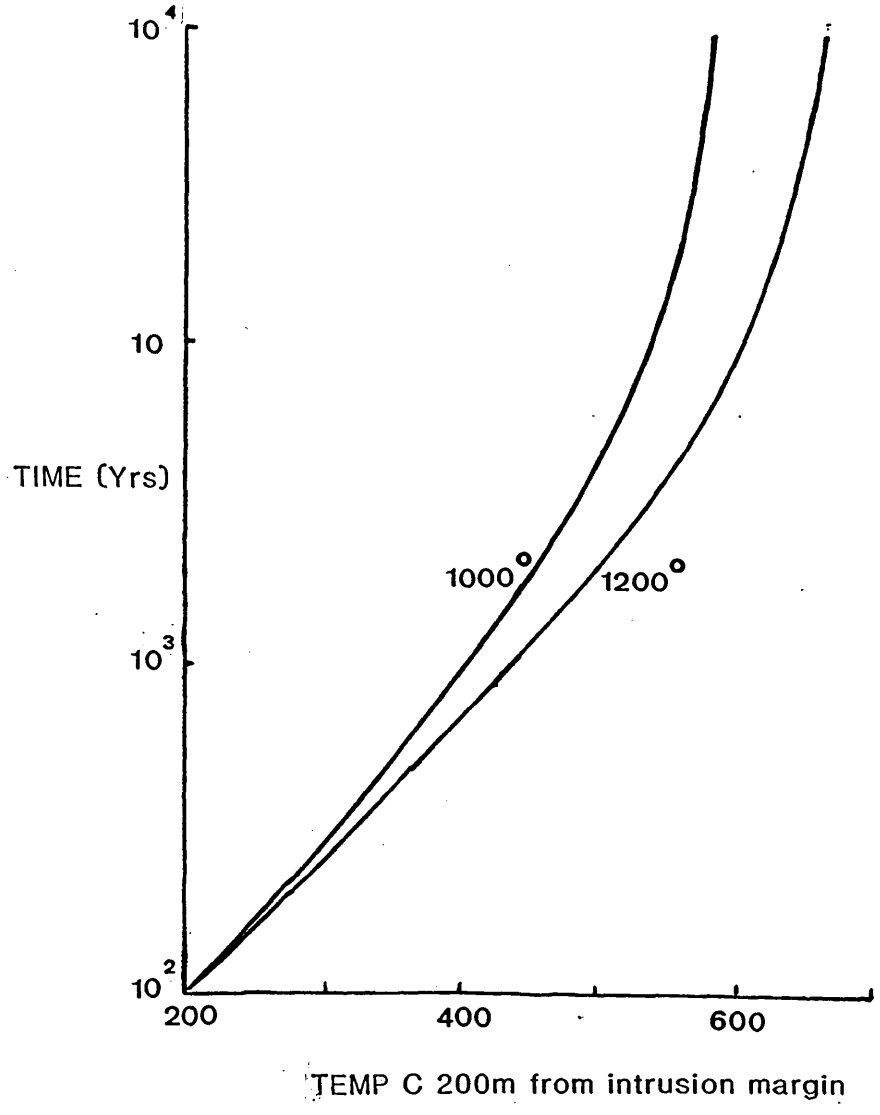

FIGURE 5.14 Temperature vs. time plot showing the country-rock temperature at 200 metres from the contact with magmas initially intruded at 1000°C and 1200 C in a simple cooling pluton of radius 2.4km.

5.6.3.2 Simulation of hypothesis C

To simulate hypothesis C, an open-ended cylinder was also used, but the temperature at the boundary was kept constant. The solution to the heat flow equation for these boundary conditions is given by the equation (Carslaw and Jaeger 1980, 2nd Ed., page 336, Eqn. 7):

$$\text{Eqn. 4}\qquad V(rt) = \left[\sqrt{\frac{a}{r}}\,\operatorname{erfc}\left(\frac{r-a}{\sqrt{2kt}}\right)\right] + \left[\frac{V(r-a)\sqrt{kt}}{4\sqrt{a}\,.\,r^{3/2}}\,\operatorname{ierfc}\left(\frac{r-a}{2\sqrt{kt}}\right)\right]$$

$$+ \left[\frac{V\,(9a^2-2ar-7r^2)\,kt}{32\;a^{3/2}\,r^{5/2}}\,\operatorname{ierfc}\left(\frac{r-a}{2\sqrt{k_t}}\right)\right] + \cdots$$

where

$$\operatorname{erfc}(x) = 1-\operatorname{erf}(x)$$

$$\operatorname{ierfc}(x) = \int_x^{\infty} \operatorname{erfc}(u).du$$

$$\text{i erfc}(x) = \int_x^{\infty} i^{n-1}\operatorname{erfc}(u).du$$

It will be evident from the thermal profiles after different amounts of elapsed time that the tendency (after infinite time) will be to raise the temperature of the surroundings to the same temperature as the intrusion (Fig. 5.15). In this case, the only question that remains is, for how long was there a continuous magma throughput? After only 300 years, the rock 200m from the margin will have reached 700°C (for a 1000°C magma). This is above the granite solidus, and continuous heating for only a few tens of years more will be sufficient to supply the latent heat for the melting of substantial amounts of country-rock.

5.6.3.3 A convectively cooling pluton

The approach to modelling that has been used so

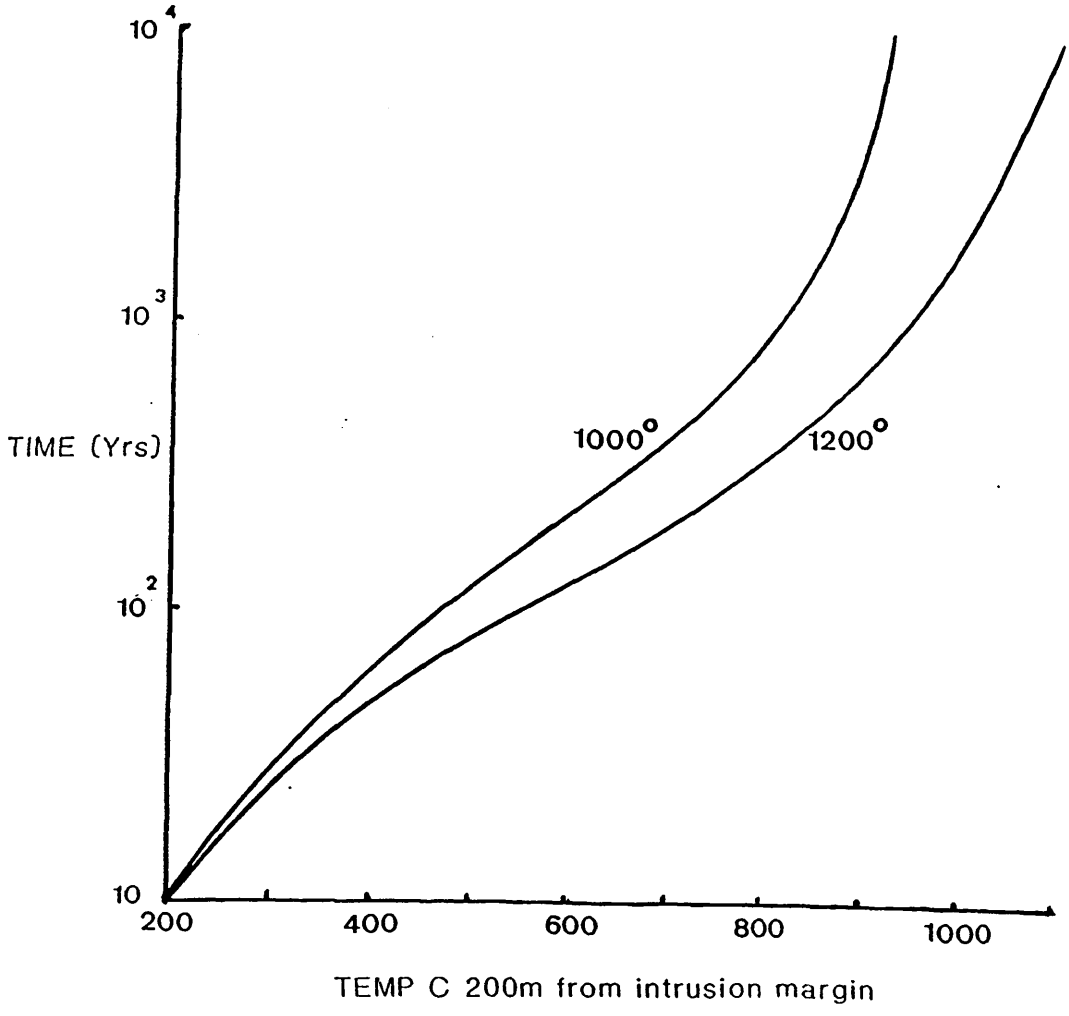

FIGURE 5.15 Temperature vs. time plot showing the country-rock heating at 200 metres from the contact with magmas at 1000°C and 1200°C where the magma remains at a constant temperature, hence there is continuous heating of the country-rock.

far is not suitable for a convective, cooling pluton. Quantitative analysis of this problem is beyond the scope of this study (R.S.J. Sparks pers. comm.). However, if the problem is approached in a simple qualitative manner, a number of reasonable deductions can be made.

1) The temperature/time curves for the country-rock outside a convectively cooling pluton will lie between the curves for a conductively cooling pluton and those for continuous heat input (Fig. 5.16).

2) At the early stages, the body of magma will remain quite hot, and therefore the cooling curves would resemble Figure 5.15.

3) At a later stage, it will cool in a manner similar to a non-convecting, cooling pluton (Fig. 5.14).

Hence, Figure 5.16 shows a region in which the cooling curve is expected to lie. This shows that after approximately 1000 years, the temperature of the country rock will lie above that of the granite solidus, and some degree of partial-melting may occur.

With a larger intrusive body, the thermal output is similar to that for the pluton of 2.4 km radius, as the flux remains almost the same. However, once it starts to crystallise, the latent heat of crystallisation may be quite substantial, but this again will be dissipated over a very long time.

5.6.4 Discussion

As a result of the modelling, hypothesis A is rejected, therefore a small cooling tonalitic intrusive body does not cause the country-rock temperature to rise above the granite solidus. Hypothesis B, i.e. a large, convective cooling pluton, cannot be rejected on theoretical grounds, as it is possible for the country-rock temperature to exceed the granite solidus after approximately 1000

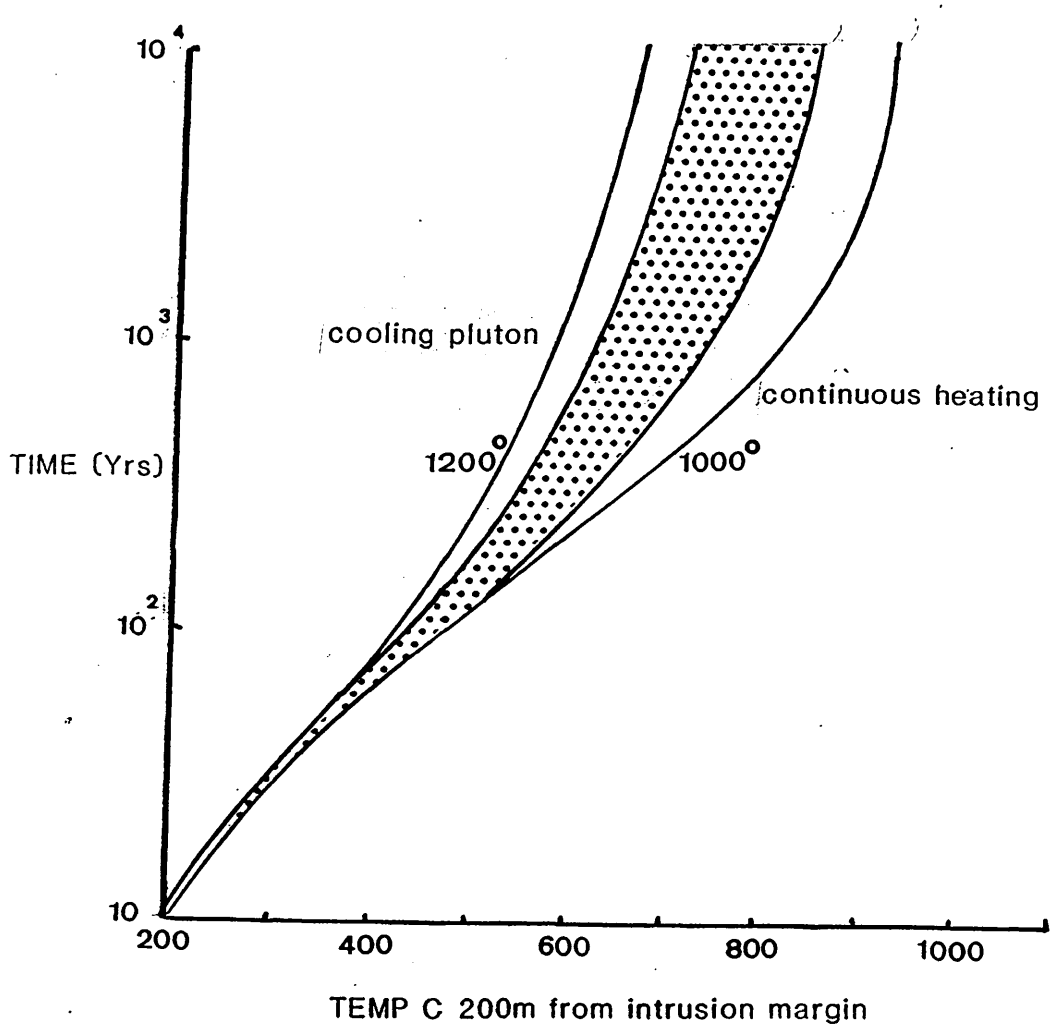

FIGURE 5.16 Temperature vs. time plot showing the likely region (shaded area) for a heating curve produced by a convective-cooling pluton with an initial temperature of 1000°C. This lies between the curve for a cooling pluton of initial temperature 1200°C, and the curve for continuous heating, where the magma remains at a constant temperature of 1000° C.

years. However, this is the only part of Glencoe where such high-grade contact metamorphic assemblages occur, and partial-melting of the country-rocks is found. To explain this, one cannot invoke regional tilting (chapters 1,2), leaving unlikely possibilities such as the concentration of convection being in the An-t-sron area, or that a laccolith-shaped intrusive body existed, with its hotter root at An-t-sron. Hypothesis C, i.e. the idea that An-t-sron formed part of a feeder system for earlier volcanic activity, can be adequately justified by the thermal modelling. This is also supported by circumstantial evidence from Glencoe and other areas:

1) The large amount of andesitic volcanism in the region.

2) The occurrence of explosion breccias in the immediate vicinity.

3) Zoned phenocrysts of plagioclase, and overgrowths on amphiboles, biotites and plagioclases suggesting a rapidly changing liquid composition. The major causes of these features is a change in the magma composition due to eruption of magma, and the input of fresh magma from a lower source, or a rapid change in the pressure and temperature conditions of the magma (chapter 3).

4) Documentation of early volcanism occurring on an incipient ring fracture in a number of more recent calderas. (e.g Long Valley see chapter 8).

5) Lack of convective movement of the xenoliths near the margin of the pluton.

In conclusion, the field, geochemical and thermal modelling evidence strongly suggests that An-t-sron is the root of or conduit for early volcanism in the Glencoe centre.

EARLY IGNEOUS ACTIVITY ASSOCIATED WITH THE FAULT. PART2 BRECCIAS AND ASSOCIATED RHYOLITE DYKES

6.1 INTRODUCTION

In the eastern part of the cauldron a number of breccia bodies can be found. Many of these are found in the Dalradian quartzite as small, elongate lenses. There are also larger breccia bodies present along the boundary between the Dalradian quartzite and the Devonian volcanics. There are also rhyolite dykes associated with the breccias, often in the form of multiple intrusions.

Clough et al. (1909) believed that the breccias were all formed by sedimentary processes, stating that the large, elongate bodies at the base of the volcanics were part of a basal conglomerate that extends to the Western side of the cauldron. They believed that the other smaller, amorphous bodies represented hollows that had been infilled by conglomerate, where the upper part had been eroded off.

More recent workers believed these smaller breccias to have been caused by the explosive release of magmatic gasses (Bailey 1960; Hardie 1963, 1968; Roberts 1974), and have described them as intrusive and explosion breccias.

Hardie (1968) interpreted the large breccia bodies as pyroclastic breccias (section 6.2.2). Roberts (1974) enlarged upon this idea by suggesting that the breccias might represent an early caldera margin. Taubeneck (1967), however, found rounded boulders of Rannoch Moor granite and rhyolite in the breccias and considered it more likely that these rocks were deposited sub-aerially by sedimentary

6.2 FIELD RELATIONSHIPS AND PETROGRAPHY

6.2.1 Distribution and outcrop of the breccias

The breccia bodies and rhyolite dykes outcrop within a band which extends from Meall a Bhuiridh, through Cam Ghleann, across Buchaille Etive Mor and Stob Beinn a Chrulaiste to Stob Mhic Mhartuin (Fig 6.01).

Much of the area is low-lying peat bog, hence outcrop is poor. Nonetheless, it has been inferred that the outcrop pattern forms an arcuate trend, which is sub-parallel to the ring-fault.

Most of the smaller breccia exposures occur in Cam Ghleann and on the slopes south of Stob Mhic Mhartuin. These outcrop as rounded hummocks, forming elongate patches of breccia, which are up to 10m wide, and may extend as far as 50m. The boundaries with the Dalradian quartzites are near vertical and hence these rocks are interpreted as breccia dykes. There are also small tapering exposures, which can be best described as veins (locality A, Plate 6.01). There are both sharp and gradational contacts with the country-rock quartzite.

The major volume of breccia in this part of Glencoe is found sandwiched between the Dalradian quartzite basement and the unconformable Devonian volcanics. This breccia layer is up to 30m thick, and is overlain by rhyolitic tuffs, agglomerates and lavas. The boundary between the breccias and the quartzites is poorly exposed, which has led to much of the ambiguity in previous interpretations (Clough et al 1909; Hardie 1963; Roberts 1974). Many of the lower contacts between breccia and quartzite observed are sub-vertical, which led Hardie (1968) to interpret this body as a "vent-breccia" (section 6.3.2). Part of the problem is due to the non-planar

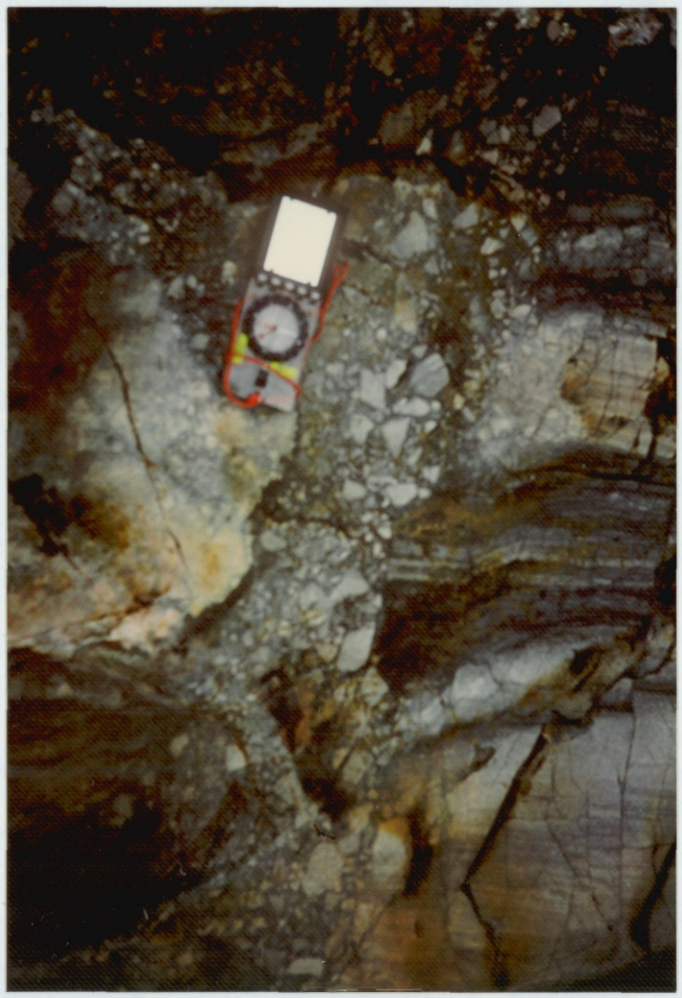

PLATE 6.01 A thin vein of intrusive breccia containing large quartzite clasts, cutting through quartzite.

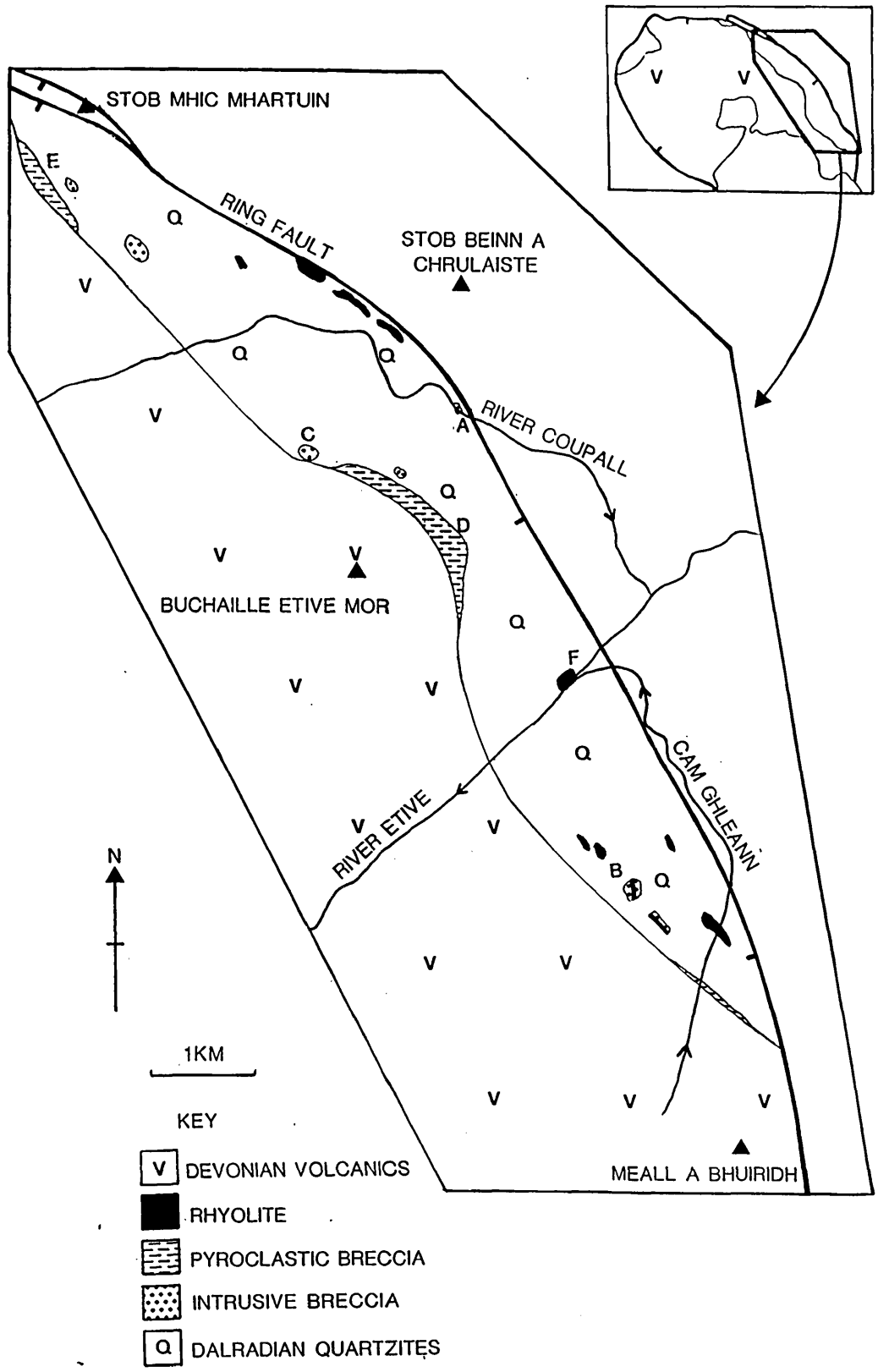

FIGURE 6.01 A sketch map of the eastern part of the Glencoe cauldron, showing the outcrop of the breccias and rhyolite dykes in relation to the Dalradian quartzites and Devonian volcanics. Major peaks and rivers are named, rocks to the east of the ring-fault are not marked.

palaeotopography of the Dalradian basement which was present at the time of breccia 'formation'. The general trend of the breccia is concordant with the overlying volcanics.

Both the breccia-dykes and the concordant band of breccia are cut by the ring-fault at a number of localities west of the Stob Mhic Mhartuin, indicating that these rocks were formed prior to ring-faulting.

6.2.2 Breccia Types

The classification of volcanic breccias has been discussed by Wright and Bowes (1963). This classification provides a workable system which is based on the relationship between clast and matrix, and the inferred genesis of the breccia body. The terminology used consists of a) intrusive breccia, whereby clasts of rock have been moved by rising streams of gas and/or magma to produce a breccia which may or may not be set in an igneous matrix. b) Explosion breccia, which is a rock formed beneath the earths surface by volcanic explosion with little movement of the clasts. c) Pyroclastic breccia is the eruptive counterpart of either an explosion breccia or an intrusive breccia. d) A vent breccia is a pyroclastic deposit which has fallen back into its conduit or crater after eruption.

Intrusive and explosion breccias. The breccia dykes, seen particularly well in Cam Ghleann (locality B on Fig. 6.01), are classified, (after Wright and Bowes 1963), as intrusive and explosion breccias (Hardie 1968). This rock-type consists of angular fragments of quartzite (2 to 60 mm in diameter), set in a fine-grained matrix. Many clasts have a fragmentary appearance, with clast fragmentation often occurring in localised zones.

The volume of the matrix is minimal, composed of quartz fragments, some of which appear to grade into quartzite clasts. Small, irregular patches of rhyolite are occsionally found between the clasts

PLATE 6.02 A typical intrusive breccia. Q = quartzite, P = pelite.

PLATE 6.03 Photomicrograph in plane polarised light of an intrusive breccia (3JG21) in which rhyolite forms part of the matrix. R = rhyolite, P = plagioclase phenocryst.

PLATE 6.04 Outcrop of a pyroclastic or vent breccia composed of sandstone clasts at locality C (Fig. 6.01).

PLATE 6.05 Photomicrograph in crossed polars of a shattered plagioclase fragment in a pyroclastic breccia (4JG18). The line drawing below depicts the feldspar fragments.

PLATE 6.06 Photomicrograph in plane polarised light of an intrusive tuff from locality F (Fig. 6.01) (1JG14). P = plagioclase phenocryst, V = volcanic clast, L = lithic (metasedimentary) clast, Q = quartzite clast.

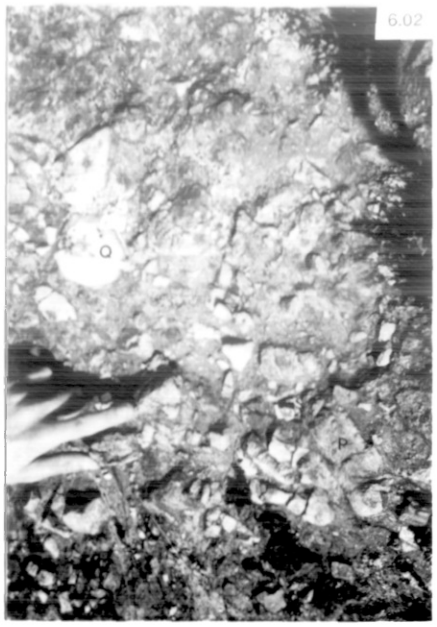

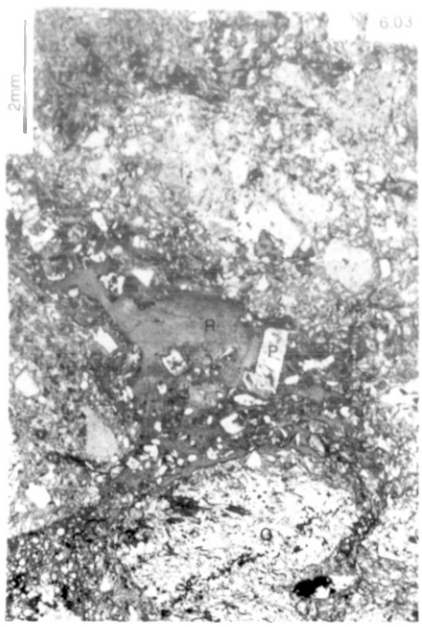



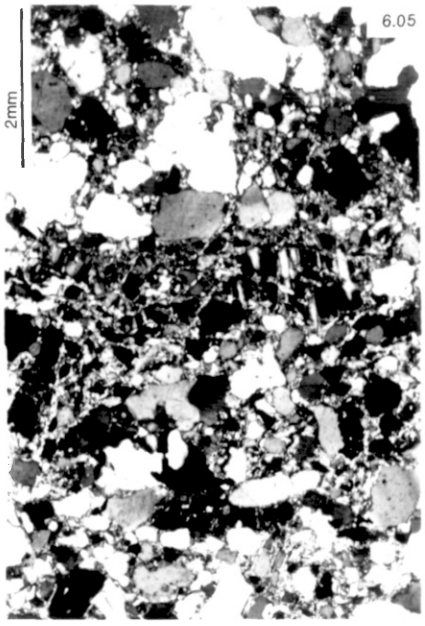

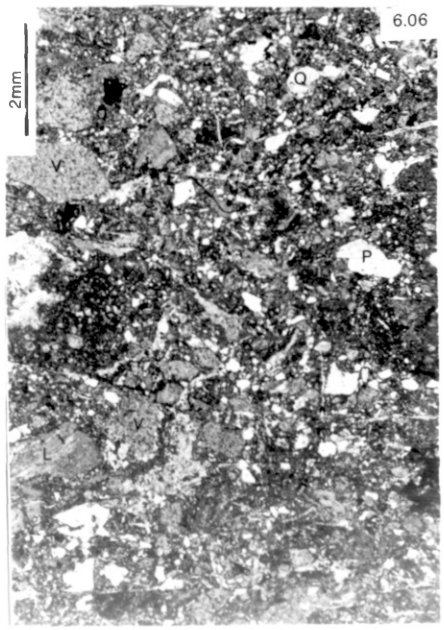

6.05



(Plate 6.02). The bodies are totally structureless and there is no layering or clast sorting.

The intrusive breccias show a cross-cutting relationship to the quartzitic country-rock (from which they have been derived). These grade into explosion breccias which have gradational boundaries with the country-rock. A breccia composed of Devonian sandstone clasts is present at locality C (on Fig. 6.01) (Plate 6.03). This is believed to be either an explosion or vent breccia (using the terminology of Wright and Bowes 1963), although no margins are seen. An indication to the explosive origin of this rock-type is given by the shattered feldspar fragment seen in Plate 6.04.

Pyroclastic breccia. The larger exposure of breccia on Buchaille Etive Mor has been named a vent breccia (Hardie 1968) or a pyroclastic breccia (using the classification of Wright and Bowes 1963). Similar deposits are also exposed in Cam Ghleann and south of Stob Mhic Mhartuin. It contains clasts of quartzite, schist, rhyolite, sandstone, andesite and occasional granite, with quartzite being the most common. Some clasts are up to 1m in size, though most have diameters between 1 and 15 cm. However, Hardie (1968) recorded a sandstone clast 30m long. Many of the fragments are angular, particularly the larger ones, but, all of the granites, most of the andesites and some of the other clast types are quite well-rounded. The clasts are set in a fine-grained quartz matrix which sometimes contains igneous fragments. The matrix to clast ratio in these rocks is higher than in the intrusive and explosion breccias, and equal proportions are present in places.

The lower part of this breccia is poorly bedded and sorted (Fig. 6.02), and contains all the very large clasts (usually bedded red sandstone and siltstone). Higher up in the sequence, bedding and sorting improves, and towards the top the breccia is well bedded. The breccia grades upwards into a tuff (locality D), which is ashy and contains pumice

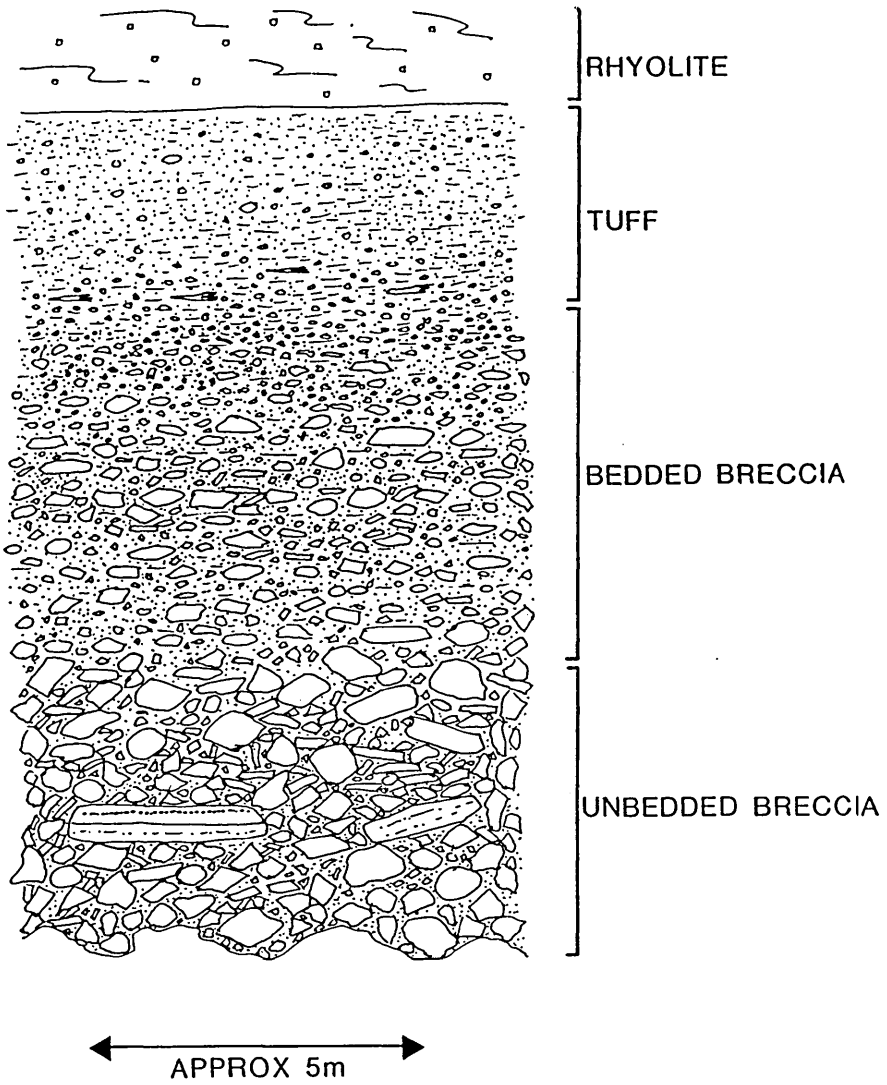

FIGURE 6.02 A sketch section through the pyroclastic breccia as seen on Buchaille Etive Mor, showing the bedding, sorting and gradation from a coarse breccia into a tuff. The deposit is overlain by rhyolitic lava.

lapilli, some of which are flattened, followed by airfall tuff (locality E). The tuffs are overlain by rhyolite.

6.2.3. Intrusive rhyolites

A number of elongate bodies of rhyolite can be found in this area, some of which intrude the explosion and intrusion breccias, and occasionally form a minor part of their matrix (Fig. 6.03). Most of the intrusions are dykes, running parallel to the breccia dykes (i.e. sub-parallel to the ring fault). The dykes vary in width from 50cm to 10m, although there is one much larger intrusion exposed in the River Etive which will be discussed later.

The rocks are geochemically similar to the extrusive rhyolites seen at Queens Cairn in the centre of Glencoe (chapter 4). Petrographically, they are poorly porphyritic, with a few small phenocrysts of feldspar and quartz. The rocks are extremely fine-grained, and unlike the Queens Cairn rhyolite, these rocks are almost structureless, but displaying some vertical flow-banding.

A much larger body of rhyolite is exposed at locality F (Fig. 6.01). Here a continuous body of rhyolite outcrops for a length of 50m parallel to the River Etive. The body is believed to be a multiple intrusion, with the oldest phases being closest to the margin. Internal contacts and flow-banding are vertical. At the northeastern margin of the intrusion a tuff with vertical flow-banding is preserved (Plate 6.05). This has been cut by later rhyolite.

No continuation of this body is exposed anywhere in the surrounding area, and as a result it is inferred to be a roughly circular intrusion.

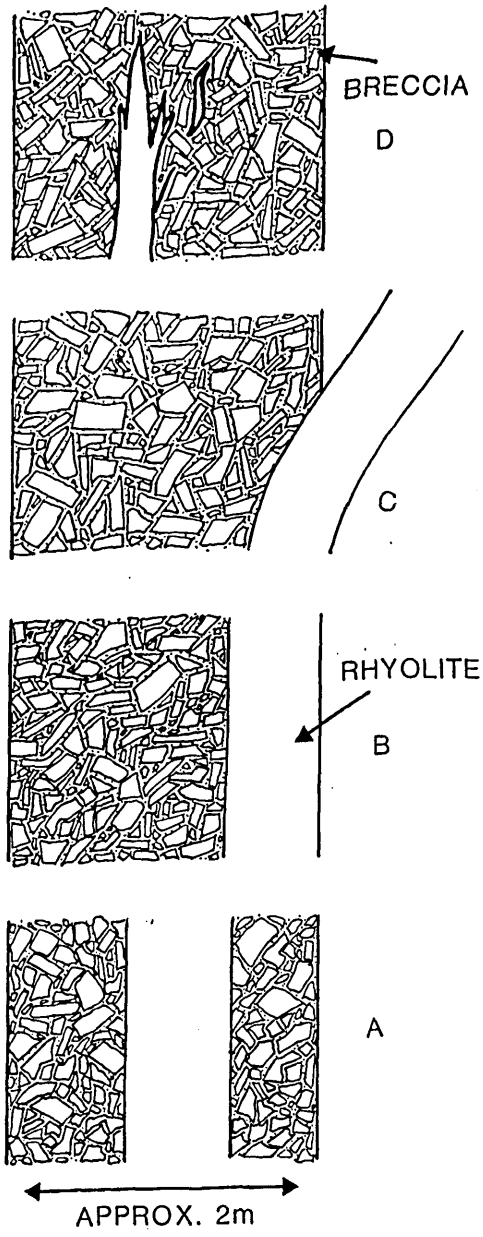

FIGURE 6.03 Sketches of the different relationships between the intrusive breccias, and the rhyolite dykes. Type A is a simple intrusive relationship. Type B shows the rhyolite intruding up the margin of the intrusive breccia. Type C shows the rhyolite dyke veering-off into the country-rock. Type D shows the termination of a rhyolite dyke, and the intimate intrusion of rhyolite between the clasts.

6.3 FORMATION OF THE BRECCIAS

6.3.1 Intrusive and explosion breccias

The presence of vertical, sometimes gradational contacts between the intrusive and explosion breccias and the country-rock has already led to the understanding that these are not sedimentary breccias. The lack of evidence of deformational processes on both macro- and microscopic scales suggests that these are not fault-breccias. Hence the writer is in agreement with the view expressed by Hardie (1963; 1968) that these are intrusive and explosion breccias, which formed below the surface by the shattering of mainly quartzitic country-rock due to the emission of magmatic gas.

The fact that both explosion and intrusive breccias (as defined by Wright and Bowes 1963) are present, suggests that the strength of the gas emissions was variable. Where there are explosion breccias, and the fragments are seen to grade into the country-rock, the force of the gas was weak, and merely caused the disruption of the quartzite, leaving the fragments more or less in situ. The intrusive breccias have sharp, discordant boundaries, which suggest that the fragments have been transported by a more powerful gas flow to their present position.

At locality C (Fig. 6.01), the clasts are composed mainly of Devonian sandstone, with minor quartzite. This indicates that the magmatic gases penetrated through the basement, to disrupt the near-surface sediments.

The planar nature of these breccia bodies suggests that the magmatic gasses were being emitted through a series of fractures.

The rhyolite dykes are usually exposed either in the centre of a breccia body, or close by (Fig. 6.03). Individual dykes run parallel to the length of the intrusive breccias, in concordance with the

arcuate breccia system as a whole. The rhyolites are considered to have intruded after breccia formation as they have suffered no post-displacement disruption, and they occasionally form part of the breccia matrix. It is therefore inferred that the intrusion of the rhyolite dykes involved the utilisation of the crustal weaknesses previously explored by the magmatic gases which created the breccias.

6.3.2. Pyroclastic breccias

Although these rocks have been called pyroclastic breccias so far, two other modes of formation have been postulated, and must be considered.

1) The breccias were considered to have a sedimentary origin (Clough et al 1909; Taubeneck 1967). This is thought unlikely, mainly due to the the presence of igneous fragments in the matrix. Also, the poor sorting and bedding, and the mixing of rounded and angular clasts, suggests that if there is a sedimentary origin, the rock must be a debris flow. However, this is unlikely due to:

a) The inferred palaeotopography at the time of deposition provides no evidence for a nearby source for the flow, such as a large, steep slope. However debris flows can travel great distances.

b) The extent, and alongstrike uniformity of the deposit on Buchaille Etive Mor seems unlikely for a debris flow.

c) The gradation into tuff does not appear consistent with a debris flow origin.

Rounded clasts of granite (derived from the Moor of Rannoch granite), are occasionally found in the breccia, which are cited as evidence for a sedimentary origin for this breccia. It is considered unlikely that the clasts have been both brought up and rounded by magmatic gasses from below

(particularly as more friable clasts, such as the sandstones and andesites are angular). However, it is conceivable that magmatic gases penetrated the Devonian sediments, disrupted a conglomerate containing rounded clasts, redepositing them in a pyroclastic breccia. This would account for much of the variation in angularity of the clasts.

2) The pyroclastic breccia has been described as representing a caldera margin that was formed prior to the main cauldron-subsidence event (Roberts 1974). This theory is based mainly on the fact that some contacts between breccia and quartzite are vertical. There are a number of reasons why the writer considers this unlikely:

a) There is a total lack of evidence for shearing in the breccia. The fragments are randomly oriented near the base of the exposure, and higher up, elongate fragments are flat-lying and undeformed.

b) This theory does not explain the presence of occasional rounded granite fragments that are found in the breccia.

c) The breccia is not continuous from Stob Mhic Mhartuin to Meall a Bhuruidh, and is not uniform. In Cam Ghleann, gently dipping rhyolites are seen directly overlying the quartzites (locality G on Fig. 6.01). Along a caldera margin one would expect to see more uniformity in the fault rocks, and not places where the quartzites are overlain by rhyolite.

d) Gently dipping bedding is seen in the upper parts of these breccias, and there are gradational contacts between the breccias and the overlying tuffs.

e) Roberts (1974) appears to have interspersed descriptions of the pyroclastic breccia with the rhyolite-associated intrusive breccias when discussing evidence for the presence of a caldera margin. This confusion is exascerbated by the lack of a location map which may help other workers to confirm such observations.

The writer is therefore in agreement with the view of Hardie (1968) that the breccias are pyroclastic in origin. Hardie (1968) believes that the outcrop of breccia on Buchaille Etive Mor represents an elongate vent or fissure infilling. This interpretation is based on the presence of vertical contacts observed along the northeastern margin of the breccia with the quartzite. He considers that the southwestern margin of the vent is obscured by overlying volcanics. The writer considers this unlikely due to: a) Many of the northeastern contacts between breccia and quartzite are not vertical. The vertical contacts that are seen are poorly exposed, and are probably a reflection of the undulating Devonian palaeotopography. b) It seem remarkably 'fortuitous' that only one margin of this apparent vent has been exposed by erosion, and not the other.

However the exposure around locality C (section 6.2.2) is consistent with the vent-infilling hypothesis. This may also be the case for other individual localities in the breccia, but not for its entire length.

In summary, it is believed that the breccia is pyroclastic, having been erupted from a number of vents similar to the one exposed at locality D (Fig. 6.01). Bedding in the upper part of the body is typical of air-fall deposits. This was immediately followed by the eruption of tuffs and rhyolites. These were probably erupted through the same vents from as the breccias. Igneous material similar to the tuffs is found in the breccia matrix, and there is a gradation from breccia into tuff, followed by rhyolite. It is common in these sorts of explosive environments for magmatic gases to 'clear' the vent of country-rock fragments prior to the eruption of igneous material (R.A. Bailey pers. comm.).

6.4.1. Conclusions

1) There are two types of breccia present in the eastern section of the Glencoe cauldron. Firstly there are elongate intrusive breccias disrupting the basement quartzites. Secondly, there is a thick deposit of pyroclastic breccia at the base of the Devonian volcanic sequence.

2) The intrusive breccias were formed by the passage of magmatic gases along an arcuate fissure system. These crustal weaknesses were then exploited by rhyolitic magmas to create rhyolite dykes.

3) At locality F (Fig. 6.01) a large intrusion of rhyolite is observed, which is interpreted as the conduit to a rhyolite dome. Here, an intrusive tuff is found, which is intruded by later rhyolite, indicating the presence of explosive and non-explosive eruptive activity.

4) On the surface there was concurrent explosive activity, fragmenting the country-rock quartzite and sediments to deposit a pyroclastic breccia up to 30m thick. The eruptions are believed to have occurred from a series of vents. On Buchaille Etive Mor, the pyroclastic breccia grades into a tuff, which contains some flattened pumices.

5) The eruption of the gases, and deposition of the breccia is believed to have cleared the vents of country-rock fragments. The rhyolitic tuffs and lavas were subsequently erupted from these vents.

6) All of the volcanic features described form an arcuate outcrop pattern, which is sub-parallel to the ring-fault. The breccias were formed prior to cauldron subsidence, as they are cut by the fault, but the arcuate outcrop pattern may indicate an inherent crustal weakness in that area, which was later to be explored by the ring-fault.

6.4.2 A 3-Dimensional Model

The close proximity of the intrusive and pyroclastic breccias is not considered to be coincidental. The two rock-types are believed to be genetically related (Fig. 6.04), and a 3-dimensional model is proposed (Fig. 6.05).

A build-up of gas pressure initiated the fracturing of the country-rock above the magma-chamber (Fig. 6.04, part 1). This enabled the release of magmatic gasses under pressure along arcuate fractures. This gas brecciated the country-rock to produce linear bands of intrusive and explosion breccia (Fig. 6.04, part 2). Some of the gasses penetrated through to the surface and erupted at a number of vents in an explosive manner. These explosions led to the deposition of pyroclastic breccias (Fig. 6.04, part 3), although some only formed vent breccias (Fig. 6.05 section 4).

Following the release of gas, rhyolitic magma (some of which may still have been exsolving gas), intruded along the fractures previously explored by the magmatic gases, to form dykes. The fine grainsize of the rhyolite suggests that these intrusions were fairly close to the surface. Much of the rhyolitic material then erupted at the surface to form tuffs and lavas (Fig. 6.04, part 4). In more modern volcanic environments rhyolite is believed to erupt from enlarged vents, and not fissures, to feed domes (R.A. Bailey pers. comm.). It is believed that the outcrop of rhyolite at locality F represents such a vent, through which tuffs and rhyolite erupted, probably on more than one occasion (section 1, Fig. 6.05). The paucity of intrusive tuffs compared to their eruptive counterparts has been noted, but it is a common feature of explosive silicic volcanism. This may be due to the destruction of eutaxitic textures in intrusive tuffs during the 'closure' of a vent after eruption. With the features of a tuff destroyed, the 'tuff' would then resemble a rhyolite

FIGURE 6.04 4-stage model showing the evolution of the breccias and rhyolitic dykes. Stage 1 shows fracturing of the country-rock above a vesiculating magma-chamber. Stage 2 shows the formation of intrusive breccias due to the release of gas from the magma-chamber. Stage 3 shows the eruption of pyroclastic material on the surface. Stage 4 shows the exploitation of the breccia-filled fractures by rhyolitic lava.

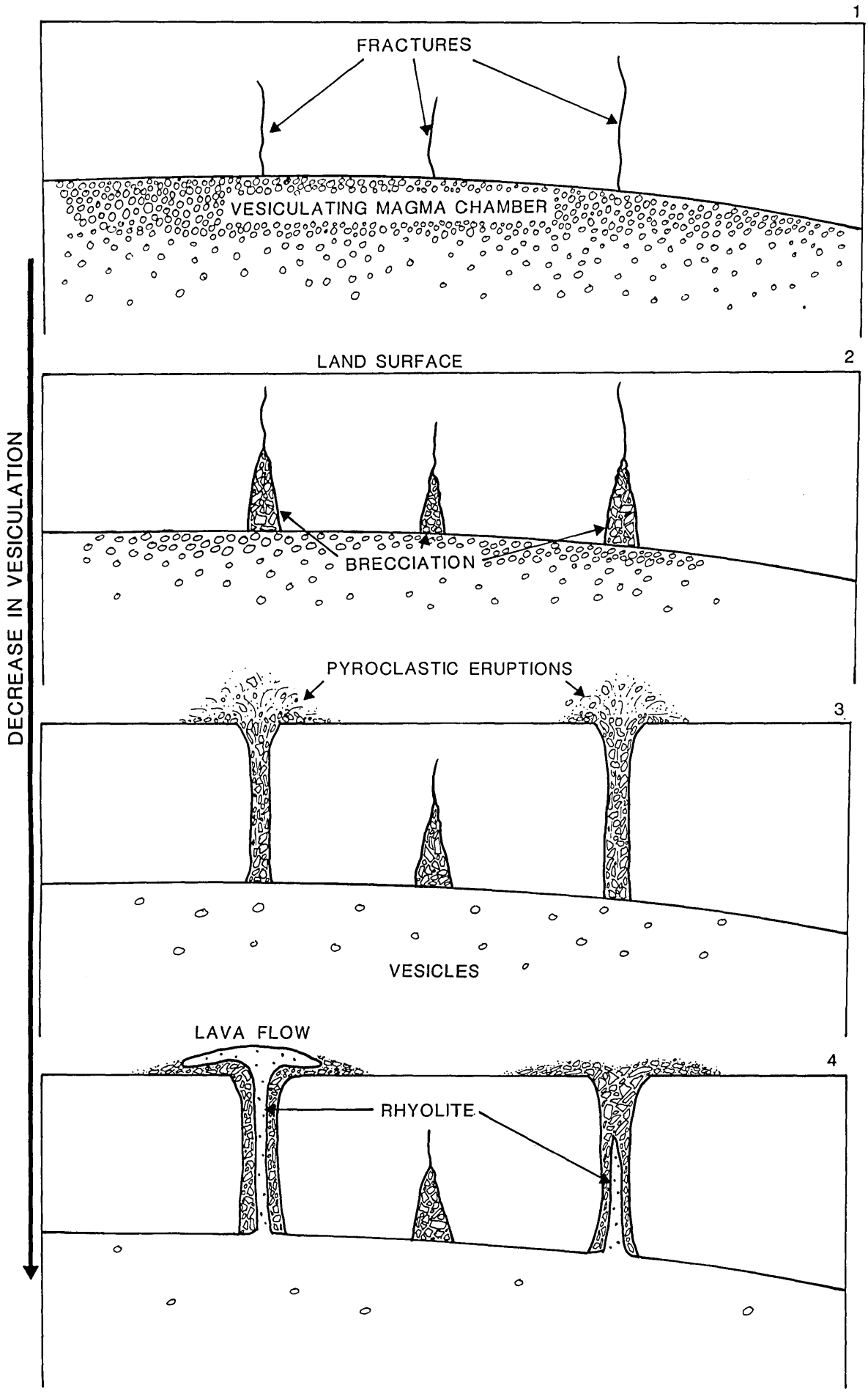
1
FRACTURES
VESICULATING MAGMA CHAMBER
LAND SURFACE
2
BRECCIATION
PYROCLASTIC ERUPTIONS
3
VESICLES
LAVA FLOW
4
RHYOLITE
DECREASE IN VESICULATION

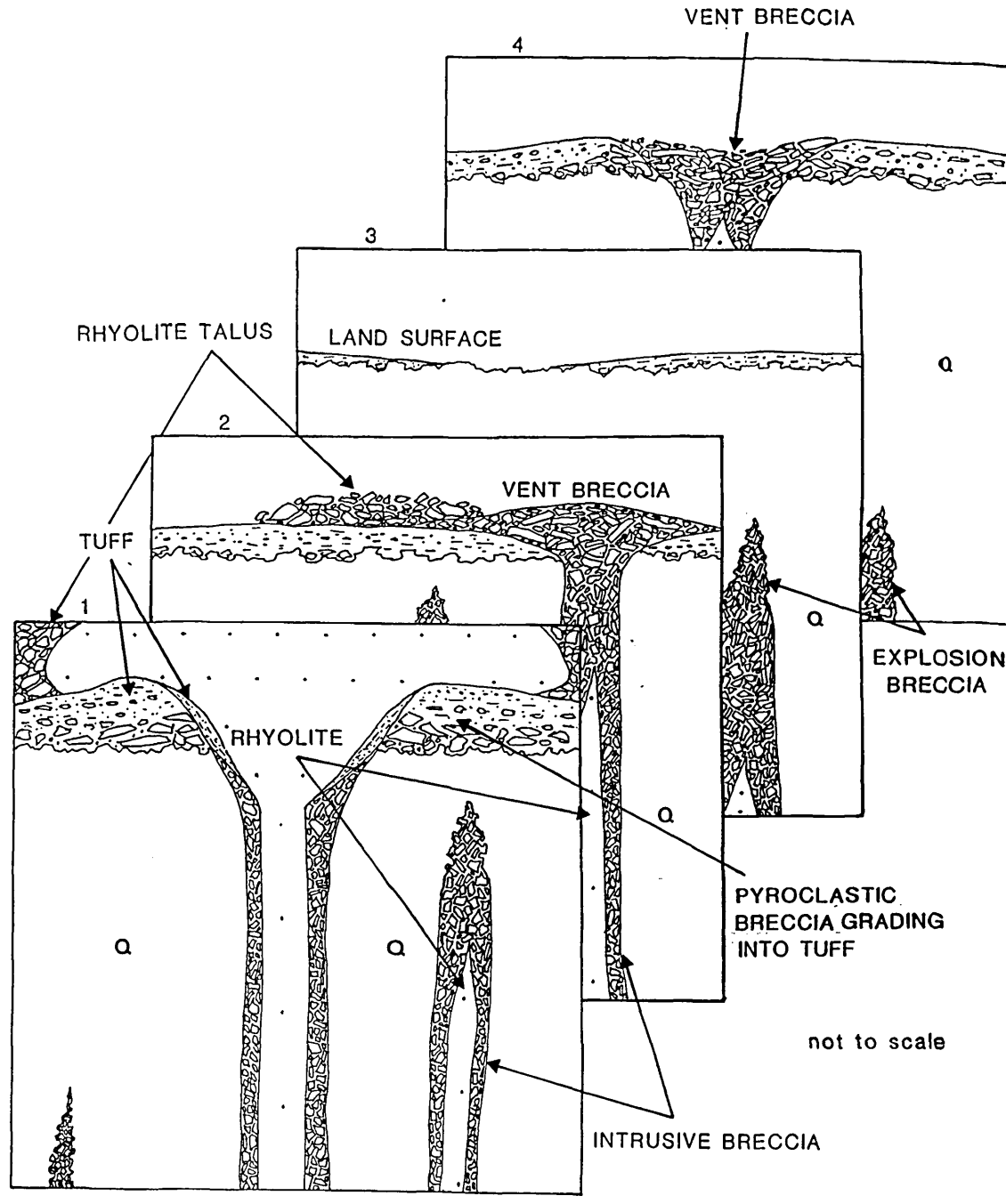

FIGURE 6.05 A 3-dimensional model showing the inferred relationship between the breccia types observed, and the tuffs and rhyolitic lavas. Q represents Dalradian quartzite. See section 6.4.2 for details

dyke or conduit (Wolff 1986). Hence it may be the case that some of the intrusive rhyolites in Glencoe were originally emplaced as tuffs.

The combination of all of the features described in this chapter have been observed in other areas, and will be discussed in chapter 8.

CHAPTER 7

THE ORIGIN AND NATURE OF THE FLINTY CRUSH-ROCK

7.1 INTRODUCTION AND TERMINOLOGY

The nature of the 'flinty crush-rock' (F.C.R.) of Glencoe, is a problem which has vexed workers in the area for many years (Clough et al. 1909; Reynolds 1956; Bailey 1960; Hardie 1963; Taubeneck 1967; Roberts 1966b, 1974). Previous work has been based on fieldwork and optical microscopy, studied in conjunction with the relationship between the F.C.R. and the ring-intrusion, aswell as wider conjectures concerning the mechanisms of ring-faulting (Reynolds 1956; Hardie 1963). Unfortunately, the fine grainsize of the F.C.R. precluded any detailed mineralogical and textural studies, which has resulted in controversy concerning the nature and formation of this rock (section 7.2). By using scanning electron microscopy (S.E.M.) one can examine the mineralogy and textures of ultra fine-grained rocks, enabling a more thorough scientific interpretation.

There has been much discussion and controversy concerning the terminology and classification of fault rocks, particularly fine-grained fault rocks (Sibson 1977; White 1982; Wise et al. 1984; Mawer 1985). The approach used in this work is based on a classification outlined by Obee (1985), which relies upon the dominant deformation mechanism active during the formation of the fault rock (Fig. 7.01). One drawback of this method is the difficulty applying it in the field, however the term 'flinty crush-rock has so far proved an adequate field term (Higgins 1971).

Three rock types from the classification (Fig.7.01) are considered in this study:

1) Cataclasite is composed of angular to subrounded host rock fragments set in an ultra

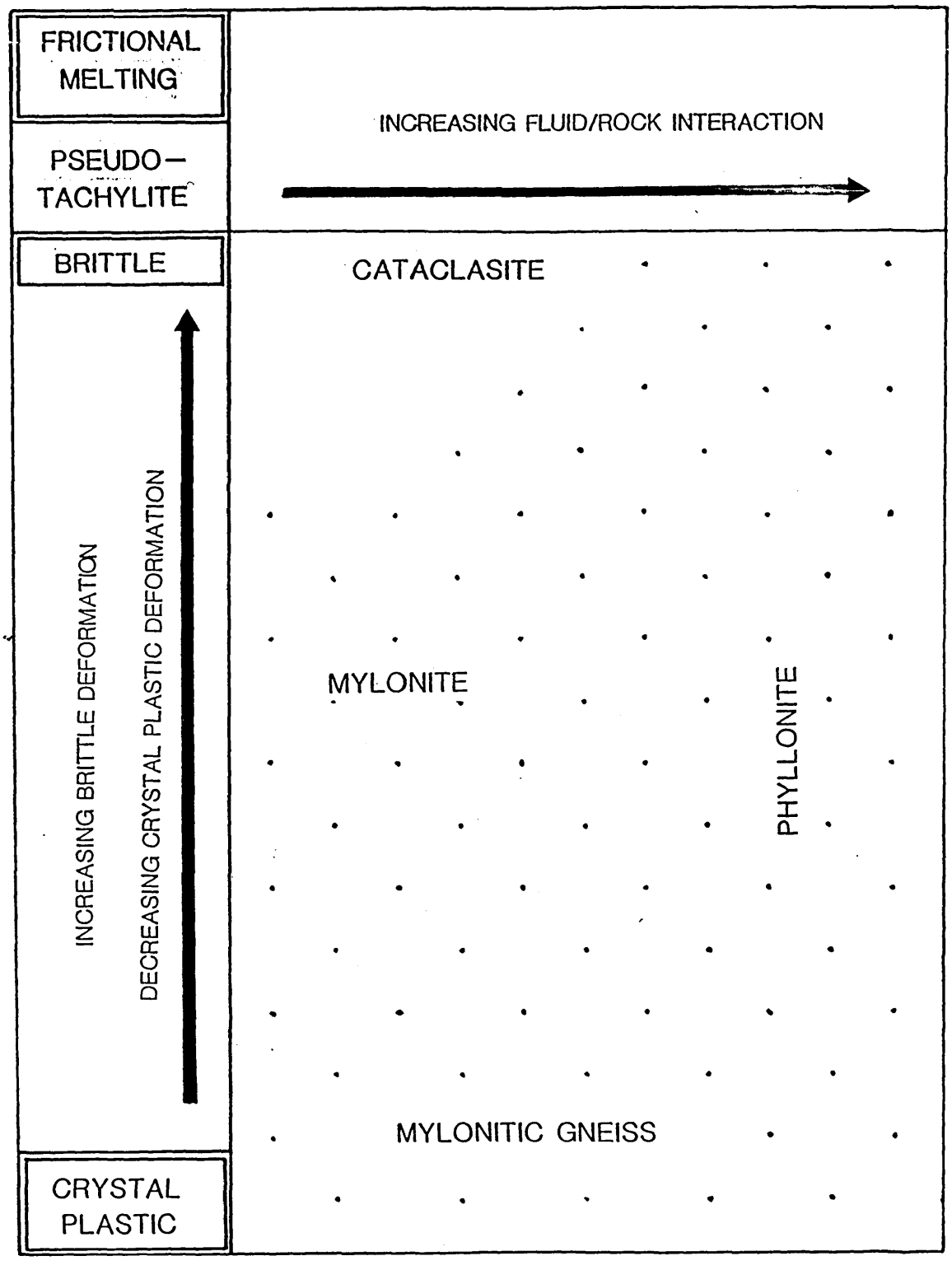

FIGURE 7.01 Mechanistic classification of fault rocks. The shaded area represents rocks that are usually foliated. (After Obee 1985)

fine-grained matrix of host rock fragments. Cataclasis is a brittle deformation process resulting from frictional sliding. This leads to grainsize reduction, grain rotation and random crystallographic orientations. It is accompanied by dilatancy, hence cataclasis is a pressure-sensitive deformation mechanism.

2) Mylonites are fine-grained, foliated fault rocks. This group of fault rocks forms by crystal-plastic processes, which usually result in a preferred crystallographic orientation. Although mylonites are not described in this work, this term has been used as a field term for some outcrops of F.C.R. by previous workers (Clough et al. 1909; Bailey 1960).

3) Pseudotachylites. These rocks have a glassy or devitrified texture, having cooled from a clast-laden silicate melt formed by frictional melting. Mechanical considerations demonstrate that this process occurs during seismic faulting events (Sibson 1975).

Also described in this work are fault breccias. These are coarse-grained, clast-supported rocks composed of angular to sub-rounded clasts, set in a fine-grained matrix derived from the host rock.

Tuffisite is another term which is considered later with respect to the F.C.R., but does not fall into any of the fault rock categories. This term was introduced by Cloos (1941) to describe an intrusive mixture of coarse blocks set in a fine-grained tuff. This definition was refined by Reynolds (1954), with the term tuffisite being restricted to fine-grained rocks, whilst the term tuffisitic breccia was introduced to represent coarse-grained, intrusive, clast-laden tuffs (Wright and Bowes 1963).

The field exposure of all the fault rocks has been described in chapter 2. These rocks are located along the ring-fault separating Dalradian basement rocks (commonly flaggy quartzites) from the ring-intrusion. The important points are summarised below:

1) The fault rocks show a gradation in grainsize from quartzitic breccia to F.C.R..

2) The F.C.R. contains rounded quartz grains, but some exposures also have euhedral feldspar 'megacrysts'.

3) The finest-grained F.C.R. is flow-banded.

4) Splays of F.C.R. up to 5m long and 5cm wide are found as sheets which diverge away from the fault zone.

5) Sheets of F.C.R. are found on non-planar surfaces, also as small pods, and sigmoidal infillings.

6) There is <u>not</u> a pervasive network of interlocking veins of F.C.R., which is distinctive of many intrusion-associated 'fault-rocks', such as the Slieve Gullion pluton in Northern Ireland (Reynolds 1956).

7) The F.C.R. is usually associated with a poorly feldsparphyric red felsite. The association is often intimate.

8) F.C.R. and red felsite are found at all outcrops of the ring-fault, except where the Devonian sediments and volcanics have been downfaulted against the Dalradian metasediments, where neither are observed.

Previous workers have offered two alternative theories as to the nature and formation of the F.C.R. (section 1.3). The rock was originally thought to have been formed by frictional melting (i.e. pseudotachylite) (Clough et al. 1909; Bailey 1960). This view was challenged by Reynolds (1956), who

considered the F.C.R. to be an ultra fine-grained intrusive breccia or tuffisite, which was formed by the brecciation of country-rock by magmatic gas es. This process, known as gas-fluidisation (Reynolds 1954), was also considered to have been the most likely method of formation by a number of other workers (Hardie 1963; Taubeneck 1967; Roberts 1966b, 1974). Other possible explanations for the formation of the F.C.R., such as thermal spallation are considered in the following discussion.

The term 'flinty crush-rock' has been used previously as a descriptive field term for all fine-grained ring-fault rocks. Some of these rocks are cataclasites. From hereon the term 'flinty crush-rock' is used solely for the rock compositions described in section 7.3.3.

7.3 F.C.R. TEXTURES AND MINERALOGY

7.3.1 Marginal breccias

The fault zones show a gradation from breccia to F.C.R.. These breccias occur mainly in the quartzites adjacent to the ring-fault, but are also observed in the schists exposed in the western part of the area (G.R. NN142571). Breccias are also present in the shear zones and shatter belts that run sub-parallel to the ring-fault (Fig. 2.04).

The quartzitic breccias are composed of rotated, clasts ranging in size from 5mm to 8cm, which are set in a fine-grained quartz matrix. The rock is clast-supported, and the texture of the clasts is similar to that of the host quartzite. Quartz crystals within the clasts are strained and show undulose extinction, but this is also observed in the unbrecciated quartzites, and is thought to have been caused by a previous deformation event. In clasts of flaggy quartzite, platey mica grains are totally

undeformed, but are smeared-out and altered in the matrix (Plate 7.01).

The matrix fills the small gaps between the rounded clasts. It is mainly composed of small rounded quartz grains. Smeared-out micas are also present, suggesting that shearing was responsible for the breccia formation, leading to grainsize reduction of the quartz crystals. There is no evidence that shattering in the absence of shearing, as is seen in the breccias described in chapter 6, was responsible for the grainsize reduction in either the fault breccias, or the cataclasites described below.

Where the fault rocks cut schistose rocks, they are dominantly composed of recrystallised micas enclosing lenses of recrystallised quartz.

7.3.2. Cataclasite

The cataclasites have similar mineralogical components to the quartzitic breccias, but have a much lower clast to matrix ratio. The rounded quartzite clasts are up to 2mm in diameter, and form less than 5% of the total rock. The clasts show no internal deformation. In addition to the quartzite clasts, individual rounded to sub-angular quartz fragments (0.2-1mm in diameter) are present, which appear to be abraded fragments derived from the quartzite clasts. They are set in a very fine-grained quartz matrix (10-200 microns). Both the larger quartz grains and the fine-grained matrix have been derived by the reduction of larger quartz crystals by brittle deformation processes.

All gradations are observed between the breccias described above, and the cataclasite. In other samples the breccias are cut by sheets of cataclasite, which in turn are cut by veins of F.C.R. (Plate 7.02), thus displaying the temporal relationship between the three types of fault-rock. This is evidence for a process of progressive deformation.

PLATE 7.01 Photomicrograph in plane polarised light of a brecciated quartzite (1JG21), with accompanying line drawing. B = undeformed biotite. Note the deformed biotites present in the breccia matrix.

PLATE 7.02 Photomicrograph under crossed polars of a fault rock (1JG35), with accompanying line drawing. This shows the cross-cutting relationship between breccia, cataclasite and F.C.R..

7·01

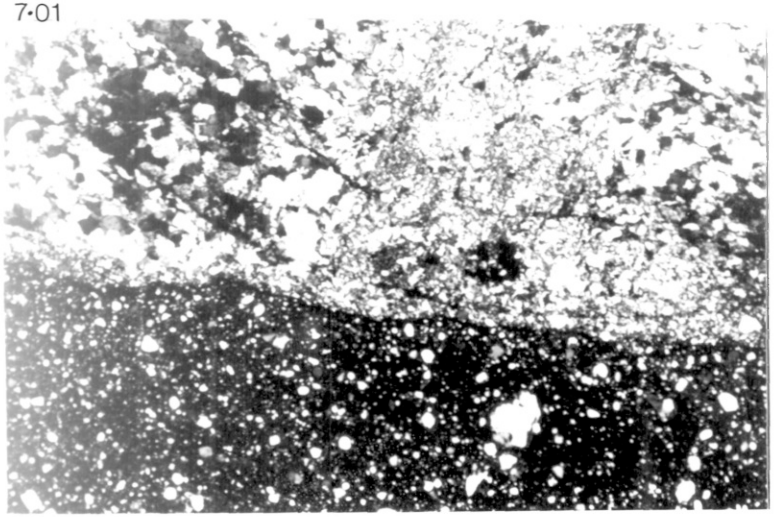

7·02

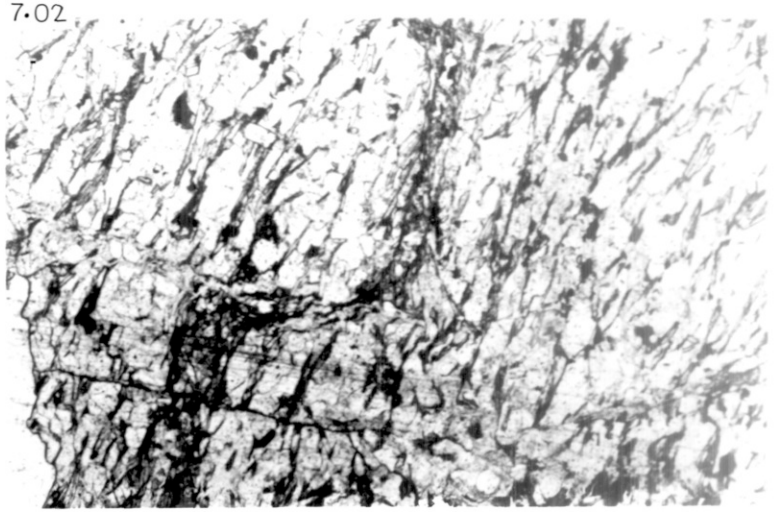

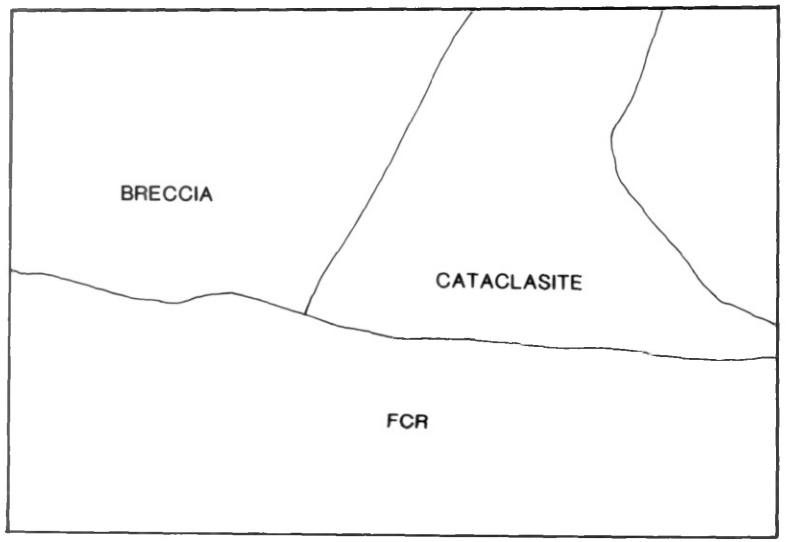

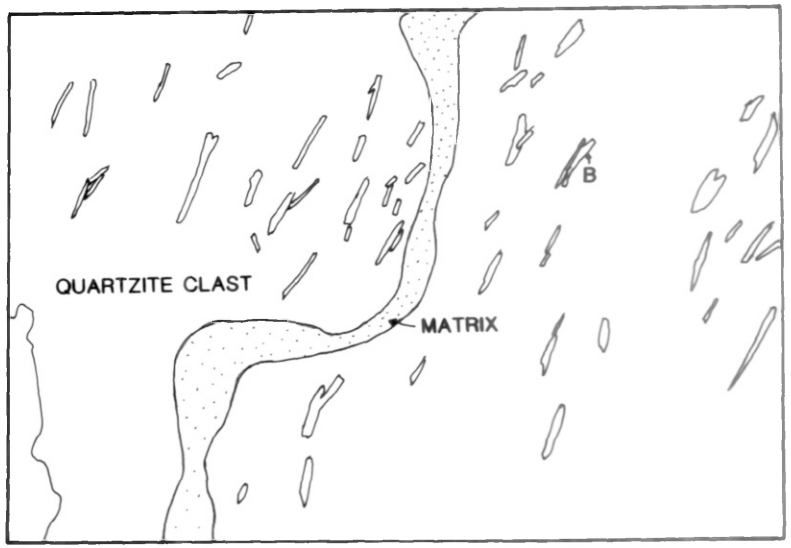

7.3.3 The Flinty Crush-Rock

The F.C.R. is composed of a number of small, but discernible particles (0.01-1mm) set in an ultra fine-grained matrix. The brown or black matrix commonly has a strongly banded fabric, which diverges around the particles, and shows eddies and swirls (see section 7.3.5). The rock is coherent, and may be 'welded'.

Four different types of particle are observed using an optical microscope: a) quartz fragments b) megacrysts c) clasts of cataclasite d) 'clasts' of red felsite (rhyolite).

a) The quartz fragments range in size from 10-100 microns, and are sub-angular to rounded. They typically form about 30% of the rock (Plate 7.03). The non-angularity of some fragments suggests that processes other than abrasion during brittle deformation may have been responsible for their generation. The fragments are evenly distributed throughout the rock.

b) Many samples of F.C.R. contain 'megacrysts'. They generally range in size from 0.5mm to 5mm. Most megacrysts are euhedral feldspars, but embayed quartz crystals and graphic intergrowth 'crystals' are occasionally found. No evidence of internal deformation or fracturing is observed. The megacrysts are surrounded by either 1) a thin layer of rhyolitic material, or 2) an overgrowth (Plates 7.04, 7.05). In sample 1JG39 an alkali feldspar crystal has an overgrowth of pure albite (plus some tiny acicular crystals which were too small to analyse) (Plate 7.04). In the same rock there are also embayed quartz crystals with a rim of pure K-feldspar (Plate 7.05). The rims may be overgrowths caused by disequilibrium reactions between the crystals and the F.C.R. matrix.

c), d) Small blebs and streaks of rhyolite and cataclasite are enclosed within the F.C.R. matrix, these are considered further in section 7.3.5.

PLATE 7.03 Photomicrograph in plane polarised light of typical F.C.R. (1JG73). Q = quartz.

PLATE 7.04 BEI micrograph of an alkali feldspar megacryst in F.C.R. (1JG39). K = k-feldspar, P = plagioclase (albite). Scale bar is 100 microns.

PLATE 7.05 BEI micrograph of a quartz megacryst in F.C.R. (1JG39). Q = quartz, K = k-feldspar. Scale bar is 100 microns.

PLATE 7.06 BEI micrograph of typical F.C.R. (1JG73). Q = quartz, P = plagioclase (albite), K = k-feldspar, B = biotite. Scale bar is 100 microns.

PLATE 7.07 BEI micrograph of typical F.C.R. matrix (1JG73). P = plagioclase, B = biotite, K = k-feldspar, Q = quartz. Scale bar is 10 microns.

PLATE 7.08 Photomicrograph of a spherulitic rhyolite (3JG64) in plane polarised light.

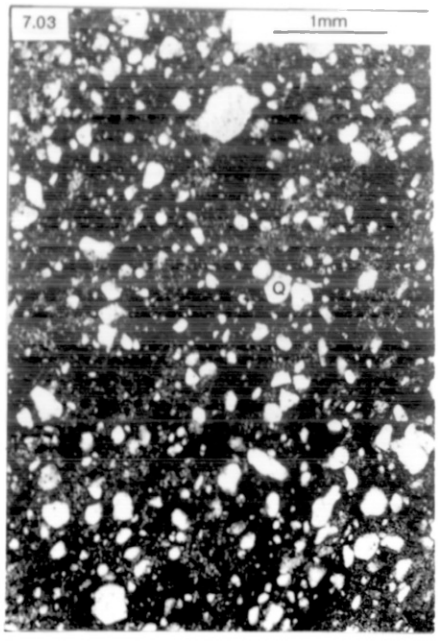
7.03
1mm
Q

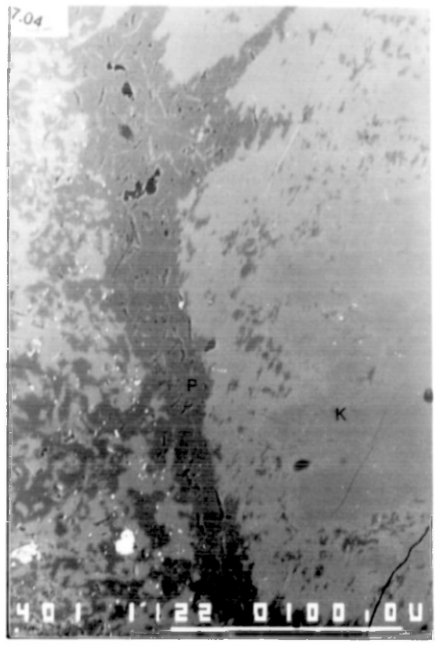
7.04
P
K

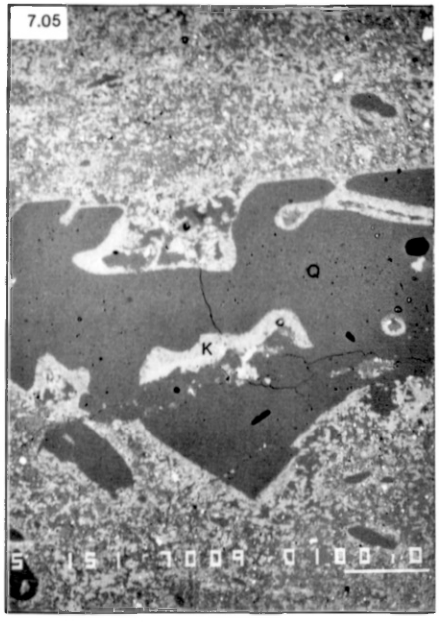
7.05
Q
K

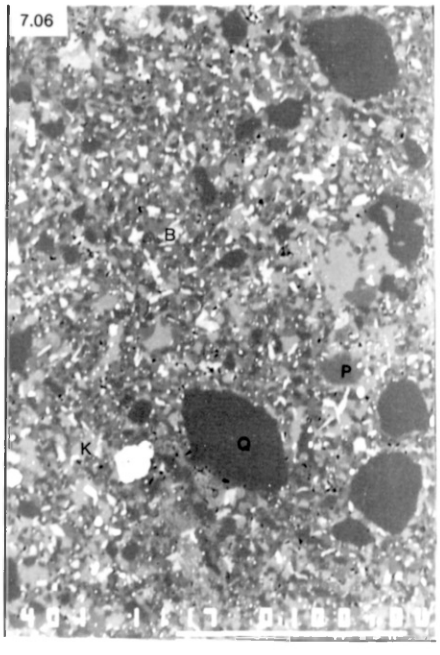
7.06
B
P
K
Q

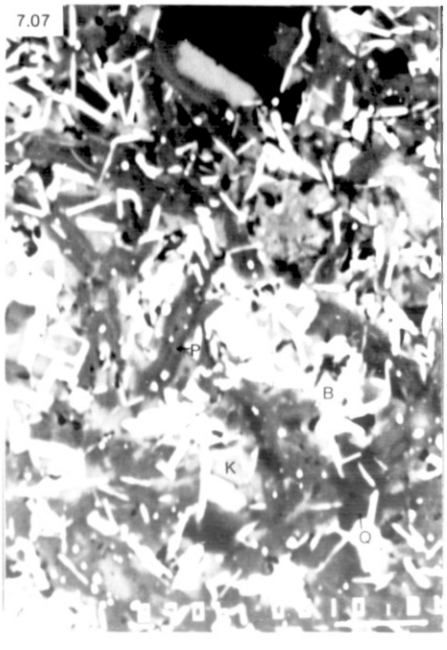
7.07
P
B
K
Q

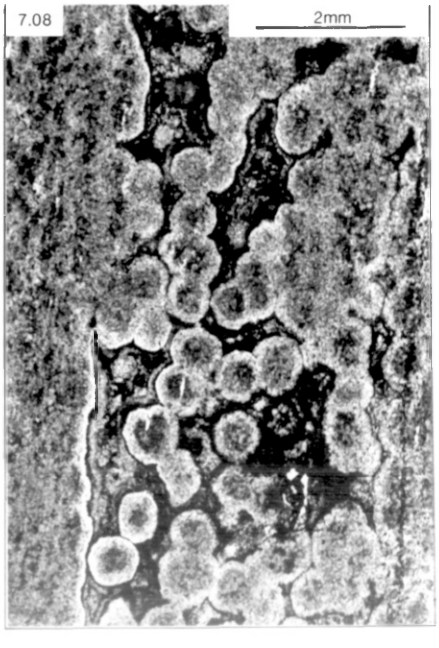
7.08
2mm

The mineralogical composition of the F.C.R. matrix is not discernible using an optical microscope. It appears as a dark (either black or browny-black), ultra fine-grained material. However, studies of the matrix can be greatly enhanced by using the S.E.M. in back-scattered electron imagery.

The black F.C.R. does not usually contain any megacrysts. It consists of an irregular intergrowth of quartz, albite and K-feldspar, enclosing tiny plates of biotite (Plate 7.06). The grainsize ranges from 1 to 10 microns; this seems to be a controlling factor in the degree of 'blackness' of the matrix in both the F.C.R. and the cataclasites, in hand-specimen and thin-section, with the darkest material having the smallest grainsize. The brown F.C.R. has a similar mineralogy, but contains more, better developed biotite plates, which are commonly replaced by chlorite (Plate 7.07).

The textures in the F.C.R. matrix suggest that it has crystallised from a melt. However, no evidence has been found to suggest that the matrix may originally have been glassy. The mineral composition of the F.C.R. is dissimilar to that of the cataclasites, breccias and Dalradian country-rock which are dominantly composed of quartz.

7.3.4. Red Felsite

The red felsite is a poorly porphyritic rhyolite of variable composition (chapter 4, section 7.4). The red colouring is uniformly pervasive throughout the rock, and may have been caused by late stage oxidation and redistribution of Fe by hydrothermal fluids.

The phenocrysts are mainly plagioclase and alkali feldspar, and commonly produce a glomeroporphyritic texture. These are unzoned, euhedral crystals, up to 5mm in length. There are also a few embayed quartz crystals of a similar size. Some samples have small remnant phenocrysts of

amphibole and biotite which have been largely pseudomorphed by chlorite.

The groundmass has a grainsize of up to 0.1mm. The texture is granular, though some samples show a spherulitic devitrification texture which is aligned in bands parallel to the flow-banding in the F.C.R. (Plate 7.08). The more acidic samples of rhyolite have a groundmass of intergrown quartz and alkali feldspar (Plate 7.09). Others contain small plates of biotite (Plate 7.10). There is a very strong similarity in both mineralogy and texture between the rhyolite groundmass and the F.C.R. matrix (Plate 7.07).

7.3.5 Mixing Relationships

It has been noted that there are often sharp boundaries between the F.C.R. and the cataclasites (section 7.3.2). These are not always planar. Often, blebs and swirls of cataclasite can be seen enclosed in the F.C.R., in a similar fashion to the rhyolite blebs described below.

Different types of mixing between the F.C.R. and the red felsite (rhyolite) have been observed in outcrop, and described in chapter 2. These vary from the interfingering of stringers of one rock type within another (immiscible mixing), to the complete mixing of the two rocks to produce a hybrid (wholesale mixing). In thin-section, details of the marginal relationships between the two media are seen, giving an important insight into the generation of the fault rocks.

As mentioned above small clasts or blebs of rhyolite are enclosed in the F.C.R.. In addition, thin stringers and tongues of rhyolite are common within the F.C.R., which are parallel to, and accentuate, the banding (Plate 7.11). Many of the blebs show eddy structures which resemble turbulent mixing between two viscous fluids (Plate 7.12).

The boundaries between the rhyolite and F.C.R.

PLATE 7.09 BEI micrograph of acidic rhyolite (1JG25). P = plagioclase, K = k=feldspar, Q = quartz. Scale bar is 10 microns.

PLATE 7.10 BEI micrograph of less acidic rhyolite (4JG20). P = plagioclase, K = k-feldspar, B = biotite. Scale bar is 10 microns.

PLATE 7.11 Photomicrograph in plane polarised light of the mixing of rhyolite and F.C.R. (3JG12). R = rhyolite, P = plagioclase megacryst.

PLATE 7.12 Photomicrograph in plane polarised light showing eddy structures in F.C.R. (1JG39). R = rhyolite, P = plagioclase megacryst.

PLATE 7.13 Photomicrograph in plane polarised light of the boundary between rhyolite and F.C.R. (4JG20), with accompanying line drawing. Note the stringers of rhyolite within the F.C.R. parallel to the boundary, and the swirl of rhyolite labelled R. P = plagioclase megacryst.

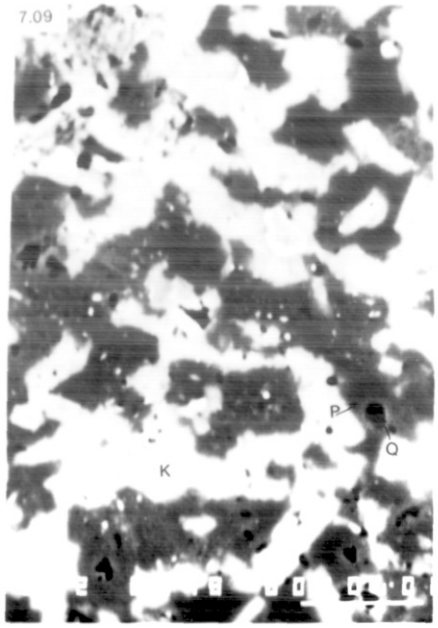
7.09
P
Q
K

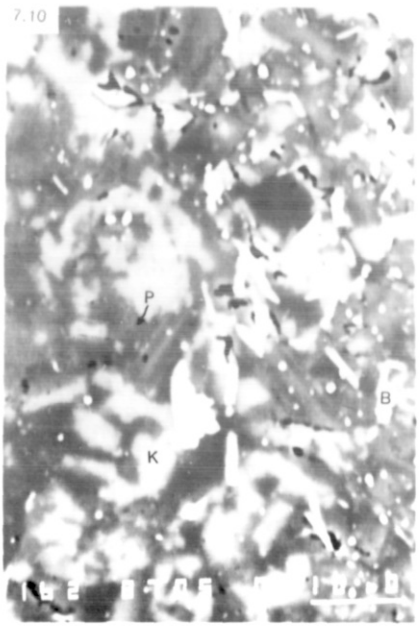
7.10
P
B
K


7.11
2mm
R
P
R

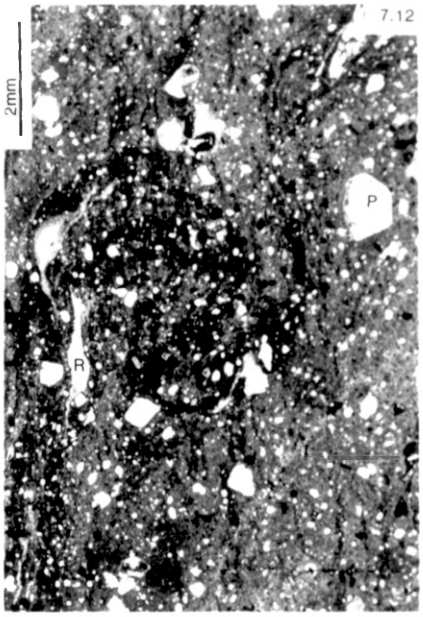
7.12
2mm
P
R

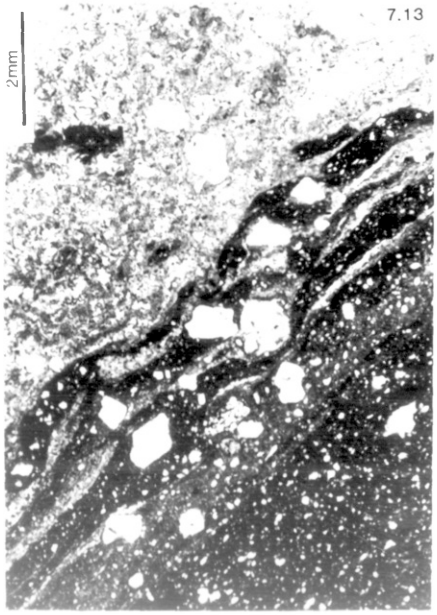
7.13
2mm

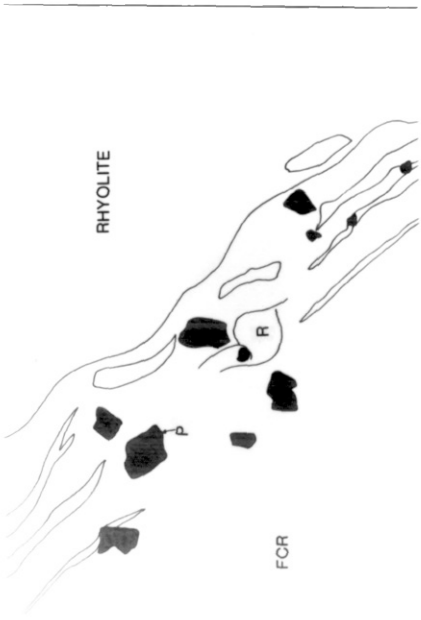
RHYOLITE
R
P
FCR

are often very sharp, with no obvious interaction between the two components (Plate 7.11). However, in other instances, the boundary is gradational, producing a hybrid zone. The hybrid material is brown in colour, and contains both rounded quartz clasts and euhedral feldspar megacrysts. Its mineral composition and matrix texture is identical to that of the brown-coloured F.C.R. described previously (Plate 7.07).

Many of the megacrysts in the F.C.R. have a thin coating of rhyolite, and others are seen spanning the boundary between rhyolite and F.C.R. (Plate 7.13). It is therefore inferred that all the megacrysts in the F.C.R. are derived from the rhyolite, and that the F.C.R. which contains the megacrysts is in fact a hybrid rock. This probably accounts for the overgrowths on many megacrysts.

The discovery of these mixing relationships promotes a number of conclusions:

1) Both the rhyolite and F.C.R. were in a fluid state at the time of mixing.

2) No deformed megacrysts are observed indicating that mixing took place after the deformation had ceased, or that deformation was entirely partitioned into the matrix without affecting the margins of the megacrysts.

3) The presence of both sharp and gradational boundaries indicates that mixing occurred under varying conditions of, for example, temperature and viscosity.

4) Mixing was progressive. Initially cataclasite mixed with probably small amounts of rhyolite to produce much of what has been described as F.C.R.. This was in some instances, then mixed with more rhyolite, leading to an increase in the amount of biotite and feldspar in the matrix.

Hence, the correct term for the F.C.R. is a tuffisite (Reynolds 1954).

7.4.1 Analytical methods

Chemical analyses have been obtained for the fault rocks, in order to test the observations and interpretations concerning their mixing and origin.

A number of whole rock analyses of the rhyolite, breccias and F.C.R. have been obtained using X.R.F. analysis (see Appendix C). However the intimate mixing of the cataclasite and rhyolite precludes any detailed investigation of the geochemistry by this method.

Bulk analyses of the fault rocks have been obtained by selected area scanning using E.D.S. x-ray analysis in the S.E.M.. Areas ranging between 100 and 1000 square microns were analysed, which gave reasonable totals providing that care was taken to avoid holes in the slide (details of the method used are given in appendix A, and the analyses are given in appendix E).

7.4.2 Results

Variations in the chemistry between the different rock-types are illustrated in plots of Al_2O_3, Na_2O+K_2O and CaO against SiO_2 (Fig. 7.02). In general, most of the F.C.R. is poorer in silica than the cataclasites and quartzitic breccias, and richer in silica than the majority of the rhyolites.

The plot of Al_2O_3 against SiO_2 has a well-defined slope, which perhaps indicates mixing between the Al-poor cataclasite and rhyolite which is richer in Al_2O_3. The plot of total alkalis against silica is more variable, but in general the F.C.R. analyses fall in between the high alkali compositions of the rhyolite, and the low alkali composition of the cataclasite, again indicative of mixing. Calcium is the only other element present in large enough

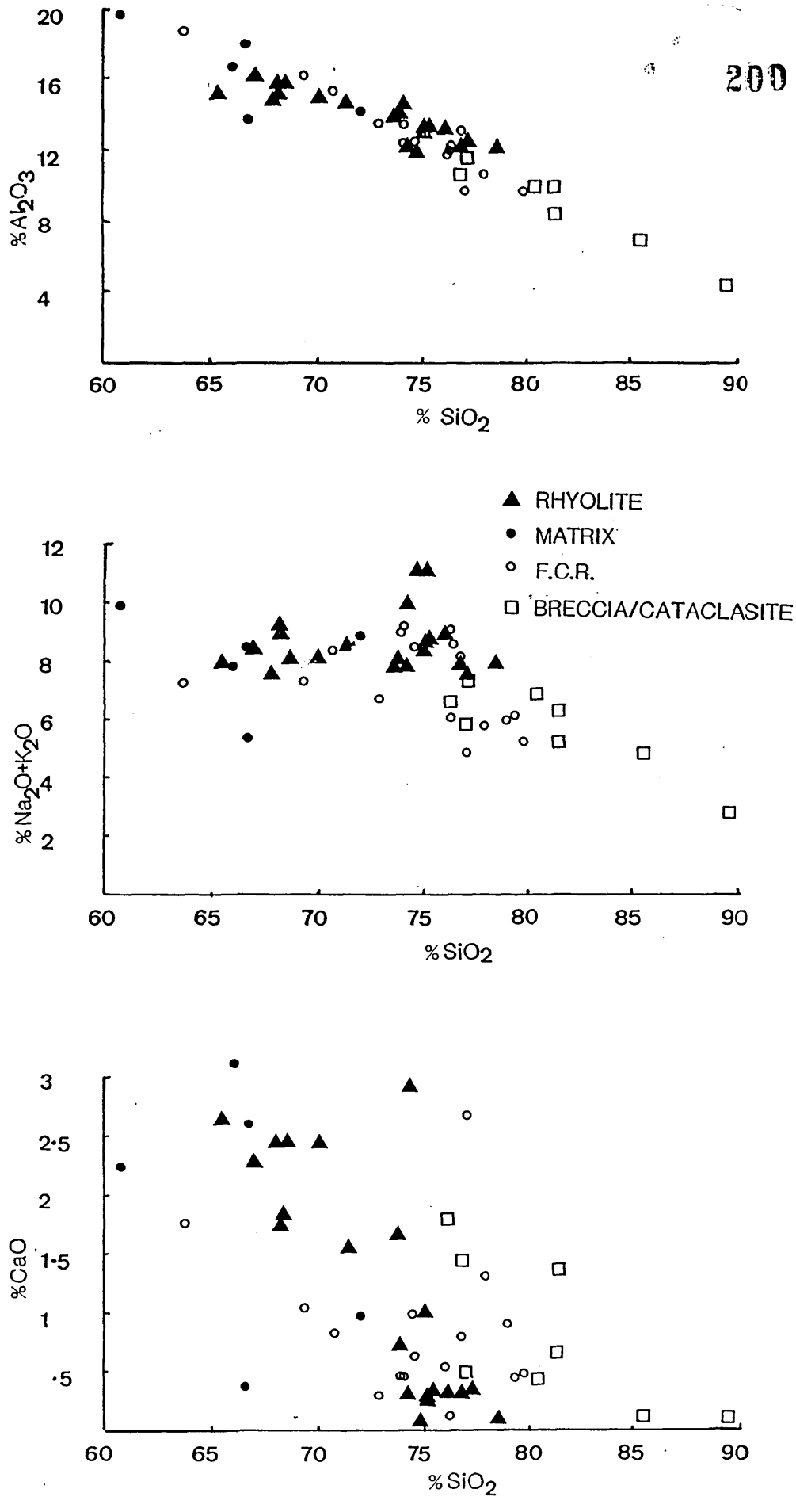

FIGURE 7.02 Binary plots of Al2O3, Na2O+K2O and CaO against SiO2 for the fault rocks.

quantities to be useful in these analyses. However the variable content of CaO in all of the rock types leads to a complex picture which cannot easily be interpreted. The range of CaO data is probably due to variable amounts of plagioclase in both the cataclasites and rhyolites.

The F.C.R. matrix compositions are mostly silica poor, and some are nearly identical to some rhyolite analyses. This implies that intimate mixing has occurred between cataclasite and more basic, less viscous rhyolite. This is consistent with petrographic evidence, whereby tongues of viscous, acidic rhyolite mix immiscibly with the cataclasite and F.C.R., but contacts between less acidic rhyolite and cataclasite or F.C.R. are gradational and produce a hybrid rock. Some matrix compositions are poorer in SiO2 than any rhyolite analyses. However, these are essentially similar to the composition of feldspar, and it is possible that a representative sample was not taken due to the small area analysed.

7.4.3. Origin of the rhyolite (red felsite)

Previous workers have either disregarded the rhyolite (Reynolds 1956; Roberts 1966b), or described it as the chilled margin of the ring-intrusion (Bailey 1960). This theory is disputed by the author due to a number of reasons:

1) A sharp boundary is seen between the rhyolite and the ring-intrusion.

2) The rhyolite is of variable thickness, and in places is not present between the F.C.R. and the ring-intrusion.

3) At certain localities the rhyolite intrudes the ring-intrusion.

4) The phenocryst phases within the rhyolite are of a different size and composition of phenocryst phases to those in the ring-intrusion.

5) If the rhyolite represents a chilled margin of an evolving intrusion, one would expect it to be

of a more basic composition than the adjacent ring-intrusion, whereas in fact it is more acidic.

Points 4) and 5) also rule out the possibility that the rhyolite or F.C.R. may have been derived by the frictional melting of the ring-intrusion during cauldron subsidence.

Two whole rock compositions of rhyolite have been included in the geochemical plots in chapter 4 as a comparison to the ring-intrusion rocks. The more acidic sample has a composition very similar to a granite (1JG61) which lies between the acidic ring-intrusion rocks and the partial-melt composition (Figs 4.02-4.05). Variable rhyolite compositions suggest that a fractionation process was operating. However, there is a low phenocryst content, and no zoned plagioclases are found indicating that crystal fractionation may not be important. Perhaps a liquid fractionation process, as has been discussed for the other rhyolites in Glencoe (chapters 4, 6), is important in the the generation of the rhyolites associated with the fault rocks. Alternatively, variable mixing between partial-melt liquids, and more basic magmas may have occurred to produce rhyolites in a similar fashion to that discussed for sample 1JG61 (section 4.5).

7.5 DISCUSSION AND INTERPRETATION

7.5.1 Summary

From this study a number of conclusions have been made:

1) The breccias and cataclasites were formed by a process of frictional sliding. Deformation was progressive in terms of grainsize reduction from breccia through cataclasite to F.C.R..

2) The rhyolite (red felsite) is not the chilled margin of the ring-intrusion.

3) The F.C.R. is a mixed rock composed of quartz grains and megacrysts set in a matrix of feldspar, quartz and biotite.

4) The F.C.R. has a chemical composition that falls between rhyolite and cataclasite. The F.C.R. matrix has a composition similar to the more basic rhyolites.

5) The rhyolite and cataclasite/F.C.R. acted as fluids at the time of mixing. The megacrysts present in the F.C.R. were derived from the rhyolite.

6) Less acidic rhyolite compositions mixed thoroughly with the cataclasite/F.C.R.. The physical relationship between the more acidic rhyolite and cataclasite/F.C.R. is that of liquid immiscibility.

7) There are no glassy or devitrification textures in the F.C.R..

7.5.2 Discussion of previous models for the origin of the F.C.R.

7.5.2.1 The pseudotachylite theory

It was originally believed that the F.C.R. was a pseudotachylite derived by frictional melting (Clough et al. 1909; Bailey 1960).

In this study, qualitative S.E.M. analysis shows the presence of crystallised melt in the matrix. In previous studies of pseudotachylites, it has been shown theoretically that pseudotachylite could be generated during a caldera collapse/cauldron subsidence event (Maddock 1986). Pseudotachylites are generally produced by the faulting of anhydrous crustal rocks at a high strain rate, i.e. similar conditions to those inferred for cauldron-subsidence. When examining this theory, a number of questions must be addressed:

1) What are the source rocks for the pseudotachylite?

2) What would be the composition of the melt?

3) What would be the physical relationship

between the melt and the host lithologies?.

In the case of Glencoe, there are two possible source rocks: a) Dalradian basement rocks, which in the case of Stob Mhic Mhartuin are quartzites. b) A mixture of Dalradian basement and ring-intrusives.

The first case can be ruled out, as one would anticipate that a pseudotachylite derived from a Dalradian quartzite would be rich in quartz, and have a high silica content. This is not the case.

In considering the composition of a fault-generated pseudotachylite melt we must examine the contribution of different minerals. Some workers suggest that pseudotachylite compositions represent either granite minimum melt (Sinha-Roy 1981), or total melt compositions (Masch 1973; Sibson 1975). Recent detailed studies of pseudotachylite matrix compositions have shown that they are formed by a complex process, whereby hydrous host-rock phases, such as biotite and amphibole are preferentially incorporated into the melt followed by feldspar and then quartz (Maddock 1986). An additional observation is that there is rarely intimate mixing between cataclasite and fault-generated pseudotachylite (Maddock 1986). Also, the most salient feature of a pseudotachylite is the occurrence of heterogeneously nucleated quenched crystals.

From this evidence one can rule out the contribution of the ring-intrusives to the F.C.R. matrix as:

1) If the matrix were partially or wholly derived from the ring-intrusives, one would expect it to have a more basic composition.

2) Although some megacrysts have a reaction rim, they are not wholly or partially consumed.

3) Most of the F.C.R. shows a very thorough mixing of cataclastic fragments and matrix.

4) No quenched crystals are observed.

One must also consider the crystalline state of the ring-intrusion at the time of cauldron-subsidence. In some areas it is clear that

the intrusion adjacent to the fault was emplaced prior to ring-faulting (chapters 2,5). In many other localities it is believed that the ring-intrusives adjacent to the fault were emplaced at the time of faulting. If this is the case, the response of partially molten rocks to stress must be examined.

Experimental studies have shown that partially crystalline rocks with a melt fraction of up to 30% can deform in a brittle fashion under shear stresses (Van der Molen and Paterson 1979). As a result of such a process, melt segregation, and the fracturing and concentration of crystals is observed. It is conceivable that the red rhyolite may represent a melt segregation from such a process. However, there are no fractured phenocrysts in either the rhyolite or the ring-intrusion (except in localities where the intrusion was wholly crystalline before cauldron-subsidence), and as has been mentioned previously, the phenocryst content of the rhyolite is totally different in crystal size and composition to the ring-intrusion.

It is therefore concluded that the F.C.R. is not a pseudotachylite, nor has the F.C.R. matrix been derived from the ring-intrusion by a deformational process.

7.5.2.2 The gas-fluidisation theory

The gas-fluidisation theory as originally proposed by Reynolds (1956) states that a fine-grained intrusive breccia was carried along the ring-fault by magmatic gasses which cored and brecciated the country-rock. This also entrained liquid droplets of magma, which mixed with the fine-grained breccia to produce F.C.R..

The presence of igneous material mixing thoroughly with both angular and rounded quartz fragments is evidence in favour of this theory. Roberts (1966b) believed the F.C.R. to be the vanguard of the ring-intrusion, hence the composition

of the F.C.R. matrix need not bear any similarity to the adjacent ring-intrusion. Also, cauldron-subsidence is a consequence of catastrophic explosive volcanism.

There is however a lot of evidence against gas-fluidisation being responsible for the formation of many of the Glencoe ring-fault rocks.

1) Cataclasis is responsible for much of the deformation within the quartzites. In the breccias formed by magmatic gasses (chapter 6), randomly oriented and undeformed micas are seen in the matrix (Hardie 1963). Whereas in the fault rocks described earlier (section 7.3), micas are smeared out in the matrix which surrounds internally undeformed clasts.

2) Many of the immiscible mixing textures between the rhyolite and cataclasite/F.C.R. indicate that the igneous material was not present in the form of liquid droplets, but as a coherent, non-vesiculating liquid (Plate 7.11).

3) One of the best cited examples of gas-fluidisation is the Tertiary intrusion at Slieve Gullion, Northern Ireland. Here, one finds a wide, pervasive network of F.C.R. veins, which spreads out radially for up to 50m away from the ring-fault. There is also a gradational boundary between the F.C.R. and the ring-intrusion. The veins are planar, up to 1cm wide, with sharp, straight boundaries. None of these features are seen in Glencoe. The veins and pods of F.C.R. that intrude rocks away from the ring-fault have undulose margins, and tend to be much thicker than those seen at Slieve Gullion. All of these pods and veins are within 5m of the fault.

It is clear that a gas-fluidisation process as proposed by Reynolds (1956), and supported by Hardie (1963, 1968), Roberts (1966b, 1974) and Taubeneck (1967) is not responsible for many of the features of the Glencoe ring-fault. However, the role of magmatic gases in the generation of the fault rocks may still be important, as is discussed below.

7.5.3. Alternative Hypotheses

Recent experimental studies have indicated that the stresses caused by thermal expansion during seismic faulting may enhance the fragmentation of the fault rocks, particularly quartzitic fault rocks (Moore and Sibson 1978). Random fracturing in the quartz grains occurs, and the ensuing fragmentation results in grainsize reduction. Intense heating of quartzo-feldspathic rocks produces a minor amount of melt, which is of granite minimum melt composition (Moore 1980). It is likely that this process, which is known as thermal spalling, has aided the fragmentation of the country-rock in the case of Glencoe.

A dynamic model of cataclasis, explosive volcanism, and rhyolitic intrusion is proposed for the generation of the fault rocks (Fig. 7.03). A basic 3-stage process is envisaged.

The initial stage (Fig. 7.03a) involves the explosive eruption of the magma, probably via a central vent or vents. The loss of material from the top of the magma chamber causes instability in the cap-rock, which produces a sub-circular fracture. This cylindrical block may then begin to subside, leading to the formation of breccias and cataclasites along the ring-fault. Some of this fragmentation may have been aided by thermal spalling. The downdrop could have been incremental, with movement of a few metres along each step, as has been inferred from a contemporary caldera-collapse (Filson *et al.* 1973).

In the second stage (Fig. 7.03b), it is envisaged that eruption shifts from a central vent to the ring-fault. As a result, gas-propelled magma droplets would be entrained along the fault, and able to mix intimately with fragments of wall-rock formed by cataclasis and thermal spalling to produce the F.C.R.. It is likely that this is laminar flow, as more turbulent mixing would be expected to lead to the erosion and incorporation of any loose wall-rock

FIGURE 7.03 A 3-stage model for fault-rock formation during cauldron-subsidence. Details of the fault are shown in enlarged circles.
A: Initial explosive activity with resultant ring-fracture. Movement along this fracture leads to brecciation and cataclasis, aided by thermal spalling. Note the presence of early ring-intrusion, which may have been cut by the fault.
B: Main phase of activity. Gas, magma droplets and lithic fragments (the latter derived by cataclasis) are blasted up the ring-fracture to be erupted as tuffs. The magma droplets and lithic fragments which do not reach the surface 'weld' together to form F.C.R..
C: Final phase, which is at the cessation of explosive activity, and leads to the deposition of air-fall tuffs. Viscous rhyolite from the top of the magma-chamber intrudes up the ring-fault, mixing turbulently with partially solidified F.C.R.. This is followed, or accompanied by more voluminous ring-intrusion of porphyritic magma.

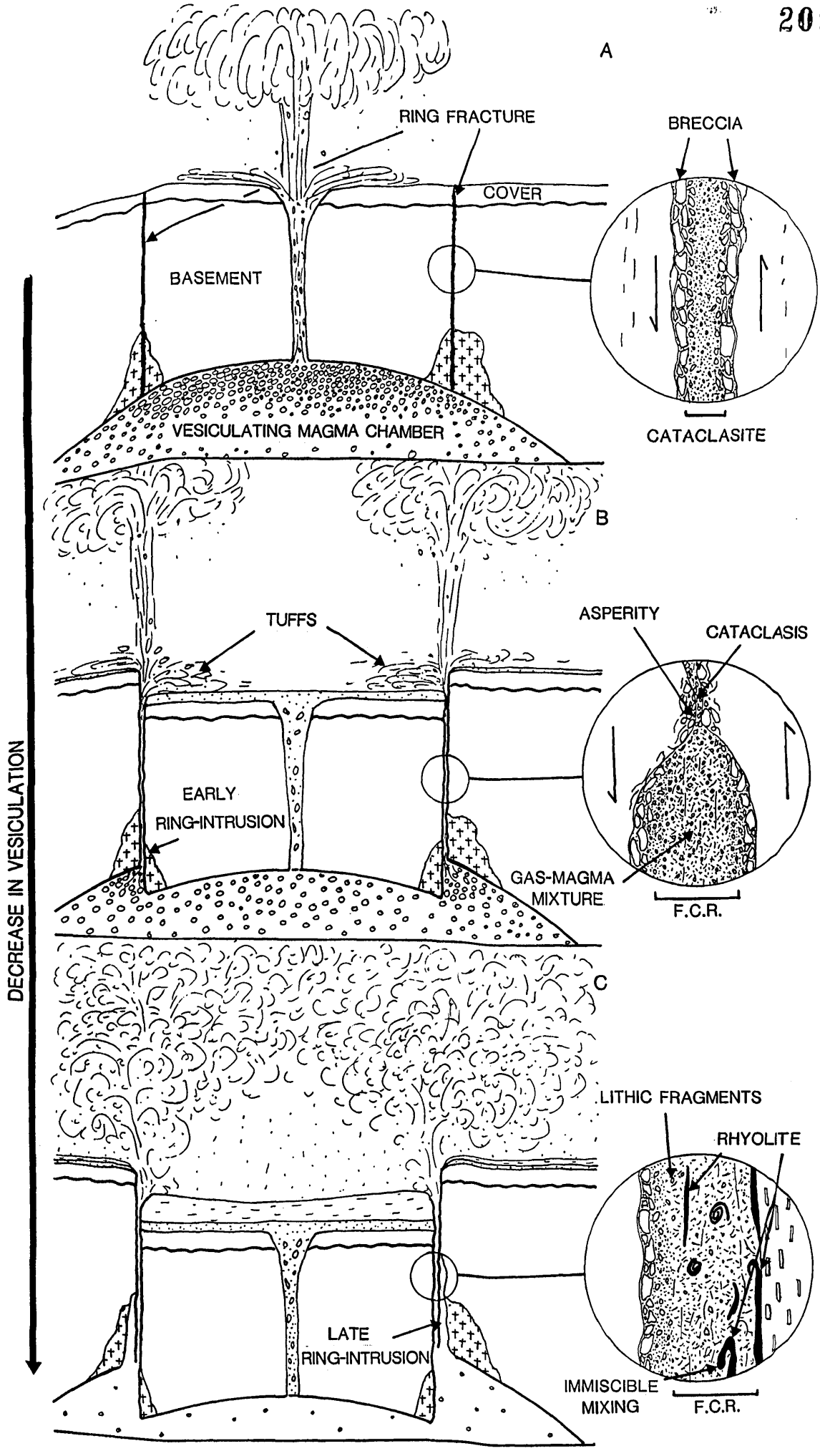
A
RING FRACTURE
COVER
BASEMENT
VESICULATING MAGMA CHAMBER
BRECCIA
CATACLASITE
B
TUFFS
ASPERITY
CATACLASIS
EARLY
RING-INTRUSION
GAS-MAGMA
MIXTURE
F.C.R.
C
DECREASE IN VESICULATION
LITHIC FRAGMENTS
RHYOLITE
LATE
RING-INTRUSION
IMMISCIBLE
MIXING
F.C.R.

material by the magma/gas mixture. Whereas breccias, grading into cataclasites are still seen along the fault adjacent to the F.C.R.. Some thin streaks of rhyolite within the F.C.R. could in fact be flattened pumice clasts which were caught up in the blast. Flattening parallel to the fault may have been exacerbated due to the stress caused by conduit closure after eruption (Wolff 1986). Cataclasites may continue to be generated at certain points where continued subsidence leads to the frictional sliding of asperities along the fault plane (Fig. 7.03b inset). This second stage could be considered a gas-fluidisation process (Reynolds 1954, 1956). However, the author believes that the country-rock fragments entrained in the gas/magma mixture were derived by deformational processes and not by gas-coring.

Finally (Fig. 7.03c), in the latter stages of eruption, the gas content of the magma will have substantially decreased. However, magmatic pressure may prolong the intrusion of rhyolitic magma up the fault plane. The magma would be liquid and non-vesiculating, but would be able to mix with unconsolidated F.C.R. plastered along the fault plane. This would be under a turbulent flow regime, in the form of immiscible liquid mixing, as depicted in Plate 7.11.

This model is a continuous, dynamic, interactive process, and none of the stages are thought to have acted independently of each other. It is likely that there is a certain amount of overlap, with different processes occurring at any one time at different localities along the fault plane.

At higher crustal levels, where Devonian sediments and volcanics have been downfaulted against the Dalradian basement, the simple, coherent ring-fault or faults is commonly replaced by an anastomosing fault system (chapter 2). Neither F.C.R. nor rhyolite is found, instead the faults are marked by a rubbly, incoherent black, fine-grained rock. It

is likely that the different mechanical and thermal properties of the Devonian cover rocks have not permitted the 'welding' of the magma/quartz fragment rock to produce F.C.R.. Instead, one finds a loose, unwelded 'tuff' mixing with friction-generated cataclasite.

The relative timing of the faulting and ring-intrusion remains an enigmatic problem. Field studies have shown that much of the ring-intrusion was emplaced prior to cauldron-subsidence (chapters 2,5). Previous workers have concluded that the intrusion found immediately adjacent to the fault was emplaced simultaneously with faulting, due to the lack of deformation and chilling of the inner margin of the ring-intrusion, and the lack of thermal metamorphism within the subsided block (Clough et al. 1909; Bailey 1960; Roberts 1974). It is possible that some portions of the ring-intrusion were emplaced adjacent to the fault immediately or soon after faulting. The fault rocks would most probably be at a high temperature, and would then be able to thermally buffer the ring-intrusion from the cold, subsided block. This would explain the lack of a chilled margin against the fault, aswell as the lack of deformation of the marginal ring-intrusion. An example of this is the inner ring-intrusion at Stob Mhic Mhartuin (see chapter 2), which is completely bounded by F.C.R., but has neither chilled nor deformed margins.

CHAPTER 8

THE RELATIONSHIPS BETWEEN THE GLENCOE CAULDRON AND YOUNGER CALDERAS

8.1 INTRODUCTION

The Glencoe cauldron is interpreted as the deep-seated equivalent of an ash-flow caldera (Roberts 1968,1974). As such, it can provide important information regarding likely processes occurring beneath presently active caldera structures, and place constraints on the interpretation of geophysical data from such areas. Conversely, data from active calderas may help interpret some of the features observed in Glencoe.

Ash-flow calderas are caused by the evacuation of a zoned magma-chamber, resulting in the deposition of thick sequences of tuffs. Calderas are known to range in size, shape and style, as a result of the interaction of a number of volcano-tectonic processes (Smith et al. 1961; Smith and Bailey 1968; Lipman 1984; Walker 1984). Large ash-flow calderas are calc-alkaline or alkaline in nature, and are situated in regions of crustal extension.

A comparative study has been made of some Tertiary and Recent calderas in the western U.S.A.. The Long Valley caldera, California, has been studied in detail. Long Valley, Valles and Yellowstone calderas still possess a partially liquid magma-chamber beneath them, and as a result of a number of integrated studies of these areas, a greater understanding of such volcanic processes has been achieved (Smith et al. 1961; Christiansen and Blank 1969; Bailey et al. 1976).

Long Valley caldera forms an elliptical depression 17Km by 32Km (Fig. 8.01), and is of

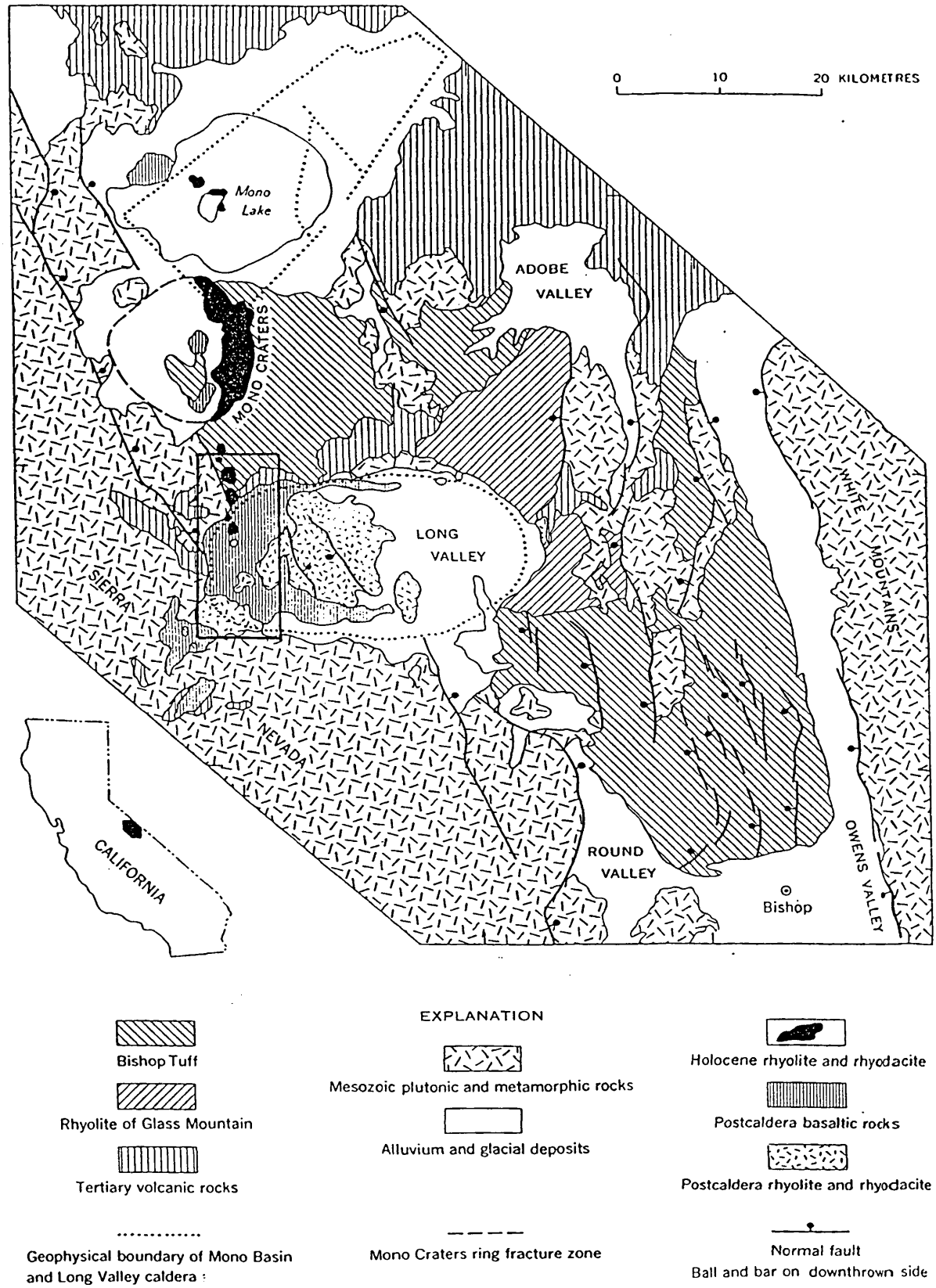

FIGURE 8.01 Generalised geological map of the Long Valley - Mono Basin area. Rectangular area marked represents the field shown in Figure 8.02 (after Bailey et al. 1976).

comparable size to Glencoe. It is situated in a graben structure on the western edge of the Basin and Range Province. The whole region has been volcanically active since early Mesozoic times, but volcanism in Long Valley has occurred only in the last 3my. After the eruption of early basalts in Long Valley, a magma chamber grew and evolved, erupting a suite of rocks with a range of composition. The magma chamber evolution culminated in the eruption of the Bishop Tuff 0.7my ago, which led to caldera-collapse. Post-collapse volcanics are also of variable composition and were erupted up to 550 years B.P.. Recent volcanological and seismic studies have indicated that the area is a potential volcanic hazard.

8.2 A 3-DIMENSIONAL VIEW

Large volume, caldera-collapse related ash-flow tuff eruptions are linked to subvolcanic granitic plutons of batholithic dimensions (Smith 1960; Lipman 1984). For example, in the San Juan Mountains of Colorado, a number of calderas exist which have been caused by the eruption of tuff from separately differentiated magma-chambers and cupolas, many of which overlap each other (Steven and Lipman 1976; Lipman 1984). The erosional edifices of such a field of calderas would presumably resemble the Grampian Highland region, where a number of overlapping granitoids, cauldrons and associated volcanics are exposed.

The magma-chambers of ash-flow calderas crystallise to form zoned plutons. In the Grampian Highlands, the Etive, Ballachulish and Ben Nevis plutons are concentrically zoned. Within the Etive pluton is a vertical fault-bounded screen of volcanic rock, which may be the remnant of a cauldron (Anderson 1937; Clayburn *et al.* 1983).

Geophysical studies summarised in Hill et al. (1985) have located the magma-chamber beneath Long Valley caldera. Prior to caldera-collapse, the depth to the roof of the magma-chamber is believed to have been approximately 6Km (Bailey et al. 1976). The rocks exposed in the Glencoe area are thought to be just above the magma-chamber, at approximately 5Km depth (chapter 5).

Long Valley magma-chamber, like most magma chambers related to ash-flow calderas, operated in an open system, and periodically erupted a variety of volcanics over a length of time. After the consolidation of one magma-chamber, the centre of activity migrates, and new (often chemically-related) chambers evolve, commonly overlapping onto other plutons. A similar picture is viewed to the southeast of Glencoe, where the cauldron, and ring-intrusion has been invaded by the Cruachan granitoid, which is part of the Etive pluton. This is also a ring-shaped intrusive, and may have been related to a later cauldron-subsidence event. (It is worth noting that other parts of the Etive pluton were emplaced prior to the formation of the Glencoe magma-chamber and subsequent cauldron subsidence).

Subvolcanic calc-alkali magma-chambers are known to rise to high crustal levels, and due to their longevity, induce partial-melting in the country-rock (Lipman 1984). As a consequence, partial-melt material is incorporated into the magma, and has a significant effect upon its chemical composition. Major element modelling of the Glencoe intrusives has suggested that upper crustal partial-melt material was added to a basaltic magma which then fractionated to produce the range of rocks analysed (chapters 4, 5).

On a more general regional level, there are clear comparisons between the Long Valley area and the Grampian Highlands. In both areas early basaltic volcanism occurs, with the magma travelling rapidly through the upper crust from a deep source. However

when basaltic magma resides in the upper crust to form a magma-chamber, its heat induces partial-melting, and a fractionating, layered magma-chamber results.

8.3 EARLY VOLCANISM

The earliest volcanism in both Long Valley and the Grampian Highland regions was basaltic, with the lavas having been erupted directly from a lower crustal or mantle source. This was then followed by a period of magma-chamber growth. Material was erupted from the developing magma-chamber in Long Valley, prior to caldera-collapse. This consisted of evolved latites and rhyolites, indicating the rapid development of magmatic stratification. These lavas were erupted as domes and flows, and were commonly situated above the incipient ring-fracture.

The voluminous outpourings of rhyolite were believed to have been hot and fluid. Depositional structures such as flow-banding, folding and autobrecciation are observed, which closely resemble similar structures seen in the centre of the Glencoe cauldron at Queens Cairn (Ferguson 1966). The rhyolite and latite eruptions in Long Valley, have left a remnant subsurface feeder system close to the ring-fault. These high-level intrusives have been expanded by post-caldera magma which fed later basaltic and rhyolitic eruptions. In addition, some recent seismic activity (in 1983) is believed to have been caused by the intrusion of magma beneath the southern moat of the caldera (R. Bailey pers. comm.). Hence, one can invisage a group of poorly defined small intrusions of various compositions abutting against the ring-fault. This would be very similar to the ring-intrusion at Glencoe, which is of variable width and composition.

8.4 ASH-FLOW TUFF ERUPTIONS

At approximately 0.7Ma, a massive pyroclastic eruption occurred in Long Valley, resulting in the deposition of the Bishop Tuff, and leading to caldera-collapse. The volume of rhyolitic material erupted is estimated to be 600 cubic kilometres, with vertical displacement along the ring-fault being in the region of 2km (Bailey et al. 1976).

The tuff deposits cover a vast area, and are of variable thickness outside the caldera. The intra-caldera tuff deposit is not exposed, but seismic and drilling evidence suggest that it is at least 1Km thick, and hence of similar proportions to Tertiary intra-caldera tuffs exposed in the San Juan Mountains, Colorado (Steven and Lipman 1976, Lipman 1984). The original caldera walls have slumped, hence enlarging the topographic depression. It is anticipated that large slump deposits in the form of breccias are associated with the intra-caldera tuff, similar to those described by Lipman (1984) in Tertiary ash-flow calderas.

The caldera-collapse along a coherent ring-fault described from Long Valley is analogous to cauldron-subsidence in Glencoe. It has been suggested that the ash-flow tuffs exposed in the subsided block in Glencoe were deposited as a result of the Glencoe cauldron-subsidence (Roberts 1974). Although the author believes that cauldron-subsidence in Glencoe led to the eruption of voluminous ash-flow tuffs, she disputes the theory that the tuffs presently observed in Glencoe were derived from that particular subsidence event due to:

1) The Glencoe ash-flow tuffs are very thin (maximum thickness of 300m) when one considers that there must have been at least 1Km of subsidence along the ring-fault. (This estimate is based on the observation that at the present day 1Km of thickness

of volcanics are exposed within the subsided block, and no volcanics are exposed outside the ring-fault.)

2) Intra-caldera ash-flow tuffs are deposited in a depression and are conformably overlain by subsequent deposits such as lake sediments. They are not eroded until much later. In Glencoe the tops of the tuff sheets appear to have been eroded, and are uncomformably overlain by lavas and sediments.

3) No slump deposits are seen associated with the Glencoe tuffs.

The author believes it is more likely that the ash-flow tuffs exposed within the Glencoe cauldron were derived from earlier caldera-forming eruptions elsewhere (perhaps Etive or Ben Nevis), and that a large tuff deposit associated with the Glencoe cauldron-subsidence has been eroded away.

8.5 THE INYO-MONO VOLCANIC CHAIN

The 11Km Inyo-Mono volcanic chain is a series of domes and craters aligned along a fracture zone which extends northwards from the northwest corner of Long Valley caldera towards Mono Lake (Fig. 8.01). There have been a number of eruptive episodes along the chain, the most recent being 550 years ago.

Explosive eruptions have led to the deposition of pyroclastic breccias, which form thick drapes close to the vents, and grade into surge, flow and airfall deposits (Miller 1985). Following the explosive activity rhyolite flows issued from many of the vents. These flows formed pancake-shaped domes, which are mantled by auto-brecciated talus deposits.

Recent drilling beneath and adjacent to one of the Inyo domes (Obsidian dome) has located its conduit, and also a dyke which runs beneath the length of the chain (Eichelberger et al. 1985; Miller 1985) (Fig.8.02). The conduit is about 40m wide, and has a margin of intrusive breccia, caused by

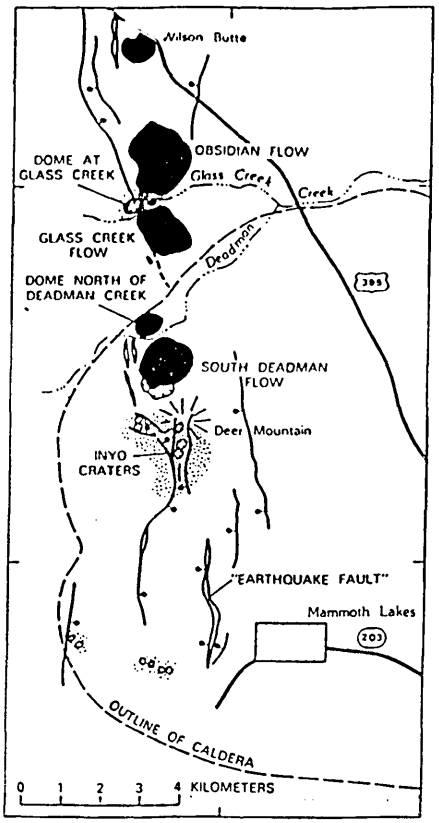

FIGURE 8.02 Map of the Inyo volcanic chain. black areas are rhyolite, hatched circles are phreatic vents, stipples are phreatic explosion debris, elongate lens patterns are fissures (after Miller 1985).

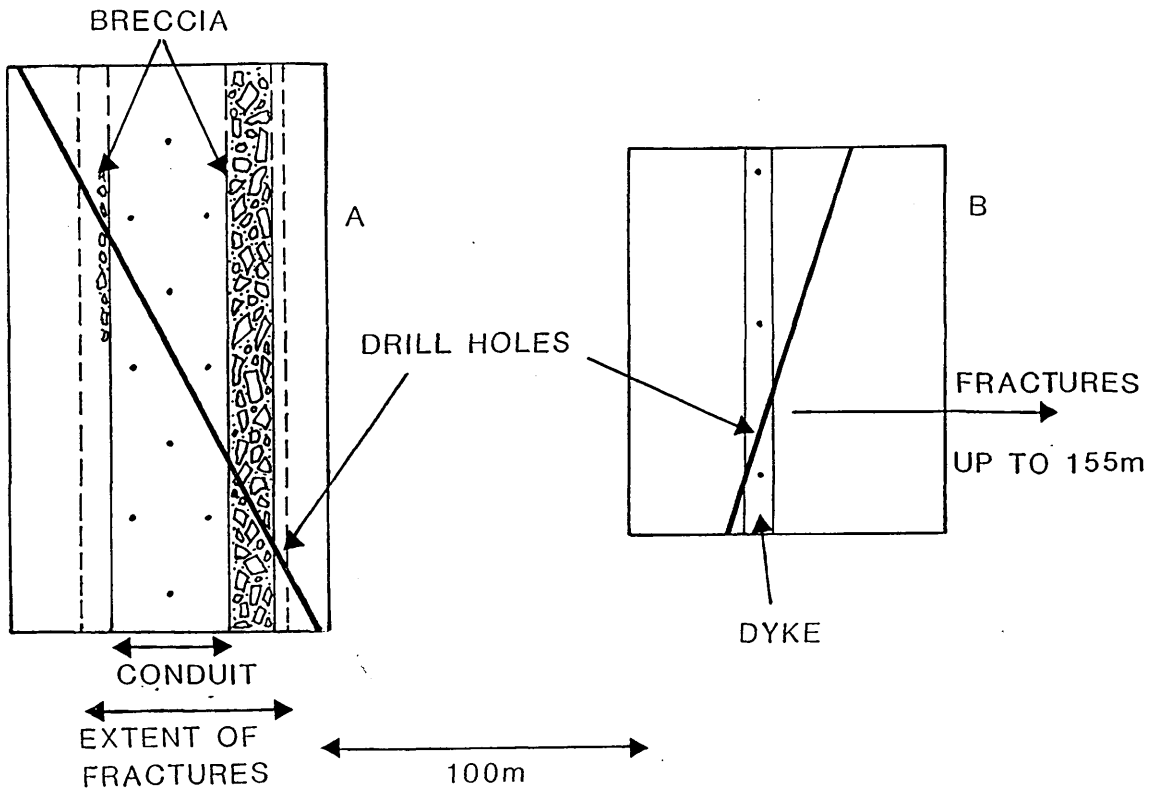

FIGURE 8.03 A - Cross-section of the conduit beneath obsidian dome. B - Cross-section of the rhyolite dyke beneath Glass Creek. Adjacent rock in both A and B is Cretaceous granite (redrawn after Eichelberger et al. 1985).

explosive activity which occurred before the extrusion of the dome (Fig. 8.03). The conduit is thought to be the enlargement of the rhyolite dyke close to the point of eruption. It is therefore anticipated that the dyke, or a series of dykes, runs beneath the whole chain, enlarging and erupting at various places along its length. The Inyo craters are phreatic, probably caused by the heat input due to the emplacement of the dyke at depth (Miller 1985).

The 3-dimensional view of the Inyo-Mono chain seems very similar to the picture described of the eastern portion of the Glencoe cauldron in chapter 6. In both cases one finds:

1) A rhyolite dyke or aligned group of dykes each just a few metres wide.

2) A rhyolite conduit, some tens of metres wide with brecciated margins, which is believed to be the enlargement of one of the aforementioned rhyolite dykes. The brecciation is thought to have occurred prior to the influx of rhyolite lava into the conduit.

3) Pyroclastic breccias which are particularly thick close to the vents (vent breccias).

4) The gradation from pyroclastic breccia through tuff (ash-flow followed by airfall), to rhyolite lava.

The Long Valley area is a potential volcanic hazard. It is hoped that comparative studies with well-constrained older regions may lead to a better understanding and anticipation of volcanism in Long Valley. Current workers believe that the Inyo-Mono chain is the most likely centre for future activity (Hill et al. 1985; R.A. Bailey pers. comm.). In Glencoe the equivalent rocks to the Inyo-Mono chain were erupted early in the volcanic sequence, prior to cauldron-subsidence. Hence, one must examine the possibility that the Inyo-Mono chain may represent the 'early warning' to future extensive volcanism, particularly as recent studies suggest that an expanding, young magma-chamber is present beneath the

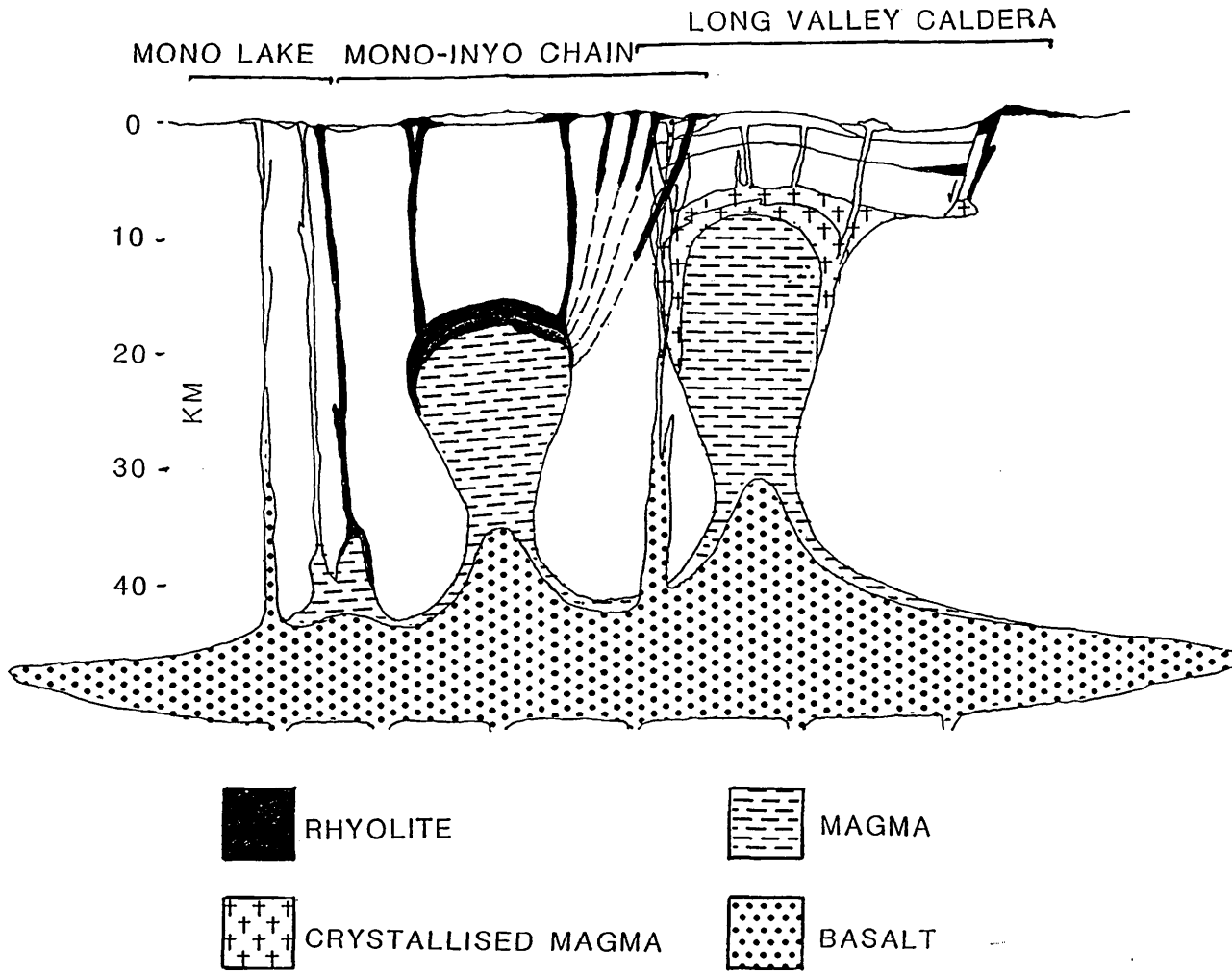

FIGURE 8.04 Schematic cross-section of the Long Valley, Mono-Inyo chain and Mono Lake volcanic complexes showing the hypothetical configuration of their inferred magma-chambers (redrawn after Bailey 1982).

northern part of the chain, adjacent to the crystallising Long Valley magma-chamber (Fig. 8.04)(Bailey 1982).

CHAPTER 9

CONCLUSIONS

The important conclusions concerning individual aspects of the study are given at the end of the relevant chapters. However, they are synthesised and summarised below. Many of the salient points are also illustrated in the cross-section (Fig. 9.01), which is drawn along the line A-B shown in Figure 1.07. (N.B. The vertical depths shown in Figure 9.01 are conjectural). A flow diagram showing the sequence of events is given in Fig. 9.02.

The conclusions of this study are:

1) The intrusive and volcanic rocks of Glencoe have crystallised from subduction-related magmas, and are part of an intrusive and volcanic suite of rocks exposed in the Grampian highlands.

2) The igneous rocks of Glencoe were derived from a zoned magma-chamber. Ring-faulting and its associated volcanism and intrusion was just one event in the evolution of the magma-chamber. The magma-chamber behaved as an open system.

3) Fractional crystallisation, accompanied by upper crustal partial-melting led to magma-chamber zonation, and were responsible for the geochemical and mineralogical variations of the ring-intrusion.

4) Much of the ring-intrusion was emplaced prior to cauldron-subsidence, and probably represents the feeder system for early volcanism. An-t-sron represents the root of a large early volcanic centre.

5) Early explosive volcanism, prior to ring-faulting, occurred in the eastern part of the area, along a trend sub-parallel to the later ring-fault, demonstrating that a pre-existing line of weakness existed.

6) Much of the intrusion present immediately adjacent to the fault was emplaced contemporaneously

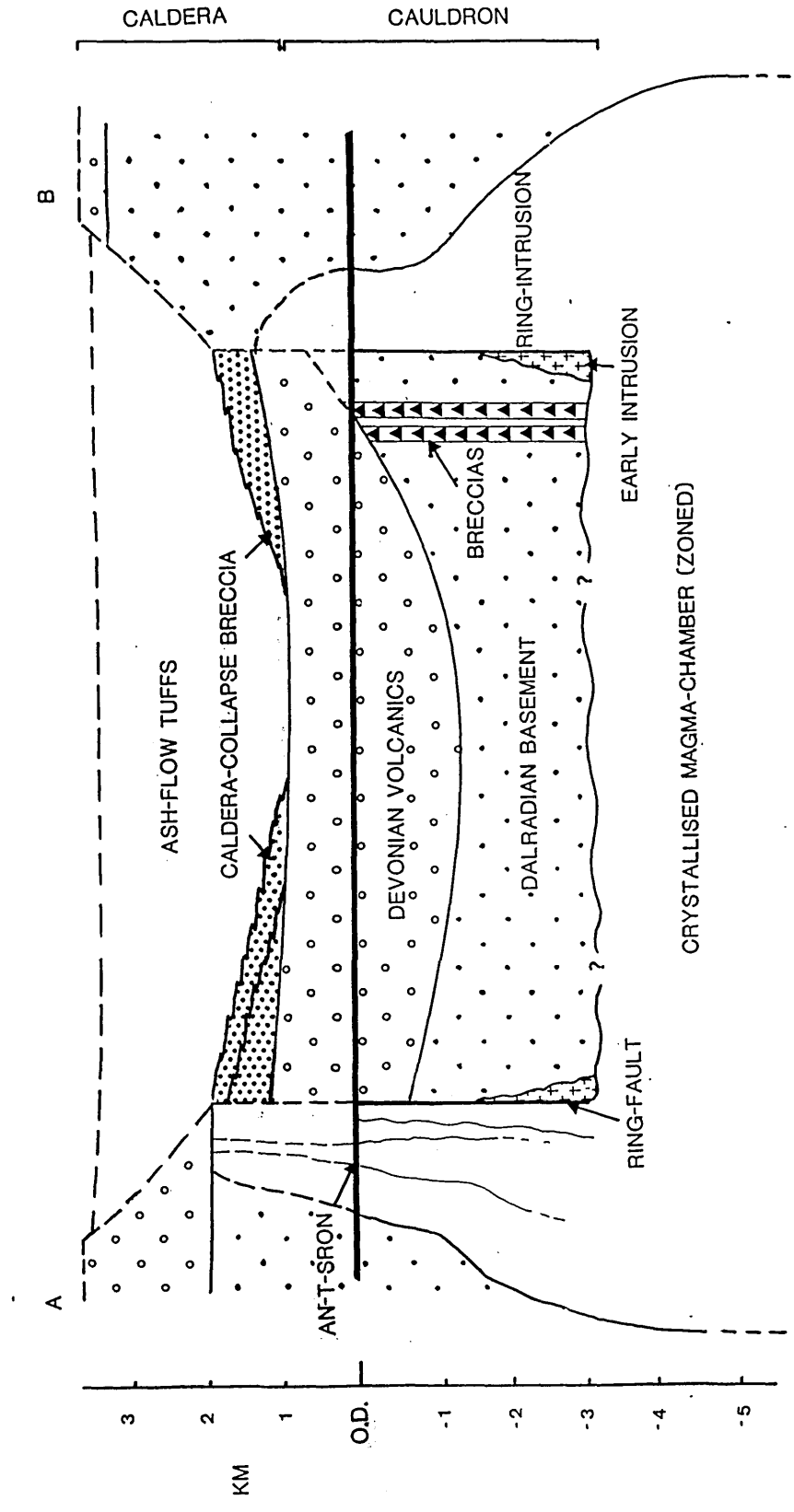

FIGURE 9.01 A schematic cross-section showing many of the conclusions reached in this study regarding the Glencoe cauldron-subsidence. A-B represents the vertical section of line A-B on Fig. 1.07. O.D. = present day sea-level.

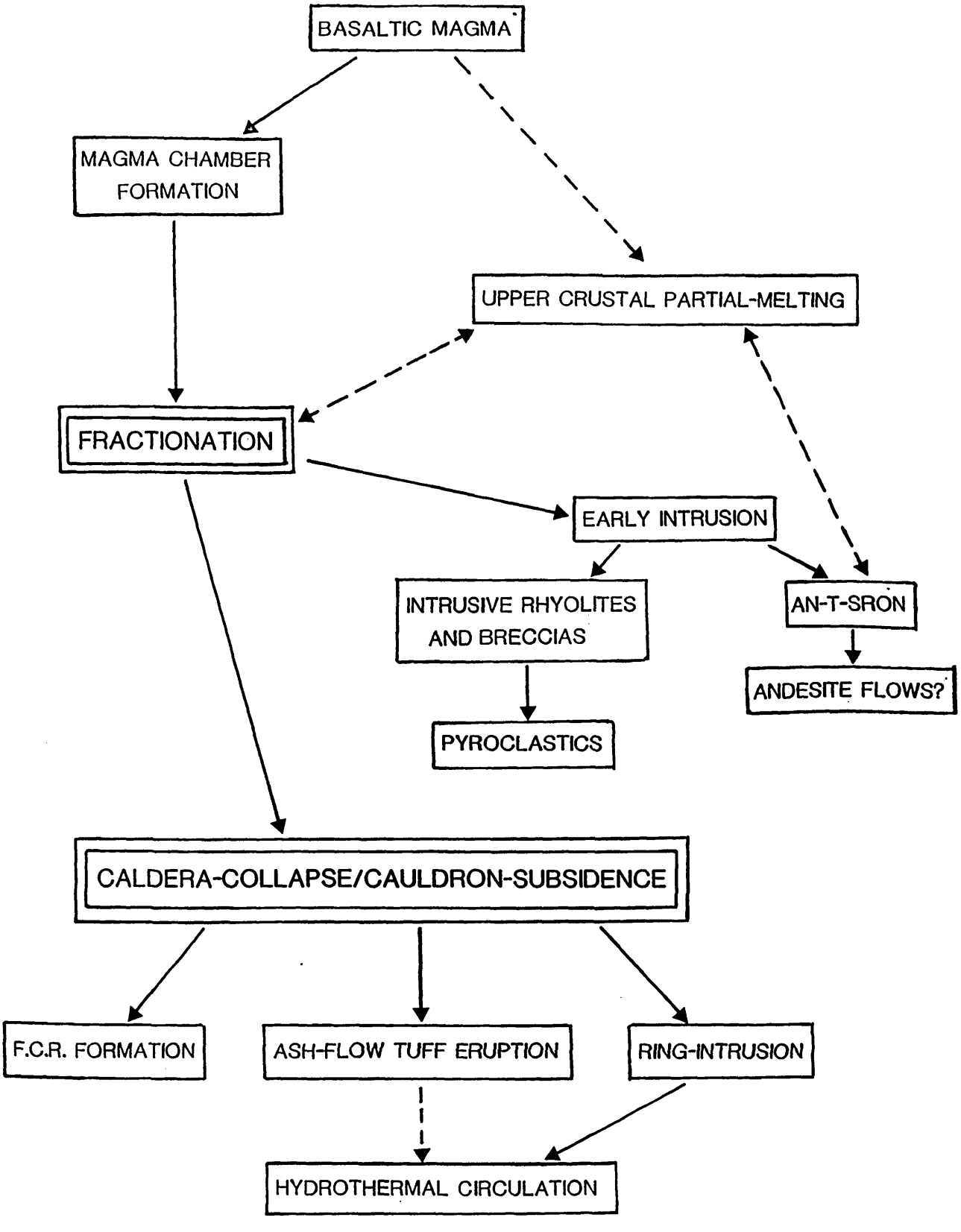

FIGURE 9.02 A flow diagram showing the sequence of magmatic events in Glencoe during the Lower Devonian.

with faulting.

7) The 'flinty crush-rock' is a fine-grained tuffisite formed by the interaction of fault-rock and magma as a result of the eruption of large volumes of tuff up the ring-fault.

8) There is no evidence to suggest that more than one phase of subsidence has occurred, however, the ring-fault exposures at An-t-sron indicate re-activation of the fault shortly after subsidence.

9) The nature of the fault rocks changes from a coherent tuffisite which is found adjacent to the basement rocks, to a rubbly, unconsolidated 'fault-rock' which is found adjacent to the Devonian volcanics and sediments. This is interpreted to be the transformation from a cauldron (in the basement rocks) to a caldera (in the cover rocks) (Fig. 9.01).

10) Field evidence, and comparisons with more recent calderas suggest that the thick ash-flow tuffs presently exposed in Glencoe were probably not deposited as a result of the Glencoe cauldron-subsidence, but were probably erupted from another volcanic centre in the region before cauldron-subsidence/caldera-collapse occurred in Glencoe.

11) Many of the characteristics of the Glencoe cauldron-subsidence have been observed or inferred in more recent, less eroded environments. By comparing and contrasting ancient and modern regions, a 3-dimensional picture of cauldron-subsidence/caldera--collapse can be drawn.

REFERENCES

Anderson, J.G.C., 1937
The Etive granite complex.
J. Geol. Soc. vol.93 pp.487-533
Anderton, R., Bridges, P.H., Leeder, M.R. and Sellwood, B.W., 1979
A dynamic stratigraphy of the British Isles.
George Allen and Unwin.
Bailey, E.B., 1960
The geology of Ben Nevis and Glencoe. (Sheet 53)
2nd ed. Mem. Geol. Surv. U.K.
Bailey, E.B. and Maufe, H.B., 1916
The geology of Ben Nevis and Glencoe.
Mem. Geol. Surv. Scotland
Bailey, R.A., 1969
Form of the Glencoe magma chamber and the main fault intrusion.
In, International Association of Volcanology Symposium on Volcanoes and their roots, International Association of Volcanology, Oxford, England pp.80.
Bailey, R.A., 1982
Other potential eruption centres in California: Long Valley-Mono Lake, Coso and Clear Lake volcanic fields.
Calif. Div. of Mines and Geol. Spec. Publ. No.63 pp.17-28
Bailey, R.A., Dalrymple, G.B. and Lanphere M.A., 1976
Volcanism, structure and geochronology of Long Valley caldera, Mono County, California.
J. Geophys. Res. vol.81 pp.725-744
Bluck, B.J., 1985
The Scottish paratectonic Caledonides.
Scott. J. Geol. vol.21 pp.437-464
Bowen, N.L., 1928
The evolution of igneous rocks.
Princeton Univ. Press
Bussell, M.A., 1979

Structures at the south-west margin of the Glencoe fault intrusion on An-t-sron.
Scott. J. Geol. vol.15 pp.279-287

Carslaw, H.S. and Jaeger, J.C., 1980
Conduction of heat in solids, 2nd ed.
Oxford Univ. Press

Cawthorn, R.G., 1976
Some chemical controls on igneous amphibole compositions.
Geochim. Cosmochim. Acta vol.40 pp.1319-1328

Christiansen, R.L. and Blank, H.R., 1969
Volcanic evolution of the Yellowstone rhyolite plateau and eastern Snake River plain, U.S.A.
In, International Association of Volcanology Symposium on Volcanoes and their roots, International Association of Volcanology, Oxford, England.

Clayburn, J.A.P., 1981
Age and petrogenetic studies of some magmatic and metamorphic rocks from the Grampian Highlands.
D. Phil Thesis, Oxford

Clayburn, J.A.P., Harmon, R.S., Pankhurst, R.J., and Brown, J.F., 1983
Sr, O and Pb isotope evidence for the origin and evolution of the Etive igneous complex, Scotland.
Nature vol.303 pp.492-497

Cloos, H., 1941
Bau und tatigkeit von tuffschloten untersuchungen an dem Schwabischen Vulkan.
Geol. Rdsch. vol.32 pp.705-800

Clough, C.T., Maufe, H.B. and Bailey, E.B., 1909
The cauldron subsidence of Glencoe, and the associated igneous phenomena.
J. Geol. Soc. vol.65 pp.611-678

Eichelberger, J.C., Lysne, P.C., Miller, C.D. and Younker, L.W., 1985
Research drillings at Inyo Domes, California: 1984 results.
EOS vol.66 No.17 pp.186-187

Ferguson, D., 1966
The stucture of the Queens Cairn rhyolite.

Scott. J. Geol. vol.2 pp.153-158

Fettes, D.J., 1979
A metamorphic map of the British and Irish Caledonides.
In, The Caledonides of the British Isles reviewed. Eds. Harris, A.L., Holland, C.H. and Leake, B.E. pp.307-321

Filson, J., Simkin, T. and Lew, L., 1973
Seismicity of a caldera collapse: Galapagos Islands 1968.
J. Geophys. Res. vol.78 pp.8591-8622

Fowler, M.B., 1985
A geochemical and mineralogical investigation of the mobility of uranium and other lithophile elements during high-grade metamorphism.
PhD. Thesis, London Univ.

Fridrich, C. and Mahood, G., 1987
Reverse zoning in the resurgent intrusions of the Grizzly Peak cauldron, Sawatch Range, Colorado.
Geol. Soc. Amer. Bull. vol.95 pp.779-787

Frost, C. and O'Nions, K., 1985
Caledonian magma genesis and crustal recycling.
J. Petrol. vol.26 pp.515-544

Gill, J.B., 1977
Role of trace element partition coefficients in models of andesite genesis.
Geochim. Cosmochim. Acta vol.42 pp.709-724

Halliday, A. and Stephens, W.E., 1984
Crustal controls on the genesis of the 400 Ma old Caledonian granites.
Phys. Earth Plan. Int. vol.35 pp.89-104

Hardie, W.G., 1963
Explosion breccias near Stob Mhic Mhartuin, Glencoe, Argyll, and their bearing on the origin of the nearby flinty crush-rock.
Trans. Edin. Geol. Soc. vol.19 pp.426-438

Hardie, W.G., 1968
Volcanic breccia and the Lower O.R.S. unconformity, Glencoe, Argyll.
Scott. J. Geol. vol.4 pp.291-299

Hawthorne, F.C., 1983
The crystal chemistry of amphiboles
Can. Mineral. vol.21 pp.174-480
Henderson, P., 1982
Inorganic geochemistry.
Pergamon Press
Higgins, M.W., 1971
Cataclastic rocks
U.S.G.S. Prof. Pap. No.687
Hildreth, W., 1979
The Bishop Tuff: Evidence for the origin of compositional zonation in silicic magma chambers.
Geol. Soc. Am. Spec. Pap. 180 pp.43-75
Hill, D.P., Bailey, R.A. and Ryall, A.S., 1985
Active tectonic and magmatic processes beneath Long Valley caldera, eastern California: an overview.
J. Geophys. Res. vol.90 pp.11111-11120
Hyndmann, D.W., 1972
Petrology of igneous and metamorphic rocks.
McGraw Hill (International Series in the Earth and Planetary Sciences)
James, R.S. and Hamilton, D.L., 1969
Phase relations in the system NaAlSiO3-KAlSiO3-
-CaAlSi2O8-SiO2 at 1 kilobar water vapour pressure.
Contrib. Mineral. Petrol. vol.21 pp.111-141
Johnson, M.R.W., 1963
Some time relations of movement and metamorphism in the Scottish Highlands.
Geol. en Mijn. vol.42 pp.121-142
Kille, I.C., 1987
Minor Tertiary intrusions around Loch Scridain, Isle of Mull.
PhD thesis, London Univ.
Lambert, R. and McKerrow, W.S., 1976
The Grampian Orogeny.
Scott. J. Geol. vol.12 pp.271-292
Leake, B.E., 1978
Nomenclature of amphiboles
Can. Mineral. vol.16 pp.501-520
Le Maitre, R.W., 1979

A new generalised petrological mixing model.
Contrib. Mineral. Petrol. vol.71 pp.133-137

Lipman, P., 1984
The roots of ash-flow calderas in Western North America: windows into the tops of granitic batholiths.
J. Geophys. Res. vol.89 pp.8801-8841

Luhr, J.F. and Carmichael, I.S., 1981
The Colima volcanic complex, Mexico: part II. Late-Quaternary cinder cones.
Contrib. Mineral. Petrol. vol.76 pp.127-147

Luth, W.C., Jahns, R.H. and Tuttle, O.F., 1964
The granite system at pressures of 4 to 10 kilobars.
J. Geophys. Res. vol.69 pp.759-773

McBirney, A.R., Baker, B.H. and Nilson, R.H., 1985
Liquid fractionation part I: Basic principles and experimental simulations
J. Volc. Geotherm. Res. vol.24 pp.1-24

Maddock, R.H., 1986
The petrology and geological significance of some fault-generated pseudotachylites.
PhD thesis, London Univ.

Mann, A.C., 1983
Trace element geochemistry of high alumina basalt-andesite- dacite-rhyodacite lavas of the Main Volcanic Series of Santorini Volcano, Greece.
Contrib. Mineral. Petrol. vol.84 pp.43-57

Masch, L., 1973
Investigation of the molten state and deformation of the pseudotachylites of the Silvretta (Austria, Switzerland).
Neues Jahrb. Miner. Mh. Jg. vol.11 pp.485-509

Mawer, C.K., 1985
Comment and reply on "Fault-related rocks: suggestions for terminolgy."
Geology vol.13 pp.378-379

Miller, C.D., 1985
Holocene eruptions at the Inyo volcanic chain, California: Implications for possible eruptions in Long Valley caldera.

Geology vol.13 pp.14-17

Moore, H.E., 1980

Rock textures and microstructures related to cataclastic processes.
PhD thesis, London Univ.

Moore, H.E., and Sibson, R.H., 1978

Experimental thermal fragmentation in relation to seismic faulting.
Tectonophys. vol.49 pp.T9-T17

Nakada, S., 1983

Zoned magma chamber of the Osuzuyama acid rocks, southwest Japan.
Jour. Petrol. vol.24 pp.471-494

Norrish, K. and Chappell, B.W., 1977

In, physical methods in determinative mineralogy. Ed. Zussmann, J. pp.201-272

Norrish, K. and Hutton, J.T., 1969

An accurate x-ray spectrographic method for the analysis of a wide range of geological samples.
Geochim. Cosmochim. Acta vol.33 pp.431-453

Obee H.K., 1985

Fault rock and deformation studies of a major continental fault system.
PhD thesis, London Univ.

Otten, M.T., 1984

The origin of brown hornblende in the Artfjallet gabbro and dolerites.
Contrib. Mineral. Petrol. vol.86 pp.189-199

Parker, R.J., 1977

Factors affecting the quality of major element rock analysis by x-ray fluorescence combined with flux-fusion sample preparation.
Technical report No. XRF-2B, Imperial College 33pp.

Parker, R.J., 1979

A computer-based system of XRF analysis and its applications to a study of volcanic rocks from Vulsini, Central Italy.
PhD. thesis, London Univ.

Parker, R.J., 1980

Preperation of rock samples for X.R.F. analysis.

Technical report No. XRF-3, Imperial College 12pp.

Piwinskii, A.J. and Wyllie, P.J., 1968
Experimental studies of igneous rock series: A zoned pluton in the Wallowa Batholith, Oregon.
J. Geol. vol.76 pp.205-234

Platten, I.M., 1983
Partial melting of a semi-pelite and the development of marginal breccias around a late Caledonian minor intrusion in the Grampian Highlands of Scotland.
Geol. Mag. vol.120 pp.37-49

Potts, D.J., Thorpe, O.W. and Watson, J.S., 1981
Determination of rare-earth element abundances in 29 international rock standards by instrumental neutron activation analysis: a critical appraisal of calibration errors.
Chem. Geol. vol.34 pp.331-352

Reynolds, D., 1954
Fluidisation as a geological process and its bearing on the problem of the intrusion of granites.
Amer. J. Sci. vol.252 pp.577-614

Reynolds, D., 1956
Calderas and ring complexes.
Nederlander Geol. Mijnb. Gen. Ver. Geol. Series 16 pp.355-379

Richardson, S.W., 1968
Petrology of the metamorphosed syenite in Glen Dessary, Inverness-shire.
J. Geol. Soc. vol.124 pp.9-51

Roberts, J.L., 1963
Source of the Glencoe ignimbrites.
Nature vol.199 pp.901

Roberts, J.L., 1966(a)
Ignimbrite eruptions in the volcanic history of the Glencoe cauldron subsidence.
Geol. J. vol.5 pp.173-184

Roberts, J.L., 1966(b)
The emplacement of the main Glencoe fault intrusion.
Geol. Mag. vol.103 pp.299-316

Roberts, J.L., 1974
The evolution of the Glencoe cauldron

Scott. J. Geol. vol.10 pp.269-282

Roberts, J.L. and Treagus, J.E., 1977
Dalradian rocks of the Loch Leven area.
Scott. J. Geol. vol.8 pp.165-184

Roberts, J.L. and Treagus, J.E., 1979
Stratigraphical and structural correlation between the Dalradian rocks of the S.W. and central Highlands of Scotland.
In, The Caledonides of the British Isles reviewed. Eds. Harris, A.L., Holland, C.H., Leake, B.E. pp. 199-204

Robie, R.A. and Waldbaum, D.R., 1968
Thermodynamic properties of minerals and related substances at 298.15 K (25.0 C) and one atmosphere (1.013 bars) pressure and at higher temperatures.
U.S.G.S. Bull. No.1259

Rock, N.M.S., 1982
Chemical mineralogy of the Monchique alkaline complex, southern Portugal.
Contrib. Mineral. Petrol. vol.81 pp.64-78

Rutter, M.J., 1985
Tertiary magmatism in northern Sardinia.
PhD thesis, London Univ.

Saunders, A.D., Tarney, J. and Weaver, S.D., 1980
Transverse geochemical variations across the Antarctic peninsula: Implications for the genesis of calc-alkaline magmas.
Earth Planet. Sci. Lett. vol.57 pp.344-360

Sibson, R.H., 1975
Generation of pseudotachylite by ancient seismic faulting.
Geophys. J. Roy. Astr. Soc. vol.43 pp.775-794

Sibson, R.H., 1977
Fault rocks and fault mechanisms.
J. Geol. Soc. vol.133 pp.191-213

Sinha-Roy, S., 1981
Pseudotachylite form a thrust zone in mylonite gneisses of major Bergen arc, southwest Norway.
Neues. Jahrb. Mineralogie. Abh. vol.141 pp.150-160

Smedley, P., 1986

The relationship between calc-alkali volcanism and within-plate continental rift volcanism: evidence from Scottish Palaeozoic lavas.
Earth Plan. Sci. Lett. vol.77 pp.113-128

Smith, R.L., 1960
Ash flows
Geol. Soc. Amer. Bull. vol.71 pp.795-842

Smith, R.L. and Bailey, R.A., 1968
Resurgent cauldrons
Geol. Soc. Amer. Mem. vol.116 pp.613-662

Smith, R.L., Bailey, R.A. and Ross, C.S., 1961
Structural evolution of the Valles caldera, New Mexico, and its bearing on the emplacement of ring dykes.
U.S.G.S. Prof. Paper 424-D pp.145-149

Soper, N.J. and Anderton, R., 1984
Did the Dalradian slides originate as extensional faults ?
Nature vol.307 pp.357-360

Steiner, J.C., Jahns, R.H. and Luth, W.C. 1975
Crystallisation of alkali feldspar and quartz in the haplogranite system NaAlSi3O8-KAlSi3O8-SiO2-H2O at 4Kb.
Geol. Soc. Amer. Bull. vol.86 pp.83-98

Stephenson, D., and Upton, B.J.G., 1982
Ferromagnesian silicates in a differentiated alkaline complex. Kungnat Fjeld, South Greenland.
Mineral. Mag. vol.46 pp.283-300

Steven, T.A., and Lipman, P.W., 1976
Calderas of the San Juan volcanic field, southwestern Colorado.
U.S.G.S. Prof. Pap. No.958 35pp.

Taubeneck, W., 1967
Notes on the Glencoe cauldron subsidence.
Geol. Soc. Amer. Bull. vol.78 pp.1295-1316

Taylor, S.R., Arculus, R., Perfit, M.R. and Johnson, R.W., 1981
Island arc basalts.
In, Basaltic volcanism on the terestrial planets ('basaltic volcanism study project'), Pergamon Press

pp.193-213

Thirlwall, M.F., 1981
Implications for Caledonian plate tectonic models of chemical data from volcanic rocks of the British Old Red Sandstone.
J. Geol. Soc. vol.138 pp.123-138

Thirlwall, M.F., 1982
Systematic variation in chemistry and Nd-Sr isotopes across a Caledonian calc-alkali volcanic arc: implications for source materials.
Earth Plan. Sci. Lett. vol.58 pp. 27-50

Thompson, R.N., 1982
Magmatism of the British Tertiary Volcanic Province.
Scott. J. Geol. vol.18 pp.49-107

Thompson, R.N., Morrison, M.A., Hendry, G.L. and Parry, S.J., 1984
An assessment of the relative roles of crust and mantle in magma genesis: an elemental approach.
Phil. Trans. Roy. Soc. Lond. A-310 pp.549-590

Tindle, A.G. and Pearce, J.A., 1981
Petrogenetic modelling of in situ fractional crystallisation in the Zoned Loch Doon Pluton, Scotland.
Contrib. Mineral. Petrol. vol.78 pp.196-207

Turcotte, D.L. and Schubert, D., 1982
Geodynamics
J. Wiley and sons.

Tuttle, O.F. and Bowen, N.L., 1958
Origin of granite in the light of experimental studies in the system NaAlSi3O8-KAlSi3O8-SiO2-H2O.
Geol. Soc. Amer. Mem. vol.74 pp.153

Van der Molen, I. and Paterson, M.S., 1979
Experimental deformation of partially melted granite.
Contrib. Mineral. Petrol. vol.70 no.3 pp.299-318

Walker, G., 1984
Downsag calderas, ring faults, caldera sizes and incremental caldera growth.
J. Geophys. Res. vol.89 pp.8407-8416

Whipple, E.R., 1974
A study of Wilsons determination of ferrous iron in

silicates.
Chem. Geol. vol.14 pp.223-238

White, S.H., 1982
Fault rocks of the Moine Thrust: a guide to their nomenclature.
Textures and Microstructures vol. 4 pp.211-221

Wise, D.U. Dunn, J.E., Engelder, J.T., Geiser, P.A., Hatcher, R.D., Kish, S.A., Odom, A.L. and Schamel, S., 1984
Fault-related rocks: suggestions for terminology.
Geology vol.12 pp.391-394

Wolff, J.A., 1986
Welded-tuff dykes, conduit closure, and lava dome growth at the end of explosive eruptions.
J. Volc. Geotherm. Res. vol.28 pp.379-384

Wones, D.R. and Gilbert, M.C., 1981
Amphiboles and the igneous environment.
In,Reviews in mineralogy 9: Amphiboles, eds. Veblen, D.R. and Ribbe, P.H. pp.355-390

Wood, D.A., Gibson, I.L. and Thompson, R.N., 1976
Element mobility during zeolite facies metamorphism of the Tertiary basalts of eastern Iceland.
Contrib. Mineral. Petrol. vol.55 pp.241-254

Wright, A.E. and Bowes, D.A., 1963
Classification of volcanic breccias.
Geol. Soc. Amer. Bull. vol.74 pp.79-86

APPENDIX A

ANALYTICAL TECHNIQUES

A1 WHOLE ROCK ANALYSES

A1.1 Sample Preparation

The rocks were split into approximately 3cm cubes after the removal of weathered surfaces by a mechanical splitter. They were then crushed in a steel jaw-crusher, which was carefully cleaned between specimens. A representative sample of each rock was powdered in an agate tema mill for up to 20 minutes to produce a suitable grainsize (200 mesh).

A1.2 Major element analysis by x-ray fluorescence spectrometry (X.R.F.).

Major element oxide concentrations (SiO_2, TiO_2, Al_2O_3, Fe_2O_3T, MnO, MgO, CaO, Na_2O, K_2O and P_2O_5) were determined on a Phillips PW 1212 semi-automated X.R.F. spectrometer at Imperial College using a chromium tube operating at 60 kV and 32 mA.

The method of Norrish and Hutton (1969) was used for sample preparation. Approximately 4g of powder was dried overnight at 110°C, and then ignited overnight at 950 C. Approximately 0.2800g of accurately weighed ignited powder was mixed with 1.5g of Johnson Matthey Spectroflux 105, which had been dried at 400°C for 4 hours. This mixture was then fused in platinum crucible for about 10 minutes to allow homogenisation. The melt was poured onto a hot-plate and pressed under a plunger to produce a glass disc.

After correction for machine drift and dead time, the data was processed using programs CHECK, SORD and PWMAJ (Parker 1977, 1979, 1980). A calibration line for each element was calculated using a set of international rock standards that were

run before the samples. Precision data for major elements using this equipment and method have been obtained by Kille (1987) during the period of the present study, and are given in Table A1. Duplicate analyses of 5 samples were determined by inductively coupled plasma atomic emission spectrometry (I.C.P.), which shows good agreement with X.R.F. data (Table A2).

A1.3 Trace element analysis by X.R.F.

The concentrations of Cu, Ni, V, Cr, Nb, Zr, Y, Th, Sr, Rb, Zn and Ba were also determined using the Phillips PW 1212 X.R.F.. A chromium tube operating at 60 kV and 32 mA was used to analyse Ba; a tungsten tube operating at 60 KV and 32 mA was used to analyse Cu, Ni, V, Nb, Zn, Zr and Cr; a molybdenum tube operating at 90 KV and 20 mA was used to analyse Y, Sr, Rb and Th.

Briquettes were prepared by mixing5.0g of dried rock powder with 6-8 drops of polyvinyl acetate. Boric acid was used to form strong walls, and the briquette was placed in a hydraulic press and subjected to a pressure of 8 tons per square inch for 30 seconds. The briquettes were dried overnight prior to analysis.

Programs TRANS and PTRAC (Parker 1979) were used to process the data, incorporating matrix, tube contamination and peak interference corrections.

The trace element concentrations for 4 U.S.G.S. standard rocks compared with their consensus values is given in Table A3. Table A4 shows precision data for selected trace elements obtained from 10-12 analyses of a basaltic glass (Kille 1987). The detection limits for selected trace elements were calculated using the formula (Norrish and Chappell 1977):

$$\text{D.L. (in ppm)} = \frac{6}{m}\sqrt{\frac{Rb}{Tb}}$$

TABLE A1 PRECISION DATA FOR MAJOR ELEMENTS ANALYSED BY X.R.F..VALUES ARE GIVEN AS WEIGHT PERCENT OXIDE. THE DATA WAS OBTAINED FROM 16 DETERMINATIONS OF 10 SEPARATE PREPARATIONS OF A BASALTIC GLASS (KILLE 1987).

.	MEAN	STANDARD DEVIATION
SiO2	55.080	0.2025
TiO2	1.5225	0.0090
Al2O3	13.6181	0.0968
Fe2O3T	12.7075	0.0706
MnO	0.2294	0.0201
MgO	3.2475	0.0584
CaO	6.7763	0.0262
Na2O	2.6794	0.1580
K2O	2.0538	0.0193
P2O5	0.2131	0.0068
LOI	1.1743	0.0842
TOTAL	99.9781	0.2873

TABLE A2 COMPARATIVE MAJOR AND TRACE ELEMENT DATA FOR 5 SAMPLES ANALYSED BY X.R.F. AND I.C.P.

SAMPLE	1JG9		1JG18		1JG27	
.	X.R.F.	I.C.P.	X.R.F.	I.C.P.	X.R.F.	I.C.P.
SiO2	67.32	67.56	53.71	53.90	61.36	60.22
TiO2	.50	.48	1.08	1.06	.98	.99
Al2O3	16.12	15.96	17.33	17.30	16.32	16.01
Fe2O3T	2.97	3.18	7.52	7.42	5.54	5.56
MnO	.03	.05	.07	.11	.08	.08
MgO	1.06	1.29	5.60	5.41	3.08	3.11
CaO	2.18	2.17	5.72	5.61	4.02	4.04
Na2O	4.60	4.44	3.64	3.63	4.37	4.31
K2O	3.91	4.02	2.55	2.54	3.42	3.37
P2O5	.40	.16	.32	.30	.37	.34
Ba	1711	1700	1470	1512	1095	1160
Cr	14	27	93	158	32	61
Cu	13	14	34	29	25	92
Sr	866	806	1281	1225	869	823
V	50	45	131	130	109	100
Zn	64	68	93	89	69	76
Zr	194	216	220	190	228	185

TABLE A2 (continued)

SAMPLE	1JG61		1JG76	
.	X.R.F.	I.C.P.	X.R.F.	I.C.P.
SiO2	71.04	70.15	65.76	65.00
TiO2	.34	.33	.67	.66
Al2O3	15.29	15.14	16.64	16.50
Fe2O3T	1.77	1.72	3.78	3.81
MnO	.04	.03	.06	.05
MgO	.32	.44	1.40	1.51
CaO	.88	.85	1.84	1.79
Na2O	4.85	4.68	4.85	4.72
K2O	5.12	5.18	4.05	4.09
P2O5	.07	.06	.20	.18
Ba	1917	1988	1753	1781
Cr	7	16	13	57
Cu	12	5	12	13
Sr	250	236	758	705
V	19	15	59	55
Zn	34	46	53	65
Zr	255	252	328	334

TABLE A3 TRACE ELEMENT ANALYSES OF U.S.G.S. STANDARD ROCKS BY X.R.F. 1 = THIS WORK, 2 = U.S.G.S. CONSENSUS VALUES (1982). ALL VALUES ARE GIVEN IN PPM.

.		G-2	AGV	BCR	W-1
V	1	41.6	121.3	381.4	272.5
.	2	36 ± 5	123 ± 12	404 ± 40	260 ± 25
Cr	1	11.1	8.3	15.2	131.8
.	2	9 ± 2	12 ± 3	16 ± 4	120 ± 14
Ni	1	6.7	15.9	18.5	74.3
.	2	4.9 ± 2.3	17 ± 4	13 ± 4	75 ± 9
Cu	1	17.2	53.6	18.9	104.5
.	2	11 ± 4	60 ± 6	19 ± 4	114 ± 10
Zn	1	85.3	82.5	124.8	77.9
.	2	85 ± 7	88 ± 2	129 ± 1	84 ± 6
Rb	1	166.4	66.6	47.4	22.6
.	2	170 ± 3	67 ± 1	47 ± .6	21.4 ± .3
Sr	1	467.4	660.1	327.6	186.9
.	2	478 ± 3	662 ± 9	330 ± 5	187 ± 7
Y	1	11.3	21.0	38.4	25.7
.	2	11.4 ± 2.3	21 ± 6	39 ± 7	26 ± 4
Zr	1	323.8	229.3	185.8	92.3
.	2	300 ± 30	225 ± 18	191 ± 5	100 ± 9
Nb	1	15.7	11.0	10.4	7.2
.	2	13 ± 4	15 ± 3	14 ± 3	8 ± 2
Ba	1	1838.9	1211.5	705.3	136.9
.	2	1880 ± 20	1221 ± 16	678 ± 16	162 ± 5

TABLE A4 PRECISION DATA FOR TRACE ELEMENTS ANALYSED BY X.R.F.. VALUES ARE GIVEN IN PPM. THE DATA WAS OBTAINED FROM 10-12 DETERMINATIONS OF 10 SEPARATE PREPARATIONS OF A BASALTIC GLASS (KILLE 1987).

.	MEAN	STANDARD DEVIATION	NOMBER OF DETERMINATIONS
V	292.77	9.33	11
Cr	12.81	2.73	11
Ni	5.46	1.79	11
Cu	14.64	2.31	11
Zn	114.11	1.65	10
Rb	72.88	1.51	12
Sr	223.45	3.13	12
Y	49.31	1.69	12
Zr	195.77	2.45	11
Nb	12.83	4.25	11
Ba	511.78	23.28	11

where:

$$m = \frac{Rp - Rb}{\text{standard concentration}}$$

Rp = peak counting rate, counts/sec.

Rb = background counting rate, counts/sec

Tb = background counting time.

standard concentration is given in ppm

The average detection limit for the 4 U.S.G.S. standard rocks is given in Table A5.

A1.4 Ferrous iron determination

FeO was determined in selected samples by wet chemical methods. A cold HF decomposition procedure was used in order to liberate ferrous iron, which was then measured by titration with potassium dichromate (Whipple 1974).

A1.5 Rare earth element analysis

Rare earth element (REE) concentrations were determined on a Phillips PV 8210 I.C.P. at Kings College.

0.500g of dried powder was mixed with 1.500g of lithium metaborate and fused in a platinum dish at 1000°C for 30 minutes. The fused bead was dissolved using a magnetic stirrer in a beaker containing 60ml of 2N HCl and 40ml of de-ionised water.

The solution was passed through an ion-exchange column containing Bio-Rad AG50W-X8 resin. The unwanted elements were removed by elution first with 300ml of 1.75N HCl, then 200ml of 1.75N HNO_3. The REE were then eluted with 100ml of 6N HNO_3, followed by 100ml of 8N HNO_3, and the resultant solution was evaporated to dryness on a hotplate. The REE salts were dissolved in 5.0ml of 2N HNO_3 just before analysis.

During the analytical run, machine drift was

TABLE A5 AVERAGE DETECTION LIMITS FOR SOME TRACE ELEMENTS DETERMINED BY X.R.F.. ALL VALUES ARE GIVEN IN PPM

V	9.6
Cr	5.4
Ni	4.5
Cu	5.8
Zn	7.4
Rb	3.6
Sr	4.1
Y	2.9
Zr	7.3
Nb	14.2
Ba	36.8

monitored using a composite REE solution, and line interference of certain elements on REE was manually corrected using interference standards. The precision of the preparation method has been tested by analysing 7 separate fusions of a hawaiite (Rutter 1985). The precision results and detection limits are given in Table A6. Precision errors for both REE and a range of incompatible elements are shown in Fig. A1. Table A7 shows the comparison between the literature values and this work for the international rock standard NIM-G.

A1.6 Instrumental Neutron Activation Analysis (I.N.A.A.)

I.N.A.A. was used to determine the concentrations of Hf, Ta, U and selected REE. Irradiations were undertaken at the University of London Reactor Centre at Silwood Park, and counting was done on a lithium-drifted germanium detector at the same site.

100mg of dried rock powder were irradiated for 5 days in sealed polythene capsules within a thermal neutron flux. International standard Soil-5 was used for calibration. Two standards were placed one at each end of a polythene irradiation tube which contained 13 samples in total. Table A8 shows the comparison between recommended values, and this work for Soil-5.

The samples were counted initially 5 days after removal from the reactor, and again 1 month later. Recounting enables a more accurate measurement of certain peaks due to the loss of interfering elements which have a short decay time, such as Sm. The data was processed using Nuclear Data software. This included a peak search routine, decay time correction and spectral interference correction.

Table A9 shows the comparison between the I.N.A.A. and I.C.P. methods for measuring certain REE concentrations.

TABLE A6 PRECISION DATA FOR R.E.E. ELEMENTS ANALYSED BY I.C.P.. VALUES ARE GIVEN IN PPM. THE DATA WAS OBTAINED FROM SEVEN SEPARATE ANALYSES OF A HAWAIITE, AND FROM SIX REAGENT BLANK SOLUTIONS (RUTTER 1985). THE CALCULATED DETECTION LIMIT IS THREE TIMES THE STANDARD DEVIATION OF THE REAGENT BLANK.

	HAWAIITE		REAGENT BLANK		
	MEAN	STANDARD DEVIATION	MEAN	STANDARD DEVIATION	CALCULATED DETECTION LIMIT
La	37.4	1.7	0.5	0.2	0.6
Ce	77.2	3.4	0.7	0.5	1.5
Pr	8.4	0.1	-	-	-
Nd	36.7	0.1	0.1	0.07	0.21
Sm	7.23	0.15	0.1	0.02	0.06
Eu	2.11	0.05	-	-	-
Gd	5.78	0.31	-	-	-
Dy	3.94	0.04	0.006	0.01	0.03
Ho	0.79	0.01	0.01	0.01	0.04
Er	1.84	0.04	0.07	0.02	0.06
Yb	1.20	0.04	0.02	0.005	0.015
Lu	0.17	0.01	-	-	-

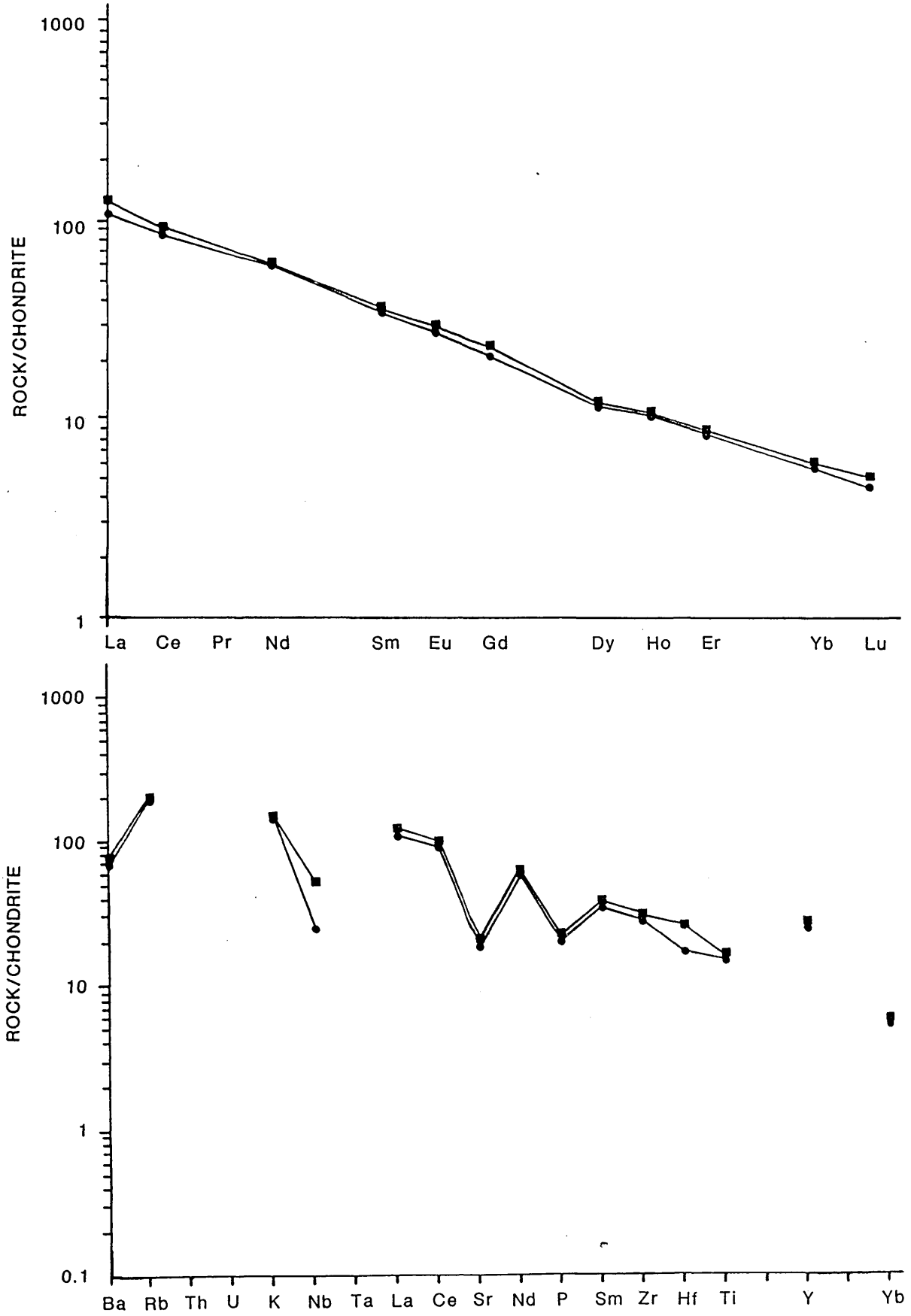

FIGURE A1 Chondrite-normalised plots for REE (top) and selected incompatible elements (bottom) graphically displaying the precision errors given in Table A6.

TABLE A7 REE ANALYSIS BY I.C.P. OF AN INTERNATIONAL ROCK STANDARD, NIM-G. LITERATURE VALUE IS POTTS ET AL. (1981). ALL VALUES GIVEN IN PPM.

.	THIS WORK	LIT VALUE
La	113	114
Ce	193	210
Pr	20	21
Nd	73	76
Sm	14	16
Eu	0.32	0.35
Gd	14	16
Dy	18	18
Ho	3.9	4.2
Er	13	13
Yb	14	14
Lu	2.0	2.2

TABLE A8 REE AND SOME TRACE ELEMENT ANALYSES BY I.N.A.A. STANDARD SOIL-5. ALL VALUES GIVEN IN PPM

	THIS WORK	RECOMMENDED VALUE
La	28.8	28.1 ± 1.5
Ce	61.4	59.7 ± 3.0
Nd	31.6	29.9 ± 1.6
Sm	5.59	5.49 ± 0.39
Eu	0.84	1.18 ± 0.08
Yb	1.62	2.24 ± 0.20
Lu	0.26	0.336 ± 0.044
Hf	7.11	6.30 ± 0.30
Ta	0.72	0.764 ± 0.056
U	2.88	3.04 ± 0.51

TABLE A9 COMPARATIVE REE DATA FOR 5 SAMPLES ANALYSED BY ICP AND INAA

SAMPLES	1JG18		1JG61		2JG1	
.	I.C.P.	I.N.A.A	I.C.P.	I.N.A.A	I.C.P.	I.N.A.A
La	24.63	27.27	54.54	50.23	19.79	19.15
Ce	49.56	53.97	100.56	91.27	39.60	38.03
Nd	25.09	28.02	38.84	39.19	20.22	20.39
Sm	4.45	5.17	5.67	5.73	3.74	4.33
Eu	1.49	1.71	1.29	1.31	1.41	1.36
Yb	1.41	1.53	1.69	1.69	1.24	1.25
Lu	.23	.16	.28	.18	.22	-

SAMPLES	3JG29		3JG32	
.	I.C.P.	I.N.A.A	I.C.P.	I.N.A.A
La	27.03	28.74	27.70	31.77
Ce	53.39	59.31	48.00	54.90
Nd	25.12	26.93	16.70	19.47
Sm	4.37	4.98	2.35	2.93
Eu	1.24	1.34	.56	.67
Yb	1.27	1.30	.73	.83
Lu	.22	-	.13	.11

A2 MINERAL ANALYSIS

Minerals were analysed at Imperial College using a Cambridge Instruments Microscan 5 microprobe fitted with a Link Systems energy dispersive x-ray detector. An accelerating voltage of 15kV and a specimen current on a Co standard of 4.0nA were used, for count times of 100 seconds. All analyses are points on C-coated polished thin-sections. Calibration was calculated using metal oxides, pure metals and end-member minerals. A set of duplicate analyses of a jadeite standard mineral analysed during the course of this work is given in Table A10. Mineral analyses were recalculated using program SUPREC written by J.C. Rucklidge (University of California at Berkeley).

A3 SCANNING ELECTRON MICROSCOPY (S.E.M)

S.E.M. studies used a JEOL 733 superprobe operating in back-scattered electron imaging (BEI) mode. Similar machine parameters and specimen preparation procedures as for the microprobe were used, with a similar EDS x-ray analyser.

A number of BEI photomicrographs are shown in chapter 7. Contrast on the image is a function of the atomic number (z) contrast in the sample, such that the brightness of an image increases with increasing z.

Semi-quantitative bulk analyses of the fault rocks were obtained by scanning small areas of the thin-sections (1-1000 square microns) with the beam for 200 seconds, again at the same operating conditions as the microprobe. Care was taken to analyse representative samples of the fine-grained rocks, and to avoid holes in the slide.

TABLE A10 PRECISION DATA FOR A JADEITE STANDARD
ANALYSED THROUGHOUT THIS STUDY

1SUPER RECAL — JADEITE STANDARD PRECISION RUN

	1	2	3	4	5	6	7	8
NA2O	14.94	15.27	14.98	15.45	15.16	14.94	14.91	15.21
MGO	.18	0.00	0.00	0.00	.24	0.00	.27	0.00
A2O3	25.15	24.99	24.93	25.40	24.38	25.16	24.87	25.27
SIO2	58.85	59.49	59.44	59.69	59.34	59.39	59.16	59.02
CAO	.43	.32	.12	0.00	.54	.14	.59	.06
TIO2	0.00	.03	0.00	0.00	.05	0.00	.04	.13
C2O3	.07	.21	0.00	.01	0.00	0.00	.05	.07
MNO	.21	0.00	.09	.01	.05	.07	0.00	.06
FEO	.23	.25	0.00	0.00	.27	.16	.07	0.00
SUM	100.06	100.56	99.56	100.56	100.03	99.86	99.96	99.82
SI	1.986 *	1.996 *	2.007 *	1.998 *	2.003 *	2.001 *	1.995 *	1.991 *
AL	.014 2.000	.004 2.000	-I 2.007	.002 2.000	-I 2.003	-I 2.001	.005 2.000	.009 2.000
AL	.985 *	.984 *	.992 *	.999 *	.970 *	.999 *	.983 *	.996 *
TI	0.000 *	.001 *	0.000 *	0.000 *	.001 *	0.000 *	.001 *	.003 *
CR	.002 *	.006 *	0.000 *	.000 *	0.000 *	0.000 *	.001 *	.002 *
FE	.006 *	.007 *	0.000 *	0.000 *	.008 *	.005 *	.002 *	0.000 *
MG	.009 *	0.000 *	0.000 *	0.000 *	.012 *	0.000 *	.014 *	0.000 *
CA	.016 *	.012 *	.004 *	0.000 *	.020 *	.005 *	.021 *	.002 *
MN	.006 *	0.000 *	.003 *	.000 *	.001 *	.002 *	0.000 *	.002 *
NA	.977 2.002	.993 2.002	.981 1.980	1.002 2.002	.992 2.004	.976 1.986	.975 1.997	.995 1.999
O	6.000 *	6.000 *	6.000 *	6.000 *	6.000 *	6.000 *	6.000 *	6.000 *
WO	41.91	62.12	62.78	0.00	48.04	43.72	57.83	55.85
EN	24.41	0.00	0.00	0.00	29.70	0.00	36.82	0.00
FS	33.68	37.88	37.22	100.00	22.26	56.28	5.36	44.15
F/M	1.380	0.000	0.000	0.000	.750	0.000	.145	0.000
F/FM	.589	0.000	0.000	0.000	.428	0.000	.127	0.000

1 STD1
2 STD2
3 STD3
4 STD4
5 STD5
6 STD6
7 STD7
8 STD8

1SUPER RECAL — JADEITE STANDARD PRECISION RUN

	9	10	11	12
NA2O	15.40	15.14	15.34	14.94
MGO	0.00	.08	.19	-.03
A2O3	25.33	25.05	25.35	24.76
SIO2	59.36	59.27	59.52	59.02
CAO	.04	.25	.46	.04
TIO2	0.00	.03	.07	-.01
C2O3	.06	.05	.12	-.01
MNO	0.00	.05	.12	-.01
FEO	0.00	.11	.22	-.00
SUM	99.89	100.03	101.38	98.69
SI	1.991 *	1.996 *	1.984 *	2.009 *
AL	.009 2.000	.004 2.000	.016 2.000	0.000 2.009
AL	.998 *	.991 *	.979 *	.993 *
TI	0.000 *	.001 *	.002 *	-.000 *
CR	.002 *	.001 *	.003 *	-.000 *
FE	0.000 *	.003 *	.005 *	-.000 *
MG	0.000 *	.004 *	.009 *	-.002 *
CA	.001 *	.009 *	.016 *	.001 *
MN	0.000 *	.002 *	.003 *	-.000 *
NA	1.007 2.008	.999 1.999	.991 2.010	.986 1.978
O	6.000 *	6.000 *	6.000 *	6.000 *
WO	100.00	51.47	46.76	-171.64
EN	0.00	22.06	26.36	226.07
FS	0.00	26.48	26.88	45.57
F/M	1.380	1.200	1.020	0.000
F/FM	.589	.546	.505	0.000

9 STD9
10 AVERAGE
11 AVERAGE PLUS SIGMA
12 AVERAGE MINUS SIGMA

APPENDIX B

SAMPLE LOCALITIES

NUMBER	ROCK TYPE	LOCALITY
1JG9	monzonite	lower An-t-sron. NN137562
1JG10	dioritic gabbro	lower An-t-sron. NN136561
1JG11	granite	Loch Etive. NN107454
1JG12	granite	Glen Etive. NN141475
1JG13	diorite	Glen Etive. NN192511
1JG14 .	intrusive tuff	confluence of River Etive and Cam Ghleann. NN241538
1JG18 .	dioritic gabbro	River Etive, 1Km W of Kingshouse. NN249546
1JG21 .	quartzitic breccia	Stob Mhic Mhartuin, between faults. NN210574
1JG24 .	rhyolite	Stob Mhic Mhartuin, inner fault. NN210574
1JG25 .	F.C.R.	Stob Mhic Mhartuin, inner fault. NN210574
1JG27 .	diorite	Stob Mhic Mhartuin, inner intrusion. NN210574
1JG29 .	diorite	Stob Mhic Mhartuin, inner intrusion. NN209574
1JG34 .	F.C.R.	Stob Mhic Mhartuin, inner fault. NN209574
1JG35 .	F.C.R.	Stob Mhic Mhartuin, inner fault. NN209574
1JG37 .	F.C.R./cataclasite	Stob Mhic Mhartuin, between faults. NN208576
1JG39 .	F.C.R.	Stob Mhiic Mhartuin, outer fault. NN208576
1JG41 .	diorite	Stob Mhic Mhartuin, outer intrusion. NN208576
1JG42	diorite	Devils Staircase. NN217575
1JG43	dioritic gabbro	Devils Staircase. NN219569
1JG51	diorite	Coire an Easain. NN255494
1JG55	diorite	Coire an Easain. NN258490

1JG56	dioritic gabbro	1Km E of Stob Beinn a Chrulaiste. NN235563
1JG58	diorite	Loch Etive. NN026330
1JG59	diorite	Old Quarry, Loch Awe. NN129291
1JG60	diorite	Old Quarry, Loch Awe. NN129291
1JG61	granite	Clachaig Quarry. NN130568
1JG73	F.C.R.	main fault, 100m N of Atriochtan. NN142570
1JG76	monzonite	An-t-sron. NN134548
1JG80	monzonite	250m N of Atriochtan. NN145577
2JG1	gabbro	Cam Ghleann, within the main fault. NN251524
2JG4	rhyolite	Queens Cairn, 500m E of meeting of three waters NN185564
2JG9	monzonite	Crossroads Quarry, W of Atriochtan. NN138567
2JG14	granite	dyke, Crossroads Quarry. NN138567
2JG15	granite	dyke, Crossroads Quarry. NN138567
2JG19	granite	dyke, River Coe. NN131566
2JG20	diorite	River Coe. NN133566
2JG21	diorite	River Coe. NN135567
2JG22	diorite	Loch Linnhe Quarries, Ballachulish. NN021589
2JG25	pelite	lower An-t-sron. NN127556
2JG26	dioritic gabbro	Cam Ghleann, within the main fault. NN251524
2JG33	F.C.R./diorite	Cam Ghleann, within the main fault. NN251524
2JG34	diorite	Cam Ghleann. NN250525
2JG35	diorite	Cam Ghleann. NN249526
2JG36	diorite	Cam Ghleann. NN248527
2JG37	diorite	Cam Ghleann. NN248528
2JG38	diorite	Cam Ghleann. NN247529
3JG10	migmatite	River Coe. NN134566

3JG12	F.C.R.	main fault, 250m N of Atriochtan. NN142573
3JG13	F.C.R.	main fault, 250m N of Atriochtan. NN142573
3JG14	monzonite	250m N of Atriochtan. NN142573
3JG17	diorite	Fionn Ghleann. NN127541
3JG20	dioritic gabbro	lower An-t-sron. NN137565
3JG21	intrusive breccia	Cam Ghleann, 200m W of stream. NN258522
3JG27	diorite	upper Cam Ghleann. NN248518
3JG30	diorite	River Coupall, 1Km SE of Laggangarbh. NN233556
3JG32	rhyolite	River Coupall. NN233556
3JG33	rhyolite	500m SE of Stob Beinn a Chrulaiste. NN229562
3JG47	dioritic gabbro	Coire an Easain. NN255494
3JG49	monzonite	Coire an Easain. NN251495
3JG50	dioritic gabbro	Coire an Easain. NN253496
3JG54	diorite	Sron a Choire Odhair. NN200579
3JG55	dioritic gabbro	Sron a Choire Odhair. NN201580
3JG56	calc-schist	Crossroads Quarry, W of Atriochtan. NN138567
3JG57	monzonite	Allt Choire Odhair Mhoir. NN200586
3JG58	diorite	Allt Choire Odhair Mhoir. NN197583
3JG59	monzonite	Allt Choire Odhair Mhoir. NN197583
3JG60	diorite	dyke, River Coe. NN134566
3JG64	monzonite	Stob Mhic Mhartuin, small intrusion between faults. NN208575
3JG65	F.C.R.	Stob Mhic Mhartuin, between faults. NN208575
4JG2	granite	pod in schists, lower An-t-sron. NN128562

4JG5	granite	Dalness, River Etive, just E of footbridge. NN166509
4JG7	monzonite	Dalness, River Etive, just E of footbridge. NN166509
4JG11	dioritic gabbro	Ghleann Fhaolain. NN157517
4JG12	dioritic gabbro	SE of Dalness, lower Beinn Ceitlein. NN174517
4JG13	monzonite	Se of Dalness, lower Beinn Ceitlein. NN175516
4JG18	pyroclastic breccia	500m SE of Laggangarbh. NN221553
4JG20	F.C.R.	250m N of Atriochtan. NN142573
4JG21	rhyolite	500m SE of Stob Mhic Mhartuin. NN210573

NOTES ON TABULATION OF WHOLE ROCK ANALYSES

Major elements calculated on a dry basis.

All Fe reported as Fe2O3.

U, Hf and Ta were analysed by I.N.A.A., REE were analysed by I.C.P., except samples 1JG29, 1JG55, 1JG56, 3JG17, 3JG20 and 3JG54 which were analysed by I.N.A.A., other trace elements were analysed by X.R.F..

FeO for some samples was determined by wet chemical methods.

All major elements are given as weight % oxide.
All trace elements are given as ppm.

APPENDIX C

MAJOR AND TRACE ELEMENT DATA

SAMPLE	1JG9	1JG10	1JG18	1JG27	1JG29	1JG41
SiO2	67.32	56.33	53.71	61.36	60.02	62.71
TiO2	.50	1.10	1.08	.98	1.01	.78
Al2O3	16.12	18.66	17.33	16.32	17.55	16.33
Fe2O3T	2.97	6.78	7.52	5.54	5.87	4.86
MnO	.03	.09	.07	.08	.08	.06
MgO	1.06	3.12	5.60	3.08	2.69	2.04
CaO	2.18	5.44	5.72	4.02	4.85	4.01
Na2O	4.60	3.94	3.64	4.37	4.22	4.03
K2O	3.91	2.68	2.55	3.42	2.60	3.04
P2O5	.40	.45	.32	.37	.35	.31
LOI	1.15	.94	2.27	1.11	.81	2.08
TOTAL	100.24	99.53	99.81	100.65	100.05	100.25
V	50	122	131	109	97	82
Cr	14	18	93	32	25	15
Ni	12	21	63	18	22	14
Cu	13	18	34	25	27	16
Zn	64	75	93	69	60	60
Rb	93	56	87	88	54	67
Sr	866	1539	1281	869	1246	1162
Y	19	20	21	19	22	23
Zr	194	242	220	228	318	223
Nb	8	7	3	17	7	8
Ba	1711	1750	1470	1095	1689	1321
Th	10	3	3	6	5	7
Hf	-	-	6.37	-	7.40	-
Ta	-	-	.79	-	.95	-
U	-	-	.95	-	1.65	-

SAMPLE	1JG42	1JG43	1JG51	1JG55	1JG56	1JG61
SiO2	60.45	53.11	58.76	61.94	56.73	71.04
TiO2	.90	1.55	1.16	.92	1.26	.34
Al2O3	16.20	16.66	16.68	17.44	17.34	15.29
Fe2O3T	5.72	8.19	7.00	4.63	7.23	1.77
MnO	.07	.12	.07	.07	.10	.04
MgO	3.43	4.65	3.32	2.07	3.84	.32
CaO	4.52	5.57	6.03	3.46	5.85	.88
Na2O	3.88	4.20	3.59	4.39	3.99	4.85
K2O	3.10	2.57	2.07	3.97	2.19	5.12
P2O5	.31	.68	.52	.27	.46	.07
LOI	1.34	2.08	.74	1.08	.93	.97
TOTAL	99.92	99.38	99.94	100.24	99.92	100.69
V	95	160	162	90	140	19
Cr	56	54	12	42	32	7
Ni	44	51	25	29	32	7
Cu	29	21	33	19	31	12
Zn	63	101	74	61	72	34
Rb	67	47	53	99	52	115
Sr	967	1000	1383	899	1304	250
Y	19	31	34	18	19	19
Zr	182	285	124	254	267	255
Nb	9	21	7	8	6	9
Ba	1161	1032	786	1390	1158	1917
Th	7	5	2	11	7	12
Hf	-	-	-	8.34	6.51	9.58
Ta	-	-	-	.82	.81	.99
U	-	-	-	3.00	1.31	2.33

SAMPLE	1JG76	1JG80	2JG1	2JG9	2JG20	2JG21
SiO2	65.76	64.57	52.61	67.03	60.52	61.34
TiO2	.67	.71	1.35	.66	1.07	.71
Al2O3	16.64	16.74	17.75	16.10	17.24	17.76
Fe2O3T	3.78	4.01	8.61	3.73	6.00	4.76
MnO	.06	.06	.14	.06	.05	.06
MgO	1.40	1.63	4.82	1.10	1.79	2.33
CaO	1.84	2.84	8.01	2.37	3.66	4.31
Na2O	4.85	4.70	3.51	4.43	5.02	4.83
K2O	4.05	3.57	1.24	3.79	2.38	2.93
P2O5	.20	.23	.30	.16	.38	.27
LOI	1.43	.91	.82	.87	1.36	.44
TOTAL	100.68	99.97	99.16	100.30	99.47	99.74
V	59	58	191	-	90	102
Cr	13	15	94	33	15	66
Ni	12	11	66	-	11	39
Cu	12	22	45	-	31	40
Zn	53	60	93	50	69	70
Rb	106	81	31	95	68	75
Sr	758	845	1547	666	1418	1200
Y	24	21	14	29	11	15
Zr	328	313	176	357	760	188
Nb	11	11	5	12	12	7
Ba	1753	1710	761	1870	1540	1402
Th	10	7	10	13	2	8
Hf	-	-	3.40	-	-	5.43
Ta	-	-	.52	-	-	.63
U	-	-	.44	-	-	1.54

SAMPLE	2JG26	2JG34	2JG35	2JG36	2JG37	2JG38
SiO2	53.45	59.45	60.25	59.14	59.50	59.77
TiO2	1.28	1.02	1.01	1.07	1.00	1.00
Al2O3	17.65	18.04	17.43	17.68	17.79	17.88
Fe2O3T	8.63	5.88	5.74	6.09	5.66	5.82
MnO	.13	.05	.09	.09	.06	.07
MgO	4.74	2.52	2.27	2.55	2.67	2.42
CaO	8.02	5.17	4.81	5.29	4.36	4.98
Na2O	3.78	4.85	4.51	4.70	4.59	4.65
K2O	1.21	2.56	2.75	2.54	2.83	2.64
P2O5	.26	.38	.36	.38	.34	.37
LOI	.73	.41	.66	.61	.99	.60
TOTAL	99.88	100.33	99.88	100.14	99.79	100.20
V	190	113	114	-	109	111
Cr	98	37	43	50	43	40
Ni	56	29	27	-	30	28
Cu	47	17	54	-	28	43
Zn	86	72	70	71	78	72
Rb	21	54	59	55	68	57
Sr	1545	1344	1224	1316	1284	1350
Y	12	17	17	23	16	8
Zr	186	349	354	319	359	314
Nb	4	11	5	8	10	9
Ba	815	1620	1635	1524	1523	1562
Th	0	7	7	8	4	7
Hf	3.58	-	7.61	-	-	-
Ta	.53	-	.78	-	-	-
U	.40	-	1.31	-	-	-

SAMPLE	3JG14	3JG17	3JG20	3JG27	3JG29	3JG30
SiO2	65.28	62.69	56.47	61.19	61.29	57.88
TiO2	.74	.93	1.16	.72	.75	1.06
Al2O3	16.83	16.83	18.91	16.20	16.95	18.47
Fe2O3T	4.30	5.60	6.86	5.26	5.42	6.01
MnO	.07	.10	.09	.11	.08	.08
MgO	1.28	1.98	2.39	3.40	2.55	2.42
CaO	2.71	3.51	5.83	4.14	4.85	5.37
Na2O	4.51	4.04	4.56	4.21	3.80	4.46
K2O	3.52	3.25	2.41	2.74	3.44	2.46
P2O5	.21	.26	.44	.22	.24	.39
LOI	.91	1.06	1.28	1.39	1.01	1.13
TOTAL	100.36	100.25	100.40	99.58	100.38	99.73
V	67	96	39	106	104	109
Cr	21	38	26	121	116	40
Ni	22	26	22	52	54	28
Cu	9	19	16	29	28	27
Zn	65	79	81	67	67	76
Rb	87	80	53	75	124	52
Sr	868	1001	1523	956	1030	1464
Y	22	26	39	10	13	16
Zr	365	360	409	156	164	410
Nb	11	10	8	9	3	8
Ba	1852	1528	2025	1068	1181	1788
Th	12	0	6	6	8	8
Hf	-	9.82	9.84	-	4.19	-
Ta	-	1.04	.62	-	.68	-
U	-	1.95	1.03	-	1.43	-

SAMPLE	3JG41	3JG47	3JG50	3JG54	3JG55	3JG57
SiO2	60.09	56.32	58.57	59.80	56.45	63.50
TiO2	1.00	1.25	1.05	1.02	1.31	.74
Al2O3	17.41	17.70	18.45	17.54	16.59	16.46
Fe2O3T	5.60	7.32	5.96	5.76	7.09	4.74
MnO	.08	.11	.09	.05	.13	.10
MgO	2.35	3.48	2.19	2.61	3.24	1.69
CaO	3.27	4.86	5.06	4.66	5.00	2.93
Na2O	3.69	3.70	4.37	4.32	4.66	4.36
K2O	3.13	1.93	2.71	2.68	2.75	3.41
P2O5	.36	.43	.40	.34	.37	.24
LOI	1.86	2.83	.88	1.01	1.95	1.36
TOTAL	98.84	99.93	99.73	99.79	99.54	99.53
V	96	155	112	99	143	80
Cr	31	57	29	47	66	34
Ni	24	45	20	28	38	12
Cu	24	57	32	52	25	22
Zn	75	91	85	65	78	72
Rb	79	62	61	52	68	88
Sr	1158	1692	1542	1242	766	980
Y	18	21	13	19	-	18
Zr	405	310	421	346	234	247
Nb	3	8	4	6	16	12
Ba	2072	1418	2052	1645	829	1386
Th	8	6	6	11	9	10
Hf	-	8.04	-	5.91	-	-
Ta	-	.96	-	.74	-	-
U	-	1.65	-	1.31	-	-

SAMPLE	3JG58	3JG59	4JG5	4JG7	4JG11	4JG12
SiO2	61.13	63.58	71.93	64.93	56.93	55.78
TiO2	.91	.93	.40	.75	1.32	1.07
Al2O3	17.08	16.91	14.54	16.17	17.03	15.81
Fe2O3T	5.85	6.34	2.01	4.20	7.56	7.00
MnO	.10	.05	0.00	0.00	.12	.10
MgO	2.27	1.89	.45	1.88	3.35	5.52
CaO	4.63	1.70	1.14	3.44	5.43	5.47
Na2O	4.39	3.20	4.36	4.24	4.21	4.22
K2O	2.79	3.89	4.67	3.63	2.60	2.92
P2O5	.38	.17	.10	.25	.38	.59
LOI	1.03	1.55	.59	.64	1.13	1.61
TOTAL	100.56	100.21	100.19	100.13	100.06	100.09
V	106	83	-	-	-	-
Cr	33	48	0	41	39	156
Ni	22	30	-	-	-	-
Cu	22	22	-	-	-	-
Zn	82	82	35	56	100	94
Rb	65	148	102	91	60	70
Sr	1298	609	356	686	763	1338
Y	14	48	16	17	24	16
Zr	243	370	202	199	224	195
Nb	8	20	15	15	8	1
Ba	1350	1259	1088	1210	829	2046
Th	7	16	15	13	8	13
Hf	-	-	-	-	-	-
Ta	-	-	-	-	-	-
U	-	-	-	-	-	-

SAMPLE	4JG13	2JG4	3JG32	3JG33	4JG21	2JG14
SiO2	63.95	74.77	74.22	76.33	74.45	76.91
TiO2	.73	.16	.25	.10	.20	.17
Al2O3	16.01	14.33	13.20	14.07	14.04	12.38
Fe2O2T	4.74	.89	2.02	.77	1.12	.91
MnO	.02	.03	.04	.04	.04	0.00
MgO	2.36	0.00	.85	.05	.29	0.00
CaO	3.46	.61	.89	.41	.48	.43
Na2O	4.18	4.56	2.36	1.08	4.42	2.65
K2O	3.70	4.37	5.49	6.07	4.82	6.32
P2O5	.25	.04	.08	.02	.05	.01
LOI	1.00	.59	1.20	1.11	.56	.19
TOTAL	100.40	100.35	100.60	100.05	100.47	99.97
V	-	8	35	4	-	8
Cr	37	8	33	2	0	10
Ni	-	7	24	9	-	7
Cu	-	18	15	12	-	13
Zn	37	49	32	34	17	11
Rb	91	114	169	179	132	141
Sr	897	187	287	196	337	62
Y	15	13	-	11	18	11
Zr	210	124	99	73	128	128
Nb	12	12	10	12	13	11
Ba	1228	1325	1377	671	1319	262
Th	12	15	16	10	12	12
Hf	-	-	3.06	-	-	-
Ta	-	-	.72	-	-	-
U	-	-	2.75	-	-	-

SAMPLE	2JG15	2JG19	4JG2	2JG25	1JG21	1JG24
SiO2	75.36	78.83	78.01	77.81	76.11	73.79
TiO2	.30	.10	.08	.14	.57	.35
Al2O3	12.93	12.68	12.89	12.30	11.73	14.06
Fe2O3T	1.56	.71	1.11	.82	1.93	1.98
MnO	.03	0.00	.06	0.00	.08	.05
MgO	.01	.15	0.00	0.00	.55	.47
CaO	.28	.10	.25	.30	1.80	.72
Na2O	2.67	5.18	4.73	3.84	2.21	4.54
K2O	7.47	1.63	1.64	4.84	4.34	3.54
P2O5	.01	.07	.03	.01	.05	.08
LOI	.23	.82	.89	.23	.84	.87
TOTAL	100.85	100.27	99.69	100.29	100.21	100.45
V	17	11	-	10	-	24
Cr	10	12	0	7	24	10
Ni	11	8	-	8	-	7
Cu	8	20	-	26	-	5
Zn	18	17	7	17	47	33
Rb	152	109	125	139	128	117
Sr	119	129	98	26	287	240
Y	-	12	21	13	33	24
Zr	168	69	45	108	413	259
Nb	18	8	13	16	15	14
Ba	409	125	134	81	984	927
Th	16	6	5	17	9	16
Hf	6.23	-	-	-	12.62	6.84
Ta	1.12	-	-	-	1.30	1.36
U	3.87	-	-	-	2.11	3.13

SAMPLE	1JG34	3JG64	1JG11	1JG12	1JG13	1JG58
SiO2	79.39	65.46	77.10	73.44	61.29	62.10
TiO2	.39	.51	.15	.33	.93	.91
Al2O3	9.83	15.15	13.04	14.16	16.23	17.36
Fe2O3T	2.20	3.90	1.03	2.01	5.71	4.76
MnO	.03	.05	.05	.05	.07	.06
MgO	.52	2.30	.15	.74	3.64	2.07
CaO	.45	2.62	.76	1.50	4.94	3.46
Na2O	2.29	3.40	3.75	3.66	4.20	4.86
K2O	3.82	4.52	4.80	4.61	3.08	4.05
P2O5	.11	.17	.05	.12	.30	.27
LOI	.53	1.70	.23	.48	.76	.39
TOTAL	99.56	99.78	101.11	101.10	101.15	100.29
V	28	-	8	28	110	80
Cr	16	113	8	13	60	6
Ni	9	-	6	9	43	7
Cu	6	-	9	14	28	27
Zn	23	60	25	35	72	66
Rb	128	107	188	122	67	97
Sr	110	856	113	419	935	971
Y	26	13	9	9	19	10
Zr	254	179	70	118	192	520
Nb	12	7	11	10	10	11
Ba	703	1503	188	1001	1091	2147
Th	7	15	17	12	6	9
Hf	8.88	-	3.15	4.26	-	14.01
Ta	1.47	-	1.25	.91	-	.49
U	1.77	-	5.36	3.31	-	5.04

SAMPLE	1JG59	1JG60	2JG22	3JG49	3JG60
SiO2	57.93	57.30	62.54	64.74	59.94
TiO2	.95	1.05	.80	.66	.85
Al2O3	16.37	16.48	16.35	15.55	15.87
Fe2O3T	6.71	6.89	4.84	4.18	5.13
MnO	.09	.10	.05	.03	.04
MgO	4.60	4.67	2.74	2.14	3.46
CaO	5.96	6.26	4.16	3.41	4.63
Na2O	3.72	3.78	4.22	4.13	3.91
K2O	2.25	2.07	3.32	3.75	3.17
P2O5	.38	.38	.29	.20	.27
LOI	.78	.56	.61	.78	2.46
TOTAL	99.74	99.54	99.92	99.57	99.73
V	121	130	108	74	106
Cr	76	79	71	54	91
Ni	54	63	33	36	59
Cu	29	28	17	11	26
Zn	72	79	63	49	58
Rb	47	44	77	98	66
Sr	1194	1224	1268	759	1026
Y	16	17	18	40	33
Zr	93	83	199	206	207
Nb	7	8	1	8	8
Ba	1046	1112	1435	1157	1181
Th	4	5	15	10	11
Hf	-	3.79	-	-	-
Ta	-	.61	-	-	-
U	-	1.50	-	-	-

FeO DETERMINATIONS

SAMPLE	1JG9	1JG10	1JG18	1JG51	1JG55	1JG56
FeO	1.59	5.16	3.99	5.29	2.44	3.87

SAMPLE	1JG61	1JG76	1JG80	2JG1	2JG26	2JG38
FeO	.91	1.73	1.75	5.04	5.84	3.54

SAMPLE	3JG17	3JG30	3JG55	3JG33	2JG14	2JG15
FeO	2.94	3.17	3.84	.65	.53	.66

SAMPLE	2JG25	1JG24	1JG34	1JG58	1JG59	1JG60
FeO	.44	.98	1.12	2.76	4.57	4.82

RARE EARTH ELEMENT DATA

SAMPLE	1JG18	1JG29	1JG55	1JG56	1JG61	2JG1
La	24.63	32.60	36.89	36.01	54.54	19.79
Ce	49.56	67.46	74.21	67.42	100.56	39.60
Pr	6.24	-	-	-	10.87	5.02
Nd	25.09	30.70	32.59	32.32	38.84	20.22
Sm	4.45	5.95	5.37	5.82	5.67	3.74
Eu	1.49	1.78	1.46	1.86	1.29	1.42
Gd	3.76	-	-	-	4.17	3.33
Dy	3.22	-	-	-	3.46	2.77
Ho	.56	-	-	-	.62	.66
Er	1.69	-	-	-	1.93	1.52
Yb	1.41	1.70	1.81	1.73	1.69	1.24
Lu	.23	.15	.20	.16	.28	.22

SAMPLE	2JG21	2JG26	2JG35	3JG17	3JG20	3JG29
La	29.32	17.95	31.48	41.49	31.02	27.03
Ce	50.21	36.40	65.00	85.37	65.33	53.39
Pr	7.02	-	7.63	-	-	6.53
Nd	20.20	20.00	29.63	43.22	35.72	25.12
Sm	4.58	3.41	5.00	7.73	6.20	4.37
Eu	1.33	1.30	1.59	1.95	2.08	1.24
Gd	3.72	2.86	4.08	-	-	3.59
Dy	3.21	2.65	3.50	-	-	2.91
Ho	.58	.60	.62	-	-	.51
Er	1.76	1.45	1.88	-	-	1.61
Yb	1.51	1.18	1.59	2.72	1.78	1.27
Lu	.28	.19	.27	.34	.19	.22

SAMPLE	3JG47	3JG54	3JG32	2JG15	1JG21	1JG24
La	26.45	35.76	27.70	34.88	31.10	43.74
Ce	58.30	73.50	48.00	66.86	65.10	77.62
Pr	7.57	-	4.96	6.91	8.30	9.32
Nd	32.00	26.53	16.70	23.40	32.00	34.93
Sm	5.47	5.94	2.35	3.46	4.77	5.19
Eu	1.77	1.95	.56	.56	1.10	.94
Gd	4.88	-	1.73	2.58	4.10	4.25
Dy	4.45	-	1.34	2.29	5.12	3.93
Ho	.80	-	.32	.43	1.50	.72
Er	2.35	-	.83	1.45	2.95	2.30
Yb	2.00	-	.73	1.47	2.62	2.02
Lu	.33	.23	.13	.24	.48	.32

NORMATIVE COMPOSITIONS CALCULATED USING FE2O3/FEO = 0.75

SAMPLE	1JG9	1JG10	1JG18	1JG27	1JG29	1JG41
QZ	20.67	6.43	0.00	10.15	10.98	15.88
CO	.62	.12	0.00	0.00	0.00	0.00
OR	23.91	15.86	16.04	20.24	15.38	17.99
AB	38.50	33.34	37.19	36.98	35.71	34.10
AN	10.74	24.98	11.89	14.80	21.23	17.48
NE	0.00	0.00	7.31	0.00	0.00	0.00
DI	0.00	0.00	12.11	2.59	1.05	.84
HY	4.37	10.54	0.00	8.60	6.33	6.68
OL	0.00	0.00	7.71	0.00	0.00	0.00
MT	1.87	3.96	4.34	3.23	3.44	2.84
IL	.95	2.09	2.05	1.86	1.90	1.48
AP	.40	1.04	.78	.88	.83	.73

SAMPLE	1JG42	1JG43	1JG51	1JG55	1JG56	1JG61
QZ	11.46	1.28	12.83	10.52	7.46	20.57
CO	0.00	0.00	0.00	.07	0.00	.17
OR	18.34	15.20	12.25	23.49	12.90	30.29
AB	32.83	35.54	30.38	37.06	33.68	40.95
AN	17.62	19.01	23.28	15.98	23.00	4.39
NE	0.00	0.00	0.00	0.00	0.00	0.00
DI	5.08	3.77	3.09	0.00	2.94	0.00
HY	9.66	12.81	9.58	6.76	.32	1.47
OL	0.00	0.00	0.00	0.00	0.00	0.00
MT	3.33	4.78	4.09	2.70	4.22	1.03
IL	1.80	2.94	2.20	1.75	2.37	.65
AP	.73	1.61	1.23	.64	1.09	.17

SAMPLE	1JG76	1JG80	2JG1	2JG9	2JG20	2JG21
QZ	15.60	14.69	3.95	19.93	11.84	9.61
CO	1.18	.29	0.00	.85	.81	0.00
OR	23.97	21.12	7.24	22.27	13.92	17.26
AB	41.04	39.77	29.90	37.24	42.48	40.91
AN	8.43	13.22	28.93	10.76	15.30	18.08
NE	0.00	0.00	0.00	0.00	0.00	0.00
DI	0.00	0.00	7.21	0.00	0.00	.45
HY	4.97	5.61	12.56	4.43	7.06	7.85
OL	0.00	0.00	0.00	0.00	0.00	0.00
MT	2.20	2.35	5.33	2.32	3.70	3.01
IL	1.27	1.35	2.58	1.21	1.97	1.37
AP	.47	.54	.62	.31	.93	.93

SAMPLE	2JG26	2JG34	2JG35	2JG36	2JG37	2JG38
QZ	3.58	7.39	10.27	7.75	8.45	8.83
CO	0.00	0.00	0.00	0.00	0.00	0.00
OR	7.24	15.03	16.14	15.03	16.70	15.59
AB	31.99	40.91	38.29	39.86	38.81	39.34
AN	27.54	20.03	19.20	19.48	19.48	20.03
NE	0.00	0.00	0.00	0.00	0.00	0.00
DI	8.34	2.24	1.57	3.14	.30	1.57
HY	12.07	7.75	7.37	7.45	8.86	7.77
OL	0.00	0.00	0.00	0.00	0.00	0.00
MT	5.33	3.70	3.47	3.70	3.47	2.78
IL	2.43	1.97	1.97	1.97	1.97	1.97
AP	.62	.93	.93	.93	.62	.93

SAMPLE	3JG14	3JG17	3JG20	3JG27	3JG29	3JG30
QZ	17.47	15.76	4.75	12.12	12.12	7.57
CO	1.05	.88	0.00	0.00	0.00	0.00
OR	20.60	19.48	14.47	16.14	20.60	14.47
AB	38.29	34.09	38.81	35.66	31.99	37.76
AN	12.43	15.67	23.65	17.25	18.92	23.09
NE	0.00	0.00	0.00	0.00	0.00	0.00
DI	0.00	0.00	2.03	1.19	2.54	.68
HY	5.06	7.43	7.97	10.64	7.74	8.34
OL	0.00	0.00	0.00	0.00	0.00	0.00
MT	2.78	3.47	4.17	3.24	3.47	3.70
IL	1.37	1.82	2.28	1.37	1.37	1.97
AP	.31	.62	.93	.62	.62	.93

SAMPLE	3JG41	3JG47	3JG50	3JG54	3JG55	3JG57
QZ	16.22	11.60	8.53	10.38	4.45	16.30
CO	3.06	1.73	.10	0.00	0.00	.98
OR	18.37	11.13	16.14	15.59	16.14	20.04
AB	31.47	31.47	37.24	36.71	39.34	36.71
AN	13.36	21.34	22.26	20.59	16.41	12.61
NE	0.00	0.00	0.00	0.00	0.00	0.00
DI	0.00	0.00	0.00	.52	4.47	0.00
HY	8.20	11.80	7.93	8.78	8.92	6.46
OL	0.00	0.00	0.00	0.00	0.00	0.00
MT	3.47	4.63	3.70	3.47	4.40	3.01
IL	1.97	2.43	1.97	1.97	2.43	1.37
AP	.93	.93	.93	.62	.93	.62

SAMPLE	3JG58	3JG59	4JG5	4JG7	4JG11	4JG12
QZ	11.72	22.69	25.64	16.38	6.31	1.88
CO	0.00	4.72	.65	0.00	0.00	0.00
OR	16.70	22.82	27.83	21.71	15.59	17.26
AB	37.24	27.27	36.71	35.66	35.66	35.66
AN	18.64	7.42	4.64	14.47	19.75	15.58
NE	0.00	0.00	0.00	0.00	0.00	0.00
DI	1.35	0.00	0.00	.52	3.58	6.35
HY	7.61	7.62	1.90	6.18	9.91	14.04
OL	0.00	0.00	0.00	0.00	0.00	0.00
MT	3.70	3.94	1.16	2.55	4.63	4.40
IL	1.67	1.82	.76	1.37	2.58	1.97
AP	.93	.31	.31	.62	.93	1.24

SAMPLE	4JG13	2JG4	3JG32	3JG33	4JG21	2JG14
QZ	14.82	29.98	36.27	45.97	28.60	36.11
CO	0.00	1.02	2.07	5.10	.71	.31
OR	21.71	25.61	32.29	35.63	28.39	37.30
AB	35.14	38.81	32.29	8.92	37.24	22.55
AN	14.19	3.06	3.53	1.95	1.95	2.23
NE	0.00	0.00	0.00	0.00	0.00	0.00
DI	.97	0.00	0.00	0.00	0.00	0.00
HY	7.57	.40	3.30	.63	.63	.40
OL	0.00	0.00	0.00	0.00	0.00	0.00
MT	3.01	.46	1.16	.46	.69	.46
IL	1.37	.30	.46	.15	.30	.30
AP	.62	0.00	.31	0.00	0.00	0.00

SAMPLE	2JG15	2JG19	4JG2	2JG25	1JG21	1JG24
QZ	30.53	41.52	43.69	36.29	41.64	31.41
CO	0.00	1.94	2.96	.31	.10	1.77
OR	43.98	9.46	9.46	28.39	25.61	21.15
AB	22.55	44.06	39.86	32.52	18.88	38.29
AN	1.39	1.11	1.11	1.39	8.90	2.69
NE	0.00	0.00	0.00	0.00	0.00	0.00
DI	0.00	0.00	0.00	0.00	0.00	0.00
HY	.53	.80	.66	.40	1.93	2.26
OL	0.00	0.00	0.00	0.00	0.00	0.00
MT	.93	.46	.69	.46	1.16	1.16
IL	.61	.15	.15	.30	1.06	.61
AP	0.00	0.00	O.OO	0.00	0.00	.31

SAMPLE	1JG34	3JG64	1JG11	1JG12	1JG13	1JG58
QZ	49.49	18.73	33.29	30.08	9.95	8.21
CO	1.36	.24	.20	.75	0.00	0.00
OR	22.82	26.72	28.95	27.28	18.37	23.94
AB	19.41	28.85	31.47	30.94	35.66	40.91
AN	1.30	12.15	3.62	6.59	16.14	13.63
NE	0.00	0.00	0.00	0.00	0.00	0.00
DI	0.00	0.00	0.00	0.00	5.18	1.42
HY	2.23	7.70	1.20	2.86	9.07	6.42
OL	0.00	0.00	0.00	0.00	0.00	0.00
MT	1.39	2.55	.69	1.16	3.47	3.01
IL	.76	.91	.30	.61	1.82	1.67
AP	.31	.31	0.00	.31	.62	.62

SAMPLE	1JG59	1JG60	2JG22	3JG49	3JG60
QZ	8.95	8.05	12.84	15.88	10.68
CO	0.00	0.00	0.00	0.00	0.00
OR	13.36	12.25	19.48	22.27	18.93
AB	31.47	31.99	35.66	35.14	33.04
AN	21.42	21.98	15.86	12.80	16.41
NE	0.00	0.00	0.00	0.00	0.00
DI	4.22	5.11	2.30	2.60	3.85
HY	12.60	12.51	7.97	5.92	9.05
OL	0.00	0.00	0.00	0.00	0.00
MT	4.17	4.17	3.01	2.55	3.24
IL	1.82	1.97	1.52	1.21	1.67
AP	.93	.93	.62	.31	.62

AB + AN = PL

DI = WO + EN + FS

HY = EN + FS

OL = FO + FA

APPENDIX D

MINERAL ANALYSES

The following pages give mineral analyses and their recalculated formulae. The analyses are printed in numbered columns, the key to which is given beneath each block.

Analyses are given in the following order:

feldspars
pyroxenes
biotites
amphiboles
sphenes

SUPER RECAL — FELDSPARS (PHENOCRYST UNLESS STATED)

	1	2	3	4	5	6	7	8
NA2O	7.40	7.62	8.08	9.59	7.52	7.83	7.87	8.12
A2O3	24.50	24.06	22.38	22.21	23.81	23.03	23.18	23.67
SIO2	61.47	61.17	62.76	64.56	61.06	61.56	62.25	61.19
K2O	.60	.60	1.04	.22	.80	.93	.87	.42
CAO	5.22	5.23	4.52	3.11	6.06	5.09	4.98	5.56
FEO	.32	.08	.15	.09	.40	.12	.14	.34
SUM	100.51	99.76	98.93	99.78	99.65	98.56	99.29	99.30
SI	2.721 *	2.729 *	2.812 *	2.850 *	2.731 *	2.773 *	2.780 *	2.741 *
AL	1.278 *	1.264 *	1.182 *	1.155 *	1.255 *	1.223 *	1.220 *	1.249 *
FE	.012 4.010	.003 3.995	.006 3.999	.003 4.008	.015 4.001	.005 4.000	.005 4.005	.013 4.003
CA	.295 *	.298 *	.217 *	.147 *	.290 *	.246 *	.238 *	.267 *
NA	.635 *	.659 *	.702 *	.821 *	.652 *	.684 *	.681 *	.705 *
K	.034 .964	.034 .991	.059 .978	.012 .980	.046 .988	.053 .983	.050 .969	.024 .996
O	8.000 *	8.000 *	8.000 *	8.000 *	8.000 *	8.000 *	8.000 *	8.000 *
AN	30.60	30.05	22.18	15.01	29.39	24.99	24.58	26.79
AB	65.88	66.51	71.75	83.73	65.99	69.57	70.30	70.80
OR	3.51	3.45	6.08	1.26	4.62	5.44	5.11	2.41

1 1JG9 CORE
2 1JG9 RIM
3 1JG9 CORE
4 1JG9 RIM

5 1JG9 CORE
6 1JG9 RIM
7 1JG9 CORE
8 1JG9 RIM

	9	10	11	12	13	14	15	16
NA2O	6.24	6.05	6.28	6.14	6.84	9.70	5.55	8.20
A2O3	26.06	26.24	26.67	26.36	26.26	21.54	27.30	23.74
SIO2	57.52	57.09	57.86	56.28	58.54	64.25	56.03	60.64
K2O	.88	.56	.54	.51	.54	.29	.42	.42
CAO	8.43	8.76	8.68	8.90	8.04	2.84	9.44	5.76
FEO	.30	.43	.25	.44	.46	.27	.30	.15
SUM	99.43	99.13	100.28	98.63	100.68	98.89	99.04	98.91
SI	2.600 *	2.587 *	2.589 *	2.568 *	2.609 *	2.864 *	2.542 *	2.729 *
AL	1.388 *	1.401 *	1.406 *	1.417 *	1.379 *	1.132 *	1.459 *	1.259 *
FE	.011 3.999	.015 4.004	.009 4.004	.017 4.002	.017 4.006	.010 4.006	.011 4.013	.006 3.993
CA	.408 *	.425 *	.416 *	.435 *	.384 *	.136 *	.459 *	.278 *
NA	.547 *	.532 *	.545 *	.543 *	.591 *	.838 *	.488 *	.715 *
K	.051 1.006	.032 .989	.031 .992	.030 1.008	.031 1.006	.016 .991	.024 .971	.024 1.017
O	8.000 *	8.000 *	8.000 *	8.000 *	8.000 *	8.000 *	8.000 *	8.000 *
AN	40.59	42.99	41.96	43.17	38.18	13.69	47.24	27.30
AB	54.37	53.73	54.93	53.89	58.77	84.64	50.26	70.33
OR	5.04	3.27	3.11	2.94	3.05	1.66	2.50	2.37

9 1JG10 CORE
10 1JG10 MIDWAY
11 1JG10 RIM
12 1JG10 CORE

13 1JG10 MIDWAY
14 1JG10 RIM
15 1JG10 CORE
16 1JG10 RIM

SUPER RECAL — FELDSPARS (PHENOCRYST UNLESS STATED)

	17		18		19		20		21		22		23		24	
NA2O	6.37		5.96		6.54		6.11		6.27		8.71		5.12		5.29	
A2O3	26.12		25.76		25.63		25.65		26.37		22.75		27.92		27.50	
SIO2	57.24		58.07		58.34		58.31		57.45		62.67		54.83		54.76	
K2O	.57		.64		.58		.77		.54		.45		.34		.31	
CAO	8.47		7.81		7.92		7.91		8.50		4.31		11.09		10.99	
FEO	.24		.29		.41		.41		.29		.22		.49		.42	
SUM	99.01		99.53		99.42		99.16		99.42		99.11		99.79		99.27	
SI	2.595	*	2.618	*	2.629	*	2.632	*	2.592	*	2.799	*	2.485	*	2.495	*
AL	1.395	*	1.368	*	1.361	*	1.365	*	1.402	*	1.197	*	1.491	*	1.476	*
FE	.009	3.999	.011	3.997	.015	4.005	.015	4.012	.011	4.005	.008	4.005	.019	3.995	.016	3.987
CA	.411	*	.377	*	.382	*	.383	*	.411	*	.206	*	.539	*	.536	*
NA	.560	*	.608	*	.571	*	.535	*	.549	*	.754	*	.450	*	.467	*
K	.033	1.004	.037	1.022	.033	.987	.044	.962	.031	.991	.026	.985	.020	1.008	.018	1.022
O	8.000	*	8.000	*	8.000	*	8.000	*	8.000	*	8.000	*	8.000	*	8.000	*
AN		40.97		36.90		38.74		39.78		41.49		20.92		53.42		52.50
AB		55.75		59.50		57.89		55.61		55.38		76.49		44.63		45.73
OR		3.28		3.60		3.38		4.61		3.14		2.60		1.95		1.76

17 1JG10 CORE
18 1JG10 RIM
19 1JG10 CORE
20 1JG10 RIM

21 1JG10 CORE
22 1JG10 RIM
23 1JG29 CORE
24 1JG29 RIM

	25		26		27		28		29		30		31		32	
NA2O	5.09		6.31		5.82		6.03		5.10		6.51		5.11		5.66	
A2O3	27.34		26.15		26.33		26.31		28.09		26.28		27.80		27.23	
SIO2	54.88		57.15		56.83		56.99		53.83		57.59		54.68		54.56	
K2O	.36		.50		.43		.40		.22		.33		.34		.35	
CAO	10.54		8.86		9.43		8.97		10.92		8.60		10.93		9.98	
FEO	.62		.33		.35		.38		.40		.41		.39		.49	
SUM	98.83		99.30		99.20		99.08		98.56		99.72		99.25		98.27	
SI	2.508	*	2.587	*	2.575	*	2.583	*	2.469	*	2.592	*	2.489	*	2.507	*
AL	1.472	*	1.395	*	1.406	*	1.405	*	1.518	*	1.394	*	1.491	*	1.475	*
FE	.024	4.004	.012	3.994	.014	3.995	.014	4.002	.015	4.002	.015	4.002	.015	3.996	.019	4.001
CA	.516	*	.430	*	.458	*	.436	*	.537	*	.415	*	.533	*	.491	*
NA	.451	*	.554	*	.511	*	.530	*	.453	*	.568	*	.451	*	.504	*
K	.021	.988	.029	1.012	.025	.994	.023	.988	.013	1.003	.019	1.002	.020	1.004	.021	1.016
O	8.000	*	8.000	*	8.000	*	8.000	*	8.000	*	8.000	*	8.000	*	8.000	*
AN		52.23		42.45		45.06		44.06		53.50		41.40		53.11		48.36
AB		45.64		54.70		51.44		53.60		45.22		56.71		44.93		49.63
OR		2.12		2.85		2.50		2.34		1.28		1.89		1.97		2.02

25 1JG29 CORE
26 1JG29 RIM
27 1JG29 CORE
28 1JG29 RIM

29 1JG41 CORE
30 1JG41 RIM
31 1JG41 CORE
32 1JG41 RIM

SUPER RECAL FELDSPARS (PHENOCRYST UNLESS STATED)

	33	34	35	36	37	38	39	40
NA2O	8.27	9.00	7.82	9.13	6.31	8.00	8.80	1.27
A2O3	23.46	22.95	23.68	21.60	26.76	23.31	21.54	18.43
SIO2	60.62	61.86	62.25	65.29	58.57	62.76	64.04	64.19
K2O	.32	.17	.32	.41	.18	.35	.35	15.05
CAO	5.46	4.81	5.12	2.90	8.41	4.64	3.21	.24
FEO	.31	.39	.35	.32	.72	.29	.18	0.00
SUM	98.44	99.18	99.55	99.65	100.95	99.35	98.12	99.18
SI	2.739 *	2.771 *	2.768 *	2.882 *	2.599 *	2.790 *	2.870 *	2.985 *
AL	1.249 *	1.211 *	1.240 *	1.123 *	1.399 *	1.221 *	1.138 *	1.010 *
FE	.012 4.000	.015 3.997	.013 4.021	.012 4.017	.027 4.025	.011 4.023	.007 4.014	0.000 3.994
CA	.264 *	.231 *	.244 *	.137 *	.400 *	.221 *	.154 *	.012 *
NA	.724 *	.782 *	.674 *	.781 *	.543 *	.690 *	.765 *	.114 *
K	.018 1.007	.010 1.022	.018 .936	.023 .941	.010 .953	.020 .931	.020 .939	.893 1.019
O	8.000 *	8.000 *	8.000 *	8.000 *	8.000 *	8.000 *	8.000 *	8.000 *
AN	26.24	22.58	26.05	14.57	41.96	23.75	16.42	1.17
AB	71.93	76.47	72.01	82.98	56.97	74.11	81.45	11.24
OR	1.83	.95	1.94	2.45	1.07	2.13	2.13	87.59

33 1JG49 GROUNDMASS
34 1JG49 GROUNDMASS
35 1JG55 MIDWAY
36 1JG55 RIM
37 1JG55 CORE
38 1JG55 MIDWAY
39 1JG55 RIM
40 1JG55 GROUNDMASS

	41	42	43	44	45	46	47	48
NA2O	.50	1.08	2.35	5.73	9.63	7.32	8.37	4.37
A2O3	18.45	18.18	17.97	27.30	22.22	25.46	23.17	29.15
SIO2	64.11	64.18	63.86	55.20	64.52	58.75	61.08	52.43
K2O	15.07	15.49	13.67	.18	.43	.20	.32	.65
CAO	.18	.22	.34	9.99	3.66	7.70	5.07	11.30
FEO	.09	0.00	.14	.41	.32	.30	.35	.44
SUM	99.41	99.15	98.33	98.81	100.78	99.73	98.36	98.34
SI	2.984 *	2.991 *	2.988 *	2.518 *	2.834 *	2.637 *	2.758 *	2.417 *
AL	1.013 *	.998 *	.991 *	1.467 *	1.150 *	1.347 *	1.233 *	1.584 *
FE	.004 4.000	0.000 3.989	.005 3.984	.016 4.001	.012 3.996	.011 3.995	.013 4.004	.017 4.018
CA	.009 *	.011 *	.017 *	.488 *	.172 *	.370 *	.245 *	.558 *
NA	.045 *	.093 *	.213 *	.507 *	.820 *	.637 *	.733 *	.391 *
K	.954 1.008	.921 1.029	.816 1.046	.010 1.005	.024 1.016	.011 1.019	.018 .996	.038 .987
O	8.000 *	8.000 *	8.000 *	8.000 *	8.000 *	8.000 *	8.000 *	8.000 *
AN	.89	1.07	1.63	48.56	16.95	36.35	24.62	56.55
AB	4.48	9.48	20.38	50.40	80.68	62.53	73.54	39.58
OR	94.63	89.45	77.99	1.04	2.37	1.12	1.85	3.87

41 1JG55 GROUNDMASS
42 1JG55 GROUNDMASS
43 1JG55 GROUNDMASS
44 1JG55 CORE
45 1JG55 RIM
46 1JG55 CORE
47 1JG55 RIM
48 1JG56 CORE

SUPER RECAL FELDSPARS (PHENOCRYST UNLESS STATED)

	49	50	51	52	53	54	55	56
NA2O	9.05	4.71	7.73	4.60	6.50	9.53	.41	9.79
A2O3	22.28	28.76	23.98	28.81	26.24	22.24	17.93	21.02
SIO2	62.54	53.61	50.45	52.99	57.07	62.94	64.15	64.60
K2O	.39	.23	.46	.31	.24	.90	16.29	.34
CAO	3.92	11.67	5.90	11.85	8.55	2.30	.25	2.67
FEO	.39	.68	.19	.37	.60	.27	.17	.45
SUM	98.57	99.66	98.72	98.93	99.20	98.18	99.20	98.87
SI	2.810 *	2.439 *	2.724 *	2.428 *	2.584 *	2.833 *	2.998 *	2.882 *
AL	1.180 *	1.542 *	1.273 *	1.556 *	1.400 *	1.180 *	.987 *	1.105 *
FE	.015 4.005	.026 4.006	.007 4.004	.014 3.998	.023 4.007	.010 4.023	.007 3.991	.017 4.004
CA	.189 *	.569 *	.285 *	.582 *	.415 *	.111 *	.013 *	.128 *
NA	.788 *	.415 *	.575 *	.409 *	.571 *	.832 *	.037 *	.847 *
K	.022 1.000	.013 .998	.026 .986	.018 1.009	.014 .999	.052 .994	.971 1.021	.019 .994
O	8.000 *	8.000 *	8.000 *	8.000 *	8.000 *	8.000 *	8.000 *	8.000 *
AN	18.88	57.02	28.87	57.68	41.51	11.16	1.23	12.84
AB	78.88	41.64	68.45	40.52	57.10	83.65	3.64	85.21
OR	2.24	1.34	2.68	1.80	1.39	5.20	95.13	1.95

49 1JG56 RIM
50 1JG56 CORE
51 1JG56 RIM
52 1JG56 CORE

53 1JG56 RIM
54 1JG56 GROUNDMASS
55 1JG56 GROUNDMASS
56 1JG56 GROUNDMASS

	57	58	59	60	61	62	63	64
NA2O	9.32	8.27	8.88	4.60	4.08	4.94	6.75	6.95
A2O3	21.27	23.43	21.92	19.03	18.20	19.35	24.30	24.68
SIO2	64.25	62.41	63.73	64.74	65.51	64.67	60.48	59.53
K2O	.73	.77	.94	9.89	11.16	9.31	1.02	.85
CAO	2.91	5.10	3.53	.13	.30	.72	6.84	7.13
FEO	.26	.31	.19	.11	.19	.29	.30	.32
SUM	98.74	100.29	99.29	98.50	99.44	99.28	99.69	99.46
SI	2.872 *	2.765 *	2.841 *	2.974 *	2.999 *	2.951 *	2.708 *	2.677 *
AL	1.121 *	1.224 *	1.151 *	1.030 *	.982 *	1.041 *	1.282 *	1.308 *
FE	.010 4.003	.011 4.002	.007 3.999	.004 4.009	.007 3.988	.011 4.003	.011 4.001	.012 3.997
CA	.139 *	.242 *	.173 *	.006 *	.015 *	.035 *	.328 *	.344 *
NA	.808 *	.711 *	.767 *	.410 *	.362 *	.437 *	.596 *	.606 *
K	.042 .989	.044 .996	.053 .994	.580 .996	.652 1.028	.542 1.014	.058 .972	.049 .998
O	8.000 *	8.000 *	8.000 *	8.000 *	8.000 *	8.000 *	8.000 *	8.000 *
AN	14.10	24.31	17.44	.64	1.43	3.47	33.75	34.41
AB	81.69	71.32	77.19	41.15	35.21	43.10	60.26	60.70
OR	4.21	4.37	5.38	58.21	63.36	53.43	5.99	4.88

57 1JG56 GROUNDMASS
58 1JG61 CORE
59 1JG61 RIM
60 1JG61 ALKALI FELDSPAR

61 1JG61 ALKALI FELDSPAR
62 1JG61 ALKALI FELDSPAR
63 1JG80 CORE
64 1JG80 RIM

SUPER RECAL FELDSPARS (PHENOCRYST UNLESS STATED)

	65	66	67	68	69	70	71	72
NA2O	4.86	4.52	5.05	5.49	5.92	4.84	4.98	5.22
A2O3	19.23	18.42	27.73	27.79	26.11	27.75	28.10	27.45
SIO2	65.02	65.68	54.26	54.05	55.70	52.59	53.03	53.01
K2O	9.30	10.01	.34	.23	.52	.33	.32	.19
CAO	.52	.37	11.39	11.55	9.74	11.78	11.82	11.50
FEO	0.00	.23	.57	.58	.53	.58	.44	.41
SUM	98.93	99.23	99.34	99.69	98.52	97.87	98.69	97.78
SI	2.968 *	2.998 *	2.476 *	2.463 *	2.553 *	2.442 *	2.441 *	2.460 *
AL	1.034 *	.991 *	1.491 *	1.492 *	1.410 *	1.519 *	1.524 *	1.501 *
FE	0.000 4.003	.009 3.997	.022 3.988	.022 3.977	.020 3.984	.023 3.984	.017 3.982	.016 3.977
CA	.025 *	.019 *	.557 *	.564 *	.478 *	.586 *	.583 *	.572 *
NA	.430 *	.400 *	.447 *	.485 *	.526 *	.436 *	.444 *	.470 *
K	.542 .997	.583 1.001	.020 1.023	.013 1.062	.030 1.035	.020 1.042	.019 1.046	.011 1.053
O	8.000 *	8.000 *	8.000 *	8.000 *	8.000 *	8.000 *	8.000 *	8.000 *
AN	2.55	1.81	54.41	53.08	46.22	56.28	55.72	54.32
AB	43.14	39.97	43.66	45.66	50.84	41.84	42.48	44.62
OR	54.31	58.23	1.93	1.26	2.94	1.88	1.80	1.07

65 1JG80 ALKALI FELDSPAR
66 1JG80 ALKALI FELDSPAR
67 2JG1 CORE
68 2JG1 MIDWAY

69 2JG1 RIM
70 2JG1 CORE
71 2JG1 MIDWAY
72 2JG1 RIM

	73	74	75	76	77	78	79	80
NA2O	7.11	7.67	9.50	8.44	8.79	8.80	7.57	3.51
A2O3	24.88	24.53	21.63	22.52	22.45	21.94	24.20	18.29
SIO2	59.91	59.86	64.17	63.24	63.98	63.09	60.46	65.62
K2O	.49	.65	1.15	1.06	1.30	1.14	.64	11.94
CAO	5.83	5.15	3.01	4.06	3.61	3.57	5.90	.33
FEO	.21	.13	.17	.18	.13	.21	.08	.06
SUM	99.43	98.99	99.53	99.50	100.26	98.75	98.85	99.75
SI	2.685 *	2.696 *	2.854 *	2.816 *	2.828 *	2.832 *	2.720 *	3.000 *
AL	1.314 *	1.302 *	1.133 *	1.182 *	1.169 *	1.160 *	1.283 *	.985 *
FE	.008 4.007	.005 4.002	.006 3.993	.007 4.004	.005 4.002	.008 4.000	.003 4.005	.002 3.987
CA	.328 *	.297 *	.143 *	.194 *	.171 *	.172 *	.284 *	.016 *
NA	.618 *	.670 *	.819 *	.729 *	.753 *	.766 *	.660 *	.311 *
K	.028 .974	.037 1.004	.065 1.028	.060 .983	.073 .998	.065 1.003	.037 .981	.696 1.023
O	8.000 *	8.000 *	8.000 *	8.000 *	8.000 *	8.000 *	8.000 *	8.000 *
AN	33.68	29.56	13.95	19.71	17.14	17.12	28.98	1.58
AB	63.44	66.72	79.70	74.16	75.51	76.37	67.28	30.40
OR	2.88	3.72	6.35	6.13	7.35	6.51	3.74	68.02

73 2JG9
74 2JG9
75 2JG9
76 2JG9

77 2JG9
78 2JG9
79 2JG9
80 2JG15 ALKALI FELDSPAR

SUPER RECAL FELDSPARS (PHENOCRYST UNLESS STATED)

	81	82	83	84	85	86	87	88
NA2O	1.85	1.80	.64	.36	7.61	8.78	5.66	5.62
A2O3	17.98	17.96	17.97	18.09	25.02	22.91	27.94	27.93
SIO2	65.12	65.11	64.81	63.89	58.43	61.64	56.14	55.61
K2O	14.72	14.70	16.05	15.93	.57	1.05	.33	.45
CAO	.25	.15	.04	.26	6.87	4.56	10.15	10.12
FEO	.03	.14	.56	.24	.22	.17	.16	.31
SUM	99.95	99.86	100.08	98.77	98.72	99.11	100.38	100.04
SI	3.002 *	3.004 *	3.001 *	2.993 *	2.650 *	2.770 *	2.518 *	2.507 *
AL	.977 *	.977 *	.980 *	.999 *	1.337 *	1.213 *	1.476 *	1.484 *
FE	.001 3.980	.005 3.986	.022 4.003	.009 4.001	.008 3.996	.006 3.990	.006 4.000	.012 4.003
CA	.012 *	.007 *	.002 *	.013 *	.334 *	.220 *	.488 *	.489 *
NA	.165 *	.161 *	.057 *	.033 *	.669 *	.765 *	.492 *	.491 *
K	.866 1.043	.865 1.034	.948 1.008	.952 .998	.033 1.036	.060 1.045	.019 .999	.026 1.006
O	8.000 *	8.000 *	8.000 *	8.000 *	8.000 *	8.000 *	8.000 *	8.000 *
AN	1.18	.72	.20	1.31	32.22	21.02	48.83	48.59
AB	15.85	15.58	5.70	3.28	64.59	73.22	49.28	48.83
OR	82.97	83.70	94.10	95.41	3.18	5.76	1.89	2.57

81 2JG15 ALKALI FELDSPAR
82 2JG15 ALKALI FELDSPAR
83 2JG15 ALKALI FELDSPAR
84 2JG15 ALKALI FELDSPAR

85 2JG21 CORE
86 2JG21 RIM
87 2JG21 CORE
88 2JG21 MIDWAY

	89	90	91	92	93	94	95	96
NA2O	8.57	6.95	7.98	9.91	7.44	7.47	8.61	7.27
A2O3	23.82	25.63	24.73	22.15	24.53	25.05	24.19	25.05
SIO2	61.85	58.13	59.99	64.19	59.53	60.10	61.71	58.94
K2O	.29	.51	.69	.12	.73	.55	.92	.46
CAO	5.42	7.66	6.33	3.49	6.55	6.88	4.59	7.07
FEO	.43	.30	.24	.25	.26	.27	.48	.21
SUM	100.38	99.18	99.96	100.11	99.04	100.32	100.50	99.00
SI	2.742 *	2.625 *	2.683 *	2.834 *	2.685 *	2.676 *	2.736 *	2.660 *
AL	1.244 *	1.364 *	1.303 *	1.153 *	1.304 *	1.314 *	1.264 *	1.332 *
FE	.015 4.002	.011 4.001	.009 3.995	.009 3.996	.010 3.999	.010 4.000	.018 4.017	.008 4.000
CA	.257 *	.371 *	.303 *	.165 *	.317 *	.328 *	.218 *	.342 *
NA	.737 *	.609 *	.692 *	.848 *	.651 *	.645 *	.740 *	.636 *
K	.016 1.010	.029 1.009	.039 1.035	.007 1.020	.042 1.009	.031 1.004	.052 1.010	.026 1.004
O	8.000 *	8.000 *	8.000 *	8.000 *	8.000 *	8.000 *	8.000 *	8.000 *
AN	25.48	36.75	29.32	16.18	31.37	32.68	21.58	34.03
AB	72.90	60.34	66.88	83.15	64.47	64.21	73.27	63.33
OR	1.62	2.91	3.80	.66	4.16	3.11	5.15	2.64

89 2JG21 RIM
90 2JG21 CORE
91 2JG21 MIDWAY
92 2JG21 RIM

93 2JG21 CORE
94 2JG21 MIDWAY
95 2JG21 RIM
96 2JG21 CORE

SUPER RECAL — FELDSPARS (PHENOCRYST UNLESS STATED)

	97	98	99	100	101	102	103	104
NA2O	8.92	7.78	7.42	1.12	4.52	7.45	4.66	4.54
A2O3	23.07	24.01	24.87	18.76	29.13	24.04	28.65	28.92
SIO2	62.11	61.19	60.07	64.18	53.41	60.55	54.23	54.21
K2O	.61	.79	.59	14.99	.14	.32	.24	.68
CAO	4.57	5.61	6.70	.22	11.98	6.19	11.65	10.61
FEO	.30	.29	.11	.08	.62	.20	.55	.71
SUM	99.58	99.67	99.85	99.35	99.80	98.75	99.98	99.67
SI	2.773 *	2.733 *	2.584 *	2.977 *	2.426 *	2.724 *	2.455 *	2.459 *
AL	1.214 *	1.264 *	1.310 *	1.025 *	1.559 *	1.274 *	1.528 *	1.546 *
FE	.011 3.998	.011 4.007	.004 3.998	.003 4.005	.024 4.008	.008 4.005	.021 4.004	.027 4.032
CA	.219 *	.268 *	.321 *	.011 *	.583 *	.298 *	.555 *	.516 *
NA	.772 *	.674 *	.543 *	.101 *	.398 *	.650 *	.409 *	.399 *
K	.035 1.025	.045 .987	.039 1.003	.887 .998	.008 .989	.018 .967	.014 .988	.039 .954
O	8.000 *	8.000 *	8.000 *	8.000 *	8.000 *	8.000 *	8.000 *	8.000 *
AN	21.32	27.19	31.98	1.09	58.94	30.87	57.20	54.04
AB	75.29	68.25	64.10	10.09	40.24	67.23	41.40	41.84
OR	3.39	4.56	3.92	88.82	.82	1.90	1.40	4.12

97 2JG21 RIM
98 2JG21 CORE
99 2JG21 MIDWAY
100 2JG21 ALKALI FELDSPAR OVERGROWTH

101 2JG26 CORE
102 2JG26 RIM
103 2JG26 CORE
104 2JG26 RIM

	105	106	107	108	109	110	111	112
NA2O	5.10	8.80	5.00	9.06	4.69	10.00	9.28	7.22
A2O3	27.47	22.95	27.93	23.06	27.82	20.55	21.71	24.65
SIO2	55.44	64.00	54.07	62.55	54.57	65.26	63.90	58.79
K2O	.25	.33	.28	.31	1.50	.76	.21	.44
CAO	10.30	4.26	10.97	4.69	9.49	2.23	3.24	6.82
FEO	.60	.34	.57	.51	.46	.21	.24	.70
SUM	99.15	100.68	98.82	100.18	98.53	99.01	98.58	98.62
SI	2.519 *	2.811 *	2.475 *	2.775 *	2.503 *	2.907 *	2.856 *	2.667 *
AL	1.471 *	1.188 *	1.506 *	1.206 *	1.504 *	1.079 *	1.143 *	1.318 *
FE	.023 4.012	.012 4.011	.022 4.003	.019 4.000	.018 4.025	.008 3.993	.009 4.008	.027 4.011
CA	.501 *	.200 *	.538 *	.223 *	.466 *	.106 *	.155 *	.332 *
NA	.449 *	.749 *	.444 *	.779 *	.417 *	.864 *	.804 *	.635 *
K	.014 .965	.018 .968	.016 .998	.018 1.020	.088 .971	.043 1.013	.012 .971	.025 .992
O	8.000 *	8.000 *	8.000 *	8.000 *	8.000 *	8.000 *	8.000 *	8.000 *
AN	51.95	20.70	53.90	21.86	48.02	10.50	15.97	33.42
AB	45.55	77.39	44.46	76.42	42.94	85.23	82.79	64.02
OR	1.50	1.91	1.64	1.72	9.04	4.26	1.23	2.57

105 2JG26 CORE
106 2JG26 RIM
107 2JG33 CORE
108 2JG33 RIM

109 2JG33 CORE
110 2JG33 RIM
111 2JG33 GROUNDMASS
112 2JG33 GROUNDMASS

SUPER RECAL FELDSPARS (PHENOCRYST UNLESS STATED)

	113	114	115	116	117	118	119	120
NA2O	9.77	8.41	7.97	8.93	6.77	9.23	7.73	8.98
A2O3	21.36	21.06	23.44	22.36	25.54	20.94	22.71	21.74
SIO2	65.07	64.22	61.29	64.01	59.13	65.10	61.71	64.76
K2O	.55	2.34	.22	.60	.23	.49	.59	.64
CAO	2.59	2.50	5.77	3.79	7.74	2.69	5.32	3.26
FEO	.21	.12	.30	.14	.31	.08	.41	.30
SUM	99.55	98.65	98.99	99.83	99.72	98.53	98.47	99.68
SI	2.881 *	2.885 *	2.750 *	2.833 *	2.647 *	2.902 *	2.781 *	2.865 *
AL	1.114 *	1.115 *	1.239 *	1.166 *	1.347 *	1.100 *	1.206 *	1.133 *
FE	.008 4.003	.005 4.004	.011 4.000	.005 4.004	.012 4.006	.003 4.005	.015 4.003	.011 4.010
CA	.123 *	.120 *	.277 *	.180 *	.371 *	.128 *	.257 *	.155 *
NA	.339 *	.732 *	.593 *	.756 *	.588 *	.798 *	.676 *	.770 *
K	.032 .993	.134 .987	.013 .983	.034 .980	.013 .972	.028 .954	.034 .966	.036 .961
O	8.000 *	8.000 *	8.000 *	8.000 *	8.000 *	8.000 *	8.000 *	8.000 *
AN	12.37	12.19	28.21	18.34	38.19	13.47	26.59	16.08
AB	84.44	74.22	70.51	78.20	60.45	83.61	69.90	80.16
OR	3.18	13.59	1.28	3.46	1.35	2.92	3.51	3.76

113 2JG33 GROUNDMASS
114 2JG33 GROUNDMASS
115 2JG35 CORE
116 2JG35 RIM
117 2JG35 CORE
118 2JG35 RIM
119 2JG35 CORE
120 2JG35 RIM

	121	122	123	124	125	126	127	128
NA2O	7.79	9.68	5.01	2.89	8.79	9.53	7.94	7.92
A2O3	23.57	21.24	28.41	18.60	21.94	21.19	24.03	24.70
SIO2	61.08	64.71	53.76	64.50	60.12	64.92	61.86	61.38
K2O	.44	.28	.30	12.15	.19	.21	.88	.81
CAO	5.41	2.68	11.17	.26	6.96	2.93	5.65	5.69
FEO	.42	.27	.70	.31	.28	.22	.22	.01
SUM	98.71	98.86	99.35	98.71	98.28	99.00	100.58	100.51
SI	2.748 *	2.882 *	2.453 *	2.983 *	2.743 *	2.885 *	2.739 *	2.717 *
AL	1.250 *	1.115 *	1.527 *	1.014 *	1.179 *	1.110 *	1.254 *	1.288 *
FE	.016 4.013	.010 4.007	.027 4.007	.012 4.009	.011 3.933	.008 4.003	.008 4.000	.000 4.006
CA	.251 *	.128 *	.546 *	.013 *	.340 *	.140 *	.268 *	.270 *
NA	.680 *	.836 *	.443 *	.259 *	.777 *	.821 *	.682 *	.680 *
K	.025 .965	.016 .980	.017 1.007	.717 .989	.011 1.129	.012 .973	.050 .999	.046 .995
O	8.000 *	8.000 *	8.000 *	8.000 *	8.000 *	8.000 *	8.000 *	8.000 *
AN	27.01	13.05	54.24	1.30	30.14	14.34	26.82	27.11
AB	70.38	85.32	44.02	26.21	68.88	84.43	68.21	68.29
OR	2.62	1.62	1.73	72.49	.98	1.22	4.97	4.59

121 2JG35 CORE
122 2JG35 OVERGROWTH
123 2JG35 CORE
124 2JG35 ALKALI FELDSPAR OVERGROWTH
125 2JG35 GROUNDMASS
126 2JG35 GROUNDMASS
127 4JG3
128 4JG3

SUPER RECAL FELDSPARS (PHENOCRYST UNLESS STATED)

	129	130	131	132	133	134
NA2O	7.93	8.32	7.68	8.00	8.32	7.95
A2O3	23.73	23.61	23.99	23.63	23.78	23.71
SIO2	61.49	61.93	60.86	62.25	62.64	62.38
K2O	.81	.80	1.00	1.03	1.02	.94
CAO	5.43	4.92	5.40	5.01	4.80	4.98
FEO	.25	.14	.18	.22	.18	.12
SUM	99.64	99.72	99.11	100.14	100.74	100.08
SI	2.746 *	2.759 *	2.733 *	2.753 *	2.763 *	2.766 *
AL	1.249 *	1.239 *	1.259 *	1.236 *	1.236 *	1.239 *
FE	.009 4.003	.005 4.004	.007 4.009	.008 4.007	.007 4.006	.004 4.009
CA	.260 *	.235 *	.260 *	.238 *	.227 *	.237 *
NA	.686 *	.719 *	.559 *	.689 *	.712 *	.683 *
K	.046 .992	.045 .999	.057 .986	.058 .985	.057 .996	.053 .973
O	8.000 *	8.000 *	8.000 *	8.000 *	8.000 *	8.000 *
AN	26.18	23.51	24.36	24.19	22.78	24.31
AB	69.19	71.94	67.83	69.89	71.46	70.23
OR	4.65	4.55	5.81	5.92	5.76	5.46

129 4JG3
130 4JG3
131 4JG3
132 4JG3
133 4JG3
134 4JG3

SUPER RECAL — PYROXENE PHENOCRYSTS

	1	2	3	4	5	6	7	8
NA2O	.58	.84	.95	.77	.64	.64	.93	1.00
MGO	15.23	17.08	15.10	15.03	14.56	14.72	14.82	14.87
A203	2.62	2.24	3.22	2.59	2.98	2.09	2.48	2.98
SIO2	51.49	52.71	50.66	51.08	50.67	51.41	51.51	50.94
CAO	21.58	20.56	20.75	21.39	20.79	21.27	21.40	21.46
TIO2	.49	.20	.81	.70	.88	.50	.58	.79
C203	.26	.50	.01	.03	.08	.08	.07	.02
MNO	.26	.28	.18	.19	.23	.20	.12	.15
FEO	7.53	6.11	8.26	7.82	8.19	8.13	8.35	7.65
SUM	100.04	100.52	99.94	99.60	99.02	99.04	100.26	99.86

	1	*	2	*	3	*	4	*	5	*	6	*	7	*	8	*
SI	1.912	*	1.929	*	1.858	*	1.908	*	1.904	*	1.932	*	1.915	*	1.898	*
AL	.088	2.000	.071	2.000	.112	2.000	.092	2.000	.096	2.000	.068	2.000	.085	2.000	.102	2.000
AL	.027	*	.026	*	.030	*	.022	*	.036	*	.024	*	.024	*	.029	*
TI	.014	*	.006	*	.023	*	.020	*	.025	*	.014	*	.016	*	.022	*
CR	.008	*	.014	*	.000	*	.001	*	.002	*	.002	*	.002	*	.001	*
FE	.234	*	.187	*	.257	*	.244	*	.257	*	.255	*	.260	*	.238	*
MG	.843	*	.932	*	.839	*	.837	*	.816	*	.824	*	.821	*	.826	*
CA	.859	*	.806	*	.829	*	.856	*	.837	*	.856	*	.853	*	.857	*
MN	.008	*	.009	*	.006	*	.006	*	.007	*	.006	*	.004	*	.005	*
NA	.042	2.034	.060	2.039	.069	2.052	.056	2.042	.047	2.027	.047	2.030	.067	2.047	.072	2.050
O	6.000	*	6.000	*	6.000	*	6.000	*	6.000	*	6.000	*	6.000	*	6.000	*
WO		44.18		41.69		42.92		44.05		43.66		44.08		44.01		44.49
EN		43.37		48.19		43.45		43.06		42.54		42.44		42.40		42.89
FS		12.45		10.12		13.63		12.88		13.81		13.48		13.60		12.62
F/M		.287		.210		.314		.299		.325		.318		.321		.294
F/FM		.223		.174		.239		.230		.245		.241		.243		.227

1 1JG29
2 1JG29
3 1JG29
4 1JG29

5 1JG29
6 1JG29
7 1JG29
8 1JG29

SUPER RECAL — PYROXENE PHENOCRYSTS

	9	10	11	12	13	14	15	16
NA2O	.64	.68	1.10	.78	.76	.80	.71	.56
MGO	14.80	14.99	15.48	13.05	15.17	15.02	15.29	15.42
A203	3.30	3.19	3.34	3.73	2.22	2.75	3.16	3.49
SIO2	51.68	51.59	52.64	54.15	52.33	51.77	51.89	51.44
CAO	20.93	20.86	18.41	17.62	20.75	20.59	21.17	20.72
TIO2	.83	.83	.75	1.01	.60	.91	.69	.71
C203	.03	.04	.09	.16	0.00	.13	.39	.41
MNO	.27	.14	.12	.49	.26	.25	.31	.14
FEO	8.02	8.39	7.55	7.54	8.01	8.16	7.29	7.38
SUM	100.50	100.71	99.48	98.53	100.10	100.38	100.90	100.27

	9	*	10	*	11	*	12	*	13	*	14	*	15	*	16	*
SI	1.908	*	1.904	*	1.941	*	2.000	*	1.938	*	1.915	*	1.906	*	1.898	*
AL	.092	2.000	.096	2.000	.059	2.000	0.000	2.000	.062	2.000	.085	2.000	.094	2.000	.102	2.000
AL	.052	*	.042	*	.086	*	.162	*	.035	*	.035	*	.042	*	.050	*
TI	.023	*	.023	*	.021	*	.028	*	.017	*	.025	*	.019	*	.020	*
CR	.001	*	.001	*	.003	*	.005	*	0.000	*	.004	*	.011	*	.012	*
FE	.248	*	.259	*	.233	*	.233	*	.248	*	.252	*	.224	*	.223	*
MG	.814	*	.824	*	.851	*	.719	*	.838	*	.828	*	.837	*	.848	*
CA	.828	*	.825	*	.727	*	.697	*	.823	*	.816	*	.833	*	.819	*
MN	.008	*	.004	*	.004	*	.015	*	.006	*	.008	*	.010	*	.004	*
NA	.046	2.020	.049	2.028	.079	2.003	.056	1.915	.055	2.024	.057	2.026	.051	2.027	.040	2.021
O	6.000	*	6.000	*	6.000	*	6.000	*	6.000	*	6.000	*	6.000	*	6.000	*
WO		43.61		43.12		40.08		41.91		42.95		42.85		43.76		43.13
EN		42.90		43.11		46.88		43.18		43.68		43.48		43.97		44.65
FS		13.49		13.77		13.04		14.92		13.37		13.67		12.27		12.22
F/M		.314		.319		.278		.346		.306		.314		.279		.274
F/FM		.239		.242		.218		.257		.234		.239		.218		.215

9 1JG49
10 1JG49
11 1JG49
12 1JG49

13 1JG49
14 1JG49
15 2JG1
16 2JG1

SUPER RECAL — PYROXENE PHENOCRYSTS

	17		18		19		20		21		22		23	
NA2O	.46		.75		.58		.92		1.00		.70		.63	
MGO	14.84		14.25		15.58		15.56		15.31		15.99		15.09	
A2O3	3.34		3.63		3.46		3.50		3.17		1.56		.93	
SIO2	50.88		50.80		51.55		51.09		50.90		53.20		53.68	
CAO	20.98		10.70		20.58		20.73		21.63		10.99		21.79	
TIO2	.95		.71		.65		.75		.64		.68		.24	
C2O3	.19		.03		.20		.53		.16		.07		.03	
MNO	.06		.18		.14		.20		.06		.27		.20	
FEO	8.11		7.66		7.06		6.41		7.34		7.73		7.32	
SUM	99.81		88.71		99.80		99.69		100.21		91.19		99.91	
SI	1.894	*	2.044	*	1.906	*	1.893	*	1.889	*	2.083	*	1.936	*
AL	.106	2.000	0.000	2.044	.094	2.000	.107	2.000	.111	2.000	0.000	2.083	.014	2.000
AL	.040	*	.172	*	.057	*	.046	*	.027	*	.072	*	.027	*
TI	.027	*	.021	*	.018	*	.021	*	.018	*	.020	*	.007	*
CR	.006	*	.001	*	.006	*	.016	*	.005	*	.002	*	.001	*
FE	.252	*	.258	*	.218	*	.199	*	.228	*	.253	*	.227	*
MG	.823	*	.855	*	.859	*	.859	*	.847	*	.933	*	.832	*
CA	.837	*	.461	*	.815	*	.823	*	.860	*	.461	*	.864	*
MN	.002	*	.006	*	.004	*	.006	*	.002	*	.009	*	.006	*
NA	.033	2.020	.059	1.833	.042	2.018	.066	2.035	.072	2.058	.053	1.804	.045	2.009
O	6.000	*	6.000	*	6.000	*	6.000	*	6.000	*	6.000	*	6.000	*
WO		43.71		29.20		42.99		43.61		44.41		27.84		44.79
EN		43.01		54.10		45.27		45.54		43.73		56.34		43.15
FS		13.29		16.70		11.74		10.86		11.86		15.82		12.07
F/M		.309		.309		.259		.238		.271		.281		.260
F/FM		.236		.236		.206		.193		.213		.219		.219

17 2JG1
18 2JG1
19 2JG1
20 2JG1

21 2JG38
22 2JG38
23 2JG38

SUPER RECAL — BIOTITES - PHENOCRYST UNLESS STATED

	1	2	3	4	5	6	7	8
NA2O	.51	.77	.89	.75	1.18	.98	1.19	.81
MGO	14.25	15.15	13.80	14.78	15.62	15.27	16.04	16.75
A2O3	13.97	14.59	14.31	14.65	14.10	13.91	14.28	13.39
SIO2	36.12	35.88	36.05	36.87	36.50	36.62	37.10	38.06
K2O	8.45	7.80	8.55	8.77	8.05	8.55	8.46	8.80
CAO	.21	.12	.28	.03	.14	.13	.14	.10
TIO2	5.03	5.63	6.23	5.76	6.32	6.08	6.04	5.49
MNO	.20	.25	.21	.09	.02	0.00	.06	.04
FEO	14.74	14.35	15.12	13.97	12.52	13.21	13.27	11.88
H2O	3.97	3.99	3.99	4.04	4.02	4.01	4.09	4.07
SUM	98.45	98.53	99.13	99.71	98.47	98.76	100.67	99.39

SI	5.448	*		5.382	*		5.424	*		5.464	*		5.439	*		5.468	*		5.431	*		5.601	*	
AL	2.483	7.931		2.579	7.961		2.483	7.907		2.536	8.000		2.476	7.915		2.448	7.916		2.463	7.894		2.322	7.923	
AL	0.000	*		0.000	*		0.000	*		.022	*		0.000	*		0.000	*		0.000	*		0.000	*	
TI	.684	*		.635	*		.705	*		.642	*		.708	*		.683	*		.665	*		.608	*	
MG	3.204	*		3.387	*		3.094	*		3.255	*		3.469	*		3.399	*		3.500	*		3.674	*	
FE	1.859	*		1.800	*		1.902	*		1.731	*		1.560	*		1.650	*		1.624	*		1.462	*	
MN	.026	5.772		.032	5.854		.027	5.727		.011	5.672		.003	5.740		0.000	5.731		.007	5.796		.005	5.749	
K	1.626	*		1.492	*		1.640	*		1.658	*		1.530	*		1.628	*		1.580	*		1.652	*	
CA	.034	*		.019	*		.045	*		.005	*		.022	*		.021	*		.022	*		.016	*	
NA	.149	1.809		.224	1.735		.250	1.945		.215	1.878		.341	1.893		.284	1.933		.338	1.939		.231	1.899	
H	4.000	4.000		4.000	4.000		4.000	4.000		4.000	4.000		4.000	4.000		4.000	4.000		4.000	4.000		4.000	4.000	
O	24.000	*		24.000	*		24.000	*		24.000	*		24.000	*		24.000	*		24.000	*		24.000	*	
BIOT		37.04			35.10			38.40			34.80			31.06			32.68			31.80			28.54		
PHLO		62.96			64.90			61.60			65.20			68.94			67.32			68.20			71.46		
F/M		.588			.541			.523			.534			.450			.485			.466			.399		
F/FM		.370			.351			.384			.348			.311			.327			.318			.285		

1 1JG10
2 1JG10
3 1JG10
4 1JG10

5 1JG29
6 1JG29
7 1JG29
8 1JG29

SUPER RECAL — BIOTITES - PHENOCRYST UNLESS STATED

	9	10	11	12	13	14	15	16
NA2O	.65	.46	.53	.60	.39	.63	.55	.67
MGO	12.65	13.94	12.40	13.75	12.19	14.08	14.58	14.14
A2O3	13.55	13.45	13.57	13.45	13.81	13.66	13.63	13.72
SIO2	36.00	37.40	35.50	37.78	35.55	35.92	36.50	35.97
K2O	8.95	9.17	8.85	9.43	9.17	9.67	9.56	9.08
CAO	.07	.20	.14	.35	.23	.21	.18	.18
TIO2	5.40	3.62	5.27	3.52	5.45	5.73	5.63	6.29
MNO	.01	.16	.25	.17	.20	.31	.24	.25
FEO	17.35	16.23	17.89	16.29	17.61	15.94	15.13	16.00
H2O	3.92	3.95	3.89	3.97	3.90	3.98	4.00	4.00
SUM	98.55	98.58	98.30	99.31	98.50	100.13	100.00	100.30

SI	5.505	*		5.674	*		5.456	*		5.698	*		5.459	*		5.405	*		5.463	*		5.385	*	
AL	2.442	7.947		2.325	8.000		2.452	7.928		2.302	8.000		2.499	7.958		2.422	7.828		2.404	7.867		2.420	7.805	
AL	0.000	*		.078	*		0.000	*		.088	*		0.000	*		0.000	*		0.000	*		0.000	*	
TI	.621	*		.413	*		.510	*		.399	*		.629	*		.648	*		.634	*		.708	*	
MG	2.883	*		3.152	*		2.946	*		3.091	*		2.790	*		3.158	*		3.253	*		3.155	*	
FE	2.219	*		2.059	*		2.303	*		2.055	*		2.262	*		2.006	*		1.894	*		2.003	*	
MN	.001	5.724		.021	5.722		.033	5.792		.022	5.655		.026	5.707		.040	5.852		.030	5.811		.032	5.898	
K	1.746	*		1.774	*		1.740	*		1.814	*		1.796	*		1.856	*		1.825	*		1.734	*	
CA	.011	*		.033	*		.023	*		.057	*		.038	*		.034	*		.029	*		.029	*	
NA	.193	1.950		.135	1.942		.158	1.921		.175	2.046		.116	1.950		.184	2.074		.160	2.014		.194	1.957	
H	4.000	4.000		4.000	4.000		4.000	4.000		4.000	4.000		4.000	4.000		4.000	4.000		4.000	4.000		4.000	4.000	
O	24.000	*		24.000	*		24.000	*		24.000	*		24.000	*		24.000	*		24.000	*		24.000	*	
BIOT		43.50			39.75			45.08			40.18			45.05			39.31			37.17			39.21		
PHLO		56.50			60.25			54.92			59.82			54.95			60.69			62.83			60.79		
F/M		.770			.660			.821			.672			.820			.648			.592			.645		
F/FM		.435			.398			.451			.402			.451			.393			.372			.392		

9 1JG49 CORE
10 1JG49 RIM
11 1JG49 CORE
12 1JG49 RIM

13 1JG49 CORE
14 1JG70
15 1JG70
16 1JG70

SUPER RECAL — BIOTITES - PHENOCRYST UNLESS STATED

	17	18	19	20	21	22	23	24
NA2O	1.07	.83	1.12	1.15	.69	.71	.61	.74
MGO	15.61	14.32	13.58	13.88	13.90	14.18	14.20	15.25
A2O3	13.54	12.99	13.18	13.24	13.51	13.77	13.71	14.13
SIO2	36.72	36.86	35.41	36.13	36.89	36.93	37.71	36.77
K2O	8.84	9.68	9.32	9.13	9.11	9.21	9.44	8.35
CAO	.20	.02	.29	.24	.19	.17	.23	.16
TIO2	5.38	5.22	5.87	5.18	5.38	5.45	5.11	6.32
MNO	.15	.24	.14	.20	.16	.08	.25	.09
FEO	14.53	15.17	16.95	16.31	16.03	16.44	15.44	13.04
H2O	4.03	3.95	3.94	3.95	4.00	4.03	4.04	4.03
SUM	100.07	98.28	99.79	99.41	99.86	100.97	100.74	98.88

SI	5.462	*		5.587	*		5.379	*		5.476	*		5.532	*		5.486	*		5.587	*		5.467	*	
AL	2.373	7.835		2.320	7.907		2.359	7.738		2.365	7.840		2.387	7.919		2.410	7.896		2.393	7.980		2.476	7.943	
AL	0.000	*		0.000	*		0.000	*		0.000	*		0.000	*		0.000	*		0.000	*		0.000	*	
TI	.602	*		.595	*		.571	*		.590	*		.607	*		.609	*		.569	*		.707	*	
MG	3.461	*		3.235	*		3.075	*		3.136	*		3.107	*		3.140	*		3.136	*		3.380	*	
FE	1.807	*		1.923	*		2.153	*		2.067	*		2.010	*		2.042	*		1.913	*		1.621	*	
MN	.019	5.889		.031	5.784		.018	5.917		.026	5.819		.020	5.744		.010	5.801		.031	5.649		.011	5.719	
K	1.677	*		1.678	*		1.806	*		1.765	*		1.742	*		1.745	*		1.784	*		1.584	*	
CA	.032	*		.003	*		.046	*		.039	*		.031	*		.027	*		.037	*		.025	*	
NA	.309	2.017		.244	1.925		.330	2.181		.338	2.142		.201	1.974		.204	1.977		.175	1.996		.213	1.822	
H	4.000	4.000		4.000	4.000		4.000	4.000		4.000	4.000		4.000	4.000		4.000	4.000		4.000	4.000		4.000	4.000	
O	24.000	*		24.000	*		24.000	*		24.000	*		24.000	*		24.000	*		24.000	*		24.000	*	
	BIOT	34.54			37.65			41.39			40.03			39.53			39.53			38.27			32.57		
	PHLO	65.46			62.35			58.61			59.97			60.47			60.47			61.73			67.43		
	F/M	.528			.604			.706			.667			.654			.654			.620			.483		
	F/FM	.345			.377			.414			.400			.395			.395			.383			.326		

17 1JG80
18 1JG80
19 2JG21
20 2JG21
21 2JG21
22 2JG21
23 2JG21
24 2JG33

SUPER RECAL — BIOTITES - PHENOCRYST UNLESS STATED

	25	26	27	28	29	30	31	32
NA2O	.61	.72	.66	.66	.18	.38	.71	.39
MGO	13.58	14.66	13.99	15.16	12.68	13.77	12.97	13.76
A2O3	14.02	13.84	14.13	13.05	12.07	13.55	13.56	12.72
SIO2	36.01	37.10	36.32	37.35	43.32	37.82	35.72	37.53
K2O	8.98	8.61	8.77	8.21	8.63	9.67	8.98	9.37
CAO	.20	.15	.10	.32	.23	.20	.14	.22
TIO2	6.02	5.07	5.91	2.34	2.39	2.92	5.81	5.15
MNO	.25	.15	.15	.19	0.00	.17	.28	0.00
FEO	15.10	13.47	15.39	16.81	15.10	15.96	17.12	15.95
H2O	3.98	4.01	3.99	3.93	4.06	3.94	3.94	3.97
SUM	99.75	98.78	99.40	98.02	98.66	98.38	99.23	99.06

SI	5.414	*		5.537	*		5.447	*		5.693	*		6.395	*		5.748	*		5.434	*		5.665	*	
AL	2.484	7.898		2.434	7.972		2.497	7.944		2.307	8.000		1.605	8.000		2.252	8.000		2.431	7.865		2.263	7.928	
AL	0.000	*		0.000	*		0.000	*		.037	*		.494	*		.174	*		0.000	*		0.000	*	
TI	.681	*		.681	*		.667	*		.268	*		.265	*		.334	*		.665	*		.585	*	
MG	3.043	*		3.261	*		3.125	*		3.444	*		2.790	*		3.119	*		2.941	*		3.096	*	
FE	2.024	*		1.681	*		1.930	*		2.143	*		1.864	*		2.028	*		2.178	*		2.014	*	
MN	.033	5.781		.019	5.643		.019	5.741		.025	5.917		0.000	5.414		.022	5.678		.036	5.820		0.000	5.694	
K	1.722	*		1.639	*		1.678	*		1.596	*		1.625	*		1.874	*		1.743	*		1.804	*	
CA	.032	*		.024	*		.016	*		.052	*		.036	*		.033	*		.023	*		.036	*	
NA	.178	1.932		.209	1.871		.192	1.886		.195	1.843		.052	1.713		.112	2.019		.209	1.975		.114	1.954	
H	4.000	4.000		4.000	4.000		4.000	4.000		4.000	4.000		4.000	4.000		4.000	4.000		4.000	4.000		4.000	4.000	
O	24.000	*		24.000	*		24.000	*		24.000	*		24.000	*		24.000	*		24.000	*		24.000	*	
	BIOT	40.34			34.27			38.41			38.62			40.05			39.66			42.95			39.41		
	PHLO	59.66			65.73			61.59			61.38			59.95			60.34			57.05			60.59		
	F/M	.676			.521			.624			.629			.668			.657			.753			.650		
	F/FM	.403			.343			.384			.386			.401			.397			.430			.394		

25 2JG33
26 2JG33
27 2JG33
28 2JG33 GROUNDMASS
29 2JG33 GROUNDMASS
30 2JG33 GROUNDMASS
31 2JG35 CORE
32 2JG35 RIM

SUPER RECAL — BIOTITES - PHENOCRYST UNLESS STATED

	33		34		35		36		37	
NA2O	.42		.52		.25		.50		.68	
MGO	13.89		12.95		13.73		12.78		12.80	
A2O3	12.44		13.37		12.34		13.84		13.46	
SIO2	37.89		36.58		37.63		36.24		35.98	
K2O	8.96		9.05		8.91		9.04		8.85	
CAO	.24		.20		.35		.14		.10	
TIO2	4.30		5.84		4.86		5.97		7.70	
MNO	.06		.25		.15		.01		.04	
FEO	15.95		17.04		15.85		17.06		16.87	
H2O	3.94		3.97		3.94		3.97		4.00	
SUM	98.09		99.77		98.02		99.55		100.48	
SI	5.760	*	5.518	*	5.727	*	5.474	*	5.386	*
AL	2.228	7.988	2.377	7.895	2.213	7.940	2.463	7.937	2.374	7.760
AL	0.000	*	0.000	*	0.000	*	0.000	*	0.000	*
TI	.492	*	.662	*	.556	*	.678	*	.867	*
MG	3.147	*	2.912	*	3.115	*	2.877	*	2.856	*
FE	2.028	*	2.150	*	2.019	*	2.155	*	2.112	*
MN	.008	5.674	.032	5.756	.019	5.709	.001	5.711	.005	5.839
K	1.737	*	1.741	*	1.730	*	1.742	*	1.690	*
CA	.039	*	.032	*	.057	*	.023	*	.016	*
NA	.124	1.900	.152	1.926	.074	1.861	.146	1.911	.197	1.903
H	4.000	4.000	4.000	4.000	4.000	4.000	4.000	4.000	4.000	4.000
O	24.000	*	24.000	*	24.000	*	24.000	*	24.000	*
	BIOT	39.27		42.83		39.55		42.84		42.57
	PHLO	60.73		57.17		60.45		57.16		57.43
	F/M	.647		.749		.654		.749		.741
	F/FM	.393		.428		.396		.428		.426

33 2JG35 RIM AROUND AMPHIBOLE
34 2JG35 CORE
35 2JG35 RIM
36 2JG35 CORE
37 2JG35 CORE

SUPER RECAL — AMPHIBOLES

	1		2		3		4		5		6		7		8	
SIO2	44.20		43.23		42.97		44.07		42.33		44.11		45.27		44.27	
A203	9.47		9.49		9.77		9.23		10.18		9.05		9.54		10.05	
FEO	8.62		9.26		8.76		8.07		8.11		8.79		9.32		9.49	
F203	4.71		4.03		5.10		5.29		5.67		4.68		3.61		3.32	
MGO	14.25		13.79		13.55		14.41		13.68		14.13		13.76		13.21	
MNO	0.00		0.00		0.00		0.00		0.00		0.00		.15		.35	
TIO2	2.71		2.61		2.81		2.45		2.86		2.51		2.16		2.60	
CAO	11.55		11.47		11.23		11.43		11.37		11.61		11.29		10.94	
NA20	2.38		2.47		2.50		2.49		2.39		2.16		2.35		2.83	
K20	.77		.75		.89		.72		.81		.82		.68		.86	
H20	2.06		2.02		2.03		2.05		2.03		2.04		2.06		2.04	
SUM	100.72		99.11		99.72		100.21		99.43		99.90		100.19		99.96	
SI	6.428	*	6.408	*	6.339	*	6.437	*	6.259	*	6.472	*	6.591	*	6.489	*
AL	1.572	8.000	1.592	8.000	1.661	8.000	1.563	8.000	1.741	8.000	1.528	8.000	1.409	8.000	1.511	8.000
AL	.051	*	.064	*	.037	*	.026	*	.033	*	.037	*	.229	*	.225	*
TI	.295	*	.291	*	.312	*	.269	*	.318	*	.277	*	.236	*	.287	*
FE3+	.515	*	.450	*	.566	*	.581	*	.631	*	.517	*	.396	*	.366	*
MG	3.089	*	3.047	*	3.004	*	3.137	*	3.015	*	3.090	*	2.986	*	2.886	*
FE	1.048	*	1.148	*	1.081	*	.996	*	1.003	*	1.079	*	1.135	*	1.163	*
MN	0.000	*	0.000	*	0.000	*	0.000	*	0.000	*	0.000	*	.018	*	.043	*
CA	1.800	*	1.822	*	1.775	*	1.789	*	1.801	*	1.825	*	1.761	*	1.718	*
NA	.201	7.000	.179	7.000	.225	7.000	.212	7.000	.199	7.000	.175	7.000	.240	7.000	.311	7.000
NA	.470	*	.531	*	.490	*	.493	*	.486	*	.440	*	.424	*	.494	*
K	.143	.613	.142	.673	.157	.657	.134	.627	.153	.639	.153	.593	.126	.550	.161	.655
H	2.000	2.000	2.000	2.000	2.000	2.000	2.000	2.000	2.000	2.000	2.000	2.000	2.000	2.000	2.000	2.000
O	24.000	*	24.000	*	24.000	*	24.000	*	24.000	*	24.000	*	24.000	*	24.000	*
MG		74.66		72.63		73.54		76.09		75.04		74.13		72.14		70.52
FEMN		25.34		27.37		26.46		23.91		24.96		25.87		27.86		29.48
F/M		.339		.377		.360		.314		.333		.349		.386		.418
F/FM		.253		.274		.265		.239		.250		.259		.279		.295

1 1JG10 BROWN
2 1JG10 BROWN
3 1JG10 BROWN
4 1JG10 BROWN
5 1JG10 BROWN
6 1JG10 BROWN
7 1JG10 BROWN
8 1JG10 BROWN

SUPER RECAL — AMPHIBOLES

	9		10		11		12		13		14		15		16	
SIO2	44.27		43.82		44.81		44.85		51.39		42.01		43.49		42.31	
A203	10.35		10.87		9.71		9.63		4.62		10.75		10.47		10.50	
FEO	9.14		10.09		8.04		9.42		10.95		9.10		9.32		8.37	
F203	4.04		2.14		5.19		3.89		.32		2.90		3.28		4.20	
MGO	13.61		13.45		14.00		13.77		15.29		13.90		13.82		13.87	
MNO	0.00		.30		.23		.12		.31		.08		.17		.05	
TIO2	2.69		3.05		2.48		2.28		.87		4.18		3.39		3.34	
CAO	11.32		11.54		11.35		11.33		12.26		11.34		11.55		11.33	
NA20	2.55		2.64		2.14		2.43		.95		2.87		2.56		2.63	
K20	.70		.67		.76		.82		.37		.77		.71		.73	
H20	2.06		2.06		2.07		2.06		2.07		2.04		2.06		2.03	
SUM	100.73		100.63		100.79		100.60		99.40		99.94		100.82		99.36	
SI	6.427	*	6.381	*	6.486	*	6.526	*	7.428	*	6.178	*	6.325	*	6.245	*
AL	1.573	8.000	1.619	8.000	1.514	8.000	1.474	8.000	.572	8.000	1.822	8.000	1.675	8.000	1.755	8.000
AL	.198	*	.246	*	.143	*	.177	*	.215	*	.040	*	.120	*	.072	*
TI	.294	*	.334	*	.270	*	.249	*	.095	*	.462	*	.371	*	.371	*
FE3+	.441	*	.234	*	.565	*	.426	*	.035	*	.321	*	.359	*	.467	*
MG	2.945	*	2.919	*	3.021	*	2.986	*	3.294	*	3.047	*	2.996	*	3.052	*
FE	1.110	*	1.229	*	.973	*	1.146	*	1.324	*	1.119	*	1.134	*	1.033	*
MN	0.000	*	.037	*	.028	*	.015	*	.038	*	.010	*	.021	*	.006	*
CA	1.761	*	1.800	*	1.762	*	1.766	*	1.899	*	1.787	*	1.800	*	1.792	*
NA	.252	7.000	.200	7.000	.238	7.000	.234	7.000	.101	7.000	.214	7.000	.200	7.000	.208	7.000
NA	.466	*	.545	*	.362	*	.452	*	.165	*	.604	*	.521	*	.544	*
K	.130	.596	.124	.669	.140	.503	.152	.604	.068	.233	.144	.749	.132	.653	.137	.682
H	2.000	2.000	2.000	2.000	2.000	2.000	2.000	2.000	2.000	2.000	2.000	2.000	2.000	2.000	2.000	2.000
O	24.000	*	24.000	*	24.000	*	24.000	*	24.000	*	24.000	*	24.000	*	24.000	*
MG		72.63		69.76		75.10		72.01		70.75		72.96		72.18		74.59
FEMN		27.37		30.24		24.90		27.99		29.25		27.04		27.82		25.41
F/M		.377		.434		.332		.389		.413		.371		.385		.341
F/FM		.274		.302		.249		.280		.292		.270		.278		.254

9 1JG10 BROWN
10 1JG10 BROWN
11 1JG10 BROWN
12 1JG10 BROWN
13 1JG10 GREEN
14 1JG29 BROWN
15 1JG29 BROWN
16 1JG29 BROWN

SUPER RECAL — AMPHIBOLES

	17	18	19	20	21	22	23	24
SIO2	42.30	42.18	41.82	42.48	50.73	50.46	50.70	50.02
A203	10.89	11.89	11.92	11.38	4.77	4.78	4.95	5.08
FEO	8.04	6.04	6.40	7.22	9.96	11.19	8.54	10.60
F203	4.20	5.63	5.17	4.90	2.82	1.87	3.55	2.54
MGO	13.94	14.70	14.03	13.85	15.19	14.56	15.61	15.02
MNO	.28	.01	.15	.18	.22	.44	.41	.23
TIO2	4.35	3.84	3.76	3.22	.76	.63	1.05	.92
CAO	11.24	11.09	11.03	11.09	11.92	12.04	11.89	12.07
NA20	2.67	2.99	2.54	2.60	1.20	1.13	1.06	1.41
K20	.78	.75	.71	.70	.43	.51	.46	.49
H20	2.06	2.08	2.05	2.05	2.08	2.06	2.09	2.08
SUM	100.75	101.20	99.69	99.67	100.08	99.67	100.31	100.46

		*		*		*		*		*		*		*		*
SI	6.157		6.073		6.109		6.218		7.311		7.337		7.263		7.221	
AL	1.843	8.000	1.927	8.000	1.891	8.000	1.782	8.000	.689	8.000	.663	8.000	.737	8.000	.779	8.000
AL	.025	*	.090	*	.151	*	.180	*	.121	*	.156	*	.099	*	.085	*
TI	.476	*	.415	*	.413	*	.354	*	.082	*	.069	*	.113	*	.100	*
FE3+	.460	*	.610	*	.558	*	.540	*	.306	*	.205	*	.383	*	.276	*
MG	3.024	*	3.155	*	3.055	*	3.022	*	3.263	*	3.155	*	3.333	*	3.232	*
FE	.979	*	.727	*	.782	*	.884	*	1.200	*	1.361	*	1.023	*	1.280	*
MN	.035	*	.001	*	.020	*	.022	*	.027	*	.054	*	.050	*	.028	*
CA	1.753	*	1.711	*	1.726	*	1.739	*	1.841	*	1.876	*	1.825	*	1.867	*
NA	.248	7.000	.290	7.000	.274	7.000	.259	7.000	.159	7.000	.125	7.000	.175	7.000	.133	7.000
NA	.505	*	.545	*	.474	*	.479	*	.176	*	.194	*	.120	*	.261	*
K	.145	.551	.138	.683	.132	.606	.131	.610	.079	.255	.095	.289	.084	.204	.090	.352
H	2.000	2.000	2.000	2.000	2.000	2.000	2.000	2.000	2.000	2.000	2.000	2.000	2.000	2.000	2.000	2.000
O	24.000	*	24.000	*	24.000	*	24.000	*	24.000	*	24.000	*	24.000	*	24.000	*
MG		74.91		81.24		79.21		76.93		72.67		69.04		75.65		71.19
FEMN		25.09		18.76		20.79		23.07		27.33		30.96		24.35		28.81
F/M		.335		.231		.262		.300		.376		.448		.322		.405
F/FM		.251		.188		.208		.231		.273		.310		.244		.288

17 1JG29 BROWN
18 1JG41 BROWN
19 1JG41 BROWN
20 1JG41 BROWN
21 1JG49 GREEN AROUND PX
22 1JG49 GREEN AROUND PX
23 1JG49 GREEN AROUND PX
24 1JG49 GREEN

SUPER RECAL — AMPHIBOLES

	25	26	27	28	29	30	31	32
SIO2	43.14	50.22	44.80	49.13	45.01	45.20	45.98	45.92
A203	11.32	4.85	9.54	5.64	9.65	7.98	8.13	7.55
FEO	11.46	9.98	9.70	9.22	10.97	9.83	11.96	12.32
F203	1.84	2.70	3.72	3.72	2.02	3.55	2.27	2.04
MGO	12.65	15.00	13.48	15.06	13.07	13.63	13.27	12.72
MNO	.24	.21	.20	.21	.21	.20	.09	.35
TIO2	2.99	1.05	2.49	.94	2.56	1.95	1.94	1.74
CAO	11.56	11.64	11.98	12.12	11.59	11.60	12.05	11.94
NA20	2.68	1.35	1.60	1.11	1.96	1.72	1.73	1.42
K20	.85	.45	.70	.49	.78	.73	.74	.75
H20	2.05	2.07	2.05	2.07	2.04	2.02	2.04	2.01
SUM	100.78	99.52	100.25	99.71	99.86	98.41	100.20	98.76

		*		*		*		*		*		*		*		*
SI	6.318		7.283		6.537		7.127		6.600		6.719		6.747		6.844	
AL	1.682	8.000	.717	8.000	1.463	8.000	.873	8.000	1.400	8.000	1.281	8.000	1.253	8.000	1.156	8.000
AL	.272	*	.112	*	.178	*	.091	*	.267	*	.117	*	.153	*	.170	*
TI	.329	*	.115	*	.273	*	.103	*	.282	*	.218	*	.214	*	.195	*
FE3+	.203	*	.295	*	.408	*	.406	*	.223	*	.397	*	.251	*	.229	*
MG	2.762	*	3.242	*	2.932	*	3.256	*	2.856	*	3.020	*	2.903	*	2.826	*
FE	1.404	*	1.210	*	1.184	*	1.118	*	1.345	*	1.222	*	1.468	*	1.536	*
MN	.030	*	.026	*	.025	*	.026	*	.026	*	.025	*	.011	*	.044	*
CA	1.814	*	1.809	*	1.973	*	1.884	*	1.821	*	1.848	*	1.895	*	1.907	*
NA	.187	7.000	.191	7.000	.127	7.000	.116	7.000	.179	7.000	.153	7.000	.106	7.000	.094	7.000
NA	.574	*	.188	*	.325	*	.196	*	.378	*	.343	*	.386	*	.317	*
K	.159	.733	.083	.271	.130	.456	.091	.286	.146	.524	.138	.481	.139	.525	.143	.459
H	2.000	2.000	2.000	2.000	2.000	2.000	2.000	2.000	2.000	2.000	2.000	2.000	2.000	2.000	2.000	2.000
O	24.000	*	24.000	*	24.000	*	24.000	*	24.000	*	24.000	*	24.000	*	24.000	*
MG		65.83		72.40		70.81		74.00		67.57		70.77		66.25		64.14
FEMN		34.17		27.60		29.19		26.00		32.43		29.23		33.75		35.86
F/M		.519		.381		.412		.351		.480		.413		.510		.559
F/FM		.342		.276		.292		.260		.324		.292		.338		.359

25 1JG49 BROWN
26 1JG49 GREEN
27 1JG51 BROWN/GREEN
28 1JG51 GREEN
29 1JG51 BROWN/GREEN
30 1JG51 BROWN/GREEN
31 1JG51 BROWN/GREEN
32 1JG51 BROWN/GREEN

SUPER RECAL — AMPHIBOLES

	33		34		35		36		37		38		39		40	
SIO2	45.01		42.69		41.88		45.04		52.40		52.96		53.51		52.60	
A203	7.69		10.72		11.04		8.83		2.88		3.21		2.64		3.76	
FEO	11.65		5.88		9.28		7.13		7.54		8.71		9.39		9.28	
F203	2.74		4.33		2.34		3.88		3.42		3.70		1.79		3.02	
MGO	13.03		14.78		13.85		15.29		16.77		16.06		16.56		15.84	
MNO	.21		0.00		.13		.17		.23		.29		.29		.27	
TIO2	2.23		3.85		4.29		2.60		.64		.48		.36		.52	
CAO	11.71		11.15		11.43		11.18		11.53		11.93		12.10		12.08	
NA20	1.64		2.72		2.77		2.62		1.09		.78		.97		.79	
K20	1.02		.86		.89		.71		.34		.20		.16		.27	
H20	2.01		2.06		2.04		2.06		2.08		2.11		2.10		2.10	
SUM	98.93		100.03		99.94		99.51		98.92		100.43		99.87		100.53	
SI	6.715	*	6.217	*	6.159	*	6.553	*	7.540	*	7.536	*	7.642	*	7.490	*
AL	1.285	8.000	1.783	8.000	1.841	8.000	1.437	8.000	.460	8.000	.464	8.000	.358	8.000	.510	8.000
AL	.065	*	.056	*	.073	*	.079	*	.028	*	.075	*	.087	*	.121	*
TI	.250	*	.422	*	.474	*	.285	*	.069	*	.051	*	.039	*	.056	*
FE3+	.308	*	.475	*	.259	*	.425	*	.370	*	.396	*	.192	*	.324	*
MG	2.897	*	3.209	*	3.036	*	3.321	*	3.597	*	3.406	*	3.525	*	3.362	*
FE	1.453	*	.838	*	1.141	*	.869	*	.907	*	1.037	*	1.122	*	1.105	*
MN	.027	*	0.000	*	.016	*	.021	*	.028	*	.035	*	.035	*	.033	*
CA	1.872	*	1.740	*	1.801	*	1.745	*	1.778	*	1.819	*	1.852	*	1.843	*
NA	.129	7.000	.260	7.000	.199	7.000	.255	7.000	.222	7.000	.181	7.000	.149	7.000	.157	7.000
NA	.346	*	.508	*	.591	*	.485	*	.082	*	.034	*	.120	*	.061	*
K	.194	.540	.160	.667	.167	.757	.132	.617	.062	.144	.036	.070	.029	.149	.049	.110
H	2.000	2.000	2.000	2.000	2.000	2.000	2.000	2.000	2.000	2.000	2.000	2.000	2.000	2.000	2.000	2.000
O	24.000	*	24.000	*	24.000	*	24.000	*	24.000	*	24.000	*	24.000	*	24.000	*
MG		66.19		79.29		72.40		78.87		79.36		76.07		75.30		74.72
FEMN		33.81		20.71		27.60		21.13		20.64		23.93		24.70		25.28
F/M		.511		.261		.381		.268		.260		.315		.328		.338
F/FM		.338		.207		.276		.211		.206		.239		.247		.253

33 1JG51 BROWN/GREEN
34 1JG56 BROWN
35 1JG56 BROWN
36 1JG56 BROWN
37 2JG1 GREEN
38 2JG1 GREEN
39 2JG1 GREEN
40 2JG1 GREEN

SUPER RECAL — AMPHIBOLES

	41		42		43		44		45		46		47		48	
SIO2	52.80		52.96		51.28		50.50		51.66		51.51		49.93		50.44	
A203	3.47		3.31		4.32		4.75		3.97		4.17		5.65		4.66	
FEO	10.35		7.46		6.24		6.27		5.90		6.68		6.71		6.46	
F203	1.68		3.89		4.60		5.70		5.50		4.76		5.41		5.38	
MGO	16.02		15.79		16.38		16.00		16.94		16.49		15.74		16.08	
MNO	.20		.38		.54		.44		.55		.50		.38		.47	
TIO2	.28		.77		.72		.84		.74		.85		.83		.77	
CAO	12.17		11.98		11.08		10.95		11.27		11.45		11.38		11.22	
NA20	1.13		.97		1.43		1.59		1.41		1.37		1.44		1.41	
K20	.36		.18		.36		.40		.36		.29		.38		.47	
H20	2.10		2.12		2.08		2.09		2.11		2.10		2.09		2.08	
SUM	100.56		100.81		99.03		99.53		100.41		100.17		99.94		99.44	
SI	7.537	*	7.482	*	7.369	*	7.255	*	7.335	*	7.340	*	7.158	*	7.260	*
AL	.463	8.000	.518	8.000	.631	8.000	.745	8.000	.664	8.000	.660	8.000	.842	8.000	.740	8.000
AL	.121	*	.033	*	.101	*	.059	*	0.000	*	.040	*	.113	*	.050	*
TI	.030	*	.082	*	.078	*	.091	*	.079	*	.091	*	.089	*	.083	*
FE3+	.180	*	.414	*	.497	*	.616	*	.588	*	.510	*	.584	*	.583	*
MG	3.409	*	3.535	*	3.508	*	3.426	*	3.585	*	3.502	*	3.363	*	3.449	*
FE	1.235	*	.881	*	.750	*	.753	*	.701	*	.796	*	.804	*	.778	*
MN	.024	*	.045	*	.066	*	.054	*	.066	*	.060	*	.046	*	.057	*
CA	1.861	*	1.813	*	1.706	*	1.686	*	1.715	*	1.748	*	1.748	*	1.730	*
NA	.139	7.000	.195	7.000	.294	7.000	.315	7.000	.267	7.000	.252	7.000	.252	7.000	.270	7.000
NA	.174	*	.070	*	.104	*	.128	*	.121	*	.126	*	.148	*	.124	*
K	.065	.239	.032	.103	.056	.170	.073	.201	.065	.187	.053	.179	.069	.218	.086	.210
H	2.000	2.000	2.000	2.000	2.000	2.000	2.000	2.000	2.000	2.000	2.000	2.000	2.000	2.000	2.000	2.000
O	24.000	*	24.000	*	24.000	*	24.000	*	24.000	*	24.000	*	24.000	*	24.000	*
MG		73.01		79.23		81.14		80.94		82.38		80.35		79.81		80.51
FEMN		25.99		20.77		18.86		19.06		17.62		19.65		20.19		19.49
F/M		.370		.262		.232		.235		.214		.245		.253		.242
F/FM		.270		.208		.189		.191		.176		.196		.202		.195

41 2JG1 GREEN
42 2JG1 GREEN
43 2JG21 GREEN
44 2JG21 GREEN
45 2JG21 GREEN
46 2JG21 GREEN
47 2JG21 GREEN
48 2JG21 GREEN

SUPER RECAL — AMPHIBOLES

	49	50	51	52	53	54	55	56
SIO2	51.78	50.16	49.91	51.19	51.10	53.40	49.76	50.24
A2O3	4.65	4.54	4.37	4.57	4.18	2.29	4.78	4.60
FEO	6.08	7.04	10.74	3.99	5.30	7.01	8.26	7.78
F2O3	5.28	4.64	.80	7.72	5.75	3.36	3.62	3.82
MGO	16.55	15.22	16.66	16.97	17.04	17.77	16.24	16.65
MNO	.51	.55	.50	.35	.55	.40	.59	.38
TIO2	.64	.90	.88	.64	.62	.29	.85	.78
CAO	11.35	11.49	11.48	11.13	11.40	11.60	11.24	11.13
NA2O	1.35	1.58	1.83	1.83	1.37	.98	2.08	2.17
K2O	.35	.45	.35	.35	.26	.22	.40	.41
H2O	2.12	2.08	2.05	2.12	2.10	2.10	2.07	2.08
SUM	100.67	99.65	99.58	100.86	99.67	99.42	99.89	100.04
SI	7.325	7.229	7.251	7.224	7.299	7.615	7.186	7.220
AL	.675 8.000	.771 8.000	.748 7.999	.760 7.984	.701 8.000	.385 8.000	.813 7.999	.779 8.000
AL	.100	0.000	0.000	0.000	.003	0.000	0.000	0.000
TI	.068	.098	.096	.068	.067	.031	.092	.084
FE3+	.562	.503	.087	.820	.618	.361	.393	.413
MG	3.489	3.484	3.508	3.569	3.628	3.777	3.496	3.567
FE	.719	.848	1.305	.471	.633	.836	.998	.935
MN	.061	.067	.052	.042	.067	.048	.072	.046
CA	1.722	1.774	1.787	1.683	1.745	1.772	1.739	1.714
NA	.278 7.000	.225 7.000	.255 7.000	.347 7.000	.240 7.000	.175 7.000	.210 7.000	.241 7.000
NA	.092	.216	.460	.153	.139	.096	.373	.364
K	.063 .155	.083 .299	.065 .525	.063 .216	.047 .186	.040 .135	.074 .446	.075 .439
H	2.000 2.000	2.000 2.000	2.000 2.000	2.000 2.000	2.000 2.000	2.000 2.000	2.000 2.000	2.000 2.000
O	24.000	24.000	24.000	24.000	24.000	24.000	24.000	24.000
MG	81.72	79.19	72.53	87.44	83.83	81.03	76.57	78.42
FEMN	18.28	20.81	27.47	12.56	16.17	18.97	23.43	21.58
F/M	.224	.263	.379	.144	.193	.234	.306	.275
F/FM	.183	.208	.275	.126	.162	.190	.234	.216

49 2JG21 GREEN
50 2JG21 GREEN
51 2JG21 GREEN
53 2JG21 GREEN
54 2JG21 GREEN
55 2JG21 GREEN

SUPER RECAL — AMPHIBOLES

	57	58	59	60	61	62	63	64
SIO2	50.24	42.49	41.80	43.32	41.74	41.90	43.11	49.44
A2O3	4.59	10.28	10.21	10.55	10.94	10.74	10.49	5.03
FEO	7.32	8.22	8.81	9.64	9.58	10.24	9.73	9.82
F2O3	3.75	3.57	3.39	1.94	2.39	1.39	2.31	2.55
MGO	16.85	14.21	13.89	13.92	13.64	13.35	13.71	15.05
MNO	.62	.19	.21	.24	.10	.04	.13	.17
TIO2	.80	3.11	3.89	3.63	4.09	4.14	3.62	1.10
CAO	11.25	11.23	11.16	11.39	11.09	11.45	11.42	11.56
NA2O	2.00	2.84	2.79	2.83	3.11	2.59	2.62	1.53
K2O	.31	.87	.85	.76	.91	.69	.79	.51
H2O	2.08	2.02	2.02	2.05	2.03	2.01	2.04	2.05
SUM	99.82	99.03	99.02	100.27	99.62	98.54	99.97	98.81
SI	7.222	6.288	6.211	6.331	6.171	6.246	6.324	7.229
AL	.778 8.000	1.712 8.000	1.788 7.999	1.669 8.000	1.829 8.000	1.754 8.000	1.676 8.000	.771 8.000
AL	0.000	.081	0.000	.147	.077	.132	.138	.096
TI	.086	.346	.435	.399	.455	.464	.399	.121
FE3+	.406	.398	.379	.213	.266	.156	.255	.281
MG	3.610	3.134	3.076	3.032	3.006	2.966	2.998	3.280
FE	.880	1.017	1.095	1.178	1.184	1.276	1.194	1.201
MN	.075	.024	.026	.030	.013	.005	.016	.021
CA	1.734	1.781	1.777	1.783	1.757	1.829	1.795	1.811
NA	.208 7.000	.220 7.000	.212 7.000	.217 7.000	.244 7.000	.172 7.000	.205 7.000	.189 7.000
NA	.350	.595	.592	.585	.648	.577	.540	.245
K	.057 .407	.164 .759	.161 .753	.142 .726	.172 .819	.131 .708	.148 .688	.095 .340
H	2.000 2.000	2.000 2.000	2.000 2.000	2.000 2.000	2.000 2.000	2.000 2.000	2.000 2.000	2.000 2.000
O	24.000	24.000	24.000	24.000	24.000	24.000	24.000	24.000
MG	79.07	75.07	73.29	71.51	71.52	69.83	71.25	72.86
FEMN	20.93	24.93	26.71	28.49	28.48	30.17	28.75	27.14
F/M	.265	.332	.364	.398	.398	.432	.404	.373
F/FM	.209	.249	.267	.285	.285	.302	.288	.271

57 2JG21 GREEN
58 2JG33 BROWN
59 2JG33 BROWN
60 2JG33 BROWN
61 2JG33 BROWN
62 2JG35 BROWN
63 2JG35 BROWN
64 2JG35 GREEN

SUPER RECAL AMPHIBOLES

	65	66	67	68	69	70	71	72
SIO2	42.02	43.71	42.10	50.32	42.96	50.10	42.46	49.61
A203	10.41	10.00	11.65	4.84	11.77	4.72	10.80	5.59
FEO	12.77	11.10	10.39	9.81	9.01	8.34	9.43	8.30
F203	1.71	1.39	1.34	3.24	3.45	3.90	2.45	4.67
MGO	11.42	13.53	13.65	15.13	13.56	15.98	13.86	15.26
MNO	.29	.03	0.00	.43	.17	.48	.11	.50
TIO2	3.55	3.17	4.33	1.26	3.27	1.04	3.56	1.36
CAO	11.48	11.70	11.65	11.99	11.23	11.56	11.27	11.54
NA20	2.28	2.65	2.94	1.26	2.98	1.72	3.05	1.53
K20	.86	.60	.78	.36	.75	.43	.79	.54
H20	1.99	2.04	2.05	2.09	2.07	2.08	2.04	2.09
SUM	98.99	99.92	100.88	100.73	101.22	100.35	99.82	100.99

SI	6.315	*		6.428	*		6.141	*		7.226	*		6.221	*		7.200	*	
AL	1.585	8.000		1.572	8.000		1.859	8.000		.774	8.000		1.779	8.000		.799	7.999	
AL	.159	*		.161	*		.143	*		.045	*		.229	*		0.000	*	
TI	.402	*		.351	*		.475	*		.136	*		.356	*		.112	*	
FE3+	.193	*		.154	*		.147	*		.350	*		.376	*		.422	*	
MG	2.603	*		2.966	*		2.968	*		3.238	*		2.927	*		3.423	*	
FE	1.605	*		1.365	*		1.257	*		1.178	*		1.091	*		1.002	*	
MN	.037	*		.004	*		0.000	*		.052	*		.021	*		.058	*	
CA	1.849	*		1.843	*		1.821	*		1.845	*		1.742	*		1.780	*	
NA	.152	7.000		.157	7.000		.180	7.000		.155	7.000		.258	7.000		.202	7.000	
NA	.513	*		.599	*		.552	*		.195	*		.579	*		.277	*	
K	.165	.677		.113	.711		.145	.797		.066	.261		.139	.717		.079	.355	
H	2.000	2.000		2.000	2.000		2.000	2.000		2.000	2.000		2.000	2.000		2.000	2.000	
O	24.000	*		24.000	*		24.000	*		24.000	*		24.000	*		24.000	*	
MG		61.32			68.42			70.07			72.47			72.47			76.34		
FEMN		38.68			31.58			29.93			27.53			27.53			23.66		
F/M		.631			.462			.427			.380			.380			.310		
F/FM		.387			.316			.299			.275			.275			.237		

SI	6.248	*		7.099	*													
AL	1.752	8.000		.901	8.000													
AL	.120	*		.042	*													
TI	.394	*		.146	*													
FE3+	.271	*		.503	*													
MG	3.040	*		3.255	*													
FE	1.160	*		.993	*													
MN	.014	*		.061	*													
CA	1.777	*		1.769	*													
NA	.224	7.000		.231	7.000													
NA	.646	*		.194	*													
K	.148	.795		.099	.293													
H	2.000	2.000		2.000	2.000													
O	24.000	*		24.000	*													
MG		72.14			75.54													
FEMN		27.86			24.46													
F/M		.386			.324													
F/FM		.279			.245													

65 2JG35 BROWN
66 2JG35 BROWN
67 2JG35 BROWN CORE

69 2JG35 BROWN CORE
70 2JG35 GREEN RIM
71 2JG35 BROWN CORE

SUPER RECAL AMPHIBOLES

	73	74	75	76	77	78	79	80
SIO2	42.34	49.91	42.50	50.48	50.21	44.06	49.18	50.50
A203	11.31	4.65	10.98	4.46	4.65	9.68	4.91	4.70
FEO	8.85	8.73	10.77	7.13	6.56	7.79	9.84	7.81
F203	3.07	2.47	.61	4.29	4.47	4.22	2.13	4.28
MGO	13.73	15.70	13.99	16.41	16.51	14.67	15.88	15.90
MNO	.05	.39	.23	.25	.38	.22	.40	.26
TIO2	3.72	1.09	4.23	1.11	1.11	3.06	1.33	1.31
CAO	11.20	11.54	11.79	11.34	11.50	11.35	11.52	11.38
NA20	2.87	1.55	3.01	1.60	1.54	2.57	1.79	1.44
K20	.73	.42	.75	.48	.29	.86	.43	.49
H20	2.04	2.05	2.05	2.08	2.08	2.06	2.06	2.09
SUM	99.92	98.50	100.82	99.63	99.30	100.54	99.47	100.16

SI	6.207	*		7.282	*		6.223	*		7.257	*		7.228	*		6.399	*	
AL	1.793	8.000		.718	8.000		1.777	8.000		.743	8.000		.772	8.000		1.601	8.000	
AL	.150	*		.082	*		.096	*		.012	*		.017	*		.055	*	
TI	.410	*		.120	*		.465	*		.120	*		.120	*		.334	*	
FE3+	.339	*		.271	*		.057	*		.454	*		.484	*		.461	*	
MG	3.000	*		3.414	*		3.027	*		3.516	*		3.542	*		3.176	*	
FE	1.086	*		1.055	*		1.316	*		.857	*		.790	*		.946	*	
MN	.006	*		.049	*		.028	*		.030	*		.046	*		.027	*	
CA	1.759	*		1.804	*		1.945	*		1.747	*		1.774	*		1.766	*	
NA	.240	7.000		.195	7.000		.155	7.000		.254	7.000		.227	7.000		.234	7.000	
NA	.576	*		.243	*		.697	*		.192	*		.203	*		.489	*	
K	.136	.712		.078	.321		.140	.837		.088	.280		.053	.256		.159	.649	
H	2.000	2.000		2.000	2.000		2.000	2.000		2.000	2.000		2.000	2.000		2.000	2.000	
O	24.000	*		24.000	*		24.000	*		24.000	*		24.000	*		24.000	*	
MG		73.31			75.41			69.25			79.84			80.91			76.54		
FEMN		26.69			24.59			30.75			20.16			19.09			23.46		
F/M		.364			.326			.444			.252			.236			.306		
F/FM		.267			.246			.309			.202			.191			.235		

SI	6.399	*		7.157	*		7.238	*										
AL	1.601	8.000		.842	8.000		.762	8.000										
AL	.055	*		0.000	*		.032	*										
TI	.334	*		.146	*		.141	*										
FE3+	.461	*		.233	*		.462	*										
MG	3.176	*		3.445	*		3.397	*										
FE	.946	*		1.198	*		.936	*										
MN	.027	*		.049	*		.032	*										
CA	1.766	*		1.796	*		1.748	*										
NA	.234	7.000		.133	7.000		.253	7.000										
NA	.489	*		.372	*		.148	*										
K	.159	.649		.080	.452		.090	.237										
H	2.000	2.000		2.000	2.000		2.000	2.000										
O	24.000	*		24.000	*		24.000	*										
MG		76.54			73.42			77.83										
FEMN		23.46			26.58			22.17										
F/M		.306			.362			.285										
F/FM		.235			.266			.222										

73 2JG35 BROWN CORE
74 2JG35 GREEN RIM
75 2JG38 BROWN AROUND PX
76 2JG38 GREEN AROUND PX

77 2JG38 GREEN
78 2JG38 BROWN
79 2JG38 GREEN
80 2JG38 GREEN

SUPER RECAL

	81
SIO2	42.44
A2O3	10.52
FEO	9.87
F2O3	1.50
MGO	13.91
MNO	.20
TIO2	3.92
CAO	11.44
NA2O	2.90
K2O	.83
H2O	2.03
SUM	99.56

SI	6.264	*
AL	1.736	8.000
AL	.094	*
TI	.435	*
FE3+	.167	*
MG	3.060	*
FE	1.218	*
MN	.025	*
CA	1.809	*
NA	.192	7.000
NA	.638	*
K	.156	.795
H	2.000	2.000
O	24.000	*

MG	71.11
FEMN	28.89
F/M	.406
F/FM	.289

81 2JG38 BROWN

SUPER RECAL

1JG55 SPHENES

	1	2	3
A2O3	.59	.85	1.05
SIO2	30.75	30.56	30.83
CAO	27.77	27.99	27.83
TIO2	37.97	36.87	36.74
FEO	1.77	1.50	1.90
SUM	98.95	97.77	98.35

SI	1.018	*	1.023	*	1.026	*	
AL	-I	1.018	-I	1.023	-I	1.026	
AL	.027	*	.034	*	.041	*	
TI	.945	.972	.928	.962	.920	.961	
CA	.985	*	1.004	*	.993	*	
FE	.049	1.034	.042	1.046	.053	1.046	
O	5.000	*	5.000	*	5.000	*	

1 1 SPHENE
2 2 SPHENE

3 3 SPHENE

APPENDIX E

MAJOR ELEMENT ANALYSES OF THE FAULT ROCKS BY E.D.S. X-RAY ANALYSIS ON THE S.E.M.

ROCK TYPE RHYOLITE

SAMPLE	1JG25	1JG25	1JG25	1JG25	1JG24	1JG24
SiO2	75.11	75.07	75.34	76.09	78.55	77.16
TiO2	.09	.32	.21	.14	.20	.17
Al2O3	13.38	13.08	13.41	13.18	12.16	12.61
Fe2O3T	.27	1.10	1.50	.97	.83	1.40
MgO	0.00	.32	.45	.36	0.00	.42
CaO	.28	.25	.31	.30	.08	.32
Na2O	3.29	4.12	4.11	4.04	5.08	4.58
K2O	7.83	4.60	4.73	4.96	2.91	2.99
TOTAL	100.25	98.86	100.06	100.04	99.81	99.65

ROCK TYPE RHYOLITE

SAMPLE	1JG24	1JG24	3JG64	3JG64	3JG12	3JG12
SiO2	75.00	74.26	67.91	68.63	76.78	74.17
TiO2	.34	.15	.53	.56	0.00	.09
Al2O3	13.32	12.24	14.90	15.76	12.25	14.71
Fe2O3T	1.31	1.14	2.71	2.44	.70	.45
MgO	.27	.41	1.51	1.49	.04	0.00
CaO	.99	2.92	2.43	2.45	.30	.28
Na2O	4.47	4.09	4.55	5.19	2.52	2.77
K2O	3.97	3.71	3.02	2.93	5.44	7.26
TOTAL	99.67	98.92	97.56	99.45	98.03	99.73

ROCK TYPE RHYOLITE

SAMPLE	3JG64	3JG64	3JG64	3JG64	3JG64	4JG20
SiO2	68.23	67.00	73.64	69.97	68.29	71.33
TiO2	.62	.66	.51	.53	.53	.30
Al2O3	15.31	16.25	13.82	14.93	15.81	14.64
Fe2O3T	1.99	2.42	1.88	2.36	2.61	2.09
MgO	1.29	1.72	1.07	1.32	1.49	.89
CaO	1.72	2.26	1.68	2.42	1.83	1.52
Na2O	3.50	5.04	4.55	4.26	3.85	4.84
K2O	5.76	3.39	3.29	3.79	5.14	3.71
TOTAL	98.42	98.74	100.44	99.58	99.55	99.32

ROCK TYPE RHYOLITE F.C.R.

SAMPLE	3JG12	1JG25	1JG25	1JG25	1JG25
SiO2	74.76	72.92	76.28	74.62	76.19
TiO2	.03	1.07	.63	.48	.25
Al2O3	11.95	13.51	12.18	12.49	11.71
Fe2O3T	.21	2.67	2.45	1.65	1.08
MgO	0.00	.89	.72	.27	0.00
CaO	.06	.28	.11	.61	0.00
Na2O	.42	.93	.81	2.76	1.94
K2O	10.70	5.77	5.27	5.71	7.16
TOTAL	98.13	98.04	98.45	98.59	98.33

ROCK TYPE F.C.R.

SAMPLE	3JG12	3JG12	3JG12	3JG12	2JG33	2JG33
SiO2	76.80	69.38	63.74	70.82	77.91	74.42
TiO2	.11	.37	.49	.37	.47	.52
Al2O3	13.08	16.19	18.85	15.32	10.53	12.16
Fe2O3T	.53	3.32	3.97	2.08	2.11	2.41
MgO	.20	1.44	1.62	.68	.46	.53
CaO	.77	1.03	1.86	.83	1.31	.98
Na2O	2.96	2.98	3.72	3.70	3.75	3.09
K2O	5.24	4.32	3.94	4.66	1.98	4.63
TOTAL	99.69	99.03	98.19	98.46	98.52	98.74

ROCK TYPE F.C.R.

SAMPLE	2JG33	2JG33	2JG33	1JG37	1JG37	1JG39
SiO2	76.99	74.19	76.45	78.98	79.87	74.00
TiO2	.29	.42	.08	.47	.59	.38
Al2O3	9.67	12.35	12.13	11.06	9.63	13.42
Fe2O3T	2.98	1.27	.68	1.61	2.36	1.31
MgO	.75	.61	.15	.63	.78	.46
CaO	2.68	.55	.53	.91	.48	.45
Na2O	2.74	2.83	2.56	2.29	1.15	3.20
K2O	2.12	6.42	5.99	3.70	4.05	5.77
TOTAL	98.22	98.64	98.57	99.65	98.91	98.99

ROCK TYPE MATRIX

SAMPLE	4JG20	4JG20	4JG20	1JG39	3JG13
SiO2	60.81	66.80	66.05	72.11	66.65
TiO2	.64	.66	.32	.36	.51
Al2O3	19.74	13.75	16.74	14.07	18.04
Fe2O3T	4.63	4.57	2.85	1.52	4.59
MgO	2.60	4.52	1.25	.73	1.71
CaO	2.24	2.59	3.10	.96	.36
Na2O	4.57	2.25	4.60	4.13	1.53
K2O	5.33	3.11	3.21	4.70	6.92
TOTAL	100.56	98.25	98.12	98.58	100.31

ROCK TYPE BRECCIA/CATACLASITE

SAMPLE	1JG25	1JG25	1JG21	1JG73	1JG73	1JG39	3JG65
SiO2	77.02	81.36	76.80	81.37	80.31	85.47	89.48
TiO2	.37	1.57	.52	.22	.21	.06	.35
Al2O3	11.70	8.57	10.76	10.13	10.08	7.14	4.56
Fe2O3T	1.20	1.06	1.85	1.08	1.16	.36	.89
MgO	.35	.18	.87	.46	.46	.18	.37
CaO	.48	1.37	1.45	.65	.44	.11	.08
Na2O	3.04	2.72	1.62	1.51	1.11	3.02	.52
K2O	4.28	2.52	4.14	4.84	5.75	1.78	2.30
TOTAL	98.44	99.35	98.01	100.26	99.52	98.12	98.55

APPENDIX F

NORMALISATION FACTORS

The normalisation factors used in the multi-element plots are those of Thompson (1982), modified by Rutter (1985). All values are given in ppm.

Ba	6.9	Zr	6.84
Rb	0.35	Hf	0.2
Th	0.042	Ti	620
U	0.013	Y	2.0
K	12.0	Yb	0.223
Nb	0.35	Pr	0.122
Ta	0.02	Eu	0.077
La	0.328	Gd	0.276
Ce	0.865	Dy	0.343
Sr	11.8	Ho	0.078
Nd	0.63	Er	0.225
P	46	Lu	0.034

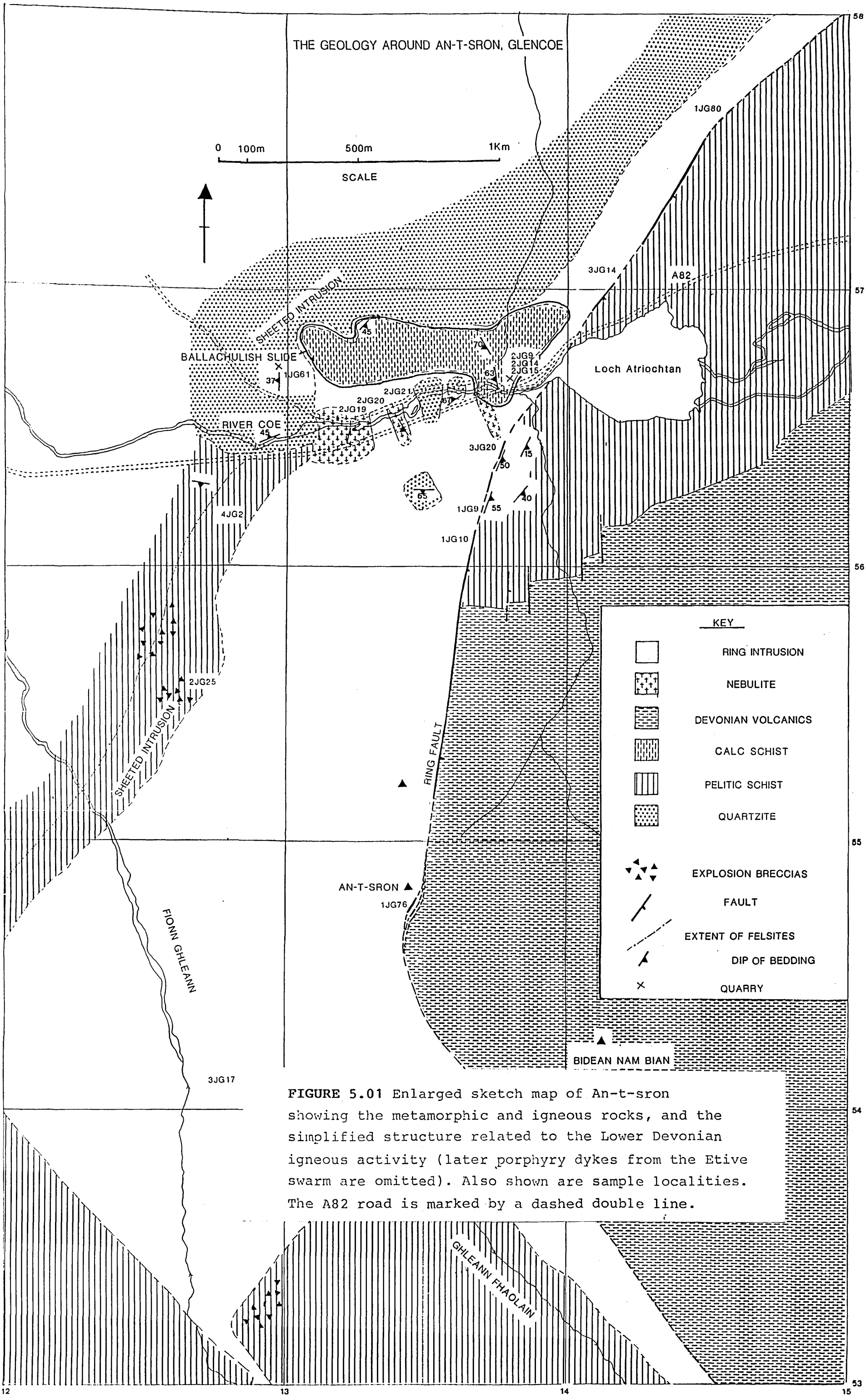

FIGURE 5.01 Enlarged sketch map of An-t-sron showing the metamorphic and igneous rocks, and the simplified structure related to the Lower Devonian igneous activity (later porphyry dykes from the Etive swarm are omitted). Also shown are sample localities. The A82 road is marked by a dashed double line.